ANL-6413

ANL-6413

MASTER

Argonne National Laboratory

CHEMICAL ENGINEERING DIVISION SUMMARY REPORT

July, August, September, 1961

DISCLAIMER

Price $3.00 . *Available from the Office of Technical Services, Department of Commerce, Washington 25, D.C.*

ANL-6413
Chemical Separations
Processes for Plutonium
and Uranium
(TID-4500, 17th Ed.)
AEC Research and
Development Report

ARGONNE NATIONAL LABORATORY
9700 South Cass Avenue
Argonne, Illinois

CHEMICAL ENGINEERING DIVISION SUMMARY REPORT

July, August, September, 1961

Stephen Lawroski, Division Director
R. C. Vogel, Associate Division Director
V. H. Munnecke, Assistant Division Director

Preceding Quarterly Reports:

ANL-6379	April, May, June, 1961
ANL-6333	January, February, March, 1961
ANL-6287	October, November, December, 1960

Operated by The University of Chicago
under
Contract W-31-109-eng-38

TABLE OF CONTENTS

TABLE OF CONTENTS

LIST OF TABLES

LIST OF TABLES

LIST OF TABLES

LIST OF TABLES

LIST OF FIGURES

LIST OF FIGURES

LIST OF FIGURES

CHEMICAL ENGINEERING DIVISION
SUMMARY REPORT

July, August, September, 1961

SUMMARY

I. Chemical-Metallurgical Processing (pages 27 to 106)

Pyrometallurgical processes for the recovery of fissionable material from discharged reactor fuels offer promise of achieving a reduction in the reprocessing costs associated with nuclear power. The principal characteristics of pyrometallurgical processes which are likely to result in reduced costs are their simplicity, compactness, low-volume dry wastes, and capability for handling short-cooled fuels with an attendant reduction in fuel inventories. Among the pyrometallurgical processes under development, melt refining, a simple melting procedure for metallic fuels, is in the most advanced state of development. This process will be used for the recovery of enriched uranium from the first core loading of the second Experimental Breeder Reactor (EBR-II). This reactor, with an integrated fuel-processing facility, is under construction at the National Reactor Testing Station in Idaho.

A fourth laboratory demonstration of the melt refining process, in which highly irradiated EBR-II prototype fuel pins were used, has been completed. Approximately 400 g of ten percent enriched uranium-five percent fissium alloy, irradiated to an estimated burnup of one total atom percent, was melt refined for one hour at 1400 C. Fission product removals were in accord with previous experiments employing inactive, low-level, and highly irradiated material. In this experiment, the fuel-handling procedures prior to melt refining were modified to limit exposure of the pins to air insofar as was practical. A substantial improvement in the product pouring yield tends to confirm the belief that low yields obtained in the high-activity-level experiments resulted from increased air oxidation of the fuel in the presence of radiation fields and fission decay heating during the fuel-handling operations.

Removal of fission product iodine from the fuel alloy during melt refining is believed to occur through volatilization of various metal iodides. Less than one percent of the total radioiodine is found in the furnace atmosphere at the completion of melt refining. Observations that additional iodine is released when the argon atmosphere in the furnace is replaced by air suggest that iodides are oxidized by air or by the moisture it contains. Iodine-131 was the only gamma activity, other than those attributable to noble gas fission products, that was detected in the furnace atmosphere after melt refining.

Nitridation rates of uranium-fissium alloy pins in an argon atmosphere containing four percent nitrogen were determined on a 2-kg scale. The results are in agreement with previous rate data from laboratory experiments with single pins.

Runs demonstrating the process for reclaiming melt refining skull material continue to show adequate purification of the uranium from fission product elements. In recent runs, over 80 percent removals of cerium, ruthenium, rhodium, palladium, zirconium, and molybdenum have been realized.

Determination of the particle size distribution of a blend of fissium skull oxides was extended into the sub-sieve range in order to assess the dusting problem created by the fine particles. Less than 1 percent of the particles were smaller than 10 μ in diameter (see Figure 2, page 44).

The reduction of uranium-fissium oxide mixtures by zinc-magnesium alloys in the presence of a flux is a basic step in the skull-recovery process. Experiments on the reduction of U_3O_8 to produce a zinc-10 weight percent uranium-12 weight percent magnesium alloy showed that increase of the volume of flux enhanced the reduction rate. The extent of reduction, however, appeared to be limited to about 96 percent. Although magnesium concentrations in the vicinity of 12 weight percent permit a reduction in solution volume because of the high solubility of uranium, concentrations of about 5 weight percent appear to be more reliable in producing complete reduction of the oxides. In a separate study in which the quantity of flux was increased as a variable, the reduction rate increased and the uranium loss to the flux decreased. A sharp decrease in reduction rate occurred when the quantity of magnesium oxide byproduct in the flux exceeded a certain value (11 weight percent under the particular conditions used in the experiments).

Since small fragments of zirconia crucibles for use in melt refining are introduced into the skull-recovery process during the skull-oxidation procedure, the extent to which such fragments are reduced to form zirconium metal in the oxide-reduction step was investigated. In 5 hr at 800 C, complete reduction occurred in zinc-12 weight percent magnesium alloy and 83 percent reduction took place in a zinc-5 weight percent magnesium alloy.

Complete reductions of thorium oxide have been achieved by 5 weight percent magnesium-zinc alloys at 750 C in the presence of a suitable halide flux. At least about 30 percent of magnesium cation in the flux is required to produce complete reduction within 2 hr.

Pressed-and-sintered beryllia crucibles (4-in. OD by 9 in. high) for retorting the uranium product from simulated skull-recovery process operations show promise. One isostatically pressed beryllia crucible has now been employed in four runs with no signs of failure. The runs consisted

of uranium dissolution, intermetallic compound precipitation, decomposition of the intermetallic compound, and final retorting. In all four runs, over 98 percent of the uranium present at the retorting step was readily dumped from the crucible as a well-agglomerated mass.

Three survey runs were made to investigate the feasibility of treating stainless steel-canned EBR-II pins by the proposed skull-recovery process or a similar process. Uranium pins and stainless steel were dissolved in a zinc-fused salt mixture which contained zinc chloride as a uranium oxidant. Dissolution was slow at 500 C but rapid at 600 C. The uranium appeared essentially completely in the molten salt while virtually all of the iron and nickel remained in the zinc phase, thus making possible a good separation of these elements from uranium. Chromium, however, distributed partially into the flux phase (15 to 20 percent), a distribution which should be reducible by decreasing the amount of excess zinc chloride employed. The results are encouraging.

The chlorination of uranium-fissium oxide mixtures to form species soluble in molten salt fluxes has been investigated briefly as a potential modification of the skull-recovery process. The oxide mixture, suspended in a molten chloride flux, was chlorinated by means of a mixture of carbon monoxide and chlorine at 800 to 850 C. Ferric chloride and zinc chloride both increased the chlorination rates. Substantial amounts of zirconium, molybdenum, and ruthenium were removed as volatile chlorides. The composition of the molten halide flux also affected the chlorination rate, the highest rates being achieved with a sodium chloride-potassium chloride-magnesium fluoride system.

In the blanket process, the high solubility of plutonium and the contrasting low solubility of uranium in high magnesium-zinc alloys are utilized to effect a separation of plutonium and uranium. A second demonstration of the blanket process largely confirmed the results of the first, namely, that rapid and complete dissolution of the blanket alloy is obtained in a 12 percent magnesium-zinc solution, and that the plutonium is retained in solution while the uranium is precipitated by addition of magnesium to a 50 percent concentration. The plutonium in the separated supernatant solution and in a succeeding wash of the uranium residue constituted 95 percent of the plutonium charged. A good separation of uranium from plutonium was thereby shown to be possible. A preliminary experiment indicated that, if desired, the uranium solubility in magnesium-rich zinc solutions may be lowered considerably by the addition of calcium (a 17 percent calcium concentration was employed in the experiment).

The possibility of separating rare earth fission products from plutonium through liquid metal extraction with calcium and calcium-rich zinc solutions is undergoing investigation. The solubility of plutonium in liquid calcium at 860 C is low (about 0.10 weight percent). The distribution ratio

of cerium between calcium and plutonium is about 0.53 on a weight basis. Thus, for a typical plutonium fuel, about 88 percent of the cerium would be removed with a loss of about 0.8 percent plutonium in two successive extractions at 860 C using a calcium/plutonium weight ratio of four. At 860 C the solubility of plutonium in calcium increases from 0.1 to 0.7 weight percent as zinc is added to 35 weight percent. The cerium distribution is not affected significantly.

A brief investigation was conducted on the precipitation of uranium carbide by adding hydrocarbon gases to uranium dissolved in zinc-magnesium and cadmium-magnesium solutions. Methane reacted somewhat faster in a cadmium-magnesium solution than in a zinc-magnesium solution. Acetylene underwent extensive pyrolysis in which elemental carbon was formed.

Materials evaluation studies are in progress to evaluate the compatibility of various materials with liquid metal systems of the types contemplated for reprocessing reactor fuels. Solutions of uranium in dilute magnesium-zinc alloys in contact with a molten halide flux were found to have good stability in tantalum and tungsten crucibles at investigated temperatures of up to 850 C. Tungsten shows considerable promise as a container material. However, there are indications of penetration of flux and metal phases into the walls of flame-sprayed-and-sintered tungsten crucibles (5 in. in diameter by 9 in. high, with a density of 92 percent of theoretical). Pressed-and-sintered tungsten crucibles are being obtained for evaluation. Various chemical etchants were evaluated for their effectiveness in revealing the depth of corrosion of refractory metals. An inert gas welding facility has been constructed to facilitate the preparation of corrosion capsules.

Porous tantalum filters have been obtained and successfully used for sampling liquid metal solutions. The tantalum filters will be used instead of porous graphite filters in those cases in which reaction of graphite with dissolved uranium is a possibility.

Twelve distillation runs have been completed in the large-scale cadmium-distillation unit. Distillation temperatures were varied from 455 to 620 C and distillation rates from 12 to 67 kg/hr, with corresponding heating efficiencies of 31 to 72 percent. In general, the unit has functioned very well. Some initial line-plugging difficulties were remedied by changes in external piping and operating procedures. Electrical resistance, liquid-level probes in the still pot proved unsatisfactory. Thermocouples at various levels are now utilized to locate liquid levels in the still pot. A freeze valve also ruptured, resulting in cadmium spillage into a catch tray. It was concluded that the valve had been improperly installed. Repairs have been made, and the spilled cadmium has been removed for possible recovery.

Equipment to measure vapor-liquid equilibrium in binary liquid metal systems has been assembled and will be used to determine activity coefficients in miscible binary metal systems, such as the cadmium-magnesium and zinc-magnesium systems. In a preliminary test of the equipment, the vapor pressure of cadmium was measured and results in good agreement with literature data were obtained. A study of the nature of liquid metal boiling and of entrainment from boiling liquid metals has been started.

A direct-cycle fuel-reprocessing plant using pyrometallurgical procedures is being designed and constructed as part of the Experimental Breeder Reactor No. II (EBR-II) project. A Laboratory and Service Building is also included. Melt refining, liquid metal extraction, and processes involving fractional crystallization from liquid metal systems are methods being examined for the recovery and purification of EBR-II fuels. Based on the results of these studies, process equipment is being designed and tested.

Construction of the Fuel Cycle Facility building was about 95 percent completed by August 29, 1961, as compared with 90 percent on June 1, 1961. Work continues on equipment for building and process services, but progress is extremely slow because of the small labor force that is now being employed by the contractor. Control equipment, such as that for the motor generator sets, was installed.

Installation of the shielding windows will probably not begin until after December 1, because of the delay in completion of the building.

Two melt refining furnaces are being built for the Facility. The bell jars and the control panels for these furnaces have been completed and shipped to Idaho.

Design and fabrication of other equipment for the Fuel Cycle Facility continues. Working drawings of the service sleeve feed-throughs have been completed and fabrication has started. The scrap-handling coffin has been received at the site. Purchase orders for the main parts of the airlocks have been let. Small scrap-handling containers have been obtained. Tools needed to handle the containers remotely are being developed.

The five-ton cranes in the process cells were greased with a radiation-resistant grease during fabrication. Subsequently, irradiation tests have revealed that other greases are more suitable for this use. Since it is not practical to remove the grease from the crane bearings, it may be possible to improve performance by adding one of the preferred greases to produce a blend of two greases in the bearings. Performance tests of bearings lubricated with blends of irradiated greases have, therefore, been initiated.

A new design grip drive clutch has been tested in the operating manipulator in the mock-up. It has proved to be superior to any of the clutches yet tested.

Development of the reference thermocouple to be used for temperature measurement in the melt refining furnaces of the Fuel Cycle Facility has been completed. The thermocouple will be used in the plant to predict the temperature and the internal heat generation rate of the fuel charge.

Design work of equipment for the skull-reclamation process continues.

Fundamental studies are being made in support of process development activities. Data basic to the various liquid metal processes are the solubilities of those elements whose separation may be attempted. The solubility of scandium in liquid cadmium has been measured. Scandium, in addition to being the first member of the first transition series of elements, is also often considered a member of the rare-earth group of elements. The solubility of scandium may be represented by two empirical equations:

$$\text{scandium (349 to 422 C):}\quad \log(\text{atom percent}) = 3.935 - 2434\ T^{-1}$$

$$\text{scandium (422 to 606 C):}\quad \log(\text{atom percent}) = 4.933 - 5335\ T^{-1} + 1.534 \times 10^{6}\ T^{-2}$$

Two different intermetallic phases have been found in the scandium-cadmium system: a hexagonal phase, probably $ScCd_3$, which is the equilibrium phase above 422 C, and another phase which has not yet been characterized.

The transformation between high-and low-temperature forms of the delta phase in the zinc-uranium system is very sluggish. The transformation temperature has been established by the X-ray diffraction examination of annealed alloys as being close to 550 C. The low-temperature form probably corresponds to uranium-rich compositions of the epsilon phase.

The utility of distribution between two immiscible liquid metals for the purification of spent reactor fuel is being investigated. The distribution of cerium and strontium between liquid zinc and lead has been measured as a function of temperature. The distribution coefficients

$$\left(\frac{\text{w/o solute in zinc-rich layer}}{\text{w/o solute in lead-rich layer}}\right)$$

found for cerium are 18.4 at 652 C, 7.9 at 703 C, and 5.0 at 736 C, whereas for strontium, values of 0.09 at 656 C, 0.11 at 703 C, and 0.15 at 740 C were obtained.

The free energy of formation of the uranium-indium intermetallic phase, UIn_3, has been measured over the range 353 to 675 C by means of a galvanic cell method. The results may be represented by the empirical equation

$$(UIn_3)\ \Delta F_f^{\circ}\ (\text{cal/mole}) = -24{,}280 + 7.441\ T + 3.875 \times 10^{-3}\ T^{2}$$

The praseodymium-zinc system is being investigated by the measurement of the zinc vapor pressure of solid alloys as a function of composition. The following phases have been found: $PrZn_{11}$, $PrZn_{8.5}$, $PrZn_{6.9-7.4}$, $PrZn_{3.4-5.6}$, $PrZn_2$, and PrZn. The phases $PrZn_{11}$ and PrZn were previously reported by other investigators.

Two series of combustions in oxygen were carried out, one with zirconium dihydride and the other with zirconium dideuteride, to determine the difference in heats of formation of the dihydride and dideuteride of zirconium. The samples were encapsulated in polyester film (Mylar) bags. A series of combustions of the Mylar material was also carried out. Results from the three series of combustions are being calculated.

The preliminary value for the heat of formation of boron trifluoride has been revised to $\Delta H^\circ_{f,298}(BF_3,g) = -270.16 \pm 0.24$ kcal/mole.

Preliminary values have been obtained for the heats of combustion and formation of the hexagonal form of boron nitride:

$$\Delta H^\circ_{C,298}(BN,c,hex) = -210.43 \pm 0.40 \text{ kcal/mole}$$
$$\Delta H^\circ_{f,298}(BN,c,hex) = -59.73 \pm 0.45 \text{ kcal/mole} \quad .$$

Preliminary values have been obtained for the heats of formation of hafnium and titanium tetrafluorides:

$$\Delta H^\circ_{f,298}(HfF_4,c) = -464.0 \text{ kcal/mole}$$
$$\Delta H^\circ_{f,298}(TiF_4,c) = -393.8 \text{ kcal/mole} \quad .$$

Exploratory experiments to develop experimental techniques for combustions of magnesium, aluminum, cadmium, and zinc in fluorine have been carried out. Calorimetric combustions with magnesium have been started.

Experimental techniques for combustions of uranium in fluorine are being developed. During one of the combustions, the cap of the bomb ruptured as a result of the heat that was generated, and fluorine and molten metal were discharged into the hood in which the experiment was being carried out. The causes of this potentially hazardous occurrence are discussed in some detail.

Construction and testing of the high-temperature enthalpy calorimeter is in progress.

II. Fuel Cycle Applications of Volatility and Fluidization Techniques (pages 107 to 148)

The volatilities of uranium and plutonium hexafluorides are the basis of a direct fluorination volatility process proposed for the recovery of uranium

and plutonium from irradiated nuclear reactor fuels. In this process fluidization techniques are also used to advantage. Progress is being made in the application of this process to uranium oxide and zirconium-matrix fuels.

The proposed process for recovery of uranium and plutonium from spent uranium oxide involves decladding by an appropriate reaction in a fluidized bed. Plutonium and uranium hexafluorides, which result from the reaction of the declad oxide fuel with fluorine, may be separated by using a combination of the variability of the rates of fluorination of the plutonium and uranium compounds and chemical reactivities of the hexafluorides.

The direct fluorination of dense uranium dioxide pellets is being examined in a 3-in.-diameter, air-cooled reactor. In order to obtain further information on the effect of temperature under process conditions, a fluorination of a 6-in.-deep bed of pellets was carried to completion at 400 C in the presence of an oxygen diluent resulting from the recycle process gas. In 11.0 hr, 86 percent of the charge was recovered as uranium hexafluoride product with an overall fluorine utilization efficiency of 82 percent. Although this batch reaction time is not considered excessive, equivalent reaction has been carried out at 500 C in 40 percent of the time. It is believed that higher rates can be obtained at 400 C by increasing the fluorine concentration, which averaged only about 16 percent in this run. Further studies of processing conditions are planned along the lines of determining the role of oxygen on overall fluorination rate, close temperature control over a wider range of reaction rates, and optimum fluorination of the pellet residues at the end of a batch reaction.

Because of a pronounced effect of the presence of oxygen on the fluorination rate, attempts are under way to measure the oxidation rate alone. In very preliminary results, oxidation of uranium dioxide pellets at 300 C was readily detected; the rate increased with temperature up to 600 C, the highest temperature employed.

Since in practice the rate of fluorination is limited by heat transfer rather than reaction kinetics, efforts have been made to enhance heat removal by utilization of a packed-fluidized-bed system. A packed-fluidized-bed system employs inert fluidizing material in the voids of a bed of larger particles so as to provide better heat transfer characteristics. A study was made of this type of heat transfer in a mockup system, showing the effect of different types and sizes of packing and different size of material fluidized in the voids of the fixed packing. The effective radial thermal conductivity was found to increase with increasing gas velocity and to be higher for larger packing. The effective thermal conductivity of packed-fluidized beds was as high as 10 Btu/(hr)(sq ft)(F/ft) compared to that for fixed beds of about 0.4 Btu/(hr)(sq ft)(F/ft). The film coefficients for the heating and cooling surfaces were found to be as much as five times that for fixed beds. Film

coefficients followed the same general trends with various particle sizes as did the effective thermal conductivities, but the variations in film coefficients were considerably smaller over the ranges of the variables. Film coefficient values and thermal conductivities in the packed-fluidized system were similar to values obtained in previous studies of packed-fluidized systems.

Laboratory-scale experiments have been performed in which fluorination reactions have been carried out with aluminum oxide as the inert bed material. It has been concluded that the use of high-purity refractory grain Alundum results in lower values of residual plutonium (~0.02 percent) than those obtained with either zirconium or calcium fluoride. It is also concluded that the use of recycled fluorine is feasible, since oxygen does not exert a deleterious effect on plutonium retention in Alundum. The use of Alundum for more than a single fuel loading may be limited not only by the accumulation of fission products but also by the increase of plutonium retention in the Alundum with reuse of the bed material. After the reuse of Alundum in five successive experiments, the plutonium concentration in the Alundum rose to approximately 0.1 percent.

Studies are being conducted on a fluidization-volatility scheme for separating and recovering uranium from zirconium-base fuels. The process involves initial separation of the zirconium by reaction of the low uranium-zirconium alloy with hydrogen chloride forming the volatile zirconium tetrachloride, which is allowed to pass out of the system. Uranium forms the solid uranium trichloride. Uranium is recovered as uranium hexafluoride by fluorination of the uranium chloride.

Laboratory studies reported in the previous quarterly (ANL-6379, page 150) indicated that, for optimum recovery of uranium from enriched uranium-zirconium alloy fuels, it is best to declad and remove the zirconium by hydrochlorination at or above 350 C. The hydrochlorination of the zirconium and the subsequent fluorination of the uranium chlorides can be carried out in a fluidized bed of granular solids. The uranium particulate is expected to be retained, for the most part, in the inert fluid-bed medium in which the primary reaction is conducted. Uranium entrained by the volatile material will be filtered by suitable means. Of those bed materials tested, Alundum, refractory aluminum oxide, was most satisfactory. In this report laboratory tests of three types of Norton's refractory grain Alundum are discussed. The purest grade of electrically fused refractory grain alumina yielded the best results.

In previous engineering-scale studies, both uranium-zirconium alloy constituents were converted to fluorides and it is believed the zirconium inhibited complete uranium recovery. Initial engineering-scale work is directed toward the evaluation of fixed beds of high-fired aluminum oxide as filters for the retention of entrained uranium particulate. The uranium is recovered from the fixed bed of aluminum oxide by fluorination. Up-flow

and down-flow systems are being tested with a 1.5-in.-diameter fluidized reaction zone and a 3.0-in.-diameter filter zone. Both up-flow and down-flow experiments show lower uranium losses may be achieved by using small filter-bed particles (200 mesh size). Higher gas velocities (in the range tested, 0.23 to 0.75 ft/sec) gave lower uranium losses in the down-flow case whereas the reverse was true for up-flow. Bed depth in the range from 3 to 12 in. has not been found critical. Overall losses were in the range from 0.1 to 0.6 percent of the uranium reacted (up to 7.6 g maximum charged as 2.7 weight percent uranium-zirconium alloy in the form of $\frac{1}{4}$-in., irregularly shaped cubes). The hydrochlorination was conducted in the range from 550 to 400 C with 20 to 70 mole percent hydrogen chloride in nitrogen.

Preliminary corrosion tests of 35- and 170-hr duration made to evaluate possible materials of construction showed rates of 0.2 mil/month (determined by weight loss) for A-nickel and Inconel exposed to zirconium tetrachloride vapor (2000 mm Hg pressure) at temperatures of 370 C. Appreciable diminution of the rate occurs with time. Sintered porous nickel coupons (possible filter material) showed significant weight loss, but quantitative values cannot be assigned because of difficulties in determining true exposed surface areas.

Studies were essentially completed this quarter on the development of a two-step fluid-bed process for converting uranium hexafluoride to uranium dioxide. This work has been conducted in an effort to provide a simpler method for preparation of ceramic reactor fuel. Equipment modifications for the first step, steam-hydrolysis of the hexafluoride to uranyl fluoride, which permitted elutriation of fines from the reaction zone, have apparently solved all of the previous operating problems associated with particle size control of the bed, and extended runs to 25 hr in duration have been made. Nominal operating conditions used for the 3-in.-diameter reactor were 100 g/min hexafluoride feed [174 lb uranium/(hr)(sq ft)], 230 C bed temperature, approximately 15-in. static bed height, 0.75 ft/sec superficial fluidizing gas velocity, steam excesses of 245 percent and a recycle solids feed rate near 15 percent. Average bed particle size was maintained near 350 μ.

The second step, reduction of uranyl fluoride to uranium dioxide, has been conducted as a batch operation. A 50-50 mixture of steam and hydrogen at temperatures near 650 C appears optimum. Static bed heights to 21 in. (L/D = 7) have been used. Material containing less than 200 ppm fluoride has been produced in periods of 3 to 4 hr, the time period depending on reactant excesses. Conversion rate also appears to be dependent on particle size, smaller particles giving somewhat better conversion times. Particle densities as determined by immersion in xylene, water, and mercury were 9.68, 9.23, and 6.22 g/ml, respectively. Reactor (nickel) corrosion in 4-hr experiments resulted in nickel content in the product of 100 to 130 ppm.

In recent engineering-scale studies, components were developed which proved valuable in fluoride volatility work. Descriptions are given of an automatic, remote-recording chain balance for weight tank applications and an all-metal fluorine analyzer. In addition, a baffled-cone gas distributor for fluid-bed reactors has been developed and appears promising in mock-up tests.

Improved operation of a small-diameter column for continuous fluid-bed calcining where criticality must be considered has been achieved in recent feasibility studies. A $2\frac{1}{4}$-in.-diameter column with 1 M aluminum nitrate feed is currently in use with vertical upward spraying of the feed, achieved by mounting the feed spray nozzle in the apex of the cone bottom, permitting use of atomizing and feed decomposition gases as the fluidizing gas medium. Runs to 6-hr duration at an air-to-liquid volume ratio of 1740 gave moderate fines production (five percent less than 140 mesh) using a 325 g bed of -20 +80 mesh aluminum oxide. A 3-hr run at an air-to-liquid ratio of 1070, achieved by increasing the feed rate from 8.7 to 14.0 ml/min while maintaining the atomizing air rate constant (0.54 scfm), gave the best results to date, only one percent less than 140 mesh material being produced. The current series of runs was carried out at bed temperatures near 330 C. The primary objective in future work will be to demonstrate reliability of the operation.

III. Reactor Safety (pages 149 to 193)

The oxidation, ignition, and combustion processes of uranium, zirconium, plutonium, and other metals and their compounds are being studied to provide information to aid in minimizing the hazards associated with handling these materials.

A program of theoretical studies has been initiated to relate quantitatively ignition results to isothermal oxidation data. Isothermal data from experiments with zirconium, covering the range from 400 to 900 C, was used to calculate theoretical temperature-time curves corresponding to shielded ignition tests. Calculations were made by a step-wise method using a simple heat transfer model. Theoretical ignition temperatures were obtained for single pieces of zirconium having specific areas of 5, 50, 500, and 5000 sq cm/g.

Previous experimental studies of zirconium by the shielded ignition method used flowing helium to shield the specimen while it was brought to temperature. Helium flow was then switched to oxygen and it was determined visually whether ignition occurred or not. It was not entirely clear how much preoxidation of the specimens occurred while the sample was heating. A brief experimental study was, therefore, made of zirconium ignition under conditions where no preoxidation could occur. Results indicated that preoxidation effects encountered in studies by the helium flow method were

negligible except for the finest foils (highest specific area) studied. Further experimental studies were made by the helium flow method to test the effect of ends or edges exposed to oxygen. Edge effects were found to be significant for large wires (low specific area). Ignition was able to occur at lower temperature at exposed sharp edges.

Comparison of theoretical ignition temperatures with experimental values was then made after it was certain that preoxidation and edge effects were not complicating the experimental results. Ignition temperatures agreed within approximately 100 C.

Efforts to calculate burning curve ignition temperatures with uranium by similar methods failed. Failure was attributed to a lack of isothermal oxidation data above 300 C. Studies were, therefore, undertaken of the isothermal oxidation of uranium between 300 and 600 C. The studies were made in a metal "heat sink" reaction cell in which specimens were pressed against metal heat sinks by a spring. This was effective in preventing excessive self-heating. Preliminary data with Argonne base uranium, "β-quenched," showed that low-temperature rates could be extrapolated to 400 C. Reaction rates then decreased slightly between 400 and 500 C. Rates began to rise rapidly with temperature above 500 C.

Studies of burning propagation along uranium and zirconium foil strips are continuing. Simultaneous measurements of propagation rates and burning temperatures have been obtained by means of a photoelectric pyrometer. Studies were concentrated on the effects of additions of halogenated hydrocarbons to the air. Results were obtained for a number of halogenated hydrocarbons. The effectiveness of the compounds in reducing burning propagation rates and temperatures was believed due to their tendency to decompose thermally at or very near to the oxidizing metal surface. Fragments produced in the decomposition were able to react with oxygen in the gaseous diffusion zone near the metal. This oxygen was, therefore, lost to the metal and was responsible for decreased rates and temperatures. Carbon tetrafluoride (CF_4) was ineffective in decreasing rates and temperatures, presumably because of insufficient thermal decomposition. Methyl and ethyl iodides were also ineffective because thermal decomposition occurred at lower temperatures at the outer edge of the diffusion boundary layer. In general, these compounds having optimum chemical stability, such as trifluorobromomethane (CF_3Br), methyl chloride (CH_3Cl), and chloroform ($CHCl_3$), were most effective.

Studies were made of the effect of halogenated hydrocarbons on burning curve ignition temperatures of uranium. Ignition temperatures were unaffected by small additions to the air of compounds containing only carbon, hydrogen, and fluorine atoms. Compounds containing bromine or chlorine atoms lowered the ignition temperatures significantly. Results suggested that there is an exothermal reaction between chlorine or bromine compounds and uranium dioxide.

Installation of apparatus in new plutonium glovebox facilities is complete. Apparatus has been assembled to study (1) burning propagation, (2) ignition, and (3) controlled oxidation. Controlled oxidations are carried out in a recording thermobalance which has been equipped with a specimen thermocouple. A magnetic amplifier is used to provide a recorded output so that there is not interference with the balance operation.

The experimental program to determine rates of reaction of molten reactor fuel and cladding metals with water is continuing. One method involves the rapid melting and dispersion of metal wires in a water environment by a surge current from a bank of condensers. A series of runs with uranium in heated water was completed. Results showed that considerably more reaction occurred in heated water than in room-temperature water. The uranium results were, therefore, consistent with previous results with zirconium. The findings added supporting evidence to the theoretical account of the zirconium-water reaction, which has been presented in previous quarterlies.

Water temperature in the uranium runs ranged from 100 to 125 C (water vapor pressure, 15 to 33 psia). Attempts to study the reaction in water at 200 C failed because of very extensive corrosion of the specimens during the run preparation period.

Particle sizes of residue from uranium runs by the condenser-discharge method are reported. Transient pressure traces from uranium indicated that the progression of slow reaction rates to explosive rates occurred over the temperature range from 1600 to 2500 C. Results were consistent with the findings for zirconium that particles smaller than 1000 μ in heated water and 500 μ in room temperature water could undergo the explosive reaction. Analyses of the hydrogen retained by the residue from uranium runs indicated that, at most, a few percent of the hydrogen generated during a run is retained by the partly oxidized metal.

A second method of studying metal-water reactions involves the rapid contact of steam with heated metal. In this method, the metal receives a "pressure pulse" of water vapor. The apparatus is entirely enclosed in a box heated to 105 C. Runs with 500 mm of water vapor reacting with molten aluminum at 800, 1000, and 1200 C are reported. Rates followed the cubic rate law; an activation energy of 21,700 cal/mole described the effect of temperature. A series of runs with aluminum-5 percent uranium alloys at 1200 C gave slightly less reaction than that obtained with pure aluminum.

The experimental work on metal-water reactions during nuclear reactor excursions was continued. Four transients were completed in TREAT on fuel pins with uranium dioxide core (20 percent enriched)

clad in 18-mil-thick stainless steel-304. The data obtained from these meltdowns in 25 C water are as follows:

	CEN Transient Number			
	64	67	65	66
megawatt-second burst:	140	185	190	230
millisecond period:	115	290	50	97
UO_2 core density, % of theor.	89 (water logged)	98	89	98
% SS-H_2O reaction:	0.8	0.3	5.2	9.0
Final appearance of fuel pin				
clad:	two small ruptures, darkened area	intact, darkened central area	fragmented, partly melted	fragmented, partly melted
core:	distorted, cracked	radial cracks	fragmented, fine particles	fragmented, coarse particles

Correlation of the data on the experiments with uranium dioxide core pins indicate a progressive increase in the amount of cladding (SS-304)-water reaction as the reactor burst becomes more energetic. For periods in the range from 48 to 121 ms, the extent of metal-water reaction is 1.2, 6.0, and 16.0 percent stainless steel reacted for energies of 200, 300, and 400 cal/g uranium dioxide, respectively. For these uranium dioxide core fuel pins, the dividing point between destructive and nondestructive transients (on fast periods of 49 to 121 ms) is a burst of about 130 Mw-sec or 174 cal/g of core. This corresponds to a peak central core temperature of 2200 C for adiabatic heating of the uranium dioxide.

An evaluation was made of previous data obtained in TREAT on mixed oxide-core fuel pins; the results indicate a threshold temperature of 2300 C (for the central core) for incipient destruction of the fuel pin. Thus, both pure and mixed oxide-core fuel pins have similar behavior with regard to the maximum allowable temperatures in transients on fuel elements submerged in nonflowing, room-temperature water.

IV. Reactor Chemistry (pages 194 to 215)

The neutron capture cross sections of neptunium-237, erbium-170, gadolinium-158, lutetium-175, ytterbium-176, and molybdenum-98 are being determined in the fast neutron energy range. Preparations have begun

for the determination of the yields of fission products in the region of mass 100 when the fissile isotopes uranium-233, uranium-235, and plutonium-239 are exposed to fast neutron (fission spectrum) flux.

Operation of a regenerative lithium hydride fuel cell system for converting nuclear energy to electricity is being studied. The thermally regenerative emf cell system is one in which heat is used to disassociate lithium hydride, which is then re-formed in an electrochemical cell with the production of electric power.

The program of research in thermoelectricity methods for direct conversion of nuclear reactor heat energy into electrical power initiated last quarter (see ANL-6379, page 242) was continued. Measurements will be made in two limited areas, namely, liquid thermocouple systems and refractory solid thermocouple systems. Seebeck coefficients, electrical conductivities, thermal conductivities, and Hall coefficients of well-characterized materials may be determined. Current efforts are concerned with design, construction, and testing of equipment, and with some exploratory measurements.

The Reactor Decontamination Program is directed toward determination of the seriousness of fuel element ruptures in boiling water reactors and the determination of methods of decontamination of contaminated surfaces. Additional data have been obtained from a 16-day run made to determine whether zirconium-niobium content would reach an equilibrium value in a stainless steel loop which simulates the action of a boiling water reactor. The data indicated that the concentrations of all fission products, except ruthenium-103, reached a near equilibrium level after about 100 hr of loop operation. The concentration of ruthenium-103 continued to decrease to nondetectable levels. Current laboratory experiments on the decontamination of stainless steel 304 are being conducted using oxalic acid-base solutions containing hydrogen peroxide.

V. Routine Operations (page 216)

The operation of the radioactive waste-processing facility and the gamma-irradiation facility continued without incident.

* * * * *

For the convenience of the reader, appropriate parts of this summary are repeated at the beginning of each of the four main sections of this report.

I. CHEMICAL-METALLURGICAL PROCESSING

Pyrometallurgical processes for the recovery of fissionable material from discharged reactor fuels offer promise of achieving a reduction in the reprocessing costs associated with nuclear power. The principal characteristics of pyrometallurgical processes which are likely to result in reduced costs are their simplicity, compactness, low-volume dry wastes and capability for handling short-cooled fuels with an attendant reduction in fuel inventories. Among the pyrometallurgical processes under development, melt refining, a simple melting procedure for metallic fuels, is in the most advanced state of development. This process will be used for the recovery of enriched uranium from the first core loading of the second Experimental Breeder Reactor (EBR-II). This reactor, with an integrated fuel processing facility, is under construction at the National Reactor Testing Station in Idaho.

A fourth laboratory demonstration of the melt refining process, in which highly irradiated EBR-II prototype fuel pins were used, has been completed. Approximately 400 g of ten percent enriched uranium-five percent fissium alloy, irradiated to an estimated burnup of one total atom percent, was melt refined for one hour at 1400 C. Fission product removals were in accord with previous experiments employing inactive, low-level, and highly irradiated material. In this experiment, the fuel-handling procedures prior to melt refining were modified to limit exposure of the pins to air insofar as was practical. A substantial improvement in the product pouring yield tends to confirm the belief that low yields obtained in the high-activity-level experiments resulted from increased air oxidation of the fuel in the presence of radiation fields and fission decay heating during the fuel-handling operations.

Removal of fission product iodine from the fuel alloy during melt refining is believed to occur through volatilization of various metal iodides. Less than one percent of the total radioiodine is found in the furnace atmosphere at the completion of melt refining. Observations that additional iodine is released when the argon atmosphere in the furnace is replaced by air suggest that iodides are oxidized by air or by the moisture it contains. Iodine-131 was the only gamma activity, other than those attributable to noble gas fission products, that was detected in the furnace atmosphere after melt refining.

Nitridation rates of uranium-fissium alloy pins in an argon atmosphere containing four percent nitrogen were determined on a 2-kg scale. The results are in agreement with previous rate data from laboratory experiments with single pins.

Runs demonstrating the process for reclaiming melt refining skull material continue to show adequate purification of the uranium from fission

product elements. In recent runs, over 80 percent removals of cerium, ruthenium, rhodium, palladium, zirconium, and molybdenum have been realized.

Determination of the particle size distribution of a blend of fissium skull oxides was extended into the sub-sieve range in order to assess the dusting problem created by the fine particles. Less than 1 percent of the particles were smaller than 10μ in diameter (see Figure 2, page 44).

The reduction of uranium-fissium oxide mixtures by zinc-magnesium alloys in the presence of a flux is a basic step in the skull-recovery process. Experiments on the reduction of U_3O_8 to produce a zinc-10 weight percent uranium-12 weight percent magnesium alloy showed that increase of the volume of flux enhanced the reduction rate. The extent of reduction, however, appeared to be limited to about 96 percent. Although magnesium concentrations in the vicinity of 12 weight percent permit a reduction in solution volume because of the high solubility of uranium, concentrations of about 5 weight percent appear to be more reliable in producing complete reduction of the oxides. In a separate study in which the quantity of flux was increased as a variable, the reduction rate increased and the uranium loss to the flux decreased. A sharp decrease in reduction rate occurred when the quantity of magnesium oxide byproduct in the flux exceeded a certain value (11 weight percent under the particular conditions used in the experiments).

Since small fragments of zirconia crucibles for use in melt refining are introduced into the skull-recovery process during the skull-oxidation procedure, the extent to which such fragments are reduced to form zirconium metal in the oxide-reduction step was investigated. In 5 hr at 800 C, complete reduction occurred in zinc-12 weight percent magnesium alloy and 83 percent reduction took place in a zinc-5 weight percent magnesium alloy.

Complete reductions of thorium oxide have been achieved by 5 weight percent magnesium-zinc alloys at 750 C in the presence of a suitable halide flux. At least about 30 percent of magnesium cation in the flux is required to produce complete reduction within 2 hr.

Pressed- and-sintered beryllia crucibles (4-in. OD by 9 in. high) for retorting the uranium product from simulated skull-recovery process operations show promise. One isostatically pressed beryllia crucible has now been employed in four runs with no signs of failure. The runs consisted of uranium dissolution, intermetallic compound precipitation, decomposition of the intermetallic compound, and final retorting. In all four runs, over 98 percent of the uranium present at the retorting step was readily dumped from the crucible as a well-agglomerated mass.

Three survey runs were made to investigate the feasibility of treating stainless steel-canned EBR-II pins by the proposed skull-recovery process or a similar process. Uranium pins and stainless steel were dissolved in a zinc-fused salt mixture which contained zinc chloride as a uranium oxidant. Dissolution was slow at 500 C but rapid at 600 C. The uranium appeared essentially completely in the molten salt while virtually all of the iron and nickel remained in the zinc phase, thus making possible a good separation of these elements from uranium. Chromium, however, distributed partially into the flux phase (15 to 20 percent), a distribution which should be reducible by decreasing the amount of excess zinc chloride employed. The results are encouraging.

The chlorination of uranium-fissium oxide mixtures to form species soluble in molten salt fluxes has been investigated briefly as a potential modification of the skull-recovery process. The oxide mixture, suspended in a molten chloride flux, was chlorinated by means of a mixture of carbon monoxide and chlorine at 800 to 850 C. Ferric chloride and zinc chloride both increased the chlorination rates. Substantial amounts of zirconium, molybdenum, and ruthenium were removed as volatile chlorides. The composition of the molten halide flux also affected the chlorination rate, the highest rates being achieved with a sodium chloride-potassium chloride-magnesium fluoride system.

In the blanket process, the high solubility of plutonium and the contrasting low solubility of uranium in high magnesium-zinc alloys are utilized to effect a separation of plutonium and uranium. A second demonstration of the blanket process largely confirmed the results of the first, namely, that rapid and complete dissolution of the blanket alloy is obtained in a 12 percent magnesium-zinc solution, and that the plutonium is retained in solution while the uranium is precipitated by addition of magnesium to a 50 percent concentration. The plutonium in the separated supernatant solution and in a succeeding wash of the uranium residue constituted 95 percent of the plutonium charged. A good separation of uranium from plutonium was thereby shown to be possible. A preliminary experiment indicated that, if desired, the uranium solubility in magnesium-rich zinc solutions may be lowered considerably by the addition of calcium (a 17 percent calcium concentration was employed in the experiment).

The possibility of separating rare earth fission products from plutonium through liquid metal extraction with calcium and calcium-rich zinc solutions is undergoing investigation. The solubility of plutonium in liquid calcium at 860 C is low (about 0.10 weight percent). The distribution ratio of cerium between calcium and plutonium is about 0.53 on a weight basis. Thus, for a typical plutonium fuel, about 88 percent of the cerium would be removed with a loss of about 0.8 percent plutonium in two successive extractions at 860 C using a calcium/plutonium weight ratio of four. At 860 C the solubility of plutonium in calcium increases from

0.1 to 0.7 weight percent as zinc is added to 35 weight percent. The cerium distribution is not affected significantly.

A brief investigation was conducted on the precipitation of uranium carbide by adding hydrocarbon gases to uranium dissolved in zinc-magnesium and cadmium-magnesium solutions. Methane reacted somewhat faster in a cadmium-magnesium solution than in a zinc-magnesium solution. Acetylene underwent extensive pyrolysis in which elemental carbon was formed.

Materials evaluation studies are in progress to evaluate the compatibility of various materials with liquid metal systems of the types contemplated for reprocessing reactor fuels. Solutions of uranium in dilute magnesium-zinc alloys in contact with a molten halide flux were found to have good stability in tantalum and tungsten crucibles at investigated temperatures of up to 850 C. Tungsten shows considerable promise as a container material. However, there are indications of penetration of flux and metal phases into the walls of flame-sprayed-and-sintered tungsten crucibles (5 in. in diameter by 9 in. high, with a density of 92 percent of theoretical). Pressed-and-sintered tungsten crucibles are being obtained for evaluation. Various chemical etchants were evaluated for their effectiveness in revealing the depth of corrosion of refractory metals. An inert gas welding facility has been constructed to facilitate the preparation of corrosion capsules.

Porous tantalum filters have been obtained and successfully used for sampling liquid metal solutions. The tantalum filters will be used instead of porous graphite filters in those cases in which reaction of graphite with dissolved uranium is a possibility.

Twelve distillation runs have been completed in the large-scale cadmium-distillation unit. Distillation temperatures were varied from 455 to 620 C and distillation rates from 12 to 67 kg/hr, with corresponding heating efficiencies of 31 to 72 percent. In general, the unit has functioned very well. Some initial line-plugging difficulties were remedied by changes in external piping and operating procedures. Electrical resistance, liquid-level probes in the still pot proved unsatisfactory. Thermocouples at various levels are now utilized to locate liquid levels in the still pot. A freeze valve also ruptured, resulting in cadmium spillage into a catch tray. It was concluded that the valve had been improperly installed. Repairs have been made, and the spilled cadmium has been removed for possible recovery.

Equipment to measure vapor-liquid equilibrium in binary liquid metal systems has been assembled and will be used to determine activity coefficients in miscible binary metal systems, such as the cadmium-magnesium and zinc-magnesium systems. In a preliminary test of the

equipment, the vapor pressure of cadmium was measured and results in good agreement with literature data were obtained. A study of the nature of liquid metal boiling and of entrainment from boiling liquid metals has been started.

A direct-cycle fuel-reprocessing plant using pyrometallurgical procedures is being designed and constructed as part of the Experimental Breeder Reactor No. II (EBR-II) project. A Laboratory and Service Building is also included. Melt refining, liquid metal extraction, and processes involving fractional crystallization from liquid metal systems are methods being examined for the recovery and purification of EBR-II fuels. Based on the results of these studies, process equipment is being designed and tested.

Construction of the Fuel Cycle Facility building was about 95 percent completed by August 29, 1961, as compared with 90 percent on June 1, 1961. Work continues on equipment for building and process services, but progress is extremely slow because of the small labor force that is now being employed by the contractor. Control equipment, such as that for the motor generator sets, was installed.

Installation of the shielding windows will probably not begin until after December 1, because of the delay in completion of the building.

Two melt refining furnaces are being built for the Facility. The bell jars and the control panels for these furnaces have been completed and shipped to Idaho.

Design and fabrication of other equipment for the Fuel Cycle Facility continues. Working drawings of the service sleeve feed-throughs have been completed and fabrication has started. The scrap-handling coffin has been received at the site. Purchase orders for the main parts of the airlocks have been let. Small scrap-handling containers have been obtained. Tools needed to handle the containers remotely are being developed.

The five-ton cranes in the process cells were greased with a radiation-resistant grease during fabrication. Subsequently, irradiation tests have revealed that other greases are more suitable for this use. Since it is not practical to remove the grease from the crane bearings, it may be possible to improve performance by adding one of the preferred greases to produce a blend of two greases in the bearings. Performance tests of bearings lubricated with blends of irradiated greases have, therefore, been initiated.

A new design grip drive clutch has been tested in the operating manipulator in the mock-up. It has proved to be superior to any of the clutches yet tested.

Development of the reference thermocouple to be used for temperature measurement in the melt refining furnaces of the Fuel Cycle Facility has been completed. The thermocouple will be used in the plant to predict the temperature and the internal heat generation rate of the fuel charge.

Design work of equipment for the skull-reclamation process continues.

Fundamental studies are being made in support of process development activities. Data basic to the various liquid metal processes are the solubilities of those elements whose separation may be attempted. The solubility of scandium in liquid cadmium has been measured. Scandium, in addition to being the first member of the first transition series of elements, is also often considered a member of the rare-earth group of elements. The solubility of scandium may by represented by two empirical equations:

$$\text{scandium (349 to 422 C): } \log(\text{atom percent}) = 3.935 - 2434\ T^{-1}$$

$$\text{scandium (422 to 606 C): } \log(\text{atom percent}) = 4.933 - 5335\ T^{-1} + 1.534 \times 10^{6}\ T^{-2} .$$

Two different intermetallic phases have been found in the scandium-cadmium system: a hexagonal phase, probably $ScCd_3$, which is the equilibrium phase above 422 C, and another phase which has not yet been characterized.

The transformation between high- and low-temperature forms of the delta phase in the zinc-uranium system is very sluggish. The transformation temperature has been established by the X-ray diffraction examination of annealed alloys as being close to 550 C. The low-temperature form probably corresponds to uranium-rich compositions of the epsilon phase.

The utility of distribution between two immiscible liquid metals for the purification of spent reactor fuel is being investigated. The distribution of cerium and strontium between liquid zinc and lead has been measured as a function of temperature. The distribution coefficients $\left(\frac{\text{w/o solute in zinc-rich layer}}{\text{w/o solute in lead-rich layer}}\right)$ found for cerium are 18.4 at 652 C, 7.9 at 703 C, and 5.0 at 736 C, whereas for strontium, values of 0.09 at 656 C, 0.11 at 703 C, and 0.15 at 740 C were obtained.

The free energy of formation of the uranium-indium intermetallic phase, UIn_3, has been measured over the range 353 to 675 C by means of a galvanic cell method. The results may be represented by the empirical equation

$$(UIn_3)\ \Delta F_f^\circ\ (cal/mole) = -24{,}280 + 7.441\ T + 3.875 \times 10^{-3}\ T^2 \quad .$$

The praseodymium-zinc system is being investigated by the measurement of the zinc vapor pressure of solid alloys as a function of composition. The following phases have been found: $PrZn_{11}$, $PrZn_{8.5}$, $PrZn_{6.9-7.4}$, $PrZn_{3.4-5.6}$, $PrZn_2$, and PrZn. The phases $PrZn_{11}$ and PrZn were previously reported by other investigators.

Two series of combustions in oxygen were carried out, one with zirconium dihydride and the other with zirconium dideuteride, to determine the difference in heats of formation of the dihydride and dideuteride of zirconium. The samples were encapsulated in polyester film (Mylar) bags. A series of combustions of the Mylar material was also carried out. Results from the three series of combustions are being calculated.

The preliminary value for the heat of formation of boron trifluoride has been revised to $\Delta H_{f,298}^\circ\ (BF_3, g) = -270.16 \pm 0.24$ kcal/mole.

Preliminary values have been obtained for the heats of combustion and formation of the hexagonal form of boron nitride:

$$\Delta H_{C,298}^\circ\ (BN, c, hex) = -210.43 \pm 0.40\ kcal/mole$$

$$\Delta H_{f,298}^\circ\ (BN, c, hex) = -59.73 \pm 0.45\ kcal/mole.$$

Preliminary values have been obtained for the heats of formation of hafnium and titanium tetrafluorides:

$$\Delta H_{f,298}^\circ\ (HfF_4, c) = -464.0\ kcal/mole$$

$$\Delta H_{f,298}^\circ\ (TiF_4, c) = -393.8\ kcal/mole.$$

Exploratory experiments to develop experimental techniques for combustions of magnesium, aluminum, cadmium, and zinc in fluorine have been carried out. Calorimetric combustions with magnesium have been started.

Experimental techniques for combustions of uranium in fluorine are being developed. During one of the combustions, the cap of the bomb ruptured as a result of the heat that was generated, and fluorine and molten metal were discharged into the hood in which the experiment was being carried out. The causes of this potentially hazardous occurrence are discussed in some detail.

Construction and testing of the high-temperature enthalpy calorimeter is in progress.

A. Pyrometallurgical Development

1. Melt Refining

(R. K. Steunenberg, L. Burris, Jr.)

Melt refining will be used to process the irradiated fuel from the first core loading of EBR-II. The metallic fuel pins, composed of approximately 50 percent enriched uranium alloyed with noble metal fission product elements, are clad with stainless steel jackets thermally bonded with sodium. The pins are declad mechanically, chopped to convenient lengths, and charged to a lime-stabilized zirconia crucible, where they are melted and held in the liquid state at 1400 C for a period of 3 to 4 hr. Volatilization and selective oxidation by the crucible result in the removal of about two-thirds of the fission products. The purified metal is cast in an ingot to be used subsequently for the preparation of new pins by injection casting. The mixture of oxides and unpoured metal remaining in the crucible in the form of a skull is recovered by a separate liquid metal process currently being developed. Experimental results are reported on (1) demonstration experiments utilizing about 400 g of highly irradiated EBR-II prototype alloy, (2) the behavior of fission products, and (3) the effect of nitrogen in the argon atmosphere which will be used in the processing cell at the EBR-II plant.

a. High-activity Level Melt Refining Experiments

(V. G. Trice, N. R. Chellew, W. H. Spicer, C. C. Honesty)

The fourth run in a series of laboratory demonstrations on the melt refining process with highly irradiated fuel alloy has been completed. In this series of experiments, short-cooled EBR-II prototype fuel pins containing 10 percent enriched uranium were irradiated in CP-5 or MTR to burnups of 0.22 to 0.75 total atom percent. Approximately 400-g charges of the fuel were then melt refined for periods of 1 to 3 hr at 1400 C in lime-stabilized zirconia crucibles. The purpose of the experiments was to seek confirmation of earlier melt refining results obtained with inactive and low-activity alloys, and to observe any effects peculiar to the high-burnup, short-cooled fuel.

Experimental results from the four experiments are summarized in Table 1. The nearly complete removal of fission products (other than noble metals) observed in previous experiments was confirmed. Some unexpected separation of zirconium from uranium was observed in all the high-activity runs. In prior studies, the addition of several hundred ppm carbon resulted in zirconium removal through carbide slagging. Since pre-irradiation analyses showed only 22 ppm of carbon to be present in this material, the amount of zirconium removed in the high-activity runs cannot be attributed completely to carbide slagging unless it is assumed that an inadvertent addition of carbon occurred during the handling operations prior to melt refining.

Table 1

SUMMARY OF RESULTS OF HIGH-ACTIVITY MELT REFINING EXPERIMENTS

	Experiment No.			
	1	2	3	4
Charge Weight (g)	387.6	392.3	362.5	364.2
Burnup (percent of total atoms)	0.56	0.22	0.74	~1.0
Cooling Time (days)	42	28	14	35
Total Activity (curies/charge)	2500	1100	5600	~4700
Melt Refining Conditions				
Time (hr)	3	3	1	1
Temperature (C)	1400	1400	1400	1400
Yield (percent)				
Active Run	72.4	69.3	52.2	73.6
Reference Run	86.7	84.0	-	84.2
Fission Product Removals (percent) $\left(1 - \frac{\text{Conc ingot}}{\text{Conc charge}}\right) \times 100$				
Rare Earths and Yttrium	99.2+	99.0+	99.0+	99.2+
Tellurium	95.4	95.7	98.9	99 +
Zirconium	9.2	18.2	20.5	11.0
Iodine	99.8	-	99.8	99.8
Cesium	99.5	-	-	a
Barium-Strontium	99.9+	-	-	99.9+
Material Balance (percent)				
Rare Earths and Yttrium — ingot	0.6	0.7	0.5	a
Rare Earths and Yttrium — skull, oxidized	85	75	75	a
Rare Earths and Yttrium — total	86	76	76	a
Tellurium — ingot	3.4	2.8	0.5	a
Tellurium — skull, oxidized	84	83	86	a
Tellurium — total	87	86	86	a
Zirconium — ingot	-	57	42	a
Zirconium — skull, oxidized	-	37	57	a
Zirconium — total	-	94	99	a
Molybdenum — ingot	74	74	-	a
Molybdenum — skull, oxidized	23	26	-	a
Molybdenum — total	97	100	-	a
Cesium — ingot	0.4	-	-	a
Cesium — skull, oxidized	0.02	-	-	a
Cesium — total	0.42	-	-	a
Barium-Strontium[b] — ingot	0.003	-	-	a
Barium-Strontium[b] — skull, oxidized	2	-	-	a
Barium-Strontium[b] — total	2	-	-	a
Iodine — ingot	0.1	-	-	a
Iodine — skull, oxidized	0.09	-	-	a
Iodine — total	0.2	-	-	a

[a] Result not yet available.

[b] Previous experiments with inactive materials indicate that barium and strontium are either retained by the crucible or are volatilized as iodides.

The data on fission product removals are not amenable to kinetic interpretation. It was found, however, that no significant differences in fission product removals could be discerned between 1- and 3-hr liquation periods at 1400 C. It had been shown in earlier studies that cerium removal was dependent upon time, temperature, charge weight, and wetted crucible area, the last representing the surface available for reaction. In the high-activity level experiments, however, the reactive surface was probably increased because of the formation of excessive amounts of uranium dioxide. Therefore, in the high-activity runs, the wetted crucible area is probably considerably less than the total oxide surface area available for reaction.

The material balances presented in Table 1 include only the material found in the ingot and the oxidized skull. (The skull was oxidized to remove it from the crucible and to pulverize it for sampling.) Those fission products which are volatilized or remain in the crucible therefore show incomplete material balances. Noble metal fission products, such as molybdenum, are accounted for in total, since they remain only in the ingot and the metallic portion of the skull. Preferential oxidation of zirconium, relative to uranium, was confirmed, the concentration of zirconium in the oxidized skull being greater than in the corresponding ingot. The incomplete balances for total rare earths, yttrium, and tellurium confirm the earlier results with inactive and low-activity fuel which showed partial penetration of the crucible by these elements. Cesium and iodine appear to have nearly completely volatilized, as anticipated. Attempts are being made to dissolve the melt refining crucible for analysis in order to obtain additional information on the fates of barium, strontium, and other fission products.

Pouring yields in the high-activity level melt refining experiments have been consistently lower than those obtained in reference experiments with unirradiated fuel pins. In Experiments 1 and 2, incomplete pours were obtained on the first attempt, and reheating with application of vacuum was employed in a second pour to obtain the total yields listed. In Experiment 3 no pour was obtained on the first attempt. In all three experiments continuous crusts, presumably of uranium oxide, covered the surface of the melt. The skull produced in Experiment 3 was examined in detail by breaking away the crucible. Throughout its volume, the skull contained a mass of oxide pin-shell fragments which indicated that oxidation of the pins had occurred prior to melting. This observation suggested that the reduced yields obtained with the highly irradiated fuel were resulting from increased oxidation during the handling operations preceding melt refining. It is reasonable to expect that the radiation field and the increased temperature of the pins due to fission product decay heat may produce a more rapid oxidation of the pins by the air atmosphere in the cave facility. The presence of activity may also increase the rate of reaction between the oxidizable materials and the oxygen of the crucible.

Additional precautions were employed in Experiment 4 to minimize air contact with the fuel during the handling operations. The melting assembly was outgassed at about 1000 C for more than 4 hr prior to introducing the assembly into the furnace. The fuel was blanketed with argon wherever possible, and the operations in which air exposure of the fuel was unavoidable were completed as rapidly as possible. The substantial increase in yield over Experiment 3 indicates that these modifications in procedure were effective. Although the yield was still short of that obtained in the reference experiment (73.6 vs. 84.2 percent), the results suggest that further improvement in yield will be possible when air is entirely avoided. Examination of the skull produced in Experiment 4 showed that, although a thin crust formed over the melt, the crust was fragile and ruptured on pouring. The skull also contained a relatively large button of metal which probably would have been poured, had it not been for the dam which was formed by a fragment of the surface crust.

The oxidation and nitridation of unirradiated and highly irradiated fuel pins are being studied in separate experiments to obtain quantitative data. It seems likely, however, that on melt refining in an argon atmosphere and on a 10-kg scale, oxidation and nitridation will not have a major effect on the pouring yield.

b. Transport of Activity in Melt Refining Systems
(N. R. Chellew, V. G. Trice, C. C. Honesty)

A previously reported investigation (ANL-6379, pages 40 to 43) has shown that when the argon atmosphere, which was employed to blanket the fuel during melt refining of highly irradiated EBR-II alloy, was pumped to a gas-storage system the major activity, other than noble gases, retained by components of the system was iodine-131. The basic components of the off-gas storage system were two high-efficiency AEC filters (glass media sheets for efficient filtering of submicron particles) and a vacuum pump compressor unit which was located downstream from the filter chamber and which pumped the furnace-contained gases to storage tanks. The equipment was recently modified to permit direct sampling of the furnace atmosphere by means of previously evacuated Pyrex bulbs.

The distributions of iodine-131 in components of the off-gas storage system in two melt refining experiments with alloy containing macro levels of fission products are compared in Table 2. The relative concentrations of iodine activity in leach solutions of the filter media, and in samples of gas from the storage tank and vacuum pump oil were related to the total amount of this activity in the charged alloy by comparison with analyses of equally irradiated (control) substitute EBR-II alloy. Apparently, no large differences in total accountable iodine concentration in the storage system resulted from variations in total melt time and in the initial iodine concentration of the fuel alloy, which differed by a factor of about three in the two runs.

The transport to the off-gas storage system of only about 0.1 percent of the total charged iodine activity in Experiment No. 3, despite a removal of 99.8 percent of the iodine activity from the ingot during the refining operation (see preceding section), is not in disagreement with previously reported observations[1] which indicated that the iodine during melt refining at high temperatures may primarily evaporate as compounds formed by complex interactions involving elements present in the irradiated alloy and materials used in the melt refining assembly. Minor activities qualitatively identified (because of their low activities relative to iodine-131) in samples of the filter leachings and/or the vacuum pump oil were barium-140, lanthanum-140, ruthenium-106, and cesium-137. The amount of free iodine released from the furnace to the gas stream of the storage system could not be accurately assessed from the present data.

Table 2

DISTRIBUTION OF IODINE-131 IN NOBLE GAS-STORAGE SYSTEM AFTER MELT REFINING HIGHLY IRRADIATED EBR-II TYPE MATERIAL

	Experiment No.	
	2	3
Charge:		
Weight (g)	392.3	362.5
Burnup (total atom percent)	0.22	0.74
Cooling Time (days)	28	14
Calculated Iodine-131 Activity (curies)	64	161
Refining Conditions	3 hr at 1400 C	1 hr at 1400 C
Volume Pumped to Storage (liters):		
Charge Outgassing to ~850 C	122[a]	b
Furnace Pressure Reduction during Refining	7[c]	(step eliminated)
Removal of Melt Atmosphere after Refining	91[d]	105[d]
Iodine-131 Distribution,[e] % of total charged in		
Primary Filter	0.3	0.09
Secondary Filter	0.02	0.002
Vacuum Pump Oil	0.01	0.002
Noble Gas Storage Tank	0.2	0.03
Copper Transfer Lines	(I^{131} present)[f]	(I^{131} present)[f]
Total Accountable	0.53	0.124

[a] Average linear velocity through filters was 1.1 ft/min.

[b] Furnace gases pumped to ventilation system of cave.

[c] Average linear velocity through filters was 0.9 ft/min.

[d] Average linear velocity through filters was 0.45 ft/min.

[e] Analyses by gamma-spectrometric techniques; corrections for decay applied.

[f] Analysis not amenable to quantitative evaluation.

[1] Chellew, N. R., and Ader, M., The Melt Refining of Irradiated Uranium: Application to EBR-II Fast Reactor Fuel. XI. Behavior of Iodine in Melt Refining, Nuclear Sci. and Eng. 9, 82-86 (1961).

In conjunction with one of the melt refining experiments conducted with highly irradiated EBR-II alloy (Exp. 4), the effect of replacement of furnace atmosphere on retention of iodine activity in the gas was followed. At the completion of a melt refining operation carried out for one hour at 1400 C, unfiltered gas samples were taken of the initial argon atmosphere over the melt and of the atmosphere after successive additions of argon or undried air had been made to the furnace. Ingot, skull, and crucible melting assembly were retained in the furnace during the sampling and atmosphere replacement operations. Analyses of the samples (extracted from the furnace in previously evacuated Pyrex bulbs having capacities of approximately 3.5 cc) were by gamma-spectrometric techniques.

The iodine-131 concentrations in the various replacement atmospheres contained at pressures varying between 590 and 740 mm are shown in Table 3. The data show that, with the addition of undried air to the furnace (Step 4) after two argon flushings, the concentration of gaseous iodine in the furnace was increased by a factor of about eight. The release of this activity to the atmosphere is apparently caused by a reaction of the oxygen or water vapor or both in the air with the iodides removed from the ingot during melt refining. This was substantiated by the appreciable reduction in gaseous iodine in the furnace by replacement of the final air atmosphere with argon. Iodine-131 was the only gamma activity, other than that attributable to noble gases, detected in the furnace atmosphere samples.

Table 3

EFFECT OF ATMOSPHERE REPLACEMENT ON IODINE-131 RETAINED IN FURNACE GAS AFTER MELT REFINING EXPERIMENT NO 4

Charge	Composition	uranium-5 weight percent fissium
	Weight	364 2 g
	Burnup	~1 total atom percent
	Cooling Time	35 days
	Refining Conditions	1 hr at 1400 C

	Atmosphere Addition[a]				
Step	Type	Time Retained (hr)	Pressure (mm)	Liters (STP)	Iodine-131 in Furnace[b] (curies x 10^3)
1	Argon (melt atmos)	21 9	590	100	1 8
2	Argon	1 0	720	122	(no sample, noble gas flushing operation)
3	Argon	0 1	740	125	(no sample noble gas flushing operation)
4	Air	23 9	690	117	14 8
5	Air	2 8	735	125	9 5
6	Argon	119 0	715	121	0 3

[a]Greater than 98 percent of the gas which was contained in the furnace was evacuated by pumping prior to each subsequent atmosphere addition

[b]Estimated accuracy of analysis, ±40 percent, activities corrected for decay to time of initial melt atmosphere sample

c. Nitride Formation on Uranium-Fissium Fuel Pins
G. A. Bennett, W. A. Pehl)

Nitridation rates obtained in a separate series of experiments with single uranium-five percent fissium pins have been reported previously (ANL-6287, page 42). A similar experiment has now been carried out on a 2-kg scale. In this experiment, 1988 g of uranium-five percent fissium pins were maintained at 350 C for a period of 24 hr in an atmosphere containing slightly over four percent nitrogen. At the end of this period, the increase in pin weight was determined. The increase in weight was then compared to the increase in weight predicted for these conditions by the data obtained from the series of experiments with single pins. The amount of nitrogen consumed in the 2-kg-scale experiment, as determined from the weight increase, was 6.9 percent greater than that predicted. This difference is of little consequence and is probably attributable to the greater roughness of the surface of the pins (particularly at the sheared pin ends) which were used in the present experiments.

2. Development of Processes Utilizing Liquid Metal Solvents
(R. K. Steunenberg, L. Burris, Jr.)

Liquid metal processes are being developed for the purposes of recovering the fissionable material remaining as a skull in the melt refining crucible and for the isolation of plutonium bred in EBR-II blanket material. Attention is also being given to the processing in liquid metal media of other fuel materials, especially future EBR-II cores, which will contain plutonium as the fissionable material. Work was also continued on the utilization of liquid metal media for the preparation of various actinide element compounds, for example, uranium and plutonium carbides and uranium silicides.

a. Demonstration of Skull Recovery Process
(R. D. Pierce, T. R. Johnson, J. F. Lenc, K. R. Tobias, R. L. Christensen, M. A. Bowden)

The program for demonstration of the process for recovery of uranium from melt refining crucible skulls has been continued. The objectives of these runs are:

1) to demonstrate the feasibility of the process;

2) to investigate the chemistry of the process;

3) to propose and investigate process modification; and

4) to reveal and evaluate problems of equipment design and operation.

Two demonstration runs (Runs 9 and 10) were completed during the quarter in which the process steps shown in Figure 1 were used. These runs differ from those reported in the previous quarterly report (ANL-6379, page 45) only in the first step. Previously, the molten salt-skull oxide slurry was transferred, for further processing, away from the zinc phase containing extracted noble metals, but, as discussed in ANL-6379, this transfer could not be satisfactorily effected. In the new scheme the zinc extract containing the bulk of the noble fission product elements is transferred and disposed of as a waste. Since the salt-skull oxide mixture remains in the crucible, the same crucible is employed for both the noble metal extraction and uranium reduction steps (Steps A and B).

FIGURE 1
SKULL-RECOVERY PROCESS FLOWSHEET

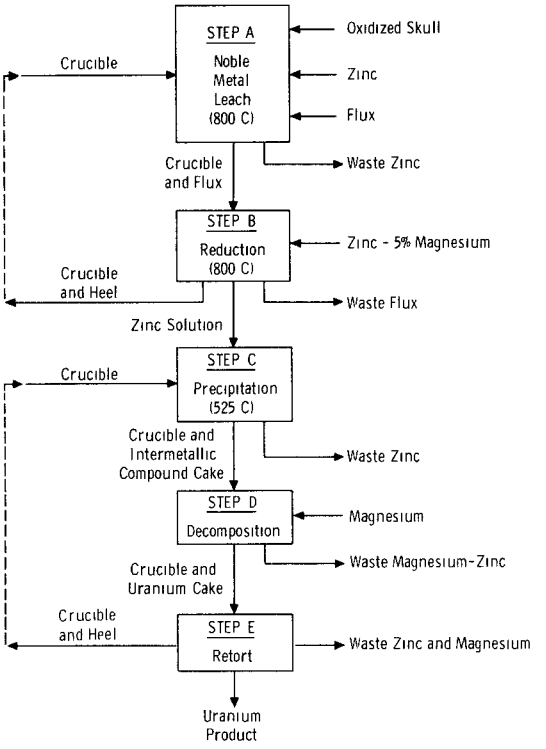

The two new demonstration runs were made to check two features of the changed flowsheet: (1) the success of the noble metal extraction and subsequent transfer operation, and (2) the feasibility of reusing a crucible containing a reduction heel and, therefore, some reduced uranium for the noble metal-extraction step of the succeeding run, i.e., the feasibility of the alternate and repeated use of the same crucible for the noble metal extraction and uranium reduction steps. All steps of the runs were successfully performed; however, as has been experienced before, some of the product stuck to the tantalum retorting crucibles. The use of beryllia crucibles, discussed in this report on page 49, appears to be a solution to this problem of sticking.

In the first of the two runs, Run 9, ruthenium-103 tracer was added to the oxidized skull charge to aid in ruthenium analysis. The molten zinc containing extracted noble metals was readily transferred away from the solidified salt phase by pressure siphoning. The removal of both ruthenium and molybdenum was over 70 percent. This value is in agreement with previous experience and appears to be a practical limit for the extraction of these elements from the salt suspension of the oxidized skull. This limitation may be a consequence of the slow diffusion of these elements from the large particles of skull oxide. Although the removal of ruthenium and molybdenum is believed adequate, better extraction could be achieved if the proportion of large particles in skull oxides could be reduced. (A particle size distribution of fission skull oxide is given in Figure 2, page 44). The ruthenium that was not removed in the noble metal-extraction step followed uranium through the balance of the process, apparently coprecipitating in both precipitation steps. The molybdenum removal improved during subsequent steps and principally during the reduction step. The improved removal during the reduction is undoubtedly brought about by the low solubility of molybdenum (~0.02 percent) in the magnesium-zinc reducing solution.

The crucible used in the noble metal leach for the second run, Run 10, contained the heel from the reduction step of Run 8 (reported in ANL-6379, page 45). The dissolved uranium in such heels must be reoxidized to prevent loss in the waste zinc from the noble metal leach. Less than 0.2 percent of the uranium was lost in the zinc waste stream from the noble metal extraction step (step A). Therefore, this run demonstrated that the oxidizing agents, such as the noble metal oxides, rare earth oxides, and U_3O_8, present in the fresh charge of skull oxide were capable of oxidizing completely the uranium present in the heel solution. If necessary, however, an oxidizing agent, such as zinc chloride, could be added.

The decontamination of uranium was typical of other demonstration runs and is presented in Table 4. The uranium loss in the zinc waste stream from the intermetallic compound precipitation step (step C) was excessively high. Although only about 2 percent of the original uranium was in solution, 7 percent transferred. Normally, the physical carryover of solids in this step is low, about 10 percent of that in solution.

A previous observation suggests an explanation for these results. Phase separations which have been attempted after precipitating intermetallic compounds of zinc and uranium from solutions containing 5 and 10 percent magnesium have exhibited a striking difference. The intermetallic compound suspended almost quantitatively in the 10 percent magnesium solutions and essentially not at all in 5 percent solutions.

Table 4

COMPOSITION OF RECOVERED PRODUCT

(Skull-recovery Demonstration Run D-10)

Element	Charge: Skull Oxide (Oxygen-free Basis) (Percent)	Product[a] (Oxygen-free Basis) (Percent)	Percent of Element Charged to Step A Found in Product
Uranium	91.0	97.5	63
Cerium	3.2	0.26	4.9
Zirconium	1.23	0.15	7.7
Ruthenium	1.69	0.38	14
Molybdenum	2.24	0.31	8.3
Palladium	0.18	$<5(10^{-4})$	<0.02
Magnesium	None	0.67	-

[a]Product oxidized completely to permit sampling.

Recent data[2] for the zinc-uranium-magnesium ternary system suggest that this difference is a result of the precipitation of different intermetallic phases, the delta and epsilon phases. Although a 5 weight percent magnesium-zinc solution was used in Run 10, it is believed that conditions encountered in the intermetallic compound precipitation step resulted in the production of some delta phase which, unlike the usual epsilon phase, suspended and transferred with the waste solution.

A drybox has been obtained and is being readied for use in future demonstration runs. The box will be filled with argon, which will be recirculated through a purification train. The drybox is expected to eliminate problems of charging and unloading hygroscopic salts and pyrophoric metals.

Particle Size Distribution of Skull Oxides

(R. D. Pierce, K. R. Tobias)

A particle size distribution of a blend of skull oxides from the oxidation of thirteen skulls, which extends the distribution into the sub-sieve range, is shown in Figure 2. This distribution was obtained in order to assess the dusting problem created by the fine particles. As Figure 2 indicates, less than 1 percent of the particles were smaller than 10μ in size. The smallest particle found was one micron in diameter.

[2]Martin, A., private communication.

FIGURE 2
PARTICLE SIZE DISTRIBUTION OF FISSIUM SKULL OXIDE

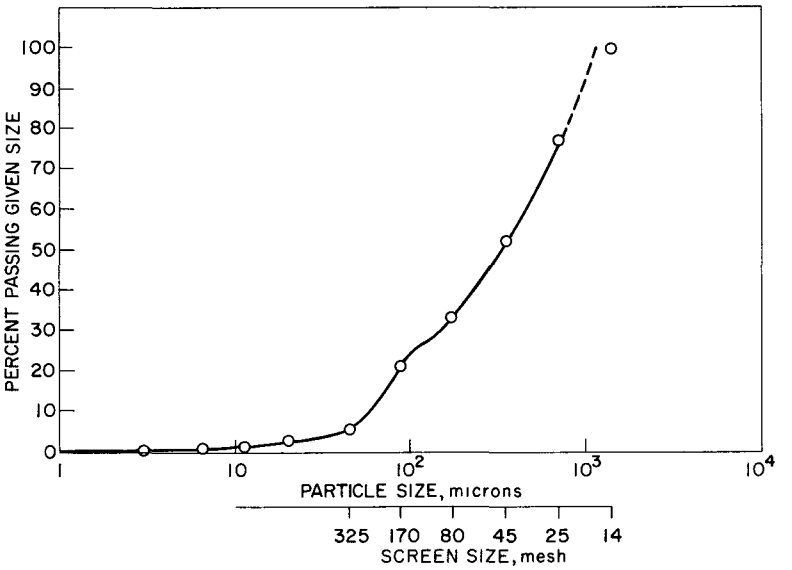

b. Pyrometallurgical Reduction Studies

(1) Reduction of U_3O_8 by Zinc-Magnesium Alloys
(J. B Knighton, J. R. Pavlik, H. E. Griffin)

One of the steps under consideration in the processing of oxidized melt refining skulls involves the reduction of a uranium-fissium oxide mixture to produce a final alloy containing about 10 weight percent uranium and 12 weight percent magnesium in zinc. At this magnesium concentration, the high solubility of uranium would permit a relatively low volume of liquid metal solution in the process. Experience with laboratory reduction studies and process demonstration experiments, however, has shown that the rates of the reduction reaction vary erratically under these conditions. Since easily reproducible behavior is considered essential in process application, additional studies have been made to determine whether an increase in the amount of flux used in the reaction would overcome the difficulty of erratic behavior.

Two reductions were performed in which the quantity of flux was varied. A calcium chloride-magnesium chloride-magnesium fluoride flux (47.5, 47.5, and 5 mole percent, respectively) was used in these experiments. In order to deal with a simpler system, U_3O_8 was substituted for the uranium-fissium oxide mixture. The results of these experiments, shown in Figure 3, indicate that increasing the quantity of flux has a beneficial effect upon the rate of reduction. In Run B, where a flux-to-metal weight ratio of one was used, the reduction was very rapid, reaching a plateau in 30 min, whereas in Run A with a flux-to-metal ratio of 2 the rate was considerably slower.

FIGURE 3
REDUCTION OF U_3O_8 TO PRODUCE 10 WEIGHT PERCENT URANIUM-12 WEIGHT PERCENT MAGNESIUM-ZINC ALLOY

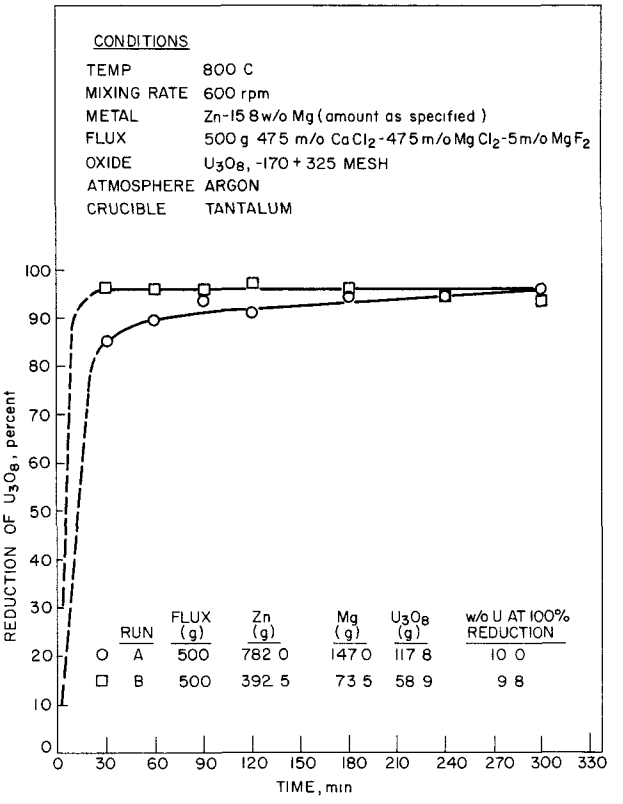

It appears that increasing the quantity of flux may eliminate the erratic reduction rates observed in this system. A more serious problem is the fact that the extent of reduction was limited to 96 or 97 percent in both experiments. Suspicion that the uranium content of the U_3O_8 was in error was removed by additional analyses. These results imply that under certain conditions the reduction reaction may be limited by a chemical equilibrium. This possibility is being explored more fully.

(2) Effect of Flux Volume on the Reduction of U_3O_8
(J. B. Knighton, J. D. Schilb, H. E. Griffin)

The effect of variations in the amount of flux on the reduction of U_3O_8 by zinc-five weight percent magnesium solution has been investigated. The flux used in the experiments had the following composition: 47.5 mole percent calcium chloride, 47.5 mole percent magnesium chloride, and 5 mole percent magnesium fluoride. The experimental results are shown in Figure 4, where the percent reduction is plotted as a function of byproduct magnesium oxide "concentration" or "loading" in the flux. (Since the magnesium oxide has a low solubility in the flux, it is suspended as a solid; thus the amount per unit volume of flux cannot properly be termed a concentration.) The magnesium oxide loading in the

flux is a value calculated from the decrease of magnesium concentration in the metal phase. It does not include magnesium and calcium oxide or oxychlorides which may be present as impurities in the original flux components.

FIGURE 4
EFFECT OF MAGNESIUM OXIDE LOADING IN FLUX ON U_3O_8 REDUCTION

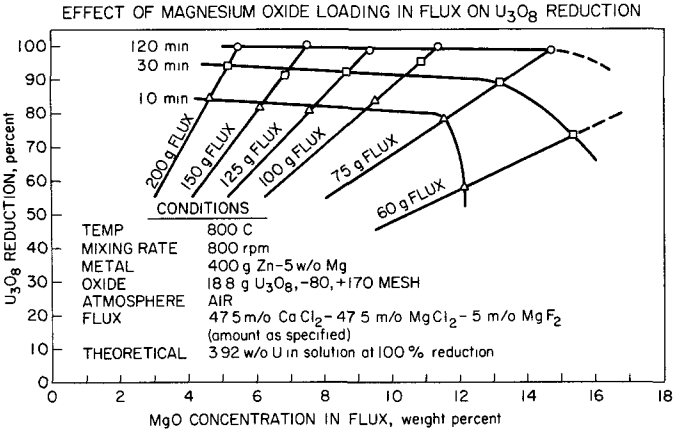

The following conclusions can be reached on the basis of the results obtained:

(a) Within the range of experimental conditions (see Figure 4), the reduction rate increases as the amount of flux is increased.

(b) The loss of uranium to the flux decreases as the amount of flux is increased.

(c) The reduction rate falls off markedly at magnesium oxide loadings in the flux exceeding about 11 weight percent. (This value, however, does not take into account the possibility of magnesium and calcium oxide impurities which may be present.)

In these experiments, the final magnesium concentrations in the metal phase ranged from 3.0 to 3.2 weight percent.

It should be noted that high percentages of reduction of uranium oxides (approaching 100 percent) have been obtained consistently with 5 weight percent magnesium-zinc solutions in which the final concentration of uranium is about 5 percent. It is suspected that the lower percentage of reduction (about 96 percent) obtained in the preceding study is related to the higher uranium concentration (about 10 percent) in the final solution.

(3) Reduction of Zirconia from a Melt Refining Crucible (J. B. Knighton, J. R. Pavlik)

In the oxidation step of the melt refining skull-recovery process, some small fragments of the zirconia crucible are introduced into

the skull oxide product. These generally amount to about one percent by weight of the oxide produced. It is therefore necessary to determine the extent to which this material is reduced to zirconium metal in the oxide-reduction step of the process.

Two reduction experiments with zirconia crucible fragments have been performed in zinc solutions containing 5 and 12 weight percent magnesium. The results of these experiments, shown in Figure 5, indicate effectively complete reduction by the 12 percent magnesium solution and 83 percent reduction by the 5 percent solution in 5 hr at 800 C.

FIGURE 5
REDUCTION OF CRUCIBLE ZIRCONIA

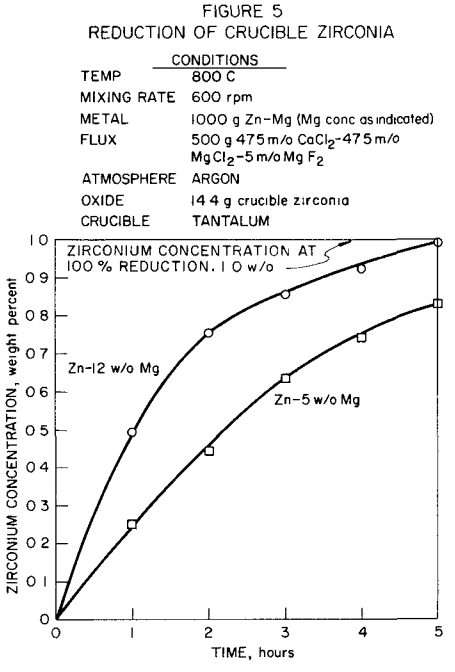

Previously reported work (see ANL-6333, page 60) indicated that a much smaller percentage of zirconia was reduced (about 4 percent in 8 hr) in comparable reducing systems, i.e., systems employing about 5 weight percent magnesium-zinc solutions. It is believed that the difference in results may be related to differences in physical properties of the zirconia that was used in the two studies. It is not certain, however, that this is the only factor which contributed to the divergence of the results.

Although the reduction rate of the crucible material is lower at the lower magnesium concentration, it is still sufficient to require consideration in the skull-recovery flowsheet. The zirconia reductions that were obtained are very likely more extensive than those that would occur under process conditions because (1) much shorter times are required for complete reduction of the uranium oxides under process conditions, and (2) the zirconium oxide appears to be stabilized through the formation of compounds with cerium oxide when the latter is present.

It is of interest to note that this reaction may represent a potential method for the production of zirconium metal directly from the oxide.

(4) Reduction of Thorium Oxide by Zinc-Magnesium Alloys
(J. B. Knighton, H. E. Griffin)

Although the reduction of thorium oxide to the metal is not related directly to EBR-II fuel processing, it is of chemical interest and may represent a potential extension of pyrochemical processing to thorium reactor fuels.

Complete reductions of thorium oxide were described in the preceding quarterly report (ANL-6379, page 59). This work is being extended to include a study of the effect of magnesium ion concentration in the flux on the reduction. Preliminary results of this investigation, shown in Figure 6, indicate that a minimum of about 30 mole percent concentration of magnesium cations in the flux is required to produce rapid, complete reductions by zinc-5 weight percent magnesium alloy in 2 hr at 750 C.

FIGURE 6
EFFECT OF MAGNESIUM CATION ON REDUCTION OF ThO_2
BY ZINC-MAGNESIUM-MOLTEN FLUX SYSTEMS

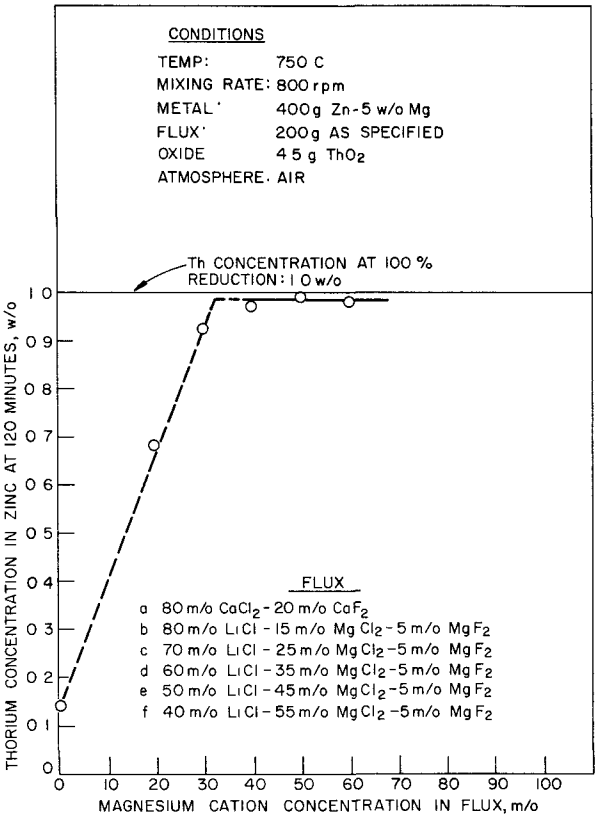

c. Retorting of Uranium Concentrates
(J. F. Lenc, M. A. Bowden)

Isolation of the uranium precipitated in the decomposition step of the proposed skull-reclamation process (see ANL-6379, Figure 5, page 46) requires a final retorting step to remove the associated zinc and magnesium. The retorted uranium product should be readily recoverable in a form suitable for remote handling. In addition, the product should be sufficiently free of any impurities that would inhibit its liquation with other fuel material upon recycle to the melt refining operation.

During the past quarter, pressed-and-sintered beryllia crucibles (4-in. OD by 9 in. high) were investigated for the retorting operation. Previously, tantalum crucibles had been employed, but the yield of readily removable uranium agglomerates (70 to 80 percent) was lower than that desired for process application. Yields of over 90 percent have resulted in seven experiments conducted to date in beryllia crucibles. The yields have increased with experience and improvements in the quality of the beryllia crucibles so that yields of over 98 percent have been realized in the last four runs (see Table 5). These latter yields were achieved in one beryllia crucible which has been successfully reused four times with no signs of failure evident. Ability to reuse this crucible is attributed to its high density (about 90 percent of the theoretical density of 3.025 g/cc) and to improved techniques used by the manufacturer for its fabrication. Further manufacturing improvements are being explored (e.g., better control of particle size, mold condition, and closer inspection).

Table 5

YIELD OF URANIUM AGGLOMERATES IN THREE-STEP[a] RETORTING EXPERIMENTS IN BERYLLIA CRUCIBLES

Scale: 150 g uranium
Crucible: 4-in OD x 9 in. high; volume: about 1150 cc.

Crucible No	Run No	Uranium Agglomerates - Percent of Total Retorted Product Easily Recovered	Condition of Beryllia Crucible after Run
1[b]	R-12	90.6	Side wall cracked circumferentially at plane coincident with liquid metal level.
2[b]	R-13	99.2	About 1 sq in. of inside surface broke away from crucible
3[c]	R-14	93.1	Porous area in crucible bottom and linear crack in side wall. Some leakage of liquid metal solution
4[c]	R-15	98.8	Crucible bottom discolored but not porous. No leakage of liquid metal solution.
4[c]	R-16	99.3	No change after second use
4[c]	R-17	98.1	No change after third use
4[c]	R-18	99.0	No change after fourth use

[a]The three steps are the last three steps of the skull-reclamation process, namely, (1) precipitation of the uranium-zinc intermetallic compound followed by removal of supernatant liquid metal, (2) decomposition of this compound with magnesium to precipitate the uranium which is again followed by removal of the supernatant liquid, and (3) final retorting to distill off the residual zinc and magnesium.

[b]Formed by cold tamping and firing to about 66 percent theoretical density.

[c]Formed by isostatically pressing and firing to about 90 percent theoretical density

The same "three-step" experimental procedure that was used previously to evaluate tantalum crucibles (ANL-6379, page 62) was employed in the current tests conducted in beryllia crucibles. In this procedure, the same crucible is used in the last three steps of the skull-reclamation process, namely, (1) precipitation of the uranium-zinc intermetallic compound followed by removal of the supernatant liquid metal, (2) decomposition of the intermetallic compound with magnesium to precipitate the uranium which is again followed by removal of the supernatant solution, and (3) final retorting of the precipitated uranium to distill off residual zinc and magnesium.

Thus far, four high-purity beryllia crucibles obtained from the Brush Beryllium Company have been tested. The first two crucibles (Nos. 1 and 2) were fabricated by cold tamping and firing beryllia powder to about 66 percent theoretical density. Subsequently, two crucibles (Nos. 3 and 4) were obtained which were formed by isostatically pressing and firing beryllia powder to approximately 90 percent theoretical density.

Crucible No. 1 remained intact through the three steps of one experiment before cracking. Results of this test were reported in ANL-6379, page 63, and Figure 14, page 64. Crucible No. 2 was also intact after one run except for the inner surface where an irregular-shaped piece of beryllia (about 1 sq in. in area) broke away from the side wall. The low density resulting from the tamping method of crucible fabrication is believed responsible for this spalling effect. Because of this condition, no attempt was made to reuse the crucible.

Some leakage of the melt through the crucible bottom was noted at the completion of the first step (intermetallic precipitation) of an experiment conducted in crucible No. 3, a high-density, isostatically pressed crucible. In addition, a horizontal crack developed in the side wall. However, the crucible remained sufficiently intact so that it was possible to complete the decomposition and retorting steps of the experiment. A possible explanation for the failure of this crucible, as suggested by the vendor, is the use of relatively coarse beryllia powder combined with mold imperfections in the forming process.

In contrast with the results experienced with the first three beryllia crucibles tested, the fourth crucible (see Figure 7) has been used in four "three-step" experiments without any evidence of deterioration, save for a small discolored area in the crucible bottom. This discoloration is attributed to the presence of impurities in the beryllia which were introduced either during fabrication or usage.

In all of the above tests, the major portion (90 to 99 percent) of the retorted uranium dumped free of the crucible in agglomerate form. The remainder of the product deposited on the side wall in the form of a thin ring. Recovery of this latter material by recycling it with the crucible appears feasible.

Figure 7

ISOSTATICALLY PRESSED BERYLLIA CRUCIBLE AFTER FOUR SUCCESSIVE RETORTING RUNS

(See procedure on page 50. Crucible size: 4 in. OD by 9 in. high. Note discolored area near bottom.)

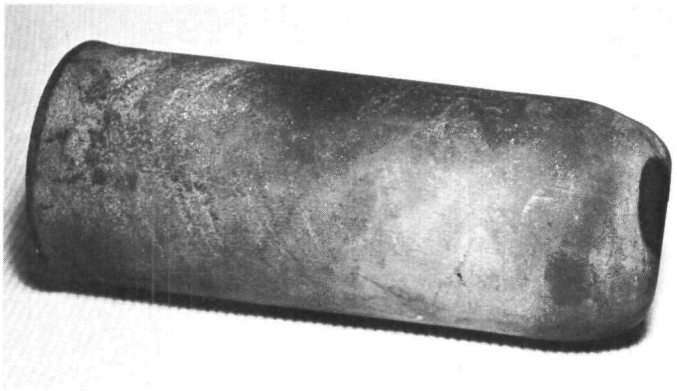

Alternative Retorting Procedures

Figure 8 shows a typical agglomerate of precipitated uranium enveloped in a zinc-magnesium matrix which dumped free from a beryllia crucible after the magnesium decomposition step of the skull-reclamation process. Tests are being made to determine whether the residual zinc and magnesium can be boiled away from the uranium at atmospheric pressure without significant uranium losses due to entrainment. If these tests are successful, two alternative simplifications to the skull-reclamation process may be possible. One simplification would be the elimination of the retorting step by adding the uranium agglomerate directly to the melt refining step; the zinc and magnesium would be removed by vaporization at atmospheric pressure and the uranium liquated with other fuel material. This process modification would depend upon the ready removal of the precipitated uranium agglomerates from the decomposition crucible after the decomposition step.

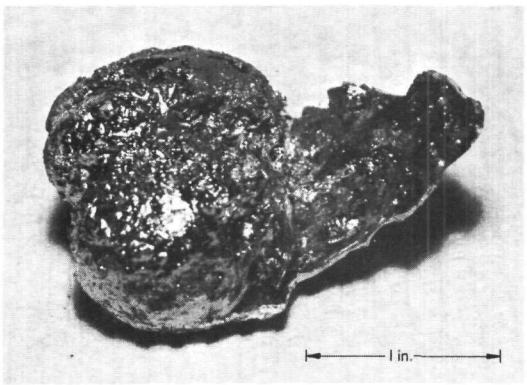

Figure 8

APPEARANCE OF URANIUM AGGLOMERATE COATED WITH MAGNESIUM-ZINC SYSTEM AFTER MAGNESIUM DECOMPOSITION STEP

If these agglomerates are not readily removable, an alternative simplification may be to retort at near atmospheric pressure in the beryllia crucible. This would eliminate the need for tight closures so that the design of remotely operated retorting equipment would be simplified.

d. Development of Alternative Processing Procedures

(1) Direct Dissolution of Canned EBR-II Fuel Pins (R. D. Pierce, K. R. Tobias, R. L. Christensen)

Three survey runs were made to investigate a possible method for treating EBR-II pins directly by the proposed skull-recovery process. This treatment could be valuable for pins which are too badly distorted for decanning or otherwise cannot be handled by decanning and melt refining. Fissium pins and stainless steel were dissolved in a zinc-fused flux mixture which contained zinc chloride as an oxidant. The intention of this step was to dissolve the stainless steel in the zinc, oxidize the uranium to the trichloride with the zinc chloride, and extract the uranium trichloride into the flux, while leaving the relatively noble stainless steel constituents in the zinc phase.

The charge data and results of three runs are summarized in Table 6. Dissolution was slow at 500 C in Run SD-123.

Table 6

DIRECT DISSOLUTION OF SIMULATED EBR-II FUEL PINS IN FLUX-ZINC SYSTEM USING CHLORIDE OXIDANT

Charge: 70 g fissium pins
10 g 304 stainless steel
1700 g zinc
500 g flux[a]. 42 mole % $MgCl_2$, 25 mole % NaCl, 17 mole % KCl, 4 5 mole % MgF_2 and 11 5 mole % $ZnCl_2$

Crucible: Unbaffled quartz, $3\frac{3}{4}$-in ID

Agitation: Runs SD-119 and SD-123, $1\frac{3}{4}$-in x $\frac{7}{8}$-in Ta paddle at 100 to 180 rpm
Run SD-124, $2\frac{3}{4}$-in x 1-in W paddle at 100 rpm

Run No	Constituent	Temp (C)	Percent in Flux after $10\frac{1}{2}$ hr	Percent in Zinc after $\frac{1}{4}$ hr	1 hr	3 hr	7 hr	$10\frac{1}{2}$ hr
SD-123	Uranium	500		-	2 2	0 7		
	Nickel			9 5	17	25		
SD-119	Uranium	600	~100[b]	0 9				0 24
	Iron		0 45[b]	-				99+[c]
	Chromium		16[b]	81 5				83 5
	Nickel		2 1[b]	~100				~100
SD-124	Uranium	500 to 600[d]					0 25	
	Iron						~100	
	Chromium						80	
	Nickel				14		~100	

[a] Freezing range of flux was found to be 470 to 445 C

[b] Entire salt phase dissolved for analysis

[c] Since the zinc was saturated with iron, this number was obtained by difference

[d] See heating pattern in Figure 9

At the end of the run (3-hr duration), the dissolution was incomplete but still progressing. At 600 C in Run SD-119 dissolution rates were rapid. The pattern of dissolution of the stainless steel, based on nickel analyses, in Run SD-124, in which the temperature was gradually increased from 500 to 600 C, is shown in Figure 9.

FIGURE 9
DISSOLUTION OF STAINLESS STEEL OF SIMULATED EBR II FUEL PINS IN FLUX-ZINC SYSTEM

(Run SD-124, see conditions in Table 6 Nickel analysis was used as representative of stainless steel dissolution)

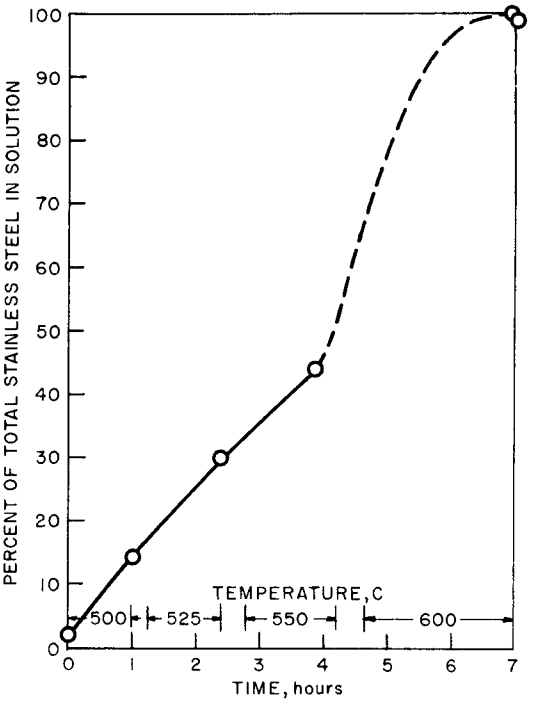

The distribution of the elements was largely as expected and, therefore, very encouraging. Uranium appeared nearly completely in the flux phase within a relatively short period of time at 600 C, and only about 0.25 percent remained behind in the zinc phase. Nearly all of the iron and nickel remained in the zinc phase, thus making possible a good separation of these elements from uranium. Chromium, however, distributed partially into the flux phase (15 to 20 percent). The separation of chromium from uranium should almost certainly be improved by proper reduction of the zinc chloride concentration.

The tantalum agitators used in Runs SD-119 and SD-123 were badly corroded, but the tungsten agitator used in Run SD-124 appeared to be unaffected by exposure to the flux-metal system. The quartz crucibles were not attacked but did crack on cooling.

(2) Chlorination of Uranium-Fissium Oxide in Molten Salt Media
(J. P. LaPlante, D. A. Wenz, H. E. Griffin)

The chlorination of uranium-fissium oxide mixtures to form compounds soluble in molten halides has received some consideration as a potential modification of the skull-recovery process by melt refining. The possible advantages of such a scheme lie mainly in the elimination of insoluble uranium and magnesium oxide-molten salt slurries through conversion of these compounds to chlorides which are soluble in chloride melts.

Chlorine, phosgene, and aluminum chloride have been used for the chlorination of uranium oxides.[3-5] Ferric chloride has also been mentioned as a catalyst.[4] In the present work a two- to three-fold excess of a carbon monoxide-chlorine mixture (2:1) was passed through 200 g of a halide flux containing about 20 g of uranium-fissium oxide in suspension. The system was agitated and maintained at a temperature of 800 to 850 C. During the course of the chlorination, filtered flux samples were taken periodically in Vycor tubes fitted with graphite filters. It was assumed that the elements not present as soluble species in the flux samples had not been chlorinated or had been removed from the system as volatile chlorides. The percentages of various elements found in the flux samples are listed in Table 7 for various chlorination times and flux compositions.

The first two experiments were identical, except for a quartz stirrer used in Experiment 1 and a tantalum stirrer in Experiment 2. The quartz was only slightly etched by the melt, whereas the tantalum suffered severe attack. It appears that the presence of tantalum decreases the percentage of soluble uranium, but increases somewhat the amount of cerium in solution. Throughout the experiments substantial amounts of zirconium, molybdenum, and ruthenium were removed from the system, presumably through the formation of volatile chlorides.[6] In Experiment 3 the presence of ferric chloride (formed by adding iron to the melt) resulted in a significant increase in the chlorination rate of uranium oxide. Addition of zinc chloride to the flux (Experiment 4) also increased the chlorination rates of uranium, molybdenum, palladium, zirconium, and ruthenium, but volatilization of ruthenium chloride appears to have been inhibited.

---

[3]Lyon, W. L., and Voiland, E. E., The Preparation of Uranium Dioxide from a Molten Salt Solution of Uranyl Chloride, HW-62431 (1959).

[4]Gibson, A. R., Buddery, J. H., and Harrison, K. T., British Patent No. 843,261 (1960).

[5]Blomgren, G. E., and Van Artsdalen, E. R., Ann. Rev. Phys. Chem. 11, 273 (1960).

[6]Bradley, D., The Preparation and Properties of the Chlorides of Uranium, Plutonium, Thorium and of the Fission Product Chlorides, AERE-C/R-2215 (1957).

Table 7

CHLORINATION OF URANIUM-FISSIUM OXIDE IN MOLTEN CHLORIDE MEDIA

Oxide	20 g uranium-fissium oxide reconstituted from screen fractions in original proportions
Flux	200 g, composition as indicated
Chlorinating Agent	CO-Cl_2 2 1 ratio 2-3 times the stoichiometric requirement
Temperature	800 to 850 C
Stirring	640 rpm
Materials	Vycor sample tubes, porcelain thermocouple well alumina crucible, tantalum or quartz stirrer

Experiment		1	2[a]	3	4	5	6
Flux		NaCl-KCl (50, 50 m/o)	NaCl-KCl (50, 50 m/o)	NaCl-KCl + 10 g Fe (50, 50 m/o)	NaCl-KCl-$ZnCl_2$ (47 5 47 5, 5 0 m/o)	LiCl-$MgCl_2$-MgF (47 5, 47 5, 5 0 m/o)	LiCl-$BaCl_2$-MgF_2 (47 5 47 5 5 0 m/o)
Time (min)	Element	Percentage of element originally present found in filtered flux sample					
30	U	72	75	96	100	7	4
	Mo	68	31	61	16	100	74
	Pd	-	48	59	67	89	73
	Ce	22	100	29	30	38	-
	Zr	-	2	<0 6	6	<1 0	<1 1
	Ru	-	<0 5	<0 6	<0 2	<0 6	-
60	U	102	73	-	100	7	-
	Mo	< 1	1 4	-	0 1	93	-
	Pd	-	43	-	69	71	-
	Ce	43	-	-	25	33	-
	Zr	6	6	-	21	<0 6	-
	Ru	75	<9	-	100	<0 3	-
90	U	99	62	94	-	7	-
	Mo	<0 5	0 2	52	-	72	-
	Pd	-	39	59	-	51	-
	Ce	43	61	34	-	34	-
	Zr	-	3	<3	-	<0 6	-
	Ru	56	<4	3	-	<0 4	-
120	U	100	57	-	-	6	-
	Mo	<0 5	0 1	-	-	77	-
	Pd	-	38	-	-	35	-
	Ce	47	89	-	-	28	-
	Zr	7	4	-	-	<0 6	-
	Ru	38	<0 3	-	-	-	-
180	U	-	-	-	100	-	100
	Mo	-	-	-	<0 5	-	1 3
	Pd	-	-	-	67	-	59
	Ce	-	-	-	26	-	51
	Zr	-	-	-	19	-	5
	Ru	-	-	-	96	-	79

[a]Tantalum stirrer

Uranium oxide chlorination was relatively ineffectual in a lithium chloride-magnesium chloride-magnesium fluoride flux (Experiment 5), while the chlorination of cerium appeared to proceed at about the same rate as in the other fluxes. In the lithium chloride-barium chloride-magnesium fluoride flux used in Experiment 6, the uranium oxide was chlorinated slowly, but completely after 3 hr.

The effects of magnesium fluoride and lithium chloride on the chlorination rate of uranium oxide were studied briefly in a separate set of experiments. The results are shown in Figure 10. Increasing the magnesium fluoride concentration in the flux and substituting lithium chloride for potassium chloride both decreased the rate of uranium oxide chlorination.

FIGURE 10
CHLORINATION OF URANIUM OXIDE

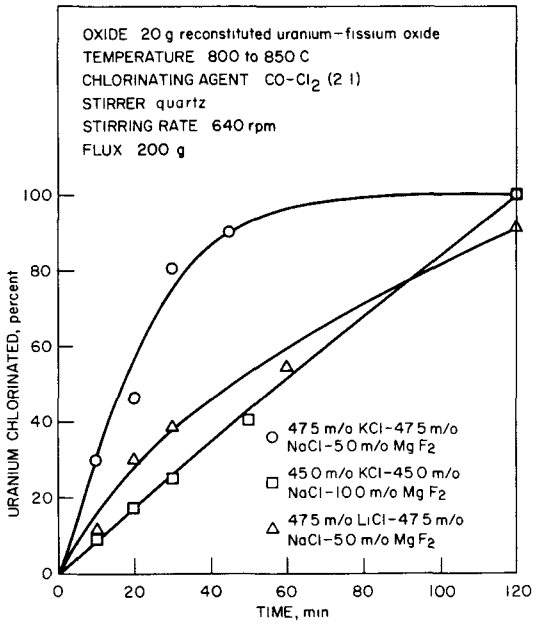

It is interesting to note that the chlorination rates of uranium oxides as a function of flux composition show the same type of periodic variation as that observed in the reduction of uranium oxides by zinc-magnesium alloy, but in reverse order (see ANL-6287, page 53). The rates of reduction decrease while the rate of chlorination increases as the atomic radii of the Group I and II cations in the flux are increased. Similarly, increasing the fluoride ion concentration enhances the reduction rate, but decreases the chlorination rate.

No further work on the chlorination procedure is being planned. The fact that the procedure apparently offers no significant advantage over the method in which uranium oxides are reduced directly is the main reason for the discontinuance of work in this area.

e. Development of Process for Recovery of Plutonium from EBR-II Blanket Material
(I. O. Winsch, T. F. Cannon)

Plutonium will be generated in the depleted uranium blanket material of the EBR-II reactor to a concentration of about one percent before the blanket material is discharged for processing. The blanket processes under investigation for the separation of plutonium from uranium by pyrometallurgical methods are based on the solubility of plutonium in magnesium-rich zinc alloys and the contrasting low solubility of uranium in these alloys.

Additional work was completed in the past quarter on a procedure in which uranium blanket material is dissolved in a 12 to 15 weight percent magnesium-zinc alloy at 800 C to give about a 14 weight percent uranium solution. On addition of magnesium to a 50 percent concentration, uranium precipitates from solution while the plutonium remains in solution. The uranium solubility in the supernatant phase is decreased by cooling to 400 C prior to removal of the plutonium-bearing supernatant phase. Isolation of the plutonium from the supernatant phase will be accomplished by distilling away the magnesium and zinc.

(1) Process Demonstration

A second process demonstration run has been completed in which the procedure outlined above was followed. About 400 g of a uranium-1 weight percent plutonium alloy in the form of $\frac{1}{2}$-in. diameter by 3-in. rods was used as charge material. All operations were conducted in helium atmospheres with tantalum vessels and tantalum auxiliaries (agitators, baffles, and thermocouple wells). Results have been summarized for each step in Table 8.

Table 8

SUMMARY OF BLANKET PROCESS DEMONSTRATION RUN NO 2

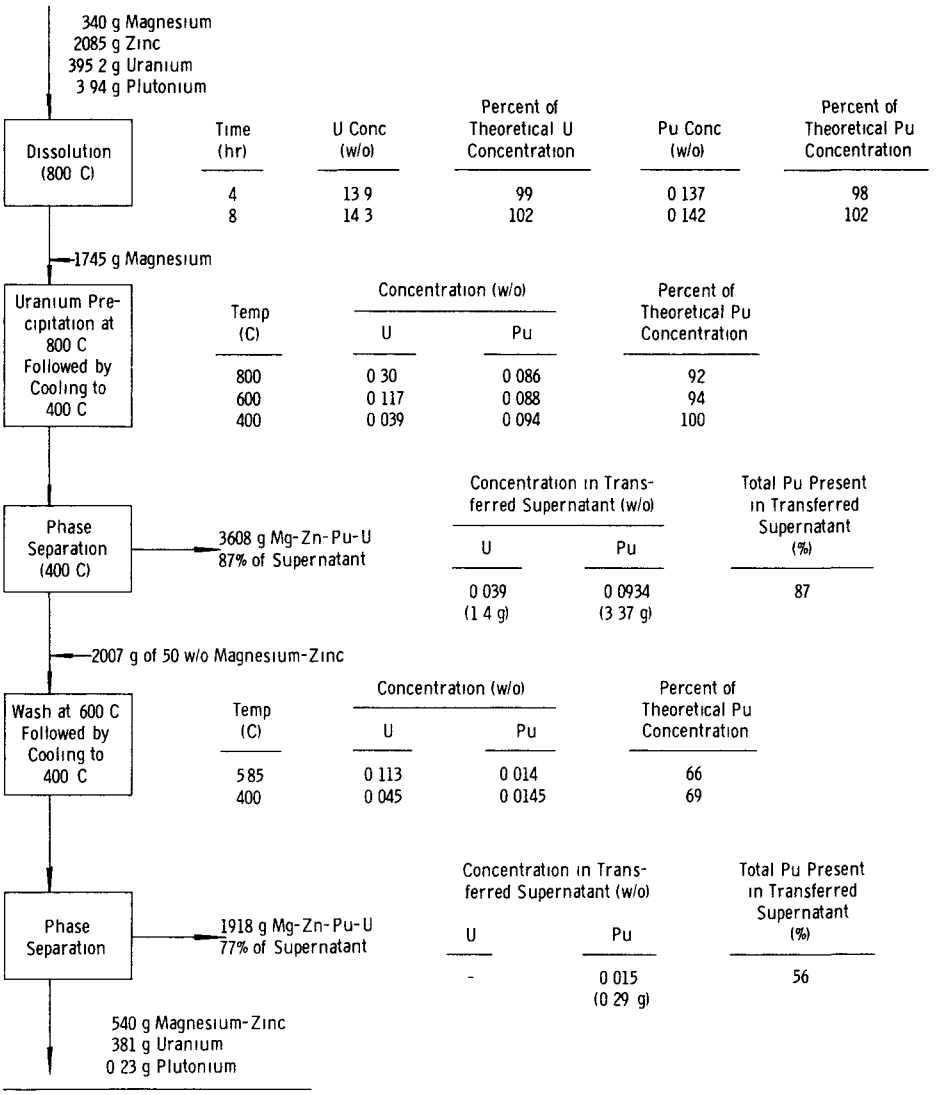

The total plutonium separated in the supernatant solutions was 3 66 g of possible 3 88 g (excludes amount removed in samples) or 95 percent of that available The uranium content is known only for the initial supernatant solution in which a total of 1 4 g was found For this solution a plutonium separation factor of 241 was realized Because of inadvertent contamination of the wash solution with uranium the uranium content of the wash solution remains unknown Extrapolating the performance of the first phase separation would give a uranium content of 0 77 g and would give an overall separation factor of 169

Analyses of solution samples showed essentially complete dissolution after 4 hr. Concentrations of uranium and plutonium remained stable (in fact, increased slightly) during an additional 4 hr allowed for the dissolution. These observations duplicate those of the first run (ANL-6379, page 75) and indicate that the dissolution step should be a straight-forward operation.

On addition of magnesium to the solution to a 50 percent concentration and during subsequent cooling from 800 to 400 C, the uranium concentration decreased from 0.3 percent at 800 C to 0.039 percent at 400 C. The plutonium concentration simultaneously increased from 92 percent to 100 percent of the theoretical value. Failure to realize theoretical plutonium concentrations immediately at 800 C can perhaps be attributed to entrapment of plutonium within the precipitated uranium and the subsequent release of the trapped plutonium upon stirring the mixture during the long cooling period. A similar behavior was noted in the first run except that the uranium concentration decreased further on cooling (to 0.025 percent at 440 C). Good plutonium recovery and separation from uranium in this step are indicated in both runs.

The 87 percent phase separation obtained in this run represents an improvement over the 70 percent separation realized in the first run. The separated plutonium-bearing phase was subsequently reheated to 800 C and sampled to determine the extent of physical carryover of uranium. The concentration of uranium was 0.039 percent which indicates that essentially no physical carryover of uranium occurred.

In the subsequent wash step, carried out at 600 C with a 50 percent magnesium-zinc solution, followed by cooling to 400 C prior to phase separation, an additional 8.0 percent of the plutonium was recovered, which brought the total plutonium recovered to 95 percent. However, the amount of plutonium appearing in solution was only about 70 percent of the available amount. While this is not a serious loss (and would not be a loss if the blanket material were reused), it indicates that a problem may exist at this point. This finding is contradictory to that of the first run in which 98.5 percent of the available plutonium at this point was found in the wash solution. One possible explanation for the failure to realize a theoretical plutonium concentration in the wash solution is the precipitation of the plutonium by impurities introduced with the wash alloy.

Because of inadvertent contamination of the wash solution with uranium, it became impossible to determine the physical carryover of uranium in this step.

In summary, 95 percent of the plutonium was recovered from the initial 1 percent plutonium-uranium alloy. Because the uranium content of the wash solution could not be determined, it is not possible to

give an overall plutonium-uranium separation factor (plutonium-uranium ratio in product divided by plutonium-uranium ratio in charge material). The separation factor for the first supernatant solution was 241. If it is assumed that no physical carryover of uranium in the wash solution occurred (as was the case for the initial phase separation), the overall uranium-plutonium separation factor would be 169.

(2) Precipitation of Uranium with Calcium from Magnesium-Zinc-Plutonium-Uranium Solutions
(I. O. Winsch, T. Cannon)

A possible further reduction of the uranium concentration in the 50 weight percent magnesium-zinc-plutonium-uranium solution resulting from the precipitation step in the blanket process may be brought about by the addition of calcium. Results presented in ANL-6379, page 66, show that the solubility of uranium in zinc decreases with the addition of calcium.

It became of interest, therefore, to determine the effect of calcium on uranium and plutonium solubility in a 50 weight percent magnesium-zinc solution. The results of an experiment showing the effect of a 17 percent calcium concentration are shown in Table 9.

Table 9

EFFECT OF CALCIUM ADDITION ON URANIUM AND PLUTONIUM SOLUBILITY IN A 50 WEIGHT PERCENT MAGNESIUM-ZINC SOLUTION

Original Charge: 1533 g Zn, 1533 g Mg, 2.83 g Pu, 3.4 g U

Temp (C)	Calcium (w/o)	Uranium in Solution		Plutonium in Solution	
		(w/o)	(% of Charge)	(w/o)	(% of Charge)
440	0	0.025	22.5	0.092	100
480[a]	16.8	0.002	2.2	0.071	92.5

[a]After calcium addition, melting point of alloy was raised to about 470 C, which necessitated the temperature change.

The uranium in solution at 480 C after the addition of calcium was reduced to about ten percent of that in solution at 440 C in the original melt. However, the addition of calcium may have resulted in precipitation of some plutonium with the uranium as shown by the 7.5-percent decrease in the plutonium concentration. This apparent precipitation of plutonium should be checked if the procedure is of interest. It is also

possible that a lower calcium concentration in the magnesium-zinc solution would effectively precipitate the uranium from solution with a less deleterious effect on the plutonium concentration.

The procedure indicates a possible method of improving the separation of plutonium from uranium, but, since an equally good separation can be obtained by evaporating the solution to cause additional uranium precipitation, it will not be pursued further at this time.

f. Development of Processes for Plutonium Reactor Fuels

(1) Calcium Extraction Studies
(M. Ader, I. O. Winsch, T. F. Cannon)

Previously reported studies (see ANL-6379, page 65) indicated the possibility of separating rare earths from plutonium and plutonium-uranium by extraction with calcium or calcium-rich zinc solutions. In a continuation of these studies, the distribution of cerium between (a) plutonium and calcium at about 860 C, and between (b) plutonium and calcium-rich zinc solutions at about 860 C and 705 C, was determined in an experiment described below. Concurrently, some data were obtained for the solubility of plutonium in calcium and calcium-zinc solutions, small amounts of cerium being present in both cases.

About 134 g of plutonium and 2.82 g of neutron-irradiated cerium were alloyed by heating in a helium atmosphere at about 700 C for $3\frac{1}{4}$ hr in a 3-in.-diameter tantalum crucible having a truncated cone-shaped bottom. The alloy was stirred with a tantalum paddle for about 30 min, and allowed to stand at room temperature over a weekend. Next, a total of 71 g of calcium sticks (nominally 99.5 percent) was added and the temperature was raised to about 860 C. The two-phase mixture was stirred for $2\frac{1}{2}$ hr, allowed to settle about 30 min, and sampled. "Bucket-type" samples (i.e., not filtered) of the light, calcium phase were taken by pressurizing the liquid into a $\frac{1}{4}$-in.-diameter tantalum tube having a closed bottom and a 0.045-in.-diameter hole in its wall. A duplicate sample was taken within about 15 min. Subsequent additions of calcium were made which enabled the determination of the cerium distribution at calcium/plutonium weight ratios of 0.53, 1.0, 1.9, and 3.8. Intervals of agitation ($3\frac{1}{2}$ hr), settling (30 min to 17 hr), and sampling at about 860 C (calcium phase only)* followed each calcium addition.

In the second part of the experiment, the effect of zinc dissolved in the calcium phase on the cerium distribution was measured at about 860 C and 705 C. Incremental additions of zinc were made to give nominal concentrations of 11, 22, and 35 weight percent (7, 15, and 25 atom percent) in the calcium phase. The experimental procedure was similar to that described above.

*The plutonium phase was not sampled because repeated sampling would have depleted the small volume of liquid plutonium (134 g = about 8 cc).

Samples were dissolved in concentrated nitric acid containing about 0.5 M hydrochloric acid and analyzed for (a) zinc by a method involving EDTA titration and complexing with potassium cyanide; (b) plutonium by alpha counting after separation of calcium, zinc, and americium-241; and (c) cerium by first removing plutonium by means of tributyl phosphate extraction, and then counting cerium-141 gamma (145-kev) activity in a single-channel analyzer adjusted to discriminate against energies less than 125 kev (for example, 60-kev americium-241 gamma activity).

The analytical data, which are given in Table 10, are averages of duplicate samples, except for the last sample taken through a graphite filter.

Table 10

EXTRACTION OF PLUTONIUM AND CERIUM FROM PLUTONIUM SOLUTIONS INTO CALCIUM-RICH SOLUTIONS

Experiment: MA-Ca-9
Conditions: Tantalum equipment; helium atmosphere
Procedure: 134 g plutonium alloyed with 2 82 g irradiated cerium at 700 C, then mixed with 71 g calcium at 860 C Subsequent additions of calcium (Part 1) as indicated below, followed by additions of zinc (Part 2)
Sampling: Unfiltered liquid samples of calcium phase pressurized into "bucket-type" tantalum tubes Data in chronological order

Temp (C)	Ca Phase/Pu Phase Weight Ratio	Calcium Phase: Weight Percent Found Zn	Pu	Ce	Percent Extracted Pu	Ce	Ce Distribution Ratio[a]
Part 1							
860 ± 3	0.53	-	0 104	0 86	0 056	22	0 53
866 ± 2	1 0_0	-	0.106	0 74	0 11	36	0 55
859 ± 3	1 9_5	-	0 099	0 54	0 20	51	0 55
856 ± 3	3 8_5	-	0 100	0 35	0 38	66	0 51
Part 2							
860 ± 4	4 3	10 7	0 119, 0 087	0.38	0 44	79	0 89
712 ± 4	3 0[b]	14 8[b]	0 060	0 41	0 19	63	0 56
860 ± 6	4 9	21 8	0 138, 0 247	0 36	0 93	87	1 3
703 ± 4	4 8	22 0	0 085	0 36	0 40	87	1 4
855 ± 3	5 9	34 3	0 70	0 33	4 0	94	2 7
704 ± 3	5 7	34 8	0 28	0.33	1 6	95	3 2
704 ± 3[c]	5 7	35 0	0.023	0.31	-	-	-

[a] Distribution Ratio = $\frac{\text{g Ce/g Ca phase}}{\text{g Ce/g Pu phase}}$

[b] Precipitation of large amount of calcium metal indicated by increase in zinc concentration on lowering temperature from 860 to 712 C Liquidus curve of Ca-Zn binary phase diagram may be incorrect (see footnote page 62)

[c] Sample filtered through Grade 60 graphite frit

The maximum differences found between duplicate samples were: plutonium, 10 percent, except for the two cases where results of each sample are shown; cerium, 2.5 percent; and zinc, 2.3 percent. This is pointed out to indicate the reliability of the data and thereby to support the computed percentage extractions and cerium distribution ratios given in Table 10. Since cerium and plutonium were determined only in the calcium phase, the remainder is assumed to be in the plutonium phase and is obtained by difference. Thus, the computed cerium distribution ratios are subject to considerable error. This is especially true after the zinc additions, because of the relatively small amounts of cerium left in the plutonium phase.

The computations are based on the following assumptions: (1) presence of two liquid phases and absence of solid phases; (2) attainment of equilibrium; and (3) 100 percent material balance for all components charged. The first assumption is reasonable for the following reasons. Plutonium (mp 640 C) and cerium (mp 804 C) are completely miscible above about 645 C from 0 to 17.5 atom percent cerium.[7] Experimental conditions of temperature and concentration were such as to preclude saturation of either phase by cerium, even after addition of zinc. Furthermore, no compounds have been reported between plutonium and cerium,[7] plutonium and calcium,[8] and cerium and calcium.[9] Although plutonium-zinc compounds exist[10] (e.g., $PuZn_2$), the finding of as much zinc in the calcium phase as nominally added indicates the absence of solid plutonium-zinc compounds. It is also reasonable to presume the absence of solid cerium-zinc compound(s) since the cerium content of the calcium-zinc phase increases with zinc concentration. Only in the case of the sample taken at 712 C and containing 14.8 percent zinc is there evidence of the presence of solids. Precipitation of a large amount (~157 g) of calcium is inferred from the increase in zinc concentration from 10.7 to 14.8 weight percent on lowering the temperature from 860 C to 712 C.*

[7]Ellinger, F. H., Land, C. C., and Cramer, E. M., Extractive and Physical Metallurgy of Plutonium and Its Alloys, W. D. Wilkinson, Ed., Interscience Publishers, Inc., New York (1960), p. 152.

[8]Coffinberry, A. S., et al., Reactor Handbook, 2nd Edition, Vol. I, C. R. Tipton, Ed., Interscience Publishers, Inc., New York (1960), p. 273.

[9]Zverev, G. D., Doklady Akad. Nauk. SSSR, 104, 242 (1955)

[10]Ellinger, F. H., Land, C. C., and Cramer, E. M., op. cit., p. 170.

*The calcium-zinc phase diagram given by Hansen and Anderko in Constitution of Binary Alloys, 2nd Edition, McGraw-Hill Book Co., New York (1958), p. 412, was used as a guide to selecting temperature and concentration conditions for the experiment. It is felt that the liquidus curve, showing the melting point of calcium-11 w/o zinc to be about 675 C, is in error.

A question arose as to whether equilibrium was attained when it was discovered that the tantalum agitator paddle had broken away from its shaft during Part 2 of the experiment. Thus, the only stirring effected was that due to the whip of the rotating shaft and convection currents. However, the consistent trend of the data tends to indicate that the combination of stirring, although inefficient, time (4 to 17 hr), and temperature yielded near-equilibrium conditions. The variation with temperature of the plutonium but not cerium content of the calcium-zinc solutions supports this view.

The last assumption is somewhat in error since weighing of the tantalum crucible and contents at the end of the experiment revealed that, of the 929 g of metal charged, 44 g, or 4.8 percent, had evaporated. The computations in Table 10 were not corrected for this loss. However, corrections were made for the removal of sample components (54 g) from the system.

In Part 1 of the experiment it was found that the solubility of plutonium in liquid calcium at about 860 C was about 0.10 percent. Small concentrations of cerium (<0.86 percent) did not appreciably affect plutonium solubility.

The distribution ratio of cerium over a sevenfold range of calcium/plutonium weight ratio (0.53 to 3.8) was fairly constant, namely, 0.53 on a weight basis (0.09 on a molar basis). The ratio of cerium to plutonium used in the present experiment was approximately twice that calculated to be present after two percent burnup of a 20 percent plutonium-uranium-fissium alloy.

Examination of the percentages of plutonium and cerium extracted, given in Part 1 of Table 10, shows that cerium can be adequately removed if one is willing to tolerate some plutonium loss. For example, two successive extractions at 860 C of a plutonium-cerium solution with approximately four times its weight of calcium will remove about 88 percent of the cerium with about 0.8 percent plutonium loss.

In Part 2 of the experiment it was found that the plutonium solubility in calcium was significantly increased by addition of zinc. At about 860 C, plutonium solubility increased from 0.1 to 0.7 weight percent as zinc concentration increased from 0 to 35 weight percent. The addition of zinc to calcium permits liquid-liquid contact at temperatures below the melting point (850 C) of calcium. At about 705 C, plutonium solubility in calcium-zinc solution was considerably lower than at 860 C. However, cerium distribution into calcium relative to plutonium did not appear to be adversely affected by additions of zinc to 35 weight percent. In fact, there appeared to be a slight improvement in the cerium-plutonium separation factor at lower temperatures.

The last sample taken in Experiment MA-Ca-9 was filtered through Grade 60 graphite to determine whether graphite was compatible with plutonium and cerium in calcium-rich solutions. That graphite cannot be used in such systems is seen by comparison of the last and next-to-last solubility values of Table 10. These data showed that at 704 C more than 90 percent of the plutonium in calcium-35 weight percent zinc solution reacted with graphite in the short time (<1 min) required for a sample to pass through the filter.

From the data obtained in this and previous experiments (see ANL-6379, pages 65 to 74), it is concluded that a practical separation of cerium and probably other rare earths from plutonium-uranium appears feasible. For example, the intermetallic zinc compound resulting from the precipitation of uranium, plutonium, and rare earths from zinc solution could be decomposed by addition of about twice as much calcium as zinc. Rare earths would remain dissolved in liquid calcium-zinc and thus could be removed from the solid solution of uranium-plutonium that precipitates. At comparable temperatures, the concentration of plutonium remaining in the liquid phase could be expected to be even lower than that found in the experiment described above, since the activity of plutonium in uranium-plutonium solid solution would be lower. In addition, lowering the temperature to about 450 C would be expected to reduce plutonium solubility in the calcium-zinc solution even further. Experiments to test these concepts are now underway.

g. Preparation of Compounds in Liquid Metal Media
(T. R. Johnson, R. L. Christensen)

Preliminary work on the preparation of refractory actinide compounds by precipitation from liquid metal solutions has been reported previously (ANL-6379, page 79). A few additional exploratory experiments were performed to investigate the feasibility of precipitating uranium carbide from zinc and cadmium solution by sparging with hydrocarbon gases. The possibility of controlling the carbon content of the product by this technique was of particular interest.

The results of this study are presented in Table 11. The reaction of methane with uranium in a zinc-12 weight percent magnesium solution at 800 C was slow. In a cadmium-2 weight percent magnesium solution the reaction was somewhat faster. In experiments with acetylene, it was found that acetylene underwent extensive pyrolysis at 600 and 800 C with the formation of elemental carbon. It is suspected that under these conditions the formation of uranium carbide results from a reaction of elemental carbon with the uranium in solution. Further studies are required to determine whether uranium carbide can be precipitated satisfactorily by this method without the deposition of carbon or if free carbon can be removed by a suitable phase-separation technique.

Table 11

REACTION OF HYDROCARBON GASES WITH URANIUM IN LIQUID METAL SOLUTIONS

Liquid Metal Solution						Hydrocarbon Gas			Reaction Conditions			U Removed from Solution (%)	Remarks
Total wt (g)	U (w/o)	U (moles)	Zn (w/o)	Cd (w/o)	Mg (w/o)	Type	Flow Rate [cc(STP)/min]	Carbon Content[a] (moles)	Time (hr)	Temp (C)	Stirring (rpm)		
375	2 4	0 04	86	-	11 6	CH_4	60	1 9	12	810	500[b]	15	Small amounts of free carbon on surface of ingot at end of run
400	7 8	0 13	81	-	11 2	C_2H_2	50	2 4	9	800	250[b]	85	Large amounts of free carbon from pyrolysis of acetylene
1000	1 0	0 04	-	97	2 0	CH_4	60	1 4	8 5	600	200[c]	30	No free carbon found on ingot
1000	0 75	0 03	-	97	2 0	C_2H_2	50	2 2	8	500 and 600	200[c]	30	Large amounts of free carbon

[a]Carbon content in the total amount of hydrocarbon gas passed into the reaction vessel

[b]Paddle stirrer 1 in x 1-1/2 in used without baffles

[c]Paddle stirrer 1-1/2 in x 3/4 in used without baffles

h. Materials and Equipment Evaluation (P. A. Nelson)

Materials evaluation studies are in progress to evaluate the compatibility of various materials with liquid metal systems of the types contemplated for reprocessing reactor fuels. Selection of materials for EBR-II processing equipment is the main objective, but data of more general interest are also being accumulated. Corrosion tests with metal coupons and runs in agitated crucibles under processing conditions are being used to evaluate materials.

(1) Solution Stability and Material Demonstration Runs (G. A. Bennett, P. Nelson, L. F. Dorsey)

Materials under consideration as container materials in the skull-reclamation process are being evaluated, not only on the basis of corrosion resistance, but also from the standpoint of compatibility with various process solutions, as indicated by solution stability. They are also being evaluated from the standpoint of general performance under processing conditions, the judgment of performance being based on such observations as embrittlement and solution penetration through connected porosity. During the last period, solution stability and material demonstration runs were conducted in Code 82 impregnated graphite, pyrolytic graphite, tantalum, and flame-sprayed-and-sintered tungsten crucibles. The crucibles were about 5 in. in diameter and 8 to 12 in. in height. Charge compositions varied from 3 to 12 weight percent magnesium and from 0.5 to 4 weight percent uranium, the remainder being zinc. In all cases a flux was used which consisted of 47.5 mole percent magnesium chloride, 47.5 mole percent calcium chloride, and 5 mole percent magnesium fluoride. Temperatures of the experiments were in the range of 750 to 850 C. Vaporization of the zinc was reduced to a negligible amount

in these runs, as contrasted with earlier runs (see ANL-6379, page 87), by the use of crucibles of lesser porosity, by the substitution of argon for helium as the experimental atmosphere, and by reduction in the temperature of the crucible top.

The details and results of the completed runs are summarized in Table 12.

Table 12

SUMMARY OF SOLUTION STABILITY AND MATERIAL DEMONSTRATION RUNS

Composition: Metal as indicated
Flux: $CaCl_2$ - 47 5 mole percent; $MgCl_2$ - 47 5 mole percent; MgF_2 - 5 mole percent
Agitation Speed: 560 rpm

Crucible Material	Charge Weight (kg)		Metal Composition (%) (Zinc by difference from 100)		Test Conditions		Solution Stability	General Observations
	Metal	Flux	U	Mg	Temp (C)	Time (hr)		
Code 82 Impregnated Graphite	1 60	0 15	0 5	4 8	750	24	Poor U concentration decreased to 0 43 percent	No apparent corrosion Graphite wet by both phases
Pyrolytic Graphite	-	-	-	-	-	-	-	Pyrolytic graphite coating separated from ATJ crucible base during crucible outgassing
Tantalum Crucible No 1	7 50	0 22	0 5	3 0	750[d] 800 850	24 24 24	Good U concentration decreased to 0 47 percent This is readily explained by 150 ppm carbon content in zinc	No apparent corrosion but crucible cracked at bottom weld on remelting of material
Crucible No 2	4 50	0 22	0 5	12 0	750[d] 800 850	24 24 24	Same as above	Same as above except that crucible withstood remelting of charge
Flame-sprayed and sintered Tungsten[a]								
Crucible No 1	4 00	0 30	3 5	5 0	750	7	-	Crucible cracked in handling subsequent to run Cracking not related to run but rather to crucible fragility
Crucible No 2	4 00	0 30	3 5	5 0	800[d] 850	20 44	Good Both Mg and U concentrations increased slightly due to zinc vaporization [b]	Crucible appearance unchanged
Crucible No 2	2 46	0 50	4 7[c]	5 4	800	49	-	No apparent effects on crucible Total metal loss was 2 percent

[a] 92 percent of theoretical density

[b] A slight loss of uranium relative to magnesium was evident which again is probably due to reaction with carbon in original zinc (C content - ~150 ppm)

[c] As uranium oxide

[d] Successive temperature changes made in same run

The following conclusions may be drawn:

1) The rate of reaction of uranium with graphite is sufficiently rapid to eliminate graphite from further consideration. This statement, however, may not apply to pyrolytic graphite, since this form of graphite has not yet been satisfactorily tested. In an attempt to test pyrolytic graphite, which had been deposited as a coating on the interior surfaces of an ATJ graphite crucible, the coating separated upon outgassing the crucible.

2) Neither tantalum nor tungsten showed evidence of corrosion in these tests. However, longer corrosion tests of tantalum (100- to 300-hr tests as described in ANL-6287, page 76) showed a slight attack (1 to 5 mils in depth) of tantalum by zinc and zinc-magnesium alloys.

3) Solution stabilities appear to be good in both tantalum and tungsten crucibles.

4) Judged by the appearance of the wall cross section of the broken flame-sprayed-and-sintered tungsten crucibles (92 percent of theoretical density), some penetration of the flux and metal phases occurred. It is not clear that the crucible was completely penetrated, but complete penetration may have occurred in certain areas. Further observations are required in this regard.

5) The flame-sprayed tungsten crucibles are rather brittle at room temperature. Figure 11 shows that these crucibles have an eneven wall thickness. This could probably be corrected by greater care in fabrication.

Figure 11

FLAME-SPRAYED TUNGSTEN CRUCIBLES

(Note uneven thickness of crucible wall)

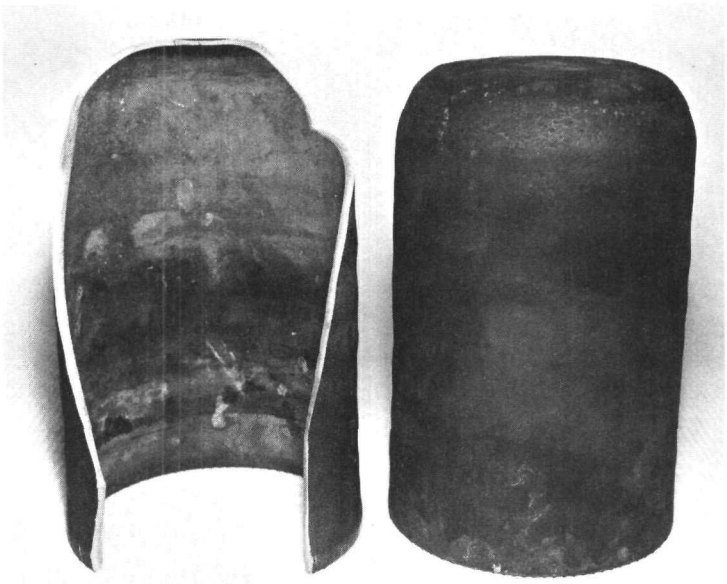

Future solution stability and material demonstration runs will be carried out in pressed and sintered tungsten crucibles, and in crucibles fabricated from a 90 weight percent tantalum-10 weight percent tungsten alloy.

(2) Etchants for Refractory Metals
(M. Kyle, A. Sanders, J. Bartos)*

Metallographic examination of the materials before and after exposure to the corroding media, usually zinc-magnesium alloys and halide fluxes, has been found to be an effective means of determining depth of corrosion. However, some difficulty has been experienced in obtaining suitable etchants for the refractory metals, especially in the presence of the zinc-magnesium matrix. Therefore, a study was undertaken to evaluate various etchants for use in determining depth of corrosion. The metals of primary interest are tantalum, tantalum-10 percent tungsten, tungsten, molybdenum, molybdenum-30 percent tungsten, and molybdenum-0.5 percent titanium. Etchant compositions of possible utility were obtained from literature sources. The etchants were tested for satisfactory etching of the subject metal after exposure to a zinc-5 percent magnesium alloy. Some etchants which were useful for etching new metal did not always clearly reveal the depth of corrosion. Table 13 presents those etchants found particularly useful for revealing the depth of corrosion.

Table 13

EVALUATION OF ETCHANTS FOR METALLOGRAPHIC DETERMINATION OF CORROSION OF REFRACTORY METALS BY ZINC-5 PERCENT MAGNESIUM ALLOY

Material	Etchant Composition	Reference	Method and Time	Comments
Ta	50 parts H_2SO_4 20 parts HNO_3 20 parts HF	(11)	Immersion 5-10 sec	Good grain boundary contrast
Ta, Ta-10% W	1 part HF 1 part HNO_3	(12)	Swabbing 30-40 sec	Slight pitting, good grain boundary contrast
Ta-10% W	60 parts glycerine 20 parts HF 20 parts HNO_3 20 parts H_2O_2	(12)	Immersion 10-15 min	Excellent grain boundary contrast
Ta-10% W	10 g NH_4F 50 ml HF 40 ml H_2O	(13)	Electrolytic 0 02 amp/ sq cm 3-5 min	Good grain boundary distinction
Mo, Mo-1/2% Ti	10 g KOH or NaOH 10 g $K_3Fe(CN)_6$ 100 ml H_2O	(13)	Swabbing at 50 C 10-30 sec	Fast etch good grain boundary contrast
Mo-30% W	1 g NaOH 35 g $K_3Fe(CN)_6$ 600 cc H_2O	(14)	Immersion 4-10 min	Grain boundaries distinct, no pitting
W	9 parts HF 1 part HNO_3	(15)	Swabbing 5-10 sec	Satisfactory grain boundary contrast

(11) Tegart, W J., Metals-Polishing, Pergamon Press, London (1959), p 96

(12) A Study of Ternary Phase Diagrams of Tungsten and Tantalum, WADC Technical Report 59-492 (March 1960), p 5

(13) Development of Tantalum-Tungsten Propulsion System Components, National Research Corporation Quarterly Report covering January 10 - April 9, 1960 NRC Project Number 11-1-032, Contract No NORD-18787

(14) Molybdenum Metal, Climax Molybdenum Company (1960)

(15) Methods and Procedures for Forming and Fabricating Tungsten Technical Data Bulletin Dec 13, 1950 Fansteel Metallurgical Corporation

*Co-operative student from the Illinois Institute of Technology.

(3) Inert Gas Welding Facility
(P. Nelson, M. Kyle, A. Sanders)

In the program for testing the corrosion resistance of refractory metals and ceramics to molten halide flux-metal systems, the material to be tested is enclosed in a 1-in.-OD by 2-in.-long tantalum capsule if the metal phase is zinc or a zinc-magnesium alloy. This tantalum capsule is enclosed in a steel capsule to protect it from atmospheric attack. Because the halide salt systems under study are very hygroscopic and because moisture contamination appears to cause tantalum failures, it is necessary to dry the salt systems and perform all capsule-loading and unloading operations in an inert gas-filled dry box. The construction of a facility which will make possible the loading and welding of capsules in argon is nearing completion.

This facility consists essentially of an argon-filled dry box containing an automatic, remotely operable, welding apparatus (see Figures 12 and 13). The facility includes an atmosphere-recirculating and purification system for removal of oxygen, nitrogen, water vapor, and hydrogen impurities from the dry box atmosphere.

Figure 12

DRY BOX WELDING FACILITY

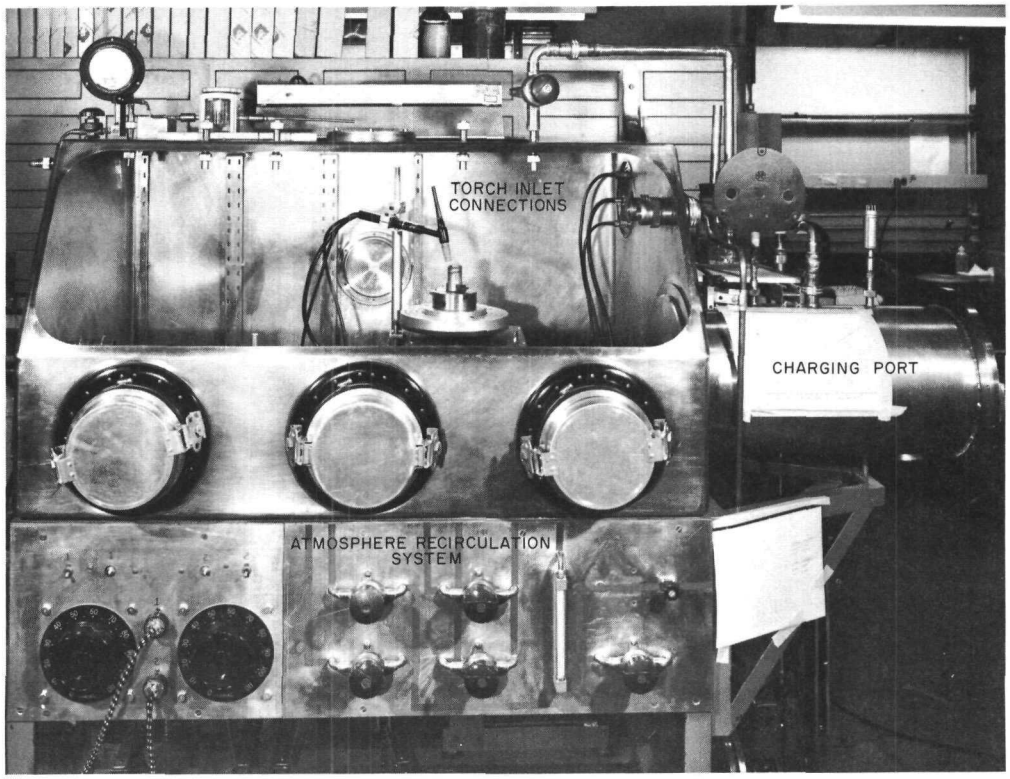

Figure 13

AUTOMATIC WELDING POSITIONER

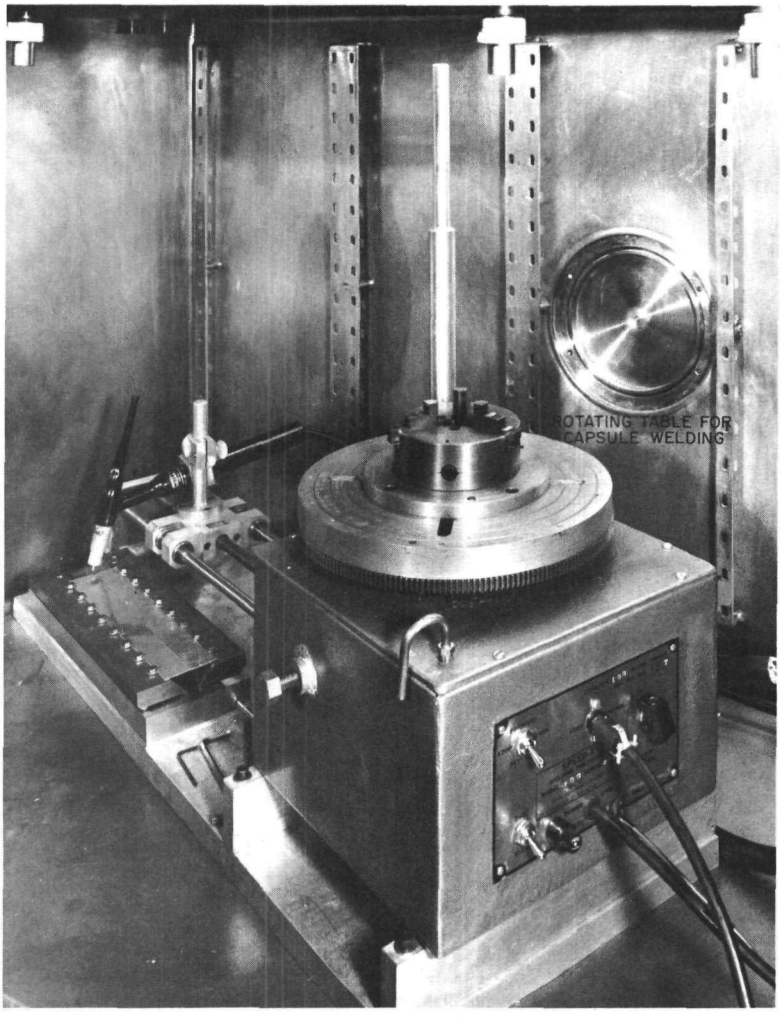

(4) Tantalum Sample Filters
(P. A. Nelson, L. Dorsey)

Liquid metal solutions have been sampled by pressurizing the solution into a tantalum tube fastened to a steel rod. The end of the tantalum tube is usually fitted with a graphite filter to remove suspended solids. Because of the reaction of graphite with uranium, the possibility of replacing graphite sample filters with tantalum filters is being investigated. A total of 500 tantalum filters, 100 of each of 5 different lots were obtained (see Table 14). The lots differed in the size and shape of powder used in making the filters and in the density and permeability obtained.

Table 14

TANTALUM SAMPLE FILTER[a] CHARACTERISTICS

(Data presented in terms of permeability index, which is defined as the flowrate of argon (cc/min) through filter measured at 70 F with a differential pressure of 15 psi, discharging to atmospheric pressure.)

Powder Size (microns)[b]	Powder Shape	Percent Voids	Permeability Index
15 to 40	irregular	49	300 ± 30
20 to 60	irregular	52	4200 ± 200
150 to 400	irregular	62	4200 ± 500
30 to 100	spherical	48	5100 ± 200
100 to 300	spherical	45	14200 ± 100
	Grade 60 graphite	48	8100 ± 2400

[a]Size of filters: 0.22-in. diameter by 0.25 in. long; filters manufactured by Kawecki Chemical Company, Boyertown, Pennsylvania.

[b]As determined by microscopic examination of sintered filters.

The permeability was measured by determining the flow rate of argon through the filters. The filters were mounted in Tygon tubing rather than tantalum sample tubes in order to ensure a good seal between the filters and the tube. The permeability values shown in Table 14 are the average of three measurements for each type of filter, and the limits shown are one standard deviation from the mean. Tests with filters mounted in tantalum tubes substantiated these values.

The fact that Grade 60 porous graphite, the type most commonly used for sample filters, has a permeability within the range obtained for the tantalum filters indicates that some of these filters will probably be satisfactory. Samples of zinc-magnesium solutions have been successfully taken by means of all the filters except the least permeable one.

i. Metal-distillation Studies

(1) Large-scale Cadmium Distillation Unit (J. DeKany, J. Arntzen, J. Hepperly)

Operation of the large-scale cadmium-distillation unit (for description see ANL-6379, page 95) with a pure cadmium feed was continued during the past quarter in order to gain operational experience and to determine the capabilities of the present equipment design. Twelve distillation runs have been performed, the data for which are given in Table 15. As shown in the table, distillations were conducted at temperatures ranging from 455 to 620 C. Induction heating to the stillpot was varied from 10 to 24 kw with an overall induction heating efficiency varying from 31 to 72 percent. The lower efficiencies occurred at the lower power inputs because heat losses represented a greater fraction of the power input. As a result of the power input variations, distillation rates ranged from 12.2 to 67 kg/hr. The latter figure represents the maximum attainable distillation rate with the present uncooled induction coil-susceptor design, because further increases in power input would result in excessive induction coil temperatures and possible coil burnout. The use of graphite as a susceptor and stillpot instead of the 304 stainless steel presently used, together with a different coil design, would increase the power input capabilities of the system so that the design capacity of 100 kg/hr would be met. Such a coil-susceptor system is being presently studied.

Table 15

DISTILLATION OF CADMIUM IN LARGE-SCALE CADMIUM-DISTILLATION UNIT

(for description of unit see ANL-6379, page 95)

Run No	Distillation Temp (C)	Condenser Pressure (mm)	Induction Power Level (kw)	Distillation Rate (kg/hr)	Weight of Cd Distillate (kg)	Power Calculated from Distillation Rate (kw)	Overall Power Efficiency (%)
13	455	5	-	67	188	-	-
5	520	17	10	12.2	38.0	3 1	31
6	525	20	23.1	65 4	104	16.6	72
14	550	30	24	66 8	323	24	70
7	562	42	17.5	36 6	127	9 3	53
8	562	42	21.2	52 2	107	13.3	63
9	560	40	20.0	41.3	233	10 5	53
10	599	74	22.8	52.9	178	13.4	59
4	604	80	15	20 6	48.5	5.3	35
15	510-610	10-90	23	60 5	269	23	67
11	618	101	22.0	53 9	107	13 7	62
12	620	104	19.4	42 4	142	10 7	55

The unit has functioned well from an operational standpoint except for some line plugging, difficulties with the electrical resistance-type liquid metal level probes, and the failure of a freeze valve. The line plugging occurred in both of the gas bubbler-type liquid level-measurement tubes and in the vapor trap associated with the feeding

apparatus. In all cases the line plugging occurred as a result of forcing cadmium up into the line by pressure during transfer operations. This situation was remedied by changes in external piping and operating procedures.

The electrical resistance liquid level probes proved to be unsatisfactory inasmuch as reproducible results could not be obtained. Readings oscillated considerably because of unstable liquid metal surfaces, resulting from either boiling or induction mixing or both. A method of liquid level measurement in the stillpot which proved to be reliable is one utilizing thermocouples at various levels on the distillation crucible inner surface. Owing to the large thermal conductivity of the molten cadmium, a drop in liquid level is readily observed by sharp changes in surface temperature of the susceptor.

During the reheat of the unit from total shutdown, a freeze valve failed, causing 200 kg of cadmium to be spilled into a tray located at the bottom of the furnace. Upon removal and examination of the valve it was concluded that the valve body had ruptured as a result of the large tensile force generated by the 4.7 percent volume expansion of the cadmium during melting. Figure 14 shows the rupture in the damaged valve.

Figure 14

PHOTOGRAPH SHOWING RUPTURE IN FREEZE VALVE OF CADMIUM DISTILLATION UNIT

(Freeze valve design was previously reported in ANL-6101, page 54).

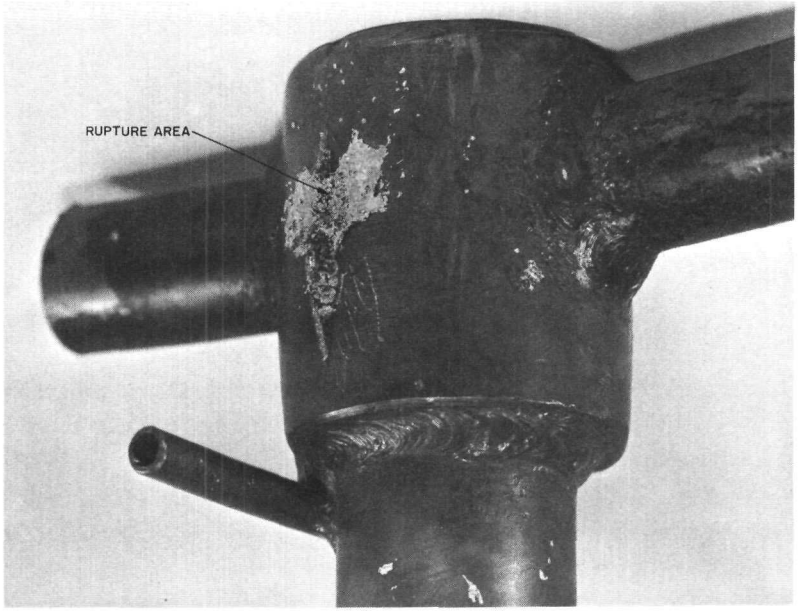

Normally, the volume contraction of the cadmium in the valve accompanying freezing would prevent such an occurrence. However, this particular freeze valve was located in a recessed well in the furnace bottom, where a temperature gradient existed that caused the cadmium to freeze preferentially in the valve from the bottom up. Consequently, the valve when frozen was filled completely with solid cadmium. As the valve was considerably smaller than the vessels to which it was connected, reheating of the furnace caused the cadmium in the valve to melt earlier than the cadmium in the vessel. Therefore, the volume expansion upon melting could not be relieved, thereby causing a great pressure buildup and subsequent valve failure. The freeze valve has been removed and will not be replaced. The spilled cadmium has been recovered.

The other freeze valves in the unit are located in positions with more uniform temperature distributions, and volume contractions can, therefore, occur during freezing. In addition, these valves may be blown free of most of the liquid metal prior to freezing.

In any liquid metal process it will be important to prevent liquid metal vapor from diffusing through instrument and service lines. For this reason, vapor traps and filters are being tested in the unit. To date, the vapor traps have been very effective in the removal of vapor from the inert gas streams and have required no maintenance. The very small amount of vapor escaping the vapor traps was completely trapped by the standard paper filters.

In the next series of runs the extent of the entrainment problem and its dependence upon the distillation rate will be determined.

(2) Vapor-Liquid Equilibrium Studies
(P. A. Nelson, H. Henryson*)

Equipment to measure vapor-liquid equilibrium in liquid metal systems has been assembled to determine activity coefficients in miscible binary metal systems such as the cadmium-magnesium and zinc-magnesium systems. In a preliminary test of the equipment, the vapor pressure of cadmium was measured and the results were in good agreement with literature data.

The equipment utilizes a modified Othmer-type equilibrium still (Figure 15). The modifications of the classical design were made 1) to remove all valves in the recycle lines, 2) to permit sampling by insertion of straight sample tubes from above, 3) to take advantage of the high thermal conductivity of liquid metals by measuring the boiling temperature in the liquid phase rather than in the vapor phase, and 4) to adjust to the fabrication techniques used for tantalum from which the still was fabricated.

*Student Aide from Princeton University.

FIGURE 15
VAPOR-LIQUID EQUILIBRIUM STILL

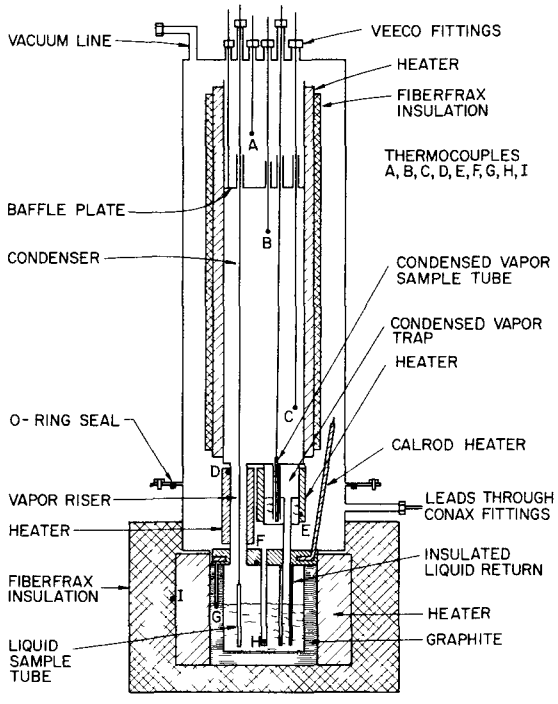

One of the most difficult accomplishments in vapor-liquid determinations at high temperatures is the measurement of the vapor temperature without superheating or condensing the vapor. Superheating would result in an inaccurate boiling point measurement, and partial condensation would result in stripping of the less volatile component from the vapor. Because of the high thermal conductivity of liquid metals, it is possible to measure the boiling temperature in the liquid phase. This eliminates the difficulty of vapor condensation, since the method permits the superheating of the vapor. That accurate boiling temperatures can be measured directly in boiling liquid metals was demonstrated by measurements made in boiling cadmium-magnesium solutions (ANL-6145, page 58). Superheating of the metal surfaces above the liquid level is accomplished by resistance elements as shown in Figure 15.

In order to reach an equilibrium condition, the still will be operated at a high rate for several hours, after which the power will be gradually reduced until boiling is barely maintained. The temperature will be maintained at a chosen value by adjusting and controlling the pressure by means of a cartesian manostat. Samples will be taken when equilibrium has been reached after suddenly raising the pressure to arrest boiling. A sample of the liquid will be obtained by inserting a sampling tube into the liquid via the vapor riser, and a sample of the condensed vapor will be obtained by inserting a sampling tube into the condensed vapor trap.

The equipment has been assembled and given preliminary tests with promising results. A stainless steel still was used for these preliminary tests with cadmium in order to conserve the tantalum still for the zinc-magnesium experiments. The boiling point of cadmium was measured over the pressure range 5 to 760 mm Hg, with the results shown in Table 16.

Table 16

VAPOR-PRESSURE MEASUREMENTS FOR CADMIUM

Temperature (C)	Vapor Pressure (mm Hg)	Calculated Vapor Pressure[a] (mm Hg)	Vapor Pressure from Literature[b]
459.9	5.7[c]	5.97	5.6
519.2	20.9	20.8	21.3
539.9	31.0	30.8	31.4
555.2	41.0	40.6	41.6
578.8	61.0	61.0	60.9
596.2	80.8	81.0	79.3
610.9	100.4	102.2	100
637.6	151.1	152.4	149
657.1	200.8	201.4	198
686.8	300.7	300.3	294
709.6	400.8	401.6	394
727.0	497.0	496.5	488
743.1	601.5	599.8	587
763.0	759.6	751.6	744

[a]Vapor pressures calculated by means of the following equation:

$$\log P_{mm} = -\frac{5665.6}{T} - 1.07186 \log T + 11.5766 \quad .$$

[b]Interpolated from compilation by D. R. Stull, Ind. and Eng. Chem., 39 (4), 541 (1947).

[c]This point was not used in deriving the correlation equations because the pressure measurement was not sufficiently accurate.

The data were fitted to an equation by utilization of the thermodynamic relationship

$$R \ln f = -\int \frac{\Delta H}{T^2} \, dT \quad ,$$

where R is the gas constant, f the fugacity, ΔH the heat of vaporization, and T the absolute temperature.

For a perfect gas and assuming that the difference in the heat capacity of the vapor and liquid is independent of temperature,

$$R \ln P - \Delta C_p \ln T = I - (\Delta H_0/T) \quad ,$$

where I and ΔH_0 are integration constants.

By linear regression correlation of the data in Table 16 and substituting of the known value for ΔC_p [$C_{p(vapor)} = 4.97$; $C_{p(liquid)} = 7.10$, $\Delta C_p = -2.13$ cal/mole],[16] the following equation was derived:

$$\log P_{mm} = -\frac{5665.6}{T} - 1.07186 \log T + 11.5766 \quad .$$

The standard deviation of the pressure measurements about this curve is 0.8 percent, which corresponds to about 0.5 C deviation in temperature. The two-constant equation

$$\log P_{mm} = -\frac{5244.1}{T} + 7.9400$$

is easier to use and is as accurate over the range of temperature for which it was derived (519 to 763 C) as the three-constant equation. However, it cannot be extrapolated with the same accuracy as the three-constant equation.

(3) Study of Entrainment during Boiling of Liquid Metals (J. Wolkoff)

The phenomenon of entrainment during the boiling of aqueous solutions has been repeatedly studied on both fundamental and applied levels. The mechanism of droplet formation from bursting bubbles and their particle size distributions have been investigated, and rational analyses have been formulated. On the applied level, the entrainment in boilers and evaporators and methods of separating the droplets from the vapor stream have received considerable attention.

Very few similar studies have been made for the boiling of liquid metals, and no fundamental experimental study of the nature and mechanism of droplet formation applied to liquid metals appears in the literature. Because of large differences, as contrasted with water, in several physical properties of liquid metals (e.g., thermal conductivity, surface tension, and density), the nature and magnitude of the boiling and entrainment phenomena may differ significantly from those of water.

A study of the entrainment from boiling liquid metals has begun. The work will include the following:

1. photographic study of the formation of droplets at the liquid-vapor interface;
2. study of nonturbulent boiling conditions and rates; and

[16] Kelley, K. K., Contributions to the Data on Theoretical Metallurgy, Bureau of Mines Bulletin 584 (1960).

3. study of solute carryover by the vapor stream.

Mercury is being used initially, but the work will be extended to include zinc, cadmium, and sodium.

B. Fuel Processing Facilities for EBR-II

1. Design and Construction
(J. H. Schraidt, M. Levenson)

a. Status of Fuel Cycle Facility Building Design and Construction
(E. J. Petkus, H. L. Stethers)

The Fuel Cycle Facility was about 95 percent complete on August 29, 1961, as compared with 90 percent complete three months earlier. The contractor is now doing finishing work, such as repairing, adjusting, and testing of equipment. Other work includes electrical and piping installation and painting. Progress is extremely slow, and the recently rescheduled completion date of October 31, 1961, is possible only if the contractor increases his work effort many fold.

Electrical and control equipment was installed during the past quarter. The installation of controls for the motor generator sets which will be used for the induction heating of the degassing, melt refining, and pin-casting furnaces was completed. Microphones were installed on the bearings of the blowers which will be used to circulate argon in the Argon Cell. The microphones will aid in the monitoring of the performance of the bearings. Wiring of the motor control center and the installation of heaters for the silver tower which will be used for the sorption of iodine resulting from the melt refining operation were also completed. Corrective work is being done on various panel boards.

The installation of heating and ventilating components is nearing completion. Testing of equipment and controls, and balancing of grilles and registers have begun.

Work is proceeding on the sealpot system on the roof of the Argon Cell (the sealpot system is a part of the Argon Cell pressure-relief system). Repairs and adjustments were made on the 20-ton crane in the high-bay area; however, the crane is still inadequate, since it will not move required loads at the required lower speeds. Leaks are being repaired in the refrigeration piping of the argon-cooling system. The control circuit of the sodium exhaust system has been tested and a protective coating has been applied to the sodium disposal box.

b. Fuel Cycle Facility Equipment
(G. J. Bernstein, A. A. Chilenskas, L. F. Coleman, J. Graae, R. H. Jahnke, M. A. Slawecki, T. W. Eckels)

Fabrication of the two melt refining furnaces for the Fuel Cycle Facility is nearing completion. The bell jars have been completed and shipped to Idaho by the vendor. The base plates and parts for the heating assembly are nearly finished and will be inspected soon. The control panels for the melt refining furnace have been shipped to Idaho by the manufacturer. The panels will be tested.

Fabrication drawings of the service sleeve feed throughs were received from Ex-Cell-O Corporation The drawings have been approved with certain modifications and returned to the vendor. Fabrication has been started.

A 200-kw emergency diesel generator will be installed to provide emergency power for the Fuel Cycle Facility Originally, it was planned to locate the unit outside the Fuel Cycle Facility in a protective housing. The unit will now be mounted in the southwest corner of the Fuel Cycle Facility basement. The required drawings for the installation of the unit are being made. A purchase order has been placed for the transfer switch which is required to transfer the load from the normal circuit to the emergency generator when the power fails.

The prototype wide-angle viewer ($82\frac{1}{2}$ degree half-angle of view) is being modified in ANL Central Shops for installation in the wall sleeve specified for the two alternative locations for this unit. One location is in the south wall of the Air Cell and the other is in the north wall of the Argon-to-Air Cell transfer lock beneath the Air Cell.

Some of the design drawings of the interbuilding coffin, which will be used to transfer fuel elements between the reactor and Fuel Cycle Facility, have been received from the vendor, but as yet the design is not complete. Fabrication of the scrap-handling coffin has been completed and the coffin is now in Idaho

The airlocks and all major associated parts have been ordered. A drawing for the large basket for use in the large lock has been completed and checked. A conceptual drawing for the gasket changing tool has been made.

One hundred special scrap-handling pails, which measure $11\frac{1}{4}$-in. ID by 6 ft long, have been delivered by the fabricator These pails are to be used to can the long pieces of stainless steel scrap resulting from the disassembly of the fuel subassembly and as a secondary container for the 3-gal scrap pails. These pails are supplied with rubber-gasketed

lug-type lids which will be capped in place with a closing tool manufactured by the Grotnes Machine Works, Inc., and modified for manipulator use. The closing tool has been tested in the mockup area with the manipulator and found to be satisfactory. The capacity of the pail is sufficient to accommodate the scrap from 12 subassemblies, giving a load of about 120 lb.

Five 3-gal scrap pails have been received for test purposes. These are standard pails which measure $10\frac{1}{4}$ in. ID by $11\frac{7}{16}$ in. high and are constructed of 22-gauge steel. These pails are supplied with a rubber-gasketed lug-type lid. The pails are intended for canning wastes such as melt refining crucibles, fume traps, Vycor pin molds, and miscellaneous small items which originate inside the Argon Cell. A slightly taller pail, measuring about 18 in. high and of the same diameter, will be used for the disposal of the shredded fuel-pin cans. These pails are to be transferred into the Air Cell and placed inside the 6-ft pail for disposal to the burial grounds.

In the plant, a vacuum lock is employed in the transfer of the pail from the Argon Cell to the Air Cell. A mockup test simulating a vacuum lock transfer has shown that conditions may arise in which the pail may be subjected to a crushing pressure of one atmosphere. Tests were performed on the five 3-gal pails and showed them capable of withstanding a pressure differential of 30 in. of Hg without permanent deformation or significant leakage.

Magnetic lifting tools utilizing permanent magnets are being considered as a means of lifting and moving the large and small scrap pails. Two permanent magnets, one large and one small, have been obtained and have been tested for load-holding capacity. On the basis of tests performed, it appears that the tool using the large magnet will have an approximate capacity of 200 lb, whereas that of the small magnet is 50 lb. In order to achieve this holding capacity with the 22-gauge lids supplied with the pails, the 6-ft pail will require a $\frac{1}{4}$-in. steel backing plate welded to the lid, and the 3-gal pail will require a $\frac{1}{8}$-in. steel backing plate. Release of the load is obtained by the squeeze motion of the double hook mounted on the operating manipulator. This motion moves the magnet away from the lid until the force exerted by the magnet becomes insufficient for holding the load. Design of both lifting tools is currently in progress.

The mechanical and electrical components for the transfer cell equipment have been shipped to Idaho by the fabricator, AMF Atomics. Work descriptions for installation of this equipment have been completed. The installation should begin in November 1961.

Eight pairs of manipulators for use in the Air Cell of the Fuel Cycle Facility have been delivered to Idaho.

Fabrication of window shutters, drives, and brackets is nearing completion. Preliminary inspection showed several discrepancies in the design and oversights in procurement and planning by the fabricator. These problems have been resolved and the equipment will soon be ready for final inspection.

c. Cranes and Manipulators
(J. Graae)

The eight manipulator carriages and the manipulator bridge power inlets have been shipped to Idaho. Installation of the latter will begin as soon as the construction of the Fuel Cycle Facility is completed. Brackets and receptacles for the Model 300 articulated manipulator arm have been completed and are being crated for shipment to Idaho, where they will be mounted on each of the operating manipulator carriages to provide power and control for the occasional use of the Model 300 articulated arm.

An operating manual for the control system for manipulators, cranes, and blister has been prepared. This manual contains key drawings, reference lists of drawings, description of the system, operating instructions, description of check-out equipment and its use, and manufacturer's equipment data.

The collapsible stand for manipulator carriages has been completed and will be tested with the prototype manipulator carriage in the mockup.

A manipulator tool storage rack and changer has been built. It has space for a dual hook, a parallel jaw hand, and a shear. It has been tested and, with a few minor modifications, should be adequate.

A single shear has been fabricated and will be tested soon. This shear can be attached to the manipulator forearm in the same manner that the dual hook and the parallel jaw hand are attached.

d. Materials Testing
(G. J. Bernstein, L. F. Coleman, J. Graae, M. A. Slawecki)

A series of experiments utilizing a new procedure to test radiation-resistant grease has been started. It is expected that the new procedure will be more representative of the operating conditions in the Air Cell than previous tests (see ANL-6379, page 103). A Timken roller bearing (432 cup - 438 cone) lubricated with NRRG-159* grease is being alternately irradiated and run in a test stand. Irradiation doses of 5×10^8 rad are followed by operation of the bearing at 40 rpm and 800-lb axial load

*Product of Standard Oil Company of California

for 38 hr. It is estimated that each of these cycles is equivalent to six months of operation in the Air Cell of the Fuel Cycle Facility. Results from the new tests are not yet available.

Three 5-ton cranes have been procured for use in the Air and Argon Cells of the Fuel Cycle Facility. At the time that these cranes were fabricated, a radiation-resistant grease was specified for the bearings; this does not appear to be as suitable for this use as the newer NRRG-159 grease. It is anticipated that complete removal of this grease will be difficult. Accordingly, tests are being conducted to determine whether a blend of this grease and NRRG-159 will be suitable. Three different mixtures of the two greases (1:3, 1:1, and 3:1) are being irradiated and tested with Timken roller bearings to determine the useful life of each blend.

The feasibility of using porous bronze bearings impregnated with radiation-resistant oil is being investigated. A number of Oilite* thrust bearings were degreased and impregnated with NRRO-359**. Previous tests have shown that this oil undergoes a very gradual increase in viscosity under irradiation. Initial samples irradiated to 1×10^9 rad are being prepared for mechanical tests.

Samples of asbestos-covered wire having an initial insulation resistance greater than 200 megohms have been irradiated to 2.28×10^{10} rad. Two of the samples were first irradiated unsealed to 2.0×10^{10} rad. Since then, they have received an additional 2.8×10^9 rad while sealed in a vial containing a desiccant. Their insulation resistance has increased to greater than 200 megohms from a resistance before sealing of 0.075 and 0.125 megohm, respectively. The third sample, sealed in a tube containing a desiccant, has received 9.3×10^9 rad while in the sealed container, plus 1.35×10^{10} rad prior to sealing. Its insulation resistance is greater than 200 megohms. The results of these tests and those of previous tests (see ANL-6287, pages 88 and 89) indicate that the reduction in insulation resistance which is observed when this type of insulation is irradiated unsealed to high dosages is probably caused by the presence of moisture. It has been found, however, that the insulation resistance may be restored to a high value by either heating or continuing irradiation in a dry atmosphere. Thus, this type of insulation will be quite adequate to dosages of at least 2×10^{10} rad in the Argon Cell where the atmosphere is extremely dry. The tests did not establish at which level moisture became a problem; therefore, no prediction can be made concerning changes in insulation resistance of asbestos-covered wire in the Air Cell where the relative humidity will range as high as 30 percent.

---

*Product of Amplex Division of Chrysler Corporation.

**Product of Standard Oil Company of California.

e. Shielding Windows
(T. W. Eckels)

Reworking of the tank units of the windows is proceeding satisfactorily and the Pittsburgh Plate Glass Company estimates that installation could be started by October 1, 1961, and could be completed within two months. However, installation cannot be started until approximately one month after Diversified Builders, Inc. have completed the Fuel Cycle Facility, and it is highly improbable that this will occur by October 30, 1961.

2. EBR-II Fuel Processing Mockup
(J. H. Schraidt)

a. Manipulator and Manipulator Removal Blister
(D. C. Hampson, J. Graae, R. Vree)

A new type grip drive clutch has been installed and tested. This clutch is a LEAR type, series 900, magnetic powder clutch. It operates on the following principle. A slotted rotor is free to turn between the poles of an electromagnet, except for the presence of a finely divided iron powder. With the electromagnet de-energized, very little torque is transmitted from electromagnet to rotor. As the electromagnet is energized, magnetized iron powder forms a bridge between the poles on the magnet. This bridge has to be sheared by the rotor, thereby resulting in the transmittal of torque.

The clutch is small enough to be adapted, with a few changes, to fit in the available space on the existing grip drive units. It is wound for 6 volts but can be wound for the 40 volts now available in the control system for the manipulators at Idaho.

Tests with this new clutch show a considerably more consistent torque transmittal for a given grip-force control setting than the friction-disc-type clutches used in the past.

The maximum grip force setting has resulted in grip forces varying between 265 lb at low speed to 415 lb at high speed of the grip drive motor. The variation may be due to inertia in the drive gears and a certain amount of eccentricity in the grip drive tubes, as well as friction in the many bearings and parts involved in the grip drive. The grip force can be regulated down to approximately 10 lb.

In order to accumulate a large amount of running time in a short elapsed time, the grip drive was operated by an automatic timer.

The timer, in turn, was turned on and off by a temperature controller which limited the grip drive motor to a safe temperature. The following average time cycle was established:

Grip Drive Opening	Grip Drive Closing	Grip Drive Slipping
12.9 sec	13.4 sec	1.0 sec

After 38 sec of running time, the drive was off for 86 sec for cooling. About 33 hr of running time have been accumulated. This means that the grip has cycled about 4,350 times and that about 1.2 hr of clutch slippage has taken place. The slippage occurs at the end of each closing cycle after the grip is completely closed and the drive has not yet reversed. This imposes a much more severe condition than expected for normal operation. Response of grip force was checked after the test and was found unchanged.

True grip force control, in the sense that a given control setting corresponds to a certain grip force within narrow limits over the entire control range, has not yet been attained. However, the grip drive no longer sticks after periods of slippage, as it did with the friction-disc clutches. This is, of course, of great importance for the proper operation of the manipulators inside the cells at Idaho.

b. Melt Refining
(D. C. Hampson, W. E. Miller)

(1) Equipment Performance

(a) Crucibles

The original plant-scale Norton crucibles, used in melt refining studies, had a bottom thickness of $\frac{3}{4}$ in. and an overall height of $9\frac{1}{4}$ in. After Norton applied the improved method of manufacture (discussed in ANL-6183, page 30), the crucible bottom thickness was increased to 1 in. to achieve an overall height of $9\frac{1}{2}$ in. It was believed that this increase in bottom thickness (from $\frac{3}{4}$ to 1 in.) has been a contributing cause of cracks that developed in the crucible bottom. Five crucibles which were manufactured by the new methods but which had the old dimensions were tested in melt refining runs. None of these crucibles cracked across the bottom. Crucibles with $\frac{3}{4}$-in.-thick bottoms, therefore, have been specified for plant use.

(b) Reference Thermocouple

In melt refining runs in the mockup furnaces, melt temperatures have been measured by shielded thermocouples immersed in

the molten uranium alloy In the remotely operated melt refining furnaces of the Fuel Cycle Facility, it will not be practical to measure melt temperatures in this direct manner Therefore, a bottom reference thermocouple was developed as an integral part of the furnace This thermocouple is in proximity of the graphite susceptor which is the externally controlled heat source of the induction furnace (see ANL-6387, page 94) In the melt refining furnaces of the Fuel Cycle Facility another heat source will be present, namely, the irradiated fuel pins inside the crucible, which is called the "internal" heat source Since two heat sources will be present, one of which may be an unknown variable, and since the thermocouple is located near the other heat source, a simple calibration curve is not sufficient to relate the temperature of the bottom reference thermocouple to the melt temperature.

All of the variables correlate well on the grid-type plot shown in Figure 16 in which the temperature of the base reference thermocouple is plotted as ordinate and the output of the motor generator power source is the abscissa (Values of both quantities will be readily available to the operators of the Argon Cell melt refining furnaces) Immersion temperatures appear as parametric curves on the plot, as do curves of constant rate of internal heat generation The latter is not required on the plot; and, in fact, a knowledge of the heat-generation rate of the fuel is not required to construct the grid for immersion temperatures Once the grid has been determined, the immersion temperature is readily obtained from the grid at the values at which the equipment is operating If the calibration includes lines of constant internal heat generation, then the operator also has available information to check fuel burnup

FIGURE 16
CALIBRATION OF BASE REFERENCE THERMOCOUPLE IN M-VI MELT REFINING FURNACE AT EQUILIBRIUM CONDITIONS

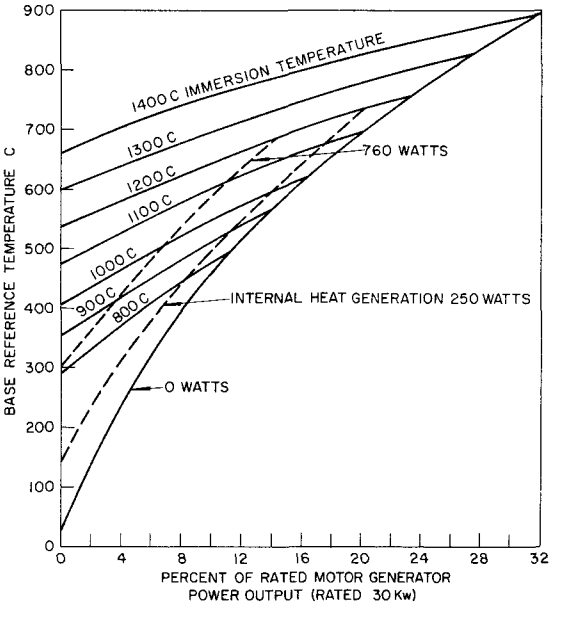

In the melt refining furnace in the mockup, heat was added to the crucible by placing resistance heaters within the crucible to simulate the fission product heat source. Only enough of the calibration grid was completed to show that there is a smooth relationship among the variables and that melt temperatures could be predicted.

To make a similar calibration grid for the Argon Cell furnaces it will only be necessary to measure accurately melt temperatures in three runs. These measurements will be made with a top reference thermocouple described in the previous quarterly (ANL-6379, page 109). In the Argon Cell melt refining furnaces, the temperature range of interest will be from melting to a melt temperature of 1400 C.

A calibration grid similar to Figure 16 will be good only for the same combination of furnace and electrical power transmission system on which the calibration runs were made. Changes in the thermal properties of the furnace would require the recalibration of the system. Experience in the mockup has shown that, after an initial break-in period (one to five runs), the thermal properties of the furnace remain essentially constant for the next 50 to 75 runs. Although the crucible is changed in every run, experience has shown that the furnace power required to maintain equilibration temperature (1400 C melt temperature) is essentially constant from run to run during the useful life of the furnace. Therefore, the variation in the thermal properties among crucibles need not be taken into account in the calibration of the base reference thermocouple. Evidently, the variation between crucibles is minimized since the crucibles are manufactured to meet specifications as to composition and dimensions.

3. Skull-reclamation Process
(J. H. Schraidt)

a. Design Considerations
(G. J. Bernstein, A. A. Chilenskas, T. W. Eckels, W. E. Miller, H. Stethers)

Development of remotely operable plant-scale equipment for the skull-reclamation process is continuing. The areas presently under study include heating and mixing techniques, and the development of suitable material transfer lines and seals.

Low-frequency induction heating is being investigated as a means of providing heat and stirring in the process vessels. Equipment is being assembled for preliminary tests with 60-cycle current. A graphite crucible, 10 in. in diameter, will be used as the containment vessel and zinc will be used as the process material. This equipment is approximately equivalent to half the scale of the proposed plant equipment. The graphite

crucible is being used because of convenience, and its use in these initial tests should not be interpreted as indicating that it is a likely candidate for process use. Two different induction coils have been designed for this work. It is anticipated that information will be obtained which would indicate whether or not adequate heating and stirring can be developed with 60-cycle current or other low frequencies up to about 1000 cycles. Mechanical stirring is also being investigated.

Two seals have been designed which will be remotely operable with the Argon Cell manipulator. These seals will be adapted for use with transfer lines, vent lines, or mechanical stirrers.

A resistance-heated line has been built for studying the problems related to transfer of molten salts and metals between furnaces. The transfer tube may be called upon to transport liquid metals, fluxes, and vapors between processing vessels. Operating temperatures will be up to 800 C. One of the major considerations in the design of the tube is remote handling. The tube must be easily and quickly detachable from the processing vessels. This requires suitable flange-seals at the point where the tube enters the vessel. Rugged construction is required since the tube will be handled by operating manipulators. The design chosen for development consists of two concentric tubes, with a single continuous resistance heater helically wound in the annulus. This type of construction has been chosen since it provides the necessary strength and ruggedness, and the outer tube affords easy attachment of flanges, braces, and handles to the line by simple welding. It has the possibility of essentially one-piece construction, i.e., the complete tube may be fabricated as a straight unit and then bent, thus eliminating welded joints in the tube itself. The first tube has been made in this manner. The inner tube has an ID of $\frac{3}{8}$ in. and an overall length of 6 ft 10 in. The heater helix was wound at a constant pitch to produce an approximately uniform heat flux along the length of the tube. The temperature distribution along the tube (both inside and outside the processing vessel) is being determined, and this information will be used to build more desirable tubes which will have a nonuniform heat flux but a more uniform temperature along the tube.

C. Pyrometallurgical Research
(H. M. Feder)

1. Chemistry of Liquid Metal Systems
(I. Johnson)

Investigations of the chemistry of liquid metal systems are being conducted to provide basic concepts and data for the rational design of methods for the reprocessing of reactor fuels. In addition, the results of these studies provide ideas and data for the formulation and testing of theories of liquid metal solutions.

a. Solubilities in Liquid Metals

The solubilities of the metals whose separations are being attempted are of prime importance in the design of fuel-reprocessing methods. The dependence of the solubility on temperature and solvent composition needs to be known. The solubility and temperature coefficients of solubility of a metallic phase in a liquid metal solvent are strongly dependent on the interatomic forces operative in the solution and, consequently, may be used to gain greater insight into the way that these forces vary with the basic properties of the solute and solvent atoms. For such fundamental studies, it is necessary to know the constitution of the solid phase in equilibrium with the saturated liquid phase.

Scandium-Cadmium System
(M. G. Chasanov, P. D. Hunt)

A scaled-down solubility apparatus was used to determine the solubility of scandium in cadmium. The total metal charged to this apparatus was 90 g, which was about one-tenth the charge used in the full-scale equipment. The charge contained 3 weight percent scandium. The sampling techniques were identical with those used with the larger apparatus (see ANL-5820, page 98). The scandium (99.9 percent) was neutron irradiated before it was added to the cadmium (99.95 percent). Scandium concentrations were determined by dissolving each sample and gamma-counting the 85-day scandium-46 present.

The measured solubilities are given in Table 17 and shown graphically in Figure 17. Over the temperature range from 349 to 422 C, the data may be represented by Equation (a), and over the range from 422 to 606 C, the data may be represented by Equation (b):

$$\text{(349 to 422 C) scandium: } \log(\text{atom percent}) = 3.935 - 2434\ T^{-1} \quad \text{(a)}$$

$$\text{(422 to 606 C) scandium: } \log(\text{atom percent}) = 4.933 - 5335\ T^{-1} + 1.534 \times 10^{6}\ T^{-2} \quad \text{(b)}$$

The relative standard deviations of Equations (a) and (b) are 0.4 and 0.8 percent, respectively. The intersection of the solubility curves at about 422 C indicates a peritectic transformation at that temperature. Thermal analysis of a furnace-cooled, 3 weight percent scandium alloy showed repeated arrests at 414 C on heating.

Hexagonal needles were isolated from a 5 weight percent alloy which had been ice quenched from 500 C. This material was found to contain 11.5 percent scandium and 88.3 percent cadmium; $ScCd_3$ would have 11.8 percent scandium. For this new phase the hexagonal

lattice parameters[17] (preliminary) are a_0 = 6.33 Å and c_0 = 4.85 Å. The X-ray density for eight atoms per unit cell is 7.55 g/cc; the pycnometric density was 7.7 g/cc. This phase is the same as the one identified in the 3 weight percent scandium-cadmium ingot from the solubility experiment; it is presumably the solid phase in equilibrium with the saturated liquid above 422 C. The equilibrium solid phase below the peritectic temperature has not yet been characterized.

Table 17

SOLUBILITY OF SCANDIUM IN LIQUID CADMIUM

Temperature (C)	Scandium (atom %)	Temperature (C)	Scandium (atom %)
606	7.04	461	3.23
578	6.05	431	2.82
558	5.43	398	2.02
523	4.52	372	1.45
502	3.95	349	1.05
475	3.47		

FIGURE 17
SOLUBILITY OF SCANDIUM IN LIQUID CADMIUM

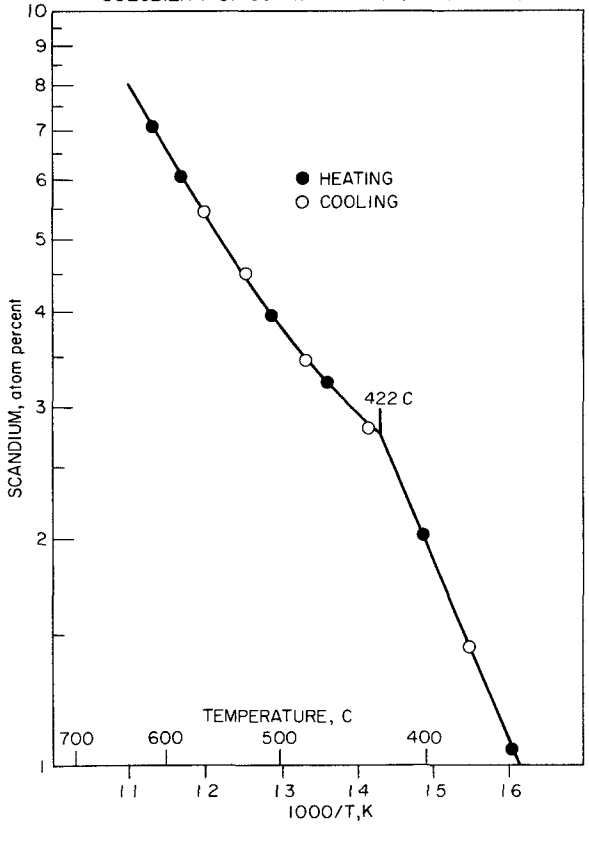

Figure 18 shows the microstructure of the 3 weight percent scandium-cadmium alloy quenched at 414 C (cooling cycle). In the photomicrograph the dark phase which is contained in envelopes of lighter material is $ScCd_3$.

The Zinc-Uranium System
(A. E. Martin, C. Wach)

As previously reported in ANL-6287, pages 102 to 104, a second zinc-uranium intermetallic phase has been found in the zinc-uranium system. In conformity with the usual nomenclature for uranium phase diagrams, the phase richer in uranium is named the delta phase and the phase richer in zinc is named the epsilon phase. The delta phase appears to have a fairly narrow composition range and its composition probably corresponds to a

[17] Schablaske, R., and Tani, B. S., personal communication.

zinc-uranium atom ratio of 8.5. The epsilon phase has a wider composition range, which has not yet been established. At temperatures near the melting point of zinc, the zinc-rich side of the epsilon field corresponds to a zinc-uranium ratio of about 11.5 to 12.

Figure 18

SCANDIUM-CADMIUM ALLOY

[Three weight percent scandium-cadmium alloy quenched at 414 C (cooling cycle); etched with 1 percent nital (1 percent nitric acid in ethanol); dark phase contained in envelopes of lighter material is $ScCd_3$. 200 X.]

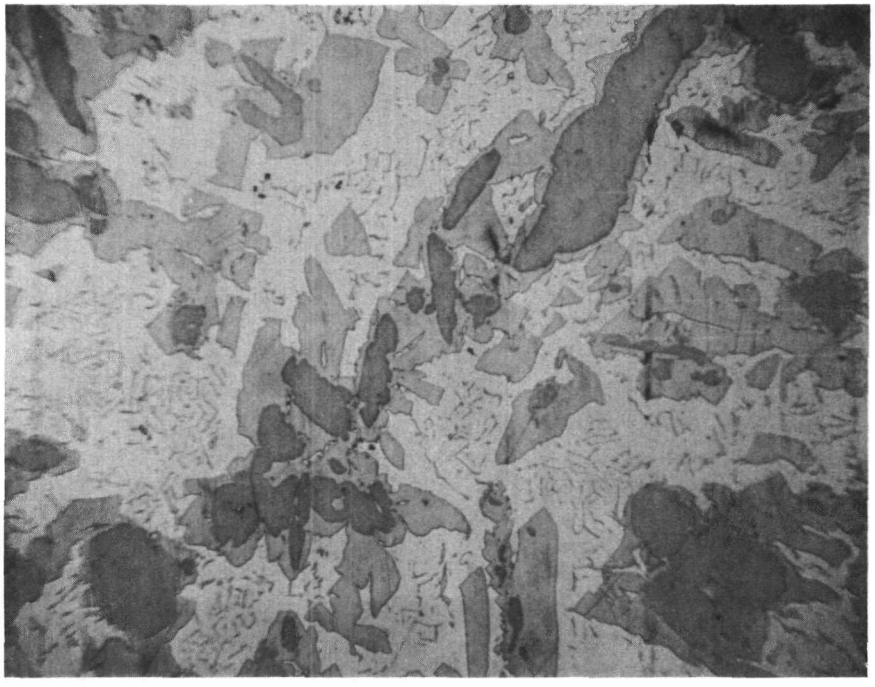

Vold[18] has reported the existence of a low-temperature form of the delta phase and indicated that the transformation temperature was probably below 550 C. This low-temperature phase will hereafter be designated as the delta-prime phase. This phase was also observed in this Laboratory, but its composition has not yet been established. However, there is no evidence that it is appreciably different from that of the delta phase. The X-ray pattern of the delta-prime phase bears resemblances to the patterns of both the delta and the epsilon phases. It is likely that the delta-prime phase merely corresponds to the uranium-rich side of the epsilon field. This possibility is currently being explored.

---

[18] Vold, C. L., and Peterson, D. T., IS-246 (1961).

The conditions of formation of the delta-prime phase have been studied in two different types of experiments. On the one hand, attempts have been made to form the delta-prime phase from the delta phase by annealing alloys containing the delta and uranium phases, with the delta phase being the dominant phase. The experiments were of long duration at various temperatures. In no case was the delta-prime phase formed. The annealing conditions included 2 weeks at 300 C, 3 weeks at 400 C, 1 week at 450 C, 1 week at 475 C, and 3 weeks at 500 C. The alloys annealed were from three different preparations. The other approach has been to study the conditions of formation of the delta-prime phase by the reaction of uranium with the epsilon phase. The epsilon material used in these studies was formed by crystallization from a zinc-rich melt. The crystals were recovered from the alloy ingot by electrolytic etching. The composition of the crystals corresponded to a zinc-uranium ratio of 11.65. Compacts were prepared from these crystals and uranium by pressing the mixture at 64,000 psi in a $\frac{1}{4}$-in. die. The compacts were sealed in Vycor tubes under a helium atmosphere and were annealed at temperatures ranging from 500 to 660 C. Compositions between the delta composition and uranium were chosen so that there would be some free uranium in the final products. As shown in Table 18, examination by X-ray diffraction of the products showed that the delta phase was formed in anneals above 600 C and may also have formed to a minor extent in the anneal at 550 C. The delta-prime phase was formed in the anneals at 550 and 500 C.

Table 18

DATA ON ZINC-URANIUM ALLOY COMPACT ANNEALS

Zinc Uranium Atom Ratios of Compacts	Annealing Conditions		Mesh Size Range of Uranium[a]	Intermetallic Phases Identified in Products by X-ray Diffraction	
	Temperature (C)	Time (weeks)		Delta	Delta Prime
5 70	660	0 7	-60, +100	Present	Absent
4 11	620	0.7	-140, +270	Present	Absent
4 11	600	4 0	-60, +100	Present	Absent
1 40	550	4 0	-140, +270	Possibly present	Present
1 32	500	3 0	-100, +270	Absent	Present

[a]Compacts were formed by mixing powdered uranium with the epsilon intermetallic compound Mesh size of latter was -100, +270

The conclusion from these experiments is that the transformation between the high- and low-temperature forms of the delta phase is very sluggish. The transformation temperature appears to be close to 550 C.

b. Liquid-Liquid Distribution

Studies of the distribution of representative fission product elements between immiscible liquid metals are being made in order to evaluate liquid metal solvent extraction processes.

The Distribution of Cerium and Strontium between Liquid Zinc and Lead

(F. Cafasso, J. Vincenzi)

For solutes which either exhibit low solubility in one of the phases or distribute very strongly into one of the phases, analyses often prove difficult. This appears to be true for both cerium, which exhibits low solubility in lead (ANL-6333, page 113), and strontium, which distributes preferentially into lead (ANL-6231, page 74). To overcome the apparent analytical problems, radiochemical methods that were more sensitive than other methods readily available were used to measure the distributions of each of the solutes in the region from 652 to 740 C. The consolute temperature of the solvent system (780 to 800 C) prevented the extension of this study to much higher temperatures.

Lead, zinc, and either activated cerium (cerium-141) or strontium (strontium-85) were melted together in an alumina crucible. After reaching the desired temperature, the melt was stirred for one hour and allowed to settle for approximately 2 hr before a sample was taken. Three samples of the equilibrium melt were taken at each of three temperatures: 652, 703, and 736 C for cerium, and 656, 703, and 740 C for strontium. All temperatures were constant to within ±2 C. Quartz tubing equipped with graphite filters and coated internally with magnesium oxide were used as sampling pipets. Both cerium and strontium were determined by gamma counting.

The results are recorded in Table 19 and are shown plotted in Figure 19 as the logarithm of the distribution coefficient versus the reciprocal of the absolute temperature. The coefficient K is defined as the ratio of the percent solute in the zinc layer to the percent solute in the lead layer. When the K values for the cerium system (K = 18.4 at 652 C, 7.9 at 703 C, and 5.0 at 736 C) are compared with earlier results (see ANL-6333, page 113) obtained for this system (K = 24.0 at 650 C, 11.7 at 700 C, and 5.7 at 730 C), it is evident that good agreement is obtained only in the 730 C region. At 650 and 700 C the cerium levels in the lead samples of the earlier experiment were in an unfavorable range for chemical analysis, whereas at 730 C this was no longer true, since at this temperature the cerium level was nearly four times greater than the level at 650 C.

Table 19

DISTRIBUTION DATA FOR CERIUM AND STRONTIUM IN THE LEAD-ZINC SYSTEM

Temperature (C)	Solute	Concentration of Solute in Zinc Layer (w/o)	Concentration of Solute in Lead Layer (w/o)	Distribution Coefficient $K = \frac{\text{w/o Solute in Zinc Phase}}{\text{w/o Solute in Lead Phase}}$
652	Ce^{141}	0 14	$7\,6 \times 10^{-3}$	18 4
703	Ce^{141}	0 11	$1\,4 \times 10^{-2}$	7 9
736	Ce^{141}	0 09	$1\,8 \times 10^{-2}$	5 0
656	Sr^{85}	$1\,9 \times 10^{-3}$	$2\,1 \times 10^{-2}$	0 09
703	Sr^{85}	$2\,3 \times 10^{-3}$	$2\,1 \times 10^{-2}$	0 11
740	Sr^{85}	$3\,2 \times 10^{-3}$	$2\,1 \times 10^{-2}$	0 15

FIGURE 19
DISTRIBUTION OF CERIUM AND STRONTIUM
BETWEEN LEAD AND ZINC
AS A FUNCTION OF TEMPERATURE

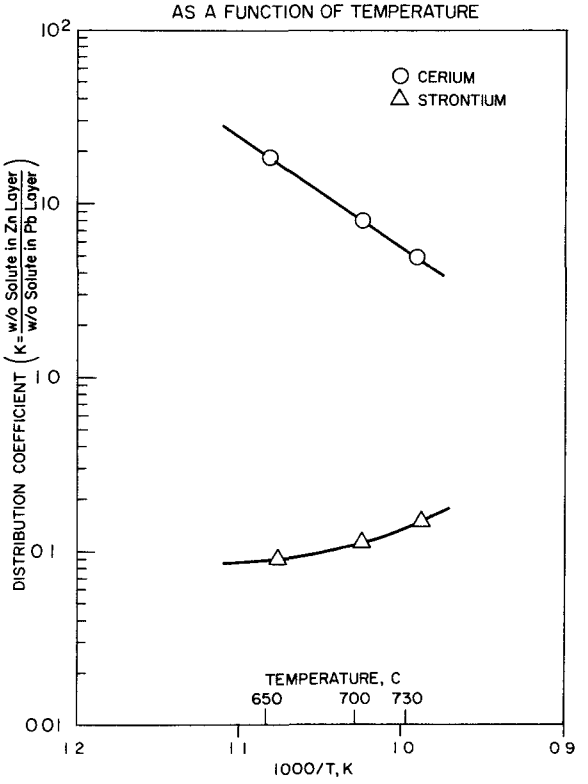

It should also be noted that the concentrations of cerium in the two experiments differ by a factor of two. It is believed, however, that the measured differences in the K values do not reflect a concentration effect but rather an improvement in the methods used in the latest experiment.

For the strontium system, K values of 0.09 at 656 C, 0.11 at 703 C, and 0.15 at 740 C were found. The 740 C value is in reasonable agreement with the value of 0.14 at 736 C reported earlier in ANL-6231, page 74.

Measurements of the simultaneous distribution coefficients of uranium, plutonium, cerium, ruthenium, zirconium, strontium, and cesium, which will be needed for an evaluation of the utility of this method, are underway.

c. Thermodynamic Studies

Thermodynamic functions for key elements in liquid metal solvents and for the more important solid intermetallic phases are being measured. Two methods are being used. Galvanic cells have proved to be especially useful for the measurement of activities in liquid metal solutions as well as for the determination of the free energy of formation of the equilibrium solid phase in solid-liquid two-phase regions. On the other hand, for systems containing several well-defined intermetallic phases, measurement of the decomposition pressure by the effusion method is proving to be most useful. The two methods supplement each other.

Thermodynamics of Uranium-Indium System (Emf Method)
(I. Johnson and R. M. Yonco)

A systematic study is being made of the thermodynamics of the systems composed of uranium and the low-melting metals. Studies of the uranium-zinc, uranium-cadmium, uranium-lead, and uranium-thallium systems have been previously reported.* Studies thus far completed on the uranium-indium system are reported below.

*For studies of the uranium-zinc system, see ANL-5924, page 132; for the uranium-cadmium system, see ANL-5996, page 116; for the uranium-lead system, see ANL-6183, page 71; and for the uranium-thallium system, see ANL-6231, page 76.

The galvanic cell used in these studies was similar to the cells used in the previous studies and may be represented by the conventional scheme

$$U \,|UCl_3,\ LiCl\text{-}KCl\ (eutectic)\,|\,U\text{-}In\ (two\ phase\ alloy) \quad .$$

The solid uranium electrode consisted of a piece of high-purity uranium welded to a tungsten lead wire. The two-phase (saturated solution of uranium in liquid indium and uranium-indium intermetallic compound) alloy was prepared from high-purity indium (99.99 percent) and solid uranium metal. A tungsten lead was used in the indium pool. The dried lithium chloride-potassium chloride eutectic (containing 3.9 percent uranium trichloride) was gettered with uranium turnings and filtered prior to use in the cell. The molten electrolyte and indium pool were contained in Morganite high-purity alumina crucibles. A tantalum protection tube for the thermocouple was used.

The emf of the cell was measured over the temperature range from 353 to 675 C. The values obtained are given in Table 20. These data may be represented by the empirical equation

$$E\ (volt) = 0.3508 - 1.075 \times 10^{-4}\, T - 5.600 \times 10^{-8}\, T^2 \quad ,$$

with an average deviation of 0.5 mv. The data are shown graphically in Figure 20.

Table 20

EMF OF URANIUM-INDIUM CELL

Cell: $U \,|UCl_3$, LiCl-KCl (eutectic) $|$U-In (2-phase alloy)

(Data in Chronological Order)

Temp (C)	Emf (v)	Temp (C)	Emf (v)	Temp (C)	Emf (v)
396	0.2539	398	0.2536	453	0.2428
659	0.2018	556	0.2232	615	0.2113
353	0.2613	413	0.2510	472	0.2391
514	0.2317	576	0.2194	635	0.2069
372	0.2584	431	0.2474	493	0.2346
540	0.2264	596	0.2152	676	0.1979

The liquid indium electrode was saturated at each temperature with respect to the uranium-indium intermetallic compound UIn_3. This compound has been characterized by Iandelli and Ferro[19] and also by

[19]Iandelli, A., and Ferro, R., Ann. Chim. (Rome) 42, 598-608 (1952).

FIGURE 20
EMF OF URANIUM-INDIUM CELL
Cell U|UCl_3, LiCl-KCl (eutectic)|U-In (2-phase alloy)

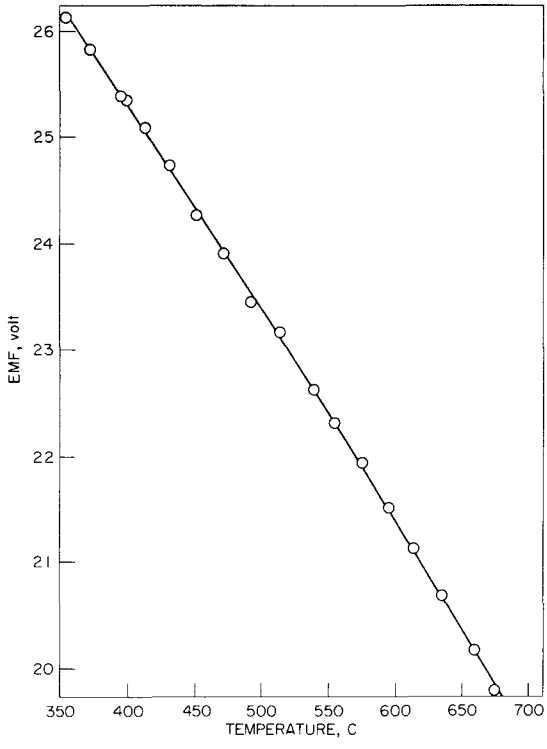

Maskrey and Frost[20] as a face-centered cubic crystal (a_0 = 4.6013 Å) which is isostructural with UPb_3, USn_3, UGa_3, UGe_3, USi_3, and UAl_3 (L 12 type). The solubility of uranium in indium has been reported by Hayes and Gordon.[21]

The free energy of formation of UIn_3, computed from the above equation is found to be

$$\Delta F_f^\circ = -24{,}280 + 7.441\,T + 3.875 \times 10^{-3}\,T^2 \ .$$

From this equation values of the enthalpy and entropy may be computed in the usual fashion. At 500 C the following values are obtained: ΔF_f° = -16.2 kcal/mole, ΔH_f° = -26.7 kcal/mole, and ΔS_f° = -13.6 cal/deg mole.

The activity coefficient of uranium in liquid indium has been estimated The values at several temperatures are given in Table 21.

Table 21

ACTIVITY COEFFICIENT OF URANIUM IN LIQUID INDIUM

Temperature (C)	Solubility U (atom %)[a]	Activity Coefficient (γ)
400	3.76×10^{-4}	0.55
500	3.42×10^{-3}	0.77
600	1.84×10^{-2}	1.1
700	7.23×10^{-2}	1.4

[a]Obtained by smoothing the data of Hayes and Gordon, J. Met. and Cer., TID-65, 130-141 (1948).

[20]Maskrey, J. T., and Frost, B. R. T., J. Inst. Metals 81, 171-181 (1953).

[21]Hayes, E. E., and Gordon, P., J. Met. and Cer. TID-65, 130-141 (1948).

Praseodymium-Zinc System (Effusion Studies)
(E. Veleckis and E. Van Deventer)

Measurements of the decomposition pressures of a number of rare earth-zinc alloys are being made as a function of alloy composition to aid in the elucidation of the intermediate phases present in these systems. In addition, from these measurements it is possible to obtain information on the relative stability of the different intermetallic phases.

Only fragmentary information about the phase relations in the praseodymium-zinc system is available. The phases PrZn and $PrZn_{11}$ have been identified by X-ray methods.[22]

The phase relations in the praseodymium-zinc system are being investigated by means of the recording effusion balance (see ANL-6333, page 115). Two different effusion crucibles were used. Low-temperature runs in the zinc-rich region of the system were made at 520 C with a crucible having an effective orifice area of 1.718×10^{-3} sq cm. High-temperature runs in the zinc-deficient portion of the system were made at 600 C with a crucible having an effective orifice area of 5.173×10^{-3} sq cm.

FIGURE 21
PRASEODYMIUM - ZINC SYSTEM
1 Vapor Pressure-Composition Isotherm at 520 C (Crucible B)
2 Praseodymium-rich Portion of the Isotherm at 600C (Crucible C)

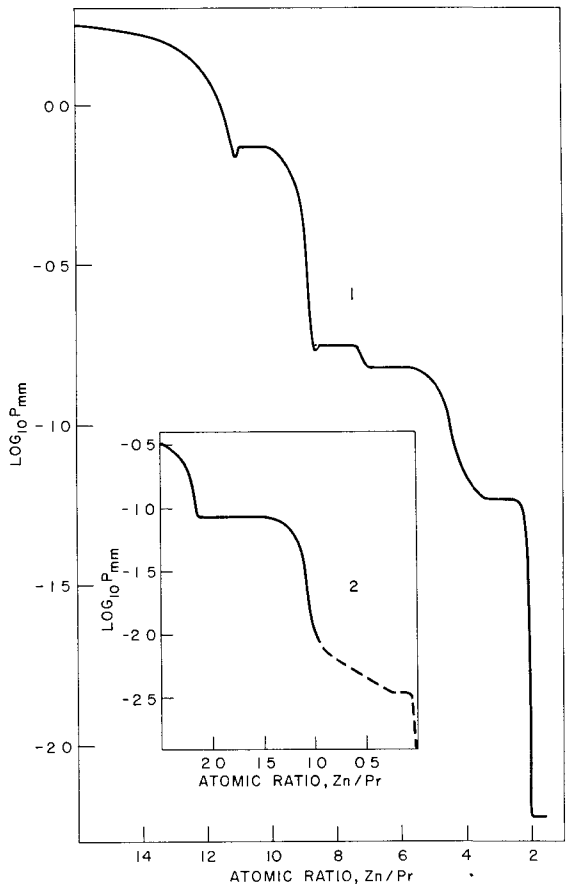

Two typical isotherms are shown in Figure 21. The isotherms suggest the existence of the following phases: $PrZn_{11}$, $PrZn_{8.5}$, $PrZn_{6.9-7.4}$, $PrZn_{3.4-5.6}$, $PrZn_2$, and PrZn. The complex behavior of the 600 C isotherm between PrZn and praseodymium may be due to diffusion problems associated with the formation of liquid solutions. This may be analogous to the lanthanum-zinc system, in which a eutectic is formed below 600 C in this region of the phase diagram. The phases found in the cerium-zinc and praseodymium-zinc systems are compared in Figure 22. The phase assignments in this system will be further verified by X-ray methods. The overall experimental accuracy in determining the compositions of the phases is estimated to be one-fifth of an atomic ratio (zinc/praseodymium) unit.

[22] Hansen, M., and Anderko, K., Constitution of Binary Alloys, McGraw-Hill Book Co., Inc., New York (1958).

FIGURE 22
RESULTS OF EFFUSION STUDIES OF CERIUM ZINC AND PRASEODYMIUM - ZINC SYSTEMS
(Region below atom ratio of 1 has not yet been investigated)

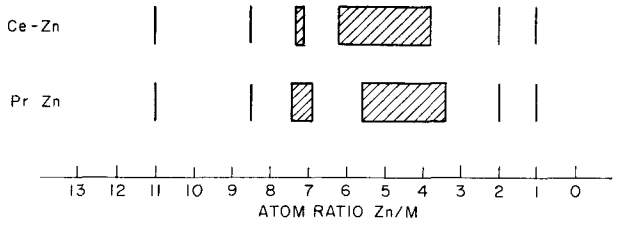

The lanthanum-zinc, cerium-cadmium, and lanthanum-cadmium systems are being studied

2 Calorimetry
(W. N. Hubbard)

Thermodynamic data are lacking for many compounds of interest in high-temperature chemistry because of the experimental difficulties involved in making the necessary measurements A program has been undertaken to help fill this gap

Part of the program consists of determinations of heats of formation at 25 C by oxygen bomb calorimetry Because some of the compounds of interest are difficult to burn in oxygen and, consequently, cannot be studied by oxygen bomb calorimetry, the new technique of fluorine bomb calorimetry has been developed for their study. The accumulation of basic heat of formation data for fluorides is a necessary preliminary adjunct to fluorine bomb calorimetry and is a valuable program on its own merit

Some of the compounds of interest are borides, aluminides, carbides, silicides, nitrides, sulfides, and selenides of metals such as uranium, zirconium, molybdenum, and tungsten One major problem in the determination of the thermodynamic properties of compounds such as these is the procurement of sufficiently pure samples. It is sometimes the case, even with "high-purity" samples, that the total uncertainty assigned to the final experimental result is due more to the uncertainty in defining the sample studied than to all the other uncertainties of the measurement combined. A program for the preparation of uranium compounds to be used in the calorimetric studies at Argonne is being carried out by Stanford Research Institute. Other compounds will be obtained from various laboratories. Boron nitride, obtained from Professor John Margrave of the University of Wisconsin, zirconium diboride, obtained from Elmer J Huber, Jr., of Los Alamos Scientific Laboratory, and zirconium dihydride and dideuteride, obtained from Howard Flotow of the Chemistry Division of this

Laboratory, are examples. Some of the compounds will be synthesized here. The disulfides of molybdenum and tungsten are examples of such compounds already studied.

The heats of formation at 25 C from oxygen or fluorine combustion calorimetry will be combined with the changes in enthalpy measured by a high-temperature enthalpy calorimeter to determine thermodynamic properties at high temperatures. A calorimetric system for measurements up to 1500 C has been designed and is now being fabricated. Design concepts for an electron beam furnace to operate up to 2500 C are being tested in the laboratory.

a. Combustion of Zirconium Dihydride and Zirconium Dideuteride in Oxygen
(D. R. Fredrickson and R. L. Nuttall)

Two series of combustions in the platinum-lined bomb have been completed to determine the heat evolved from the following reactions:

$$ZrH_2(c) + 3/2\ O_2(g) \rightarrow ZrO_2(c) + H_2O(l)$$
$$ZrD_2(c) + 3/2\ O_2(g) \rightarrow ZrO_2(c) + D_2O(l) \quad .$$

A series of calorimetric combustions in oxygen have been completed to determine the heat of combustion of the plastic polyester film (Mylar) which is used to encapsulate the zirconium dihydride and zirconium dideuteride. The calorimetric system ANL-R1-Pt-1* has been recalibrated by means of combustions of benzoic acid. The results of the calibration experiments are given in Table 22.

Table 22

CALIBRATION OF CALORIMETRIC SYSTEM ANL-R1-Pt-1*

Heat Transfer Coefficient $\alpha \times 10^4$ (sec^{-1})	Mass of Benzoic Acid (g)	Temp Rise ΔT (C)	ϵ(calorimeter) (cal/deg)
0.3397	0.70081	1.23795	3578.14
0.3429	0.70135	1.23903	3578.15
0.3410	0.70133	1.23971	3576.39
0.3411	0.69990	1.23638	3575.50
0.3367	0.70157	1.23999	3576.71

Average = 3577.18

Std Deviation of Mean = $\pm$0.47 or 0.01%

*Stainless steel bomb lined with platinum and used in a rotating bomb calorimeter.

Previous reports (ANL-6287, page 124, and ANL-6379, page 127) have described conditions and techniques for preliminary calorimetric combustion of zirconium dihydride in oxygen. Techniques for zirconium dideuteride combustions are identical. Some modifications in the setup were made prior to the final calorimetric series. The use of a platinum dish lined with zirconium dioxide, in place of an alumina dish, eliminated the formation of carbon during combustions by allowing the dish to become much hotter. Because the surface energy of fine particles may be significant, material of known particle size range was burned. The samples were ground and sieved and particles between 37 and 53 μ were used so that (1) complete combustion with no spattering could be obtained, and (2) the surface energy of the particles could be ignored.

In the final calorimetric series, combustions of zirconium dihydride were alternated with combustions of zirconium dideuteride. The results are being calculated. Preliminary results indicate a very definite difference between the heats of combustion of the two compounds.

Because the polyester film (Mylar) used to encapsulate the zirconium dihydride and zirconium dideuteride contributes approximately 7 percent of the total heat evolved, an accurate value for the heat of combustion of Mylar was determined. Five sq in. of the 100-gauge Mylar (approximately 0.5 g) was used for each combustion. The Mylar was folded six times, giving approximately a $\frac{3}{4}$-in. square. Each sample was equilibrated and weighed in the dry box to eliminate a correction for absorbed moisture. The Mylar was burned at 20 atmos oxygen pressure in a platinum crucible supported in a gimble (the conventional benzoic acid calibration setup). A platinum wire and cotton fuse were used for ignition of the sample. One ml of water was also placed in the bomb, as is customary for combustions in which water is formed in the reaction. Approximately 3000 cal were liberated during the combustion. Results are now being calculated.

b. Combustion of Boron and Boron Nitride in Fluorine (S. Wise)

(1) Combustion of Boron

Experimental work has been completed for the study of the heats of formation of boron trifluoride. A revised value of -270 ± 0.24 kcal/mole has been obtained for the standard heat of formation, ΔH_f°(25 C), of boron trifluoride gas. A manuscript entitled Fluorine Bomb Calorimetry: 3. The Heat of Formation of Boron Trifluoride, has been accepted for publication in the Journal of Physical Chemistry.

(2) Combustion of Boron Nitride

Calorimetric studies have been completed on a sample of the hexagonal form of boron nitride. A preliminary value of -210.43 ± 0.40 kcal/mole has been derived for the heat of combustion (ΔH_c°) of hexagonal boron nitride with fluorine according to the reaction:

$$BN(c,hex) + 3/2\ F_2(g) \rightarrow BF_3(g) + 1/2\ N_2(g) \quad .$$

Using the revised value for the heat of formation of BF_3, a preliminary value of -59.73 ± 0.45 kcal/mole has been derived for the standard heat of formation of hexagonal boron nitride crystal.

Combustions of the cubic form of boron nitride are also being carried out. Because of the scarcity of this material, the number of combustions in this series will be limited.

c. Combustion of Titanium and Hafnium in Fluorine
(E. Greenberg, M. H. O'Leary*)

Calorimetric combustions of titanium in fluorine have been completed. The results of the titanium experiments are presented together with the results for the previously completed combustions of hafnium (see ANL-6379, page 129).

The combustion results for titanium and hafnium, in the energy change per gram of sample burned, are presented in Table 23. Analyses of the titanium samples are not yet complete and the results are, therefore, subject to minor revision. For each of the studies, the value for the heat of formation of the tetrafluoride showed a standard deviation of the mean of about 0.1 kcal/mole.

Three of the hafnium combustions were carried out with a high-purity commercial fluorine (99.75 percent) obtained from the General Chemical Company. Although the data are somewhat limited, the results do not appear to differ significantly from the values obtained using fluorine distilled in our own laboratory (99.95 percent).

Table 24 summarizes the derived data for the formation of the titanium and hafnium tetrafluorides from the respective elements at 25 C. G is the symbol recently adopted by the International Union of Pure and Applied Chemistry (IUPAC) for Gibbs energy. No value is given for HfF_4 because of the unavailability of an entropy value at 25 C for this substance.

*Student Aide from the University of Illinois.

Table 23

RESULTS OF COMBUSTIONS OF TITANIUM AND HAFNIUM IN FLUORINE

	Titanium[a] $\Delta E_c^\circ/M$ (cal/g)	Hafnium $\Delta E_c^\circ/M$ (cal/g)
	-8197.2	-2590.5
	-8192.7	-2591.0
	-8191.1	-2592.1[b]
	-8193.4	-2594.2[b]
	-8204.0	-2594.4[b]
	-8201.4	-2594.0
	-8196.3	-2593.4
		-2593.1
		-2594.7
Average	-8196.6	-2593.1
Std. Dev. of Mean	± 1.8	± 0.5
	± 0.1 kcal/mole	± 0.1 kcal/mole
	0.02%	0.02%

[a]Impurity corrections are incomplete.

[b]High-purity commercial fluorine (99.75 percent) was used. All other experiments were carried out with ANL distilled fluorine (99.95 percent).

Table 24

DATA CALCULATED FROM COMBUSTIONS OF TITANIUM AND HAFNIUM IN FLUORINE

$$\text{Metal(c)} + 2\ F_2(g) \longrightarrow MF_4(c)$$

	TiF_4	HfF_4
$\Delta E_f^\circ = E_c^\circ$ (kcal/mole)	-392.6	-462.9
ΔH_f° (kcal/mole)	-393.8	-464.0
ΔG_f° (kcal/mole)	-372.3	-

d. Combustions of Magnesium, Aluminum, Cadmium, and Zinc in Fluorine
(E. Rudzitis, R. Terry)

The techniques of combustion of magnesium, aluminum, cadmium, and zinc have been developed simultaneously because of similarities in some of their physical and chemical properties. A preliminary calorimetric series of cadmium combustions in fluorine described in the previous report (ANL-6379, page 131) had to be discarded because of difficulties encountered in determining the unburned cadmium in the presence of a large excess of cadmium fluoride. The technique and apparatus have since been improved and satisfactory results have been obtained from calibration experiments.

The determination of electrical ignition energy, which introduces an appreciable correction to the total heat effect, presented another problem. For the above "soft" metals, this quantity is difficult to determine experimentally because of the practically instantaneous and simultaneous melting and fluorination of the ignition wire. The ignition energy and, therefore, the thermal correction was greatly decreased by developing a method whereby the metal sample could be ignited by a very fine wire (approximately one mil in diameter). Application of a similar method to the ignition of benzoic acid reduced the electrical ignition energy from the usual 3 cal to approximately 0.01 cal, which is an insignificant quantity. The benzoic acid pellet was ignited directly (without the use of a cotton thread) by a one-mil platinum wire.

A series of nine such calibration combustions yielded 3602.54 cal/C as the energy equivalent of ANL-R1-Ni4* calorimetric system. The standard deviation from the mean was 0.47 cal/C or 0.013 percent.

Currently, a calorimetric combustion series of magnesium in fluorine is in progress. Magnesium was chosen because the easier recovery of unburned metal, as compared with cadmium, will help to establish more firmly the recovery technique.

e. Combustion of Uranium in Fluorine
(J. Settle)

The calorimetric combustions of uranium in fluorine previously reported (see ANL-6333, page 124) were somewhat unsatisfactory because of the formation of considerable amounts of uranium fluorides other than uranium hexafluoride. About one-third of the uranium pin placed in the reaction vessel was recovered, after the combustion, as unreacted

*Nickel bomb used in a rotating bomb calorimeter.

metal. On the surface of the recovered metal the following compounds were found: UF_3, UF_4, and UF_5, and an unidentified phase which may be U_4F_{17} or U_2F_9 or both. Analysis of the combustion residue was necessary in order to make appropriate thermochemical corrections to the measured heat. However, because of the difficulty of analyzing the complex mixture of uranium metal and its lower fluorides, and because the heats of formation of the lower fluorides are not well known, an uncertainty of at least 0.2 percent was introduced into the calculation of the heat of formation of uranium hexafluoride.

It was realized that the determination of the heat of formation of uranium hexafluoride could be made more precisely if the amounts of lower uranium fluorides remaining after a combustion could be reduced. Many exploratory combustions were performed in an attempt to achieve this reduction through the attainment of a complete reaction of uranium metal with fluorine. These included burning a uranium pin supported by a consumable zirconium pin, burning pelleted mixtures of uranium powder and Teflon powder supported by nickel, alumina, or synthetic sapphire discs, and burning uranium powder spread in a thin layer on nickel, molybdenum, aluminum, or sintered aluminum trifluoride discs. These exploratory experiments did not yield complete combustion of the uranium. They did seem to indicate, however, that the desired result might be obtained by using relatively high fluorine pressures to burn a thin layer of uranium powder supported by a dish made of a substance that would not be shattered by thermal shock, would be resistant to alloying with liquid uranium, and would have a high thermal conductivity.

A combustion was performed in which powdered uranium, supported by an aluminum dish, was burned in fluorine at about 18 atmos pressure. The result was an apparently complete conversion of uranium to uranium hexafluoride. However, the aluminum dish suffered considerable surface fluorination. It was thought that the surface fluorination of the supporting dish might be decreased if the dish were made of a metal, such as copper, silver, or gold, which has a higher thermal conductivity than aluminum.

Silver, because it does not form compounds with uranium, was the first to be tried as a supporting dish. The uranium powder was spread on a shallow dish made from 0.030-in.-thick sheet silver. The silver dish was supported by a $\frac{3}{8}$-in.-thick aluminum disc which served as a heat sink. The aluminum disc was in contact with a nickel plate which was fastened to the bomb cap with nickel screws. Fluorine was admitted to the bomb, the uranium ignited, and additional fluorine was allowed to enter the bomb for about 45 sec, at which time the total pressure in the bomb was about 9.5 atmos. A pressure surge up to about 17 atmos occurred and the supply of fluorine was shut off from the bomb. Within about 10 sec, the cap of the bomb was ruptured at one small point, and the

gases contained in the bomb and a small amount of molten material were ejected from the bomb into the hood in which the experiment was taking place. Subsequent visual examination of the contents of the bomb revealed that all of the metal supporting plates had melted. It is thought that the following chain of events may have occurred during the combustion:

(1) The burning uranium supplied enough heat to melt and/or ignite the silver dish.

(2) The molten silver entered into an exothermal alloying reaction with the aluminum. The heat produced by the alloying reaction was sufficient to melt the aluminum.

(3) The molten aluminum entered into a further exothermal alloying reaction with the nickel, thus leading to the rupture of the vessel.

This possible series of events was deduced in the following way. During the experiment, the bomb contained 0.17 mole fluorine, 0.01 mole uranium, 0.19 mole silver, 1.48 moles aluminum, and 0.58 mole nickel fittings. The aluminum-silver eutectic[22] contains about 28 atom percent aluminum and melts at 566 C. The nickel-aluminum eutectic[15] contains about 2.7 atom percent nickel and melts at 640 C. Assuming that these eutectics were formed during the experiment, it is estimated that 10,000 cal were required to melt the two eutectics. In addition, about 14,000 cal were required to melt the 0.55 mole of nickel in the fitting which was not required for eutectic formation and an estimated 0.5 mole of nickel from the bomb cap. Thus, the least amount of heat required to accomplish the melting of the metals was about 24,000 cal. The maximum amount of heat that could have been produced by fluorination reactions was about 35,000 cal, if all of the available fluorine (0.17 mole) reacted with aluminum to form AlF_3. Because the reaction was initiated by the spontaneous ignition of uranium powder when fluorine was admitted to the reaction vessel, not all the fluorine was available to react with aluminum. In addition, because the melting had to proceed from the uranium to the silver to the aluminum, it is likely that the silver was fluorinated to some extent, thus further reducing the amount of fluorine available to react with aluminum. When the bomb ruptured, some fluorine was released to the atmosphere. It is, therefore, likely that less than 20,000 cal were produced by fluorination reactions. This estimate leads to the belief that other sources of heat contributed to the extensive melting. No values for the heats of formation of aluminum-silver compounds are available. The heats of formation of aluminum-copper compounds[23] vary from -10,000 to -16,000 cal (exothermal)/mole. It is quite possible, therefore, that the alloying of aluminum and silver may also be an exothermal process. The

---

[23] Selected Values of Chemical Thermodynamic Properties, National Bureau of Standards Circular 500, U. S. Government Printing Office, Washington, D. C. (1952).

heats of formation of aluminum-nickel compounds[16] vary from -34,000 to -38,000 cal/mole. It is reasonable to assume that these exothermal alloying reactions did supply the excess heat produced in the experiment.

If additional experiments of this type are performed, more attention will be given to the possibility of reactions between the metals used in the reaction vessel.

A new bomb cap, with a built-in nickel heat sink, has been fabricated. It is expected that more efficient transfer of heat from the reaction zone can be achieved by placing the sample support dish in direct thermal contact with the more massive bomb cap. The ANL-R1-Ni-1M* calorimetric system, in which the new bomb cap is used, has been calibrated by burning National Bureau of Standards' Sample 39h benzoic acid in oxygen. Pertinent data are presented in Table 25. The standard energy of combustion of benzoic acid 39h is 6317.96 cal/g under the conditions in which it was burned in this calorimetric system. The first column gives the energy of combustion of the mass of benzoic acid used in each experiment. The energy of combustion of the cotton thread, which was used as a fuse to ignite the benzoic acid, is 4.05 cal/mg; Column 2 lists the energy of combustion of the short length of cotton thread used in each experiment. In three of the experiments, minute specks of carbon were recovered after the combustions.

Table 25

CALIBRATION OF CALORIMETRIC SYSTEM ANL-R1-Ni-1M*

ΔE_c Benzoic Acid 39h (cal)	ΔE_c Cotton Thread (cal)	ΔE_c Carbon Residue (cal)	ΔE Ignition (cal)	$\Delta E^\dagger$ Contents (cal)	Temp Rise ΔT (C)	ϵ(calorimeter) (cal/deg)
6316 51	5 91	0 32	1 94	-24 28	1 74776	3604 84
6312 72	5 55	0 00	1 94	-24 26	1 74666	3604 57
6316 51	5 35	0 00	1 94	-24 28	1 74761	3604 65
6319.03	5 79	0 08	1 89	-24 29	1 74895	3603 59
6318 78	6 88	0 00	1 94	-24 28	1 74809	3605 83
6312 97	6 16	0 39 ± 0 20	1 94	-24 22	1 74639	3505 86 ± 0 11
6315 50	5 87	0.00	1 94	-24 23	1 74716	3605 33
6316 00	5.99	0 00	1 94	-24 28	1 74768	3604 58

Average = 3604 91 cal/deg

Std Deviation of the Mean = ±0 39 cal/deg or 0 01%

$^\dagger\Delta E$ contents = $[\epsilon^f(\text{cont.}) - \epsilon^1(\text{cont.})]\,[25 - T^1] - [\epsilon^f(\text{cont.})]\,[\Delta T]$.

*Nickel bomb used in a rotating bomb calorimeter.

Appropriate corrections for the energy of combustion of carbon are given in Column 3. The amount of electrical energy used to start the combustion is listed next. The column headed by ΔE contents gives the amount of energy absorbed by the contents of the calorimetric bomb in raising them from the initial temperature of about 23 C to the reference temperature of 25 C. The temperature rise of the calorimetric system, corrected for heat exchanged with its environment and for stirring energy, is listed as ΔT. The energy equivalent of the calorimetric system, ϵ(calor), is the sum of the energy terms divided by the corrected temperature rise.

Now that the new calorimetric system has been calibrated, the investigation of the heat of combustion of uranium in fluorine will be resumed.

f. High-temperature Enthalpy Calorimeter
(D. R. Fredrickson, R. L. Nuttall, E. D. West*)

The calorimetric system to measure changes in enthalpy up to 1500 C is being assembled.

The vacuum system for the furnace component provides a vacuum of 3.2×10^{-7} mm of Hg at room temperature. Further outgassing will be done by heating the three sets of molybdenum furnace windings. While this is being done, the performance of various thermocouples within the furnace will also be checked.

A dual vacuum system has been designed to be used for both the calorimeter and vacuum valve. Certain machined parts and the cold trap are being fabricated by the shops. Other items, such as valves and piping are being collected and the vacuum system will be assembled upon completion of machined parts.

The drop mechanism has just been completed and test drops at various drop speeds will be tried with the unit before installing it in the calorimetric system.

*Consultant, National Bureau of Standards.

II. FUEL CYCLE APPLICATIONS OF VOLATILITY AND FLUIDIZATION TECHNIQUES

The volatilities of uranium and plutonium hexafluorides are the basis of a direct fluorination volatility process proposed for the recovery of uranium and plutonium from irradiated nuclear reactor fuels. In this process fluidization techniques are also used to advantage. Progress is being made in the application of this process to uranium oxide and zirconium-matrix fuels.

The proposed process for recovery of uranium and plutonium from spent uranium oxide involves decladding by an appropriate reaction in a fluidized bed. Plutonium and uranium hexafluorides, which result from the reaction of the declad oxide fuel with fluorine, may be separated by using a combination of the variability of the rates of fluorination of the plutonium and uranium compounds and chemical reactivities of the hexafluorides.

The direct fluorination of dense uranium dioxide pellets is being examined in a 3-in.-diameter, air-cooled reactor. In order to obtain further information on the effect of temperature under process conditions, a fluorination of a 6-in.-deep bed of pellets was carried to completion at 400 C in the presence of an oxygen diluent resulting from the recycle process gas. In 11.0 hr, 86 percent of the charge was recovered as uranium hexafluoride product with an overall fluorine utilization efficiency of 82 percent. Although this batch reaction time is not considered excessive, equivalent reaction has been carried out at 500 C in 40 percent of the time. It is believed that higher rates can be obtained at 400 C by increasing the fluorine concentration, which averaged only about 16 percent in this run. Further studies of processing conditions are planned along the lines of determining the role of oxygen on overall fluorination rate, close temperature control over a wider range of reaction rates, and optimum fluorination of the pellet residues at the end of a batch reaction.

Because of a pronounced effect of the presence of oxygen on the fluorination rate, attempts are under way to measure the oxidation rate alone. In very preliminary results, oxidation of uranium dioxide pellets at 300 C was readily detected; the rate increased with temperature up to 600 C, the highest temperature employed.

Since in practice the rate of fluorination is limited by heat transfer rather than reaction kinetics, efforts have been made to enhance heat removal by utilization of a packed-fluidized-bed system. A packed-fluidized-bed system employs inert fluidizing material in the voids of a bed of larger particles so as to provide better heat transfer characteristics. A study was made of this type of heat transfer in a mockup system, showing the effect of different types and sizes of packing and different size of material

fluidized in the voids of the fixed packing. The effective radial thermal conductivity was found to increase with increasing gas velocity and to be higher for larger packing. The effective thermal conductivity of packed-fluidized beds was as high as 10 Btu/(hr)(sq ft)(F/ft) compared to that for fixed beds of about 0.4 Btu/(hr)(sq ft)(F/ft). The film coefficients for the heating and cooling surfaces were found to be as much as five times that for fixed beds. Film coefficients followed the same general trends with various particle sizes as did the effective thermal conductivities, but the variations in film coefficients were considerably smaller over the ranges of the variables. Film coefficient values and thermal conductivities in the packed-fluidized system were similar to values obtained in previous studies of packed-fluidized systems.

Laboratory-scale experiments have been performed in which fluorination reactions have been carried out with aluminum oxide as the inert bed material. It has been concluded that the use of high-purity refractory grain Alundum results in lower values of residual plutonium (~0.02 percent) than those obtained with either zirconium or calcium fluoride. It is also concluded that the use of recycled fluorine is feasible, since oxygen does not exert a deleterious effect on plutonium retention in Alundum. The use of Alundum for more than a single fuel loading may be limited not only by the accumulation of fission products but also by the increase of plutonium retention in the Alundum with reuse of the bed material. After the reuse of Alundum in five successive experiments, the plutonium concentration in the Alundum rose to approximately 0.1 percent.

Studies are being conducted on a fluidization-volatility scheme for separating and recovering uranium from zirconium-base fuels. The process involves initial separation of the zirconium by reaction of the low uranium-zirconium alloy with hydrogen chloride forming the volatile zirconium tetrachloride, which is allowed to pass out of the system. Uranium forms the solid uranium trichloride. Uranium is recovered as uranium hexafluoride by fluorination of the uranium chloride.

Laboratory studies reported in the previous quarterly (ANL-6379, page 150) indicated that, for optimum recovery of uranium from enriched uranium-zirconium alloy fuels, it is best to declad and remove the zirconium by hydrochlorination at or above 350 C. The hydrochlorination of the zirconium and the subsequent fluorination of the uranium chlorides can be carried out in a fluidized bed of granular solids. The uranium particulate is expected to be retained, for the most part, in the inert fluid-bed medium in which the primary reaction is conducted. Uranium entrained by the volatile material will be filtered by suitable means. Of those bed materials tested, Alundum, refractory aluminum oxide, was most satisfactory. In this report laboratory tests of three types of Norton's refractory grain Alundum are discussed. The purest grade of electrically fused refractory grain alumina yielded the best results.

In previous engineering-scale studies, both uranium-zirconium alloy constituents were converted to fluorides and it is believed the zirconium inhibited complete uranium recovery. Initial engineering-scale work is directed toward the evaluation of fixed beds of high-fired aluminum oxide as filters for the retention of entrained uranium particulate. The uranium is recovered from the fixed bed of aluminum oxide by fluorination. Up-flow and down-flow systems are being tested with a 1.5 in.-diameter fluidized reaction zone and a 3.0-in.-diameter filter zone. Both up-flow and down-flow experiments show lower uranium losses may be achieved by using small filter-bed particles (200 mesh size). Higher gas velocities (in the range tested, 0.23 to 0.75 ft/sec) gave lower uranium losses in the down-flow case whereas the reverse was true for up-flow. Bed depth in the range from 3 to 12 in. has not been found critical. Overall losses were in the range from 0.1 to 0.6 percent of the uranium reacted (up to 7.6 g maximum charged as 2.7 weight percent uranium-zirconium alloy in the form of 1/4-in., irregularly shaped cubes). The hydrochlorination was conducted in the range from 550 to 400 C with 20 to 70 mole percent hydrogen chloride in nitrogen

Preliminary corrosion tests of 35- and 170-hr duration made to evaluate possible materials of construction showed rates of 0.2 mil/month (determined by weight loss) for A-nickel and Inconel exposed to zirconium tetrachloride vapor (2000 mm Hg pressure) at temperatures of 370 C. Appreciable diminution of the rate occurs with time. Sintered porous nickel coupons (possible filter material) showed significant weight loss, but quantitative values cannot be assigned because of difficulties in determining true exposed surface areas.

Studies were essentially completed this quarter on the development of a two-step fluid-bed process for converting uranium hexafluoride to uranium dioxide. This work has been conducted in an effort to provide a simpler method for preparation of ceramic reactor fuel. Equipment modifications for the first step, steam-hydrolysis of the hexafluoride to uranyl fluoride, which permitted elutriation of fines from the reaction zone, have apparently solved all of the previous operating problems associated with particle size control of the bed, and extended runs to 25 hr in duration have been made. Nominal operating conditions used for the 3-in. diameter reactor were 100 g/min hexafluoride feed (174 lb uranium/(hr)(sq ft)), 230 C bed temperature, approximately 15-in. static bed height, 0.75 ft/sec superficial fluidizing gas velocity, steam excesses of 245 percent and a recycle solids feed rate near 15 percent. Average bed particle size was maintained near 350 μ.

The second step, reduction of uranyl fluoride to uranium dioxide, has been conducted as a batch operation. A 50-50 mixture of steam and hydrogen at temperatures near 650 C appears optimum. Static bed heights to 21 in. (L/D = 7) have been used. Material containing less than 200 ppm fluoride has been produced in periods of 3 to 4 hr, the time period depending

on reactant excesses. Conversion rate also appears to be dependent on particle size, smaller particles giving somewhat better conversion times. Particle densities as determined by immersion in xylene, water, and mercury were 9.68, 9.23, and 6.22 g/ml, respectively. Reactor (nickel) corrosion in 4-hr experiments resulted in nickel content in the product of 100 to 130 ppm.

In recent engineering-scale studies, components were developed which proved valuable in fluoride volatility work. Descriptions are given of an automatic, remote-recording chain balance for weigh tank applications and an all-metal fluorine analyzer. In addition, a baffled-cone gas distributor for fluid-bed reactors has been developed and appears promising in mock-up tests.

Improved operation of a small-diameter column for continuous fluid-bed calcining where criticality must be considered has been achieved in recent feasibility studies. A $2\frac{1}{4}$-in.-diameter column with 1 M aluminum nitrate feed is currently in use with vertical upward spraying of the feed, achieved by mounting the feed spray nozzle in the apex of the cone bottom, permitting use of atomizing and feed decomposition gases as the fluidizing gas medium. Runs to 6-hr duration at an air-to-liquid volume ratio of 1740 gave moderate fines production (five percent less than 140 mesh) using a 325 g bed of -20 +80 mesh aluminum oxide. A 3-hr run at an air-to-liquid ratio of 1070, achieved by increasing the feed rate from 8.7 to 14.0 ml/min while maintaining the atomizing air rate constant (0.54 scfm), gave the best results to date, only one percent less than 140 mesh material being produced. The current series of runs was carried out at bed temperatures near 330 C. The primary objective in future work will be to demonstrate reliability of the operation.

A. Laboratory Investigations of Fluoride Volatility Processes (J. Fischer)

1. Fluorination of Plutonium-Uranium Dioxide (L. Anastasia, L. Trevorrow, R. Jarry, T. Baker)

The Direct Fluorination Volatility Process for low-enrichment power reactor fuels utilizes a step in which uranium dioxide fuel is reacted with fluorine at 450 C to remove uranium and plutonium as the volatile hexafluorides. The fluorination step can be carried out in a reactor containing a fluidized bed of inert solids. Zirconium tetrafluoride, calcium fluoride, and refractory aluminum oxide have been tested for use as inert solids. In order to minimize the plutonium loss to the inert bed material, several batches of fuel might be processed with the same charge of bed material. The number of times the material could be reused would depend on the extent of uranium and, particularly, plutonium retention on the inert solids. Reuse would also depend on the capacity of the inert solids and the reaction vessel

to dissipate the heat due to the accumulated fission products. For economy in the use of fluorine, a recycle system would be used and the fluorine would become diluted with oxygen resulting from the fluorination of uranium dioxide.

Results have been previously reported (ANL-6379, pages 142 and 143) for the fluorination of mixtures of uranium and plutonium oxides in beds of zirconium tetrafluoride or calcium fluoride. This report presents the results of experiments in which fluorination reactions have been carried out with aluminum oxide as the inert bed material. The effects of reuse of the bed material and dilution of fluorine with oxygen on the plutonium retention have been investigated.

A description of the experimental equipment was given in a previous report (ANL-6379, page 139). Two grades of Norton's refractory aluminum oxide (Alundum) were used: Type 38, and Blue Label, a highly purified grade. Spectral analyses of both grades of Alundum are given in Table 31 (see page 118).

The sample to be fluorinated was prepared by mixing ground, solid solutions of plutonium-uranium dioxides with the Alundum. The resultant mixture, contained in a nickel boat, was then placed in a horizontal tube reactor. The reactor was brought to the reaction temperature, and fluorine was recycled through the system at a flow rate of 800 cc/min at a pressure of about one atmosphere. Uranium and plutonium hexafluorides formed by the reaction were removed from the gas stream by a series of two cold traps held at -80 C. At the completion of an experiment, the residue was weighed and analyzed for uranium and plutonium.

In all of the experiments, 10 hr of reaction with fluorine resulted in a residue in which the concentration of uranium was reduced to a satisfactory level ($\leq$0.01 weight percent). Therefore, further discussion of the results will deal mainly with plutonium retention in the Alundum.

In the first group of experiments, the effects of impurities in the Alundum and of reaction temperature were investigated. The results of the fluorination of uranium-plutonium dioxides from mixtures with both grades of Norton's refractory grain Alundum are listed in Table 26. In all of these experiments, except for Experiments 52 and 53, 60 mesh, high-purity, Blue Label Alundum was used; in Experiments 52 and 53, -60 + 100 mesh, Type 38 Alundum was used. At 350 and 450 C, a residual concentration of about 0.03 weight percent plutonium in the high-purity, Blue Lable Alundum was obtained after fluorination. Residual plutonium at 500 C was about 0.05 weight percent and 0.11 weight percent at 550 C. After fluorination of the oxides at 450 C, the residual plutonium concentration in Type 38 Alundum was 0.17 weight percent (Experiment 52); with the use of prefluorinated Type 38 Alundum (Experiment 53), residual plutonium was reduced to 0.11 weight percent.

Table 26

REACTION OF URANIUM-PLUTONIUM DIOXIDES, ALUNDUM MIXTURES WITH FLUORINE

Fluorine Recycle Rate: 800 cc/min
Fluorine Pressure: ~1 atmos
Alundum Particle Size: Blue Label[a]: 60 mesh
Fluorination Time: 10 hr

		Initial Sample					Residue				
Exp No	Temp (C)	Wt Al_2O_3 (g)	Wt U (mg)	Wt Pu (mg)	U (w/o)	Pu (w/o)	Wt Solids Recovered (g)	Wt U (mg)	Wt Pu (mg)	U (w/o)	Pu (w/o)
47[b]	350	1.99	810	38.7	27.0	1.29	1.83	0.09	0.53	0.005	0.029
54[d]	450	0 90	0.07	0.32	0.008	0.035	0.91	0.05	0.18	0.0056	0.020
55[b]	450	1.99	1025	43.8	34.2	1.46	1.98	0.13	0.53	0.0067	0.027
52[c]	450	2.04	825	37.9	27.4	1.26	2.11	0 74	3.60	0.035	0.17
53[b,c]	450	2.03	822	37 8	27.4	1.26	2.04	0.35	2.24	0.017	0.11
61[b]	500	2.24	800	37.9	23.9	1.13	2.31	0.21	1.39	0.009	0.060
63[b]	500	2.26	808	38.2	23.9	1.13	2.28	0.41	0.91	0.018	0.040
49[b]	550	2.41	955	45 7	27.0	1.29	2.40	0.67	3.24	0.028	0.135
56[b]	550	2.11	1090	46.5	34.2	1 46	(2.64)[e]	(0.29)	(2.38)	0.011	0.090

[a] See Table 31 (page 118) for spectral analysis of Alundum.
[b] The Alundum was prefluorinated 3 hr at 300 C and an additional hour at 400 C.
[c] Norton's Type 38 Alundum, -60 +100 mesh, was used in Experiments 52 and 53.
[d] The initial sample for Experiment 54 was the residue from Experiment 48, previously fluorinated for 10 hr (see ANL-6379, page 143).
[e] Residue weight questionable because of contamination by nickel fluoride scale from reactor wall

In Experiment 54, the residue from a previous oxide fluorination from 60 mesh high-purity Alundum (Experiment 48, see ANL-6379, page 143) was fluorinated for an additional 10 hr; the additional fluorination reduced plutonium retention from 0.035 weight percent to 0.02 weight percent. A comparison of all the results is given in Table 27.

It is noted that residual plutonium in Type 38 Alundum is somewhat higher than values obtained with the high-purity material at 450 C. It is thought that the difference in plutonium retention may be attributed to both the smaller particle size and the impurities present in Type 38 Alundum. It is also noted that plutonium retention in high-purity Alundum increases as the temperature of fluorination is increased.

The fluorinations of uranium-plutonium oxides from Alundum have all been carried out in a recycle flow system. Some dilution of the fluorine with oxygen resulted as the uranium oxide reacted with the fluorine.

Table 27

SUMMARY[a] OF PLUTONIUM FLUORINATIONS FROM SOLID SOLUTIONS OF URANIUM-PLUTONIUM DIOXIDES AND PHYSICAL MIXTURES WITH ALUNDUM

Gas Flow Rate: 800 cc/min
Total Pressure: ~1 atmos
Fluorination Time: 10 hr
Alundum Particle Size: Blue Label: 60 mesh
Type 38: -60 +100 mesh

Exp No.	Temp (C)	Plutonium[b] Volatilized (%)	Residual Plutonium (w/o)
	Norton Blue Label Alundum		
40[c]	350	99	0.028
47	350	99	0.029
48[c]	450	98	0.035
54	450	100[f]	0.020
55	450	99	0.027
65	450	98	0.029
70[d]	450	97	0.010
61	500	96	0.060
63	500	98	0.040
64[d]	500	97	0.064
38[c]	550	96	0.068
49	550	93	0.135
56	550	(95)[e]	0.090
	Norton Type 38 Alundum		
52	450	90	0.17
53	450	94	0.11
59[d]	450	97	0.058

[a] See Tables 26, 28, and 29 for complete data.
[b] Percent decrease of plutonium over amount in original sample.
[c] Previously reported in ANL-6379, page 143.
[d] 25 v/o oxygen in fluorine.
[e] See note e, Table 26.
[f] Based on amount of plutonium in initial sample of Experiment 48; see Table 26.

However, the volume of the experimental reactor system is large compared to the volume of oxygen released from the oxides during a particular experiment; therefore, dilution of the fluorine with oxygen was in the range 1 to 3 percent. In plant-size fluorination equipment, the ratio of uranium dioxide to the volume of the system will be much larger than that used in the laboratory fluorinations. Therefore, to simulate the conditions that might exist in plant-size fluorinations, several experiments were made with fluorine initially containing 25 percent oxygen. The detailed results are shown in Table 28 and are also included in Table 27 for comparison with the other fluorination experiments. At a fluorination temperature of 500 C (Experiment 64), the additional oxygen appeared to have little or no effect on the residual plutonium found in Blue Label Alundum; the value of 0.064 weight percent obtained in Experiment 64 compares with values of 0.060 and 0.040 weight percent obtained in Experiments 61 and 63, respectively (see Table 27). However, at a fluorination temperature of 450 C, with both high-purity and Type 38 Alundum, (Experiments 70 and 59), plutonium retention in the Alundum was slightly lower after fluorination with 25 percent oxygen in fluorine than with recycle fluorine. With high-purity Alundum, the comparative values were 0.010 weight percent after fluorination by oxygen-fluorine vs. 0 03 weight percent with fluorine; similarly, the level of plutonium retention in Type 38 Alundum was 0.058 weight percent after fluorination with oxygen-fluorine and this value compares with 0.11 weight percent after fluorination with fluorine. It is concluded from these results that additional oxygen causes no deleterious effects on plutonium removal from Alundum

Table 28

REACTION OF URANIUM-PLUTONIUM DIOXIDES, ALUNDUM MIXTURES WITH FLUORINE EFFECT OF OXYGEN ADDITION TO FLUORINE

Gas Flow Rate	800 cc/min
Total Pressure	~1 atmos
Oxygen to Fluorine Volume Ratio	$\frac{1}{3}$
Alundum Particle Size	Blue Label 60 mesh[a] Type 38 -60 +100
Fluorination Time	10 hr

	Initial Sample						Residue				
Exp No	Temp (C)	Wt Al_2O_3 (g)	Wt U (mg)	Wt Pu (mg)	U (w o)	Pu (w/o)	Wt Solids Recovered (g)	Wt U (mg)	Wt Pu (mg)	U (w/o)	Pu (w o)
59[b]	450	2 05	745	36 1	24 1	1 17	2 10	0 31	1 22	0 015	0 058
70[c]	450	1 94	791	35 5	27 0	1 21	1 99	0 06	0 20	0 003	0 010
64[c]	500	2 35	1034	47 1	29 1	1 33	2 36	0 38	1 51	0 016	0 064

[a] See Table 31 (page 118) for spectral analysis of Alundum

[b] Type 38 Alundum

[c] Blue Label Alundum

The possible reuse of Alundum for more than one fluorination was investigated by using a single sample of Alundum in a series of five fluorination experiments. The experimental procedure consisted of adding the solid solutions of uranium-plutonium dioxides to 4.63 g of prefluorinated Blue Label Alundum. The concentration of plutonium was about 1 weight percent in the starting mixture. This mixture was sampled and then fluorinated for 10 hr at 450 C with recycled fluorine at a flow rate of 800 cc/min. After the reaction residue was sampled, the plutonium concentration in the remaining residue was increased to 1 weight percent by the addition of uranium-plutonium oxides. The resultant mixture formed the starting material for the next experiment. This procedure was followed for Experiments 65 through 69; the results are listed in Table 29.

Table 29

REACTION OF URANIUM-PLUTONIUM DIOXIDES, ALUNDUM MIXTURES WITH FLUORINE· EFFECT OF REUSE OF NORTON'S BLUE LABEL ALUNDUM[a]

Alundum Particle Size:	60 mesh
Fluorine Recycle Rate:	800 cc/min
Fluorine Pressure:	~1 atmos
Temperature.	450 C
Fluorination Time:	10 hr

	Initial Sample						Residue				
Exp No	Residue from Exp	Wt Al_2O_3 (g)	Wt U (mg)	Wt Pu (mg)	U (w/o)	Pu (w/o)	Wt Solids Recovered (g)	Wt U (mg)	Wt Pu (mg)	U (w/o)	Pu (w/o)
65[c]	-	4 63	1327	59 8	21.1	0 95	4 65	0.42	1.35	0.009	0.029
66	65[b]	3 76	1126	52.2	22.0	1.02	3 77	0 72	3.92	0.019	0.104
67	66[b]	2 90	874	43.2	22.2	1 10	2 92	0 55	2.98	0 019	0.102
68	67[b]	2 05	582	28.7	21 1	1.04	2 12	0 41	2.41	0.018	0.106
69	68[b]	1 25	334	16.3	20.5	1.00	1.20	0 19	1.08	0 016	0 090

[a] See Table 31 (page 118) for spectral analysis of Alundum.

[b] Uranium-plutonium dioxides added to increase initial plutonium concentration to about 1 weight percent

[c] Initial Alundum sample was prefluorinated 3 hr at 300 C and an additional hour at 400 C.

A value of 0.029 weight percent plutonium in the Alundum residue after the initial fluorination is in good agreement with results obtained previously at 450 C. After the second use of Alundum, the residual plutonium concentration increased to a value of 0.104 weight percent and remained at about that level in the three subsequent fluorinations. A parallel pattern of retention is also noted with uranium. These results indicate that the plutonium concentrations in a batch of Alundum used in a fluidized-bed reactor might be expected to increase to a level of about 0.1 weight percent after the second use of Alundum and to remain at that level in any subsequent use.

On the basis of results obtained by fluorination of uranium-plutonium dioxides from mixtures with zirconium tetrafluoride, calcium fluoride, and Alundum, it is concluded that the use of high-purity refractory grain Alundum results in lower values of residual plutonium than those obtained with either the zirconium or calcium fluorides. It is also concluded that the use of a recycled fluorine stream is feasible in the design for a full-scale process fluorinator, since oxygen does not exert a deleterious effect on plutonium retention in Alundum. However, the use of Alundum for more than a single fuel loading may be limited not only by accumulation of fission products but also by the increase of plutonium retention in the Alundum with reuse of the bed material.

2. Direct Fluorination Process for Enriched Uranium-Zirconium Alloy Fuels
(C. Johnson, J. Stockbar)

The Direct Fluorination Process for the recovery of uranium from enriched uranium-zirconium alloy fuels has previously been described (ANL-6379, page 146). Brookhaven National Laboratory is also investigating this process.[24] The Direct Fluorination Process utilizes gas-metal reactions to convert the constituents of the alloy to compounds from which the uranium can be recovered by reaction with fluorine to produce volatile uranium hexafluoride. The fuel is initially reacted with hydrogen chloride in the first stage (lower zone or first vessel) of a fluid-bed reactor. Uranium remains behind in the first stage as uranium tetrachloride while zirconium tetrachloride is volatilized into the second stage (upper zone or second vessel) of the reactor, where it can be reacted with hydrogen fluoride to form zirconium tetrafluoride. The uranium compound remaining in the first stage is then reacted with fluorine to produce volatile uranium hexafluoride, which is distilled from the reaction vessel.

Data previously reported (ANL-6379, page 156) indicated that the optimum fluorination temperature, using fluorine, is 350 C and that refractory aluminum oxide (Alundum) is a suitable bed material. There are a variety of grades of Alundum differing in purity; therefore, further experimental work was done to determine what grade would be suitable for use. Three types of Norton's refractory grain Alundum were tested. They were (1) refractory grain, electrically fused, crystalline, aluminum oxide (Blue Label); (2) refractory grain, aluminum oxide, Type 38; and (3) commercial Type X, abrasive grain, aluminum oxide.

---

[24] Reilly, J. J., Regan, W. H., Wirsing, E., and Hatch, L. P. Status Report: Reprocessing of Reactor Fuels by Volatilization through the Use of Inert Fluidized Beds, BNL-663 (T-217) (May 1961).

The experimental procedure was as follows: the uranium-zirconium alloy was submerged in a bed of Alundum in the lower zone of a laboratory two-stage fluid-bed reactor (ANL-6379, page 156). The alloy was first reacted with hydrogen chloride to form volatile zirconium tetrachloride and nonvolatile uranium chlorides. The volatile zirconium tetrachloride was then converted to zirconium tetrafluoride by reaction with hydrogen fluoride in the upper zone of the reactor and collected on nickel wool which separated the two stages. The hydrochlorinations were run at gas velocities such that the granular bed in the lower zone remained static. After the hydrochlorination was completed the reactor was placed in a dry box and disassembled. The granular bed was removed, thoroughly mixed, and then replaced in the reactor. Nonvolatile uranium chlorides, remaining in the bed, were separated from the bed material by fluorination of the uranium to uranium hexafluoride. During fluorination the gas velocities were sufficient to fluidize the bed.

The data from experiments, using various grades of refractory aluminum oxide as bed materials, are given in Table 30. From these results it appears that the electrically fused refractory grain alumina ("Blue Label") is suitable for use as a bed material.

Table 30

FLUORINATION OF URANIUM RESIDUE FROM HYDROCHLORINATION OF URANIUM-ZIRCONIUM ALLOY[a]

Temp: 350 C

Two-stage fluid-bed reactor (see above for description of experiment)

Type of Alumina	Uranium Concentration (%)	
	Initial	Final
Blue Label	(1.0)[b]	5.2×10^{-3}[c]
		4.0×10^{-3}[c]
Blue Label	2.0	8.5×10^{-3}[d]
Blue Label	1.9	6.8×10^{-3}[d]
Type 38	1.5	2.7×10^{-2}[d]
Type 38	(1.5)[b]	2.7×10^{-2}[d]
Type X	(1.5)[b]	8.0×10^{-2}[d]

[a] Material fluorinated was solids remaining in lower zone of reactor after hydrochlorination.

[b] Calculated value.

[c] Fluorinations of thin beds in flat boat in horizontal reactor.

[d] Fluorination in vertical reactor. Materials mixed in dry box after hydrochlorination and returned to lower zone of reactor for reaction with fluorine.

Specifications received from the Norton Company indicate that "Blue Label" and "Type 38" contain a minimum of 99 percent pure aluminum oxide. For the Type X material, specifications give 94.4 percent aluminum oxide. Results of spectral analysis of the solids are given in Table 31.

Table 31

SPECTRAL ANALYSIS OF NORTON'S ALUNDUM

Element	Blue Label (%)	Type 38 (%)	Type X (%)
Fe	0.01	0.03	0.2
Mg	<0.01	<0.01	0.08
Na	<0.01	0.2	<0.01
Si	<0.01	0.08	0.5
Ti	<0.01	<0.01	0.8
Zr	0.01	<0.01	0.03

B. Engineering-scale Investigations of Fluoride Volatility Processes
(A. A. Jonke)

1. Direct Fluorination of Uranium Dioxide Fuel
(J. D. Gabor, J. Wehrle, R. Kinzler, D. Armstrong* and W. J. Mecham)

Pilot plant-scale work has been directed toward the optimization of process conditions for the fluorination of uranium dioxide pellet fuel. In previous work (ANL-6379, pages 159 to 171), the use of oxygen to dilute fluorine was shown to give the shortest time for complete fluorination of a batch of pellets. Also, in a series of runs to show the effect of temperature on fluorination rates, under standard operating conditions, it was found that the oxygen-diluent fluorinations proceeded at rates of about 5 times those for runs without oxygen over a range of temperatures from 350 to 500 C. Presumably the oxygen reacts with the uranium dioxide to form higher oxides which spall off the pellet surface and enter the inert fluid bed as fines. These fines are expected to present a high surface area to the fluorine reagent gas.

Batch fluorinations carried to completion to date have been nearly all at 500 C. This temperature was favored on the basis of providing a high reaction rate but still maintaining a satisfactory equipment life.

*Co-op student attending Northwestern University.

Although the effect of temperature on the reaction rate under particular conditions has been reported previously, it has appeared desirable to extend batch fluorination studies to lower temperatures in order to observe the temperature effect on the complete course of fluorination of uranium dioxide pellet charges. In the present period the fluorination of a 6-in. bed of pellets was carried to completion at 400 C (Run UOF-42).

In Run UOF-42 the temperature was controlled at 400 C by automatic regulation of the fluorine input. Off-gas recycle was used, with a recycle pump rate of 0.6 cu ft/min. Thus the fluorine was diluted with oxygen during the run. The charge was a 6-in. bed (4.4 kg) of uranium dioxide pellets and a 3-ft inert bed of Alundum (fused aluminum oxide) particles. The run was carried out for a total of 11 hr, and 86 percent of the original uranium dioxide charge was fluorinated. Although the fluorination rate had dropped to a very low value in the last hour, an appreciable amount of uranium dioxide was found unreacted in the bottom of the column. This is believed due to the low temperature noted at the column inlet. Provisions for improved heating at the point is being made for future runs.

The uranium hexafluoride collection during this run is shown in Figure 23, and the fluorine concentrations in the inlet and outlet streams are shown in Figure 24.

FIGURE 23
URANIUM HEXAFLUORIDE COLLECTION FOR RUN UOF-42

6-inch Pellet Bed
4 4-kg Charge of UO_2
0 6-cfm Recycle Rate
36-inch Alundum Inert Bed
Temperature Control Point 400 C

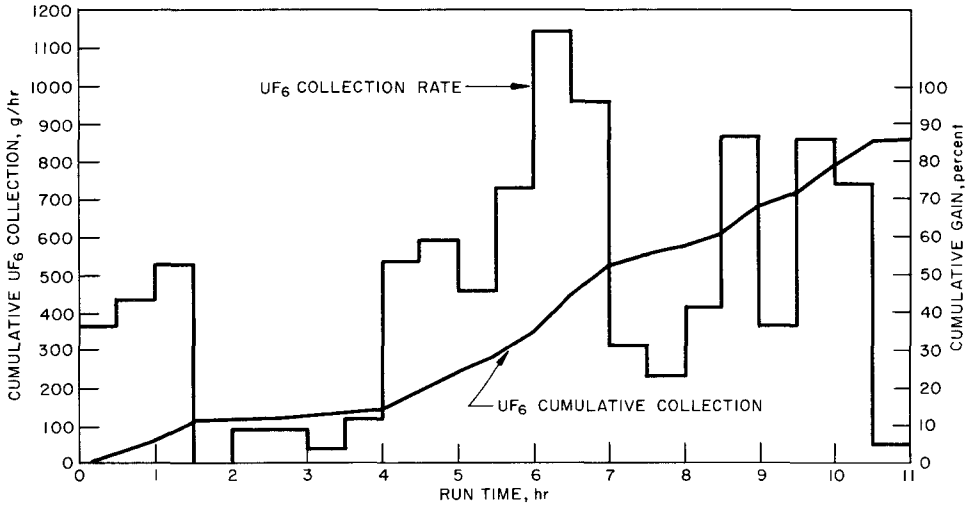

The variations in the uranium hexafluoride collection rate are due to fluctuations in the rate of fluorine introduction. An interruption of fluorine occurred at 1.5 hr because of a plug in the condenser. This plug

apparently was the result of a long-term accumulation of nonvolatile material and was not an effect of the present run. Other fluorine fluctuations resulted from the operation of the automatic temperature-control system. Temperature variations in the system in this run were more pronounced than expected; comparison is made below with a previous run.

FIGURE 24
FLUORINE CONCENTRATIONS IN INLET AND OUTLET STREAMS FOR RUN UOF-42

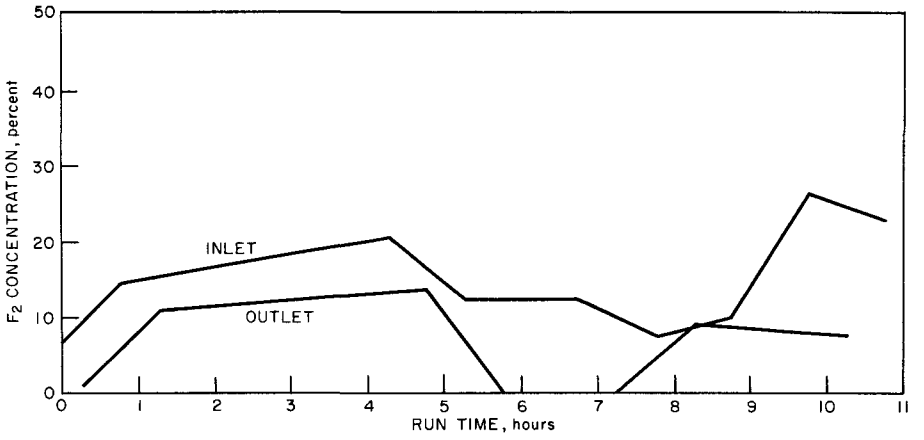

The inlet fluorine concentrations in Figure 24 follow the varying fluorine demands set by the automatic controller. The outlet concentration shows typical behavior, with a minimum about half-way through the run. This corresponds to the period of highest fluorine utilization efficiency.

From the data in Figure 23, the average fluorination rate in the period from 4.0- to 10.5-hr run time (14 to 85 percent reaction) was 490 g/hr. This rate is not very much lower than in 500 C runs, considering that in the present case the average inlet fluorine concentration was only about 16 percent. It is expected that higher rates can be obtained at 400 C at higher fluorine concentrations. Despite the variations of fluorine concentration shown in Figure 24, the overall fluorine efficiency in terms of fluorine charge being converted to uranium hexafluoride was 82.4 percent, the highest yet obtained in a batch run.

For general comparison, in Run UOF-34 (at 500 C with the same size uranium charge), 86 percent of the reaction was complete in 4.5 hr and the reaction was 95 percent complete in 6.0 hr. In UOF-34, the average inlet fluorine concentration was 42 percent and the overall fluorine utilization efficiency was 62 percent.

The fluorination rates obtained in both the runs cited above are determined by heat transfer conditions, since automatic temperature control by fluorine regulation was used. Heat transfer and temperature

control appeared to be better in Run UOF-34 than in UOF-42. Although no definite indications of caking were noted in UOF-42, it is possible that the lower temperature favored higher concentration of uranium oxide and fluoride fines in the bed, which resulted in poorer quality fluidization. In the present run (UOF-42), the control point temperature on several occasions fluctuated as much as 100 C, although for extended periods the control was close to 400 C. These fluctuations marked a comparative lack of smoothness in the system for temperature control. It is possible that the fluorine-regulation method as set up worked less well at 400 than at 500 C, because of differences in chemical kinetics affecting heat generation or in temperature gradients determined by heat loss from the reactor. Control optimization is being studied further.

In order to clarify the role of oxygen in determining the fluorination rate under these conditions, two series of runs (UOF-43 and 45) were made to determine the rate of pellet oxidation in the absence of fluorine. Analyses are not yet available for quantitative evaluation of these runs, but preliminary data show detectible oxidation at 300 C and increasing oxidation with temperatures up to 600 C. The oxide fines appear to be chiefly minus 325 mesh in samples determined thus far. This aspect of the process study will be continued along with further fluorination experiments.

2. Development of Special Engineering-scale Equipment

In recent fuel-reprocessing studies on the pilot-plant scale, equipment components were developed which proved to be of considerable value. One development concerned an automatic chain scale with remote recording for use with a process weigh tank. Another development was an all-metal fluorine analyzer for use with process off-gas. The desirable features of these components recommend them for similar use on other applications. A new baffled-cone gas distributor for fluid-bed systems has been developed and also seems promising.

a. Recording Chain Scale
(R. W. Kessie)

The ultimate standard of accurate measurement of weight has long been provided by beam balances. Also, balances are generally the most convenient method, especially where high accuracy and a wide range of weights are involved. In order to achieve the convenience of dial readings and weight recording, commercial models have abandoned the manipulation of weights required in the null-balance system and incorporated displacement systems, using springs or equivalent devices. But even with the most perfectly proportional and fully temperature-compensated system the use of displacement has a positive disadvantage

for weigh-tank applications. This is because the piping attached to the weigh tank introduces additional forces with displacement systems, and this effect is not present in a true null-balance system.

Recently, analytical balances having key-operated weights and chains have been marketed which go a long way toward more convenient balance operation. But these principles have not become commercially standard for balances of larger capacity, and no known manufacturer offers such a unit of engineering-scale capacity with a remote reading system.

In the fused salt process, large tanks containing about 500 lb of liquid (anhydrous) hydrogen fluoride were used for storage and measurement. An ordinary manual industrial scale was provided initially for this application (Fairbanks-Morse, 1000-lb capacity). The accuracy of this scale was $\frac{1}{10}$ percent or better and was a very rugged unit of low cost.

To provide remote reading, an automatic chain-balancing system was added to the manual scale. Movement of the beam from the null-balance point was made to close electrical contacts which, in turn, operated a reversible electric motor and reeled the chain in and out by means of a sprocket wheel. The chain was attached to the end of the beam and was of sufficient length to provide automatic balance over a span of about 200 lb. The remote reading of the chain position was provided electrically by means of a helipot electrical system connected to the chain pulley drive. The remote reading was recorded on a standard Brown potentiometer strip chart. The linear chart record was very convenient in determining rates of addition. Schematic diagrams of components of the electrical system are shown in Figures 25 and 26. A photograph of the weigh tank system is shown in Figure 27.

FIGURE 25
RECORDING CHAIN BALANCE CIRCUIT SCHEMATIC DIAGRAM

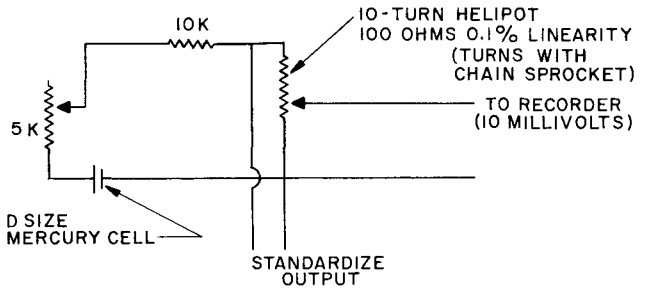

FIGURE 26
SCHEMATIC DIAGRAM OF BALANCING CIRCUIT FOR THE RECORDING CHAIN BALANCE

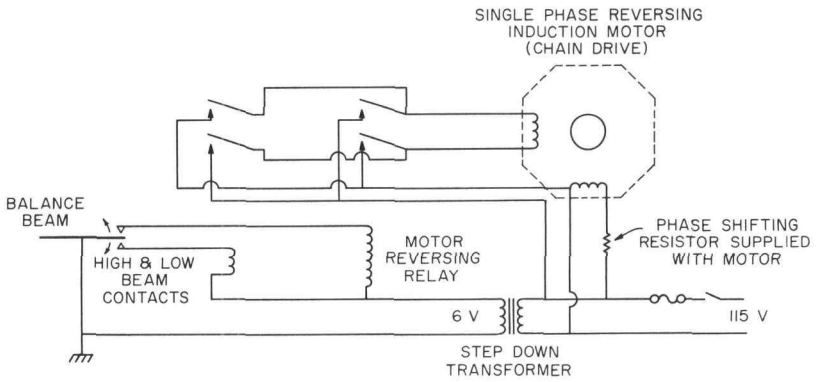

Figure 27

AUTOMATIC CHAIN SCALE ON WEIGH TANK

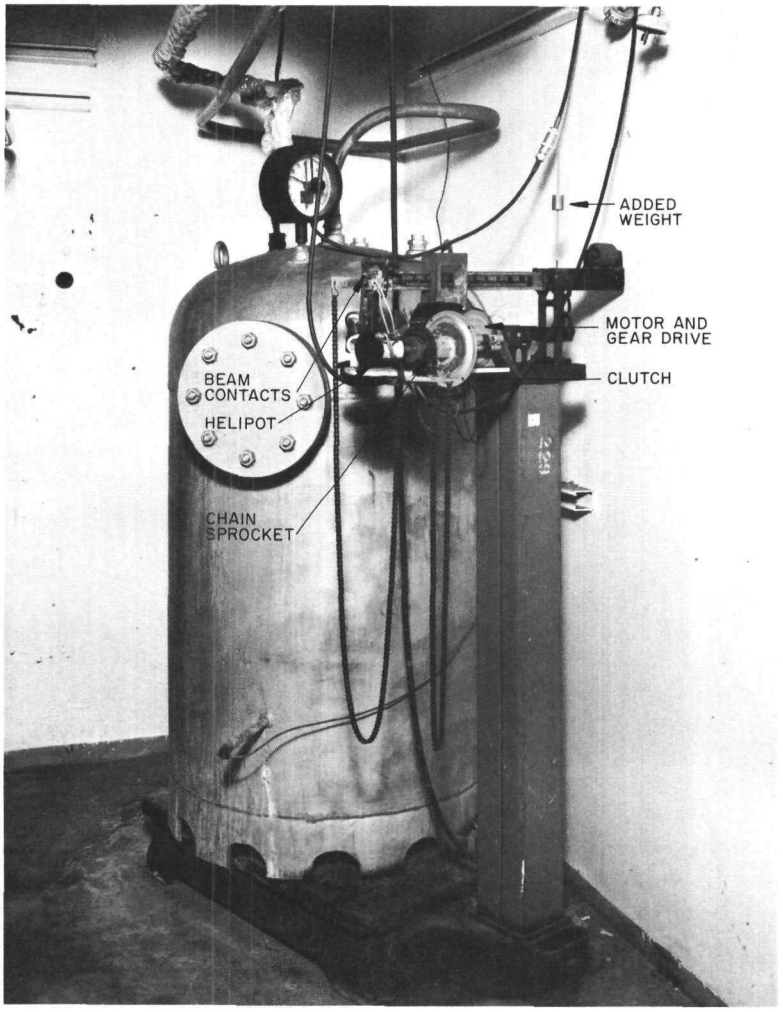

The 200-lb range on the chain was selected on the basis of convenience for the chain and the amount of space available in this installation. Manual tare weights were used for the wider weight ranges. The chain was readily reset by hand, since a clutch was provided on the motor drive.

An important part of the design was to provide compensation to the beam so that high sensitivity is retained when a chain is added to the balance beam. The loss in sensitivity is due to the load change of the chain with beam displacement. The original sensitivity was recovered by the addition of a weight to the beam above the center of gravity of the beam. The compensation required can be determined in terms of the quantities shown in the schematic diagram of Figure 28.

FIGURE 28
SCHEMATIC DIAGRAM OF BEAM LOADS: METHOD OF RECOVERING BEAM SENSITIVITY

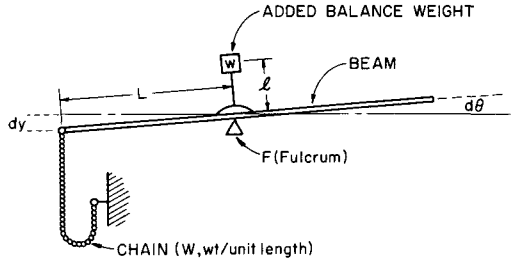

In the system shown in Figure 28, a change in torque accompanies a change $d\theta$ in the beam angle θ. The related displacement dy results in a length of chain $dy/2$ shifting its load off the beam. Since

$$dy = Ld\theta \quad ,$$

the torque change is

$$(WL/2)d\theta = wld\theta$$

or

$$wl = WL/2 \quad .$$

Therefore, attaching a weight w to the beam at a distance l above the pivot point will recover the original scale sensitivity.

The scale capacity was stated by the manufacturer to be 1000 lb. The measurement characteristics, based on experimental tests, were the following:

Original Scale:

Sensitivity: ~1 lb/in.
(load wt per inch of beam displacement Δy)

Accuracy: ±1 lb
(maximum error over full capacity; 0.1% of capacity)

Modified Scale:

Sensitivity: ~1 lb/in.
(0.1 lb to give $\frac{1}{8}$ -in. beam travel between electrical contacts)

Accuracy: $\pm\frac{1}{2}$ lb
(measured over 200-lb range of chain)

The accuracy for the modified scale is limited by nonlinearity in the chain used, which was a commercial type of the sort used on bicycles, etc.

Although the system as described worked quite satisfactorily, there are some features for which improvements are desirable. A variable-speed motor drive could be used to accommodate varying rates of weight change. The system described above used a fixed speed of about 100 lb/hr, which was adequate for that particular weigh-tank application. Also, a chain of uniform weight per unit length should be used for highest accuracy. By providing sufficient space for a long chain, wider ranges of weight could be accommodated by the automatic system.

b. Fluorine Analyzer
(J. D. Gabor)

The reaction of liquid mercury with fluorine has long been used as a method of fluorine analysis. In the common application of this method a volume of fluorine in a Pyrex flask is contacted with mercury by vigorously shaking the flask by hand. Without shaking, a thin film of fluoride prevents reaction. With a sensitive means of pressure measurement, such as a manometer, this method has been successful for analysis from about 0.5 to 99.5 percent fluorine.

In order to increase the speed and safety of this analysis, the method was modified by using a metal flask with a stirrer to provide adequate contacting. This unit was then permanently attached to the sample manifold and operated through valves, so that there was no need for uncoupling the flask for agitation or pressure measurement. In order to eliminate possible gas leakage at a stirrer shaft seal, a magnetically driven stirrer was designed.

A schematic diagram of the analyzer assembly is shown in Figure 29.

FIGURE 29
SCHEMATIC DIAGRAM OF FLUORINE ANALYZER ASSEMBLY

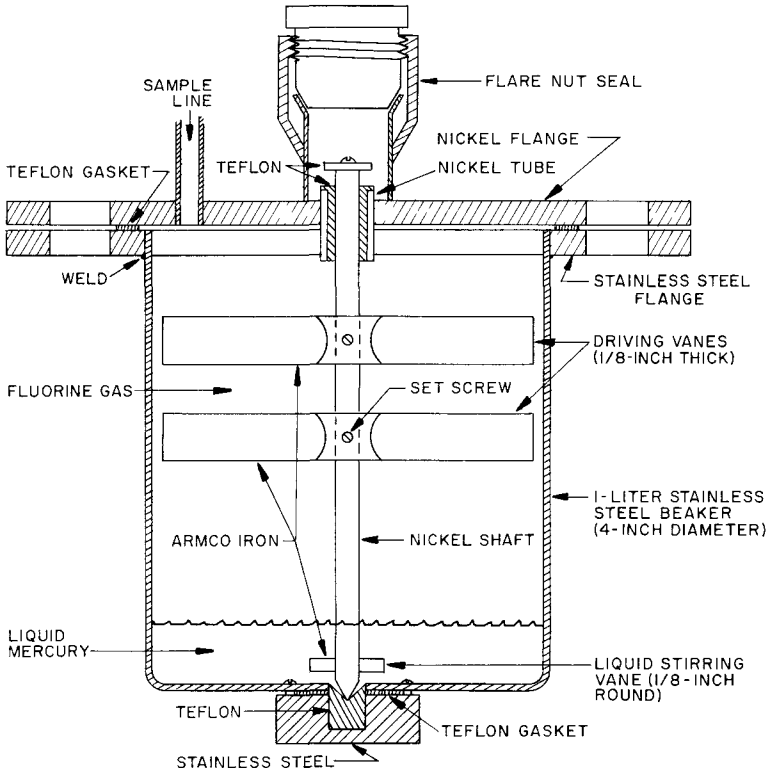

Figure 30 shows the process connections schematically. The manometer and the differential pressure transmitter are alternative means of pressure measurement. Fluorolube was used to prevent fluorination of the mercury surface in the manometer.

FIGURE 30
SCHEMATIC DIAGRAM OF FLUORINE ANALYZER SYSTEM

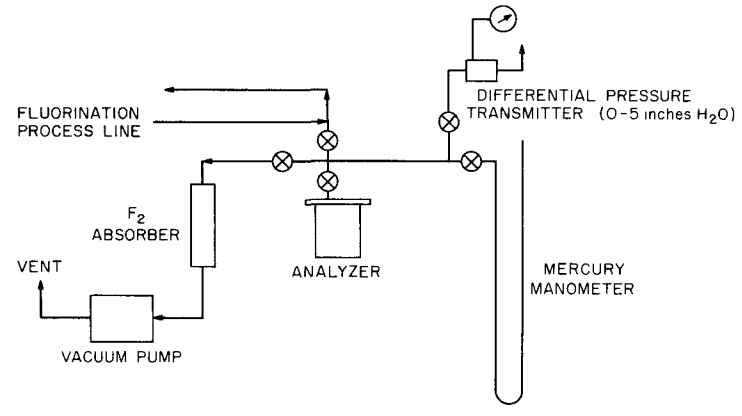

The body of the analyzer was fabricated from a one-liter stainless steel beaker. A flanged top was provided for access, and bearings were provided for aligning the stirrer shaft. Teflon was used for both top and bottom bearings.

The rotating magnetic field was provided by the field coil of a standard 3-phase induction motor. The field coil used was that from a 2-hp motor (GE SK 204 D130, frame 204). This size of unit allowed a desirably close fit around the outside of the analyzer body. To avoid overheating, the voltages to the coils were reduced with variable autotransformers.

The stirrer design was tailored to the requirements of this system. Small liquid-stirring vanes were provided because of the high density of the mercury. Large stirring vanes were provided in the vapor space, to provide adequate coupling to the magnetic field.

A small portable air blower was used to remove heat generated during operation. No difficulties have been encountered with it in about 20 fluorination runs.

It is recommended that in future models the top bearing be modified so that support is provided by the body or the lower flange rather than by the top flange. In this way re-alignment of the shaft can be avoided when the unit is re-assembled after cleaning.

c. Baffled-cone Gas Distributor
(E. Carls)

A serious disadvantage to the conventional cone bottom employed in various fluidization units is that the gas-inlet line at the apex of the cone fills with powder when gas is not flowing, and subsequent startup procedures usually require rather high pressures and sometimes mechanical vibration to aid in forcing powder out of the line and commence fluidization. The baffled-cone inlet shown in Figure 31 was designed to overcome this difficulty and still provide for a rather large solids take-off point

FIGURE 31
BAFFLED CONE GAS DISTRIBUTOR

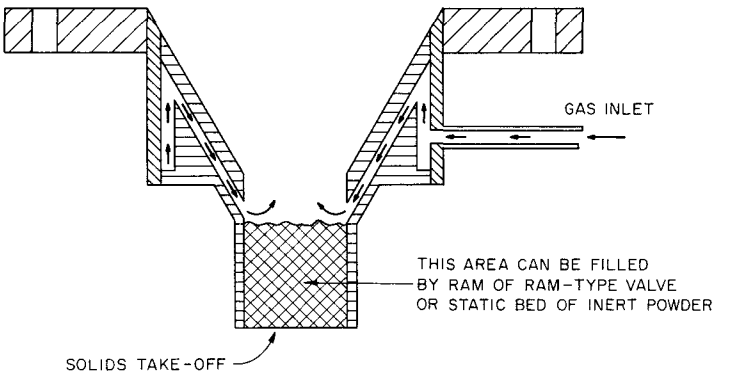

which would remove all the bed material from the unit. A distributor of this type has been tested in the glass mockup column. The startup requires no noticeable pressure drop, the fluidization pattern is very good, and no solids have been detected downstream of the baffles.

3. Heat Transfer Tests in a 'Packed-Fluidized' Bed

(E. N. Ziegler,* J. D. Gabor)

The importance of heat transfer in the fluorination of uranium dioxide pellets has led to the application of fluidization to this system. However, direct fluidization of the pellets themselves has not appeared practical, and the use of an inert material of an appropriate particle size has been adopted to provide a fluidized phase in the voids of the fixed bed of pellets. This type of system has been referred to as a 'packed-fluidized' bed. As a supplement to fluorination studies, heat transfer tests of packed-fluidized systems have been studied in mockup configurations similar to that in the fluorinator.

Bed-expansion ratios and pressure-drop behavior have been described in ANL-6101, pages 115 to 117. Heat transfer coefficients at the surface of heated pellets were reported in ANL-6231, pages 112 to 117. Initial work on the internal- and external-wall heat transfer coefficients and on the effective radial thermal conductivity was reported in ANL-6287, pages 153 to 157. In the present work, mockup tests have been extended to give wall coefficients and radial conductivities for a range of fluidized particles sizes and a range of pellet sizes and shapes in the fixed bed.

Equipment

A 4-in. column with an internal heater was used. The column had as a gas distributor a porous plate flanged to its bottom. The height of the column was only 24 in. to allow hand placement of the heater and thermocouples. The heater was $\frac{3}{8}$ in. in diameter and 16 in. long. The small heater diameter (less than packing size) was intended to cut down on flow pattern disturbance.

The packing materials were

1) Stationary packing

   a. Brass cylinders 0.5 x 0.5 in. and 0.375 x 0.375 in.

   b. Steel spheres 0.5 and 0.25 in.

---

*Summer Research Associate from Northwestern University.

2) Fluidized packing

Glass beads 0.0030-, 0.0080-, and 0.0110-in. avg diameter (corresponding to approx. 230, 85, and 65 mesh, respectively).

The packed-fluidized column is shown schematically in Figure 32. Air was used as the fluidizing medium. Eighty runs were made with various size combinations of stationary and fluidized packing. Superficial gas velocities up to 0.25 ft/sec were used, based on open column cross-sectional area and 70 F.

FIGURE 32
DIAGRAM OF PACKED-FLUIDIZED BED

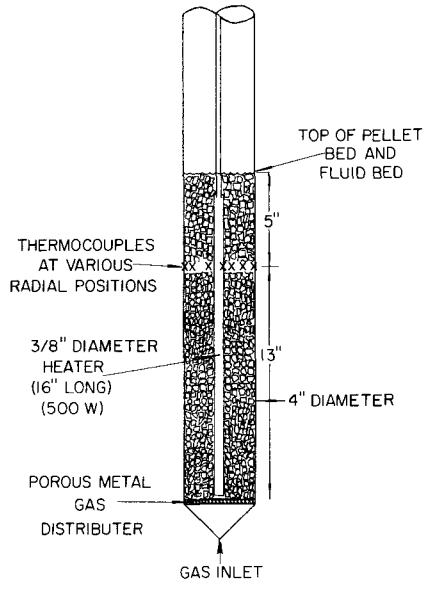

Eleven temperatures were recorded for each run at steady-state conditions. The placement of the 30-gauge iron-constantan thermocouples is shown in Figure 32. The thermocouples were attached inside the stationary packing by drilling a $\frac{1}{16}$-in. hole axially through the cylinders and cementing the insulation to the inner surface. The thermocouple junction did not touch the body of the packing and the tip extended nearly to the outer surface. Heater temperature was measured by a thermocouple soldered to the heater. Bed temperatures at six radial positions, the heater temperature, and the wall temperature were all recorded at the same vertical position, at an elevation 13 in. from the bottom of the tube. Inlet and outlet air temperatures were recorded. Pressure drops were taken across the bed for all systems, and the minimum fluidizing gas velocity noted. Heat input was measured by a calibrated variable autotransformer.

Effective Thermal Conductivity

Radial heat transfer in a cylindrical annulus may be described in terms of an effective thermal conductivity k_E such that

$$k_E = \frac{q \ln (r_2/r_1)}{2\pi L (t_1 - t_2)} ,$$

where

k_E = effective thermal conductivity along radius of cylinder, Btu/(hr)(sq ft)(F/ft)

q = total heat flow, Btu/hr

r_1, r_2 = radial distances of the cylindrical annulus at the inner heating surface and the outer cooling surface, respectively, ft

L = overall height of cylinder, ft

t_1, t_2 = temperature at the heating surface and cooling surface, respectively, F.

This equation neglects axial conduction and radiant heat transfer, and considers the temperatures constant along the column length.

For each packed-fluid bed and each gas velocity in these tests, six temperatures at different radial positions were obtained in addition to the heater and coolant wall temperatures. The temperature difference between the wall and the closest radial position was considered to apply to the film coefficient and the six intermediate radial temperatures to apply to the radial temperature gradient in the bed. Plots of $\ln(r_2/r_1)$ vs. the radial temperature differences (t_1-t_2) approximated a straight line, although appreciable scatter was noted. From the above equation, the slope of such a straight line is proportional to k_E, which is thereby an average constant value along the radius. A least-squares analysis of the data was made for all six radial temperatures and also for four of these temperatures in the central radial position. The correlation coefficients (a statistical measure of the fit of the data to the correlating equation) for the constants determined by six points were higher, indicating a slightly better fit. For the total of 80 runs, only 10 percent of these correlation coefficients had values of less than 90 percent, indicating the assumption of a constant k_E was reasonable with the present data. Values of the effective radial thermal conductivity are given in Table 32. The gas velocities corresponding to experimental determinations of incipient fluidization by pressure drop are marked in the table by a small "a." The upper limit of gas velocities was set by entrainment of the smallest size of glass beads. As expected, higher effective thermal conductivities were generally obtained at higher gas velocities, especially for the larger beads, which are less easily entrained. The thermal conductivity data indicate that in a few instances local fluidization may have occurred at velocities slightly different from that indicated by the symbol "a."

Heat Transfer Coefficients at the Wall

The heat transfer coefficients at the cooling wall surfaces were calculated by the equation

$$h = q/A\,\Delta T \quad ,$$

where ΔT is the temperature difference between the wall and the nearest radial position. The values of h so determined are given in Table 33.

Table 32

EFFECTIVE THERMAL CONDUCTIVITIES, Btu/(hr)(sq ft)(F/ft) FOR A 4-INCH-DIAMETER COLUMN

Superficial Air Velocity (ft/sec)	No Beads	Glass Beads (diameters)		
		0.0030 in.	0.0080 in.	0.0110 in.
	0.25-in. Steel Spheres			
0.017	0.238	0.35	0.49	0.42
0.074	0.281	0.92	0.39	0.40
0.128	0.246	0.92	0.41[a]	0.51
0.182	0.228	-	0.39	0.60[a]
0.243	0.225	-	1.58	0.82
	0.50-in. Steel Spheres			
0.017	0.281	0.95[a]	-	0.57
0.074	0.301	1.93	-	0.52
0.128	0.290	2.51	-	0.85
0.182	0.299	3.01	-	1.19[a]
0.243	0.298	-	-	1.64
	0.375 x 0.375-in. Brass Cylinders			
0.017	0.595	1.68[a]	0.72	1.12
0.074	0.586	2.62	3.46	1.13
0.128	0.338	6.01	4.01[a]	2.02
0.182	0.591	7.31	4.57	3.60[a]
0.243	0.449	7.12	5.44	4.70
	0.50 x 0.50-in. Brass Cylinders			
0.017	0.278	1.92[a]	1.21	0.92
0.074	0.290	4.65	2.94	1.28
0.128	0.297	5.90	7.32[a]	4.64
0.182	0.317	10.30	7.71	3.34[a]
0.243	0.329	8.60	9.36	3.81

[a]Incipient fluidization.

Table 33

COOLING WALL HEAT TRANSFER COEFFICIENTS, Btu/(hr)(sq ft)(F), FOR A 4-INCH-DIAMETER COLUMN

Superficial Air Velocity (ft/sec)	No Beads	Glass Beads (diameters)		
		0.0030 in.	0.0080 in.	0.0110 in.
	0.25-in. Steel Spheres			
0.017	10.4	13.2[a]	18.4	15.4
0.074	7.3	18.6	16.9	12.2
0.128	8.0	18.2	17.3[a]	22.1
0.182	8.5	-	17.5	20.6[a]
0.243	8.0	-	27.2	20.9
	0.50-in. Steel Spheres			
0.017	8.0	12.1[a]	-	13.6
0.074	6.9	30.6	-	12.5
0.128	6.8	16.4	-	21.9
0.182	6.5	22.7	-	22.5[a]
0.243	7.0	-	-	22.0
	0.375 x 0.375-in. Brass Cylinders			
0.017	8.1	17.5[a]	10.2	9.9
0.074	7.3	18.8	15.0	9.5
0.128	7.8	38.6	15.6[a]	12.8
0.182	7.1	32.5	17.7	16.0[a]
0.243	7.0	34.1	21.1	14.4
	0.50 x 0.50-in. Brass Cylinders			
0.017	9.5	43.7[a]	17.1	24.0
0.074	9.1	48.0	39.9	24.2
0.128	9.2	33.8	27.4[a]	57.9
0.182	9.8	38.3	23.8	31.8[a]
0.243	9.3	35.8	23.6	21.3

[a]Incipient fluidization

where

Δt_{bed} = temperature difference across bed, F

q' = rate of heat generation, Btu/(hr)(cu ft)

k_E = effective bed thermal conductivity, Btu/(hr)(sq ft)(F/ft)

r = radius of bed, ft,

and

$$\Delta t_{wall} = q/hA \quad ,$$

where

Δt_{wall} = temperature drop at wall, F

q = heat flux, Btu/hr

h = heat transfer coefficient, Btu/(hr)(sq ft)(F)

A = area, sq ft.

Table 35

COMPARISON OF TEMPERATURE DIFFERENTIALS OBTAINED DURING FLUORINATION WITH THOSE CALCULATED FROM HEAT TRANSFER TESTS

Fluorination Conditions:
6-in.-deep bed UO_2 pellets control temperature 500 C

Run Number	30	32	34
Fluid Bed	no	yes	yes
Diluent Gas	N_2	N_2	O_2
Total Gas Velocity, ft/sec	0.31	0.63	0.71
UF_6 Collection Rate, kg/hr	0.73	0.70	1.25
Heat Generation, Btu/(hr)(cu ft)	87,000	83,000	149,000
Calculated k_E, Btu/(hr)(sq ft)(F/ft)	0.55	10.0	10.5
Calculated h, Btu/(hr)(sq ft)(F/ft)	7.5	40	44
Calculated ΔT bed, C	352	18	31
Calculated ΔT wall, C	402	73	117
Calculated total ΔT, C	754	91	150
Measured ΔT, C	460	30	60

Run UOF-30 was a fluorination of a bed of uranium dioxide pellets without an inert fluidizing medium. The estimated effective thermal conductivity and wall heat transfer coefficient were taken from Tables 32 and 33. These values were taken for 0.375-in. cylinders to take into account the reduction of size of the original 0.5-in. pellets by the reaction. A temperature drop of 754 C was estimated. The actual temperature drop was about 460 C. In estimating the temperature drop, axial heat transfer and conduction through the metal bed support plate were neglected; this may account for the fact that the calculated temperature drop was higher than that obtained experimentally.

Run UOF-32 was a fluorination of a bed of uranium dioxide pellets with the presence of an inert fluidizing medium of -40 +140 calcium fluoride particles. The reactant gas was composed of nitrogen and fluorine. The calculated bed thermal conductivity and wall heat transfer coefficient were taken from Tables 32 and 33 for the appropriate conditions. A temperature difference between the wall and the center of the bed was estimated to be 91 C. The experimental value was about 30 C. Because of the presence of fluid bed above and below the pellet bed, axial heat transfer was significant and as a result the actual temperature drop was lower than that predicted.

Run UOF-34 also used a fluid-packed bed system. The reactant gas contained oxygen, which increased the reaction rate. For this case the estimated temperature drop was 150 C. The experimental value was 60 C.

The true temperatures of the gas and the pellet surfaces differ from the measured bed temperature depending on the values of heat transfer coefficient under the run conditions. In the two runs with a fluid bed these temperature differences are small, but in the absence of a fluid bed they are much higher.

4. Process Studies for the Recovery of Uranium from Zirconium-base Nuclear Fuels
(N. Levitz)

Engineering studies on a fluidization-volatility scheme for processing zirconium-base nuclear fuels have been resumed on the basis of encouraging results from Brookhaven[25] and laboratory-scale experiments conducted at ANL (ANL-6379, pages 175 to 178). Incomplete uranium recovery from the bed materials in previous work (ANL-6231, pages 120 to 123)

---

[25] Reilly, J. J., et al., Reprocessing of Reactor Fuels by Volatilization Utilizing Inert Fluidized Beds, BNL-663 (May 1961).

As with the effective thermal conductivity, higher values of heat transfer coefficients would be expected at gas velocities farther above the minimum fluidization velocities.

Heat Transfer Coefficients at the Heater Surface

For comparison, the heat transfer coefficients at the surface of the heater were calculated by the same methods as above for the cooling wall. The heater was $\frac{3}{8}$ in. in diameter and axially located. Its heating length, 16 in., was the same as the bed height. Values of h for this case are shown in Table 34. These values are higher than those for the cooling wall, as would be expected.

Table 34

HEATER WALL HEAT TRANSFER COEFFICIENT h, Btu/(hr)(sq ft)(F)
(3/8-in.-diameter heater axially located in a 4-in.-diameter column)

Superficial Air Velocity (ft/sec)	No Beads	Glass Beads (diameters) 0.0030 in.	0.0080 in.	0.0110 in.
		0.25-in. Steel Spheres		
0.017	-	36.4[a]	40.3	29.6
0.074	16.6	119.8	-	29.5
0.128	17.0	122.6	-[a]	52.0
0.182	17.5	-	54.9	59.8[a]
0.243	17.5	-	-	65.4
		0.50-in.-Steel Spheres		
0.017	11.1	32.4[a]	-	28.7
0.074	11.2	148.3	-	30.0
0.128	11.3	76.8	-	45.2
0.182	11.4	111.0	-	87.9[a]
0.243	11.2	-	-	82.7
		0.375 x 0.375-in. Brass Cylinders		
0.017	17.0	86.6[a]	30.8	27.5
0.074	17.3	76.7	87.3	31.4
0.128	24.2	116.2	88.4[a]	44.6
0.182	17.2	99.2	79.2	45.8[a]
0.243	24.1	95.6	71.4	49.1
		0.50 x 0.50-in. Brass Cylinders		
0.017	9.8	71.8[a]	26.8	24.3
0.074	9.9	64.4	62.7	25.5
0.128	9.4	114.5	84.0[a]	44.0
0.182	10.5	131.0	69.3	73.5[a]
0.243	10.6	132 9	58.3	86.5

[a]Incipient fluidization

In general the ranges of k_E and h in this work appear similar to those in the previous experiments cited above.

Heat Transfer in Fluorination Tests

Further experiments have been made to investigate heat transfer problems in the direct fluorination process. Studies have been carried out on a pilot-plant scale in a 3-in.-diameter nickel reactor in which uranium dioxide was fluorinated. External fins were provided for forced-air cooling, and the column was heated during start-up by electrical resistance heaters. Thermowells were located at various heights as shown in Figure 33. At each column height one thermowell extended to the center of the column and the thermowell on the opposite side was flush with the wall. The uranium dioxide pellets were supported on a perforated nickel disk.

FIGURE 33
THERMOWELL LOCATIONS IN FLUORINATOR

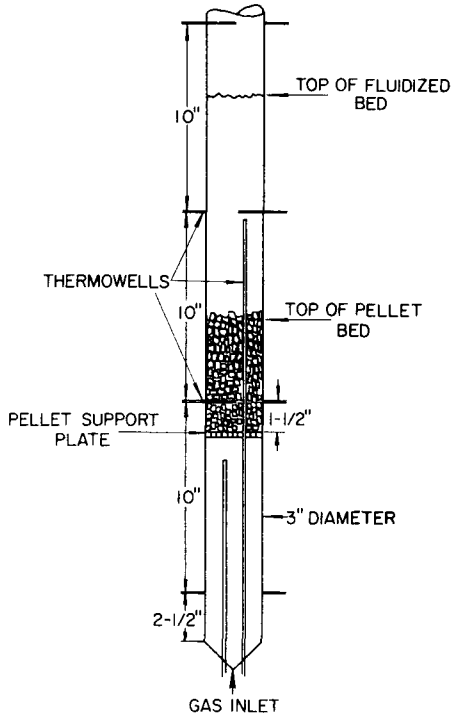

Temperature control was maintained satisfactorily at predetermined levels, even at high fluorination rates, by automatic regulation of the fluorine input. In general, heat transfer rather than reaction kinetics limited the fluorination rate. Heat transfer rates measured during fluorination runs have been compared with the results of heat transfer tests described above in the mockup equipment.

In Table 35 are compared the experimental temperature differences between the center of the bed and the wall of the column during a fluorination and those estimated from the heat transfer data. Three runs are presented in which 6-in.-deep pellet batches were fluorinated under varying conditions. The nominal control temperature in each run was 500 C as measured by an internal thermowell in the pellet bed.

The following assumptions were made in estimating the temperature drops from the center of the bed to the column wall: (1) heat transfer was all radial, and (2) heat was generated uniformly in the bed. The following equations would then apply:

$$\Delta t_{bed} = \frac{q'}{k_E}\left(\frac{r^2}{4}\right) \quad ,$$

was attributed to the presence of zirconium retained as the tetrafluoride. The new approach involves initial separation of the zirconium from the uranium by a direct hydrochlorination reaction conducted above the sublimation temperature of the zirconium tetrachloride (331 C) in beds of inert material (currently Norton Co., Type 38 Alundum). The inert material serves as a heat transfer medium. The uranium forms the solid trichloride which will be retained, for the most part, in the fluidized bed and the remainder is retained in the system by a suitable filtration scheme. Uranium recovery will be effected by fluorination to the hexafluoride.

a. Hydrochlorination and Fixed-bed Filtration Studies
(J. T. Holmes, C. Schoffstoll)

The initial engineering work is being directed toward the evaluation of fixed beds of Alundum as filters for the separation of uranium solids entrained by the volatile zirconium tetrachloride stream. Uranium retained in these beds will then be recovered by fluorination to the hexafluoride. Both up- and down-flow filtration, shown schematically in Figure 34, were investigated utilizing a 1.5-in.-diameter fluidized reaction zone and a 3.0-in.-diameter filter zone.

FIGURE 34
STATIC-BED FILTER EVALUATION APPARATUS

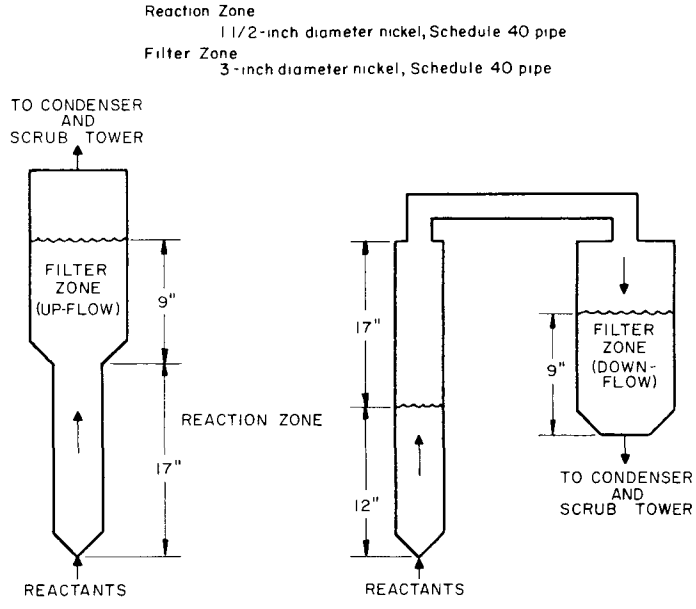

General descriptions of important filtration mechanisms can be found in references by Ranz and Wong,[26] Langmuir and Blodgett,[27] and Sell.[28]

[26] Ranz, W. E., and Wong, J. B., Impaction of Dust and Smoke Particles on Surface and Body Collectors, Ind. Eng. Chem., 44, 1371-1381 (1952).

[27] Langmuir, I., and Blodgett, K. B., General Electric Research Laboratory, Schenectady, New York, RL-225, 1944-1945.

[28] Sell, W., Forsch. Gebiete Ingenieurw, 2, Forschangsheft, 347 (Aug. 1931).

Experimental Procedure

The uranium-Zircaloy fuel alloy (2.7 weight percent uranium) in the form of irregularly shaped cubes (~$\frac{1}{4}$ in. on a side) was charged to a basket which was submerged in Alundum in the reaction zone. In the case of up-flow filtration experiments, more Alundum was charged to give the specified filter-bed height in the enlarged (upper) zone of the column. For down-flow work the procedure was similar except that the reaction column and filter column were separate units connected by a horizontal pipe. The reaction and filter beds were heated while nitrogen was passed through the column. Sufficient gas was provided to fluidize the Alundum in the reaction zone. Hydrogen chloride was added to the gas stream as the bed approached the desired temperature (350 to 400 C), and the experiment was conducted for a fixed time interval.

Experiments which investigated the effect of filter-bed depth and particle size, and gas velocity have been made (see Table 36) and evaluated on the basis of the uranium found in the zirconium tetrachloride air-cooled condenser, hydrogen chloride scrub tower, and Filter Queen air sampler located downstream from the bed filter. Negligible amounts of uranium were found in the air sampler. In all cases the experiments were conducted such that a minimum of 90 percent of the metal charged was reacted.

Table 36

URANIUM-ZIRCONIUM ALLOY HYDROCHLORINATIONS

Reaction Bed: Type 38 Norton Alundum -40 +200 mesh for Runs 3 to 6; -40 +80 mesh for Runs 7 to 11

Temperature: Reaction Bed 350 to 400 C Filter Bed 375 to 425 C

Reaction Zone: 1 61-in diameter Filter Zone 3 07-in diameter

Fuel Alloy: 2 7 weight percent uranium-Zircaloy

	Filter Bed			Reaction Bed		Uranium Reacted[c] (g)	Uranium Downstream of Filter		
Run No	Mesh Size	Depth (in)	Velocity (ft/sec)	Velocity (ft/sec)	HCl Conc[b] (m/o in N_2)		Condenser (g)	Scrub Solution (g)	Loss (%)
3A-Up-flow	-40 +200	9	0 14	0 47	72	4 7	0 015	0 001	0 3
4A-Up-flow	-40 +200	9	0 28	0 94	65	4 3	0 024	< 0 0001	0 6
5A-Up-flow	-20 +36[a]	9	0 18	0 65	61	4 1	0 011	0 012	0 6
6A-Down-flow	-40 +200	9	0 21	0 70	42	7 6	0 003	0 024	0 3
7A-Down-flow	80 +200	3	0 23	0 85	48	7 0	0 013	0 005	0 26
8A-Down-flow	-80 +200	8	0 25	0 90	48	6 3	0 005	0 006	0 18
9A Down-flow	-80 +200	12	0 25	0 90	43	7 0	0 014	0 001	0 20
13A-Down-flow	-80 +200	3	0 75	1 5	18	3 2	0 0023	0 0033	0 17
11A-Down-flow	-100 +140	3	0 25	0 90	50	7 3	0 0057	0 0019	0 10

[a] On a perforated support plate

[b] Hydrogen chloride dried with activated charcoal

[c] Represents at least 90 percent of the charge in all cases

Results

Up-flow Filtration

Experiments 3A and 4A, which showed an effect of velocity through the filter bed, were conducted with up-flow of the reactants through a continuous reaction and filter bed, that is, no support plate was used for the filter bed. The gas velocity was chosen so that the material in the filter zone remained static while the material in the reaction zone, which was of smaller cross section, was fluidized. Uranium losses were 0.3 percent at 0.14 ft/sec and 0.6 percent at 0.28 ft/sec.

Experiment 5A was made with a coarser material in the filter bed than in the fluid bed (-20 + 36 mesh as compared to -40 +200 mesh), so that a support plate for the filter bed was required. A perforated plate was used. Uranium losses of 0.3 and 0.6 percent for the fine and coarse filter bed materials, respectively, (Run 3A vs. Run 5A) indicated an effect of particle size on filtration efficiency. Partial plugging of the support plate was encountered, but it is not believed that this affected filter-bed operation. Redesign of this plate will be considered in future work.

Down-flow Filtration

Experiments 7A, 8A, and 9A show that there is no detectable effect of filtration bed height. The uranium losses were 0.26, 0.18, and 0.20 percent for 3-, 8-, and 12-in.-deep beds of -80 +200 mesh Alundum.

A possible effect of filter-bed particle size and distribution is shown in Runs 6A and 8A, and also in 7A and 11A. For the 8- and 9-in. beds, the -80 + 200 mesh Alundum allowed only 0.18 percent loss, whereas a 0.3 percent loss was noted for the coarser, -40 +200 mesh bed. Experiments 7A and 11A showed a decrease in efficiency with broad-spectrum particle sizes for 3-in.-deep beds. The losses were 0.26 and 0.10 percent for -80 +200 and -100 +140 mesh filter beds, respectively.

A study of the effect of gas velocity through a 3-in. down-flow filter bed (Runs 7A and 13A) showed lower uranium losses were achieved at the high velocity, 0.17 percent at 0.75 ft/sec as opposed to 0.26 percent at 0.23 ft/sec.

In summary, preliminary results indicate uranium losses through down-flow packed-bed filters may be reduced by the use of smaller bed particles and higher velocity, but there is no apparent effect of bed depth. Down flow, in general, gave equal or better results than up-flow filtration. The down-flow technique is limited to flow rates which do not give excessive pressure drops but is not limited with respect to bed particle size as is up-flow bed filtration where the continuous scheme is

used. The up-flow continuous-bed technique is limited to velocities below the incipient fluidization value for the filter-bed particles. Evaluation of an up-flow and down-flow filter in series is planned. The up-flow bed will be continuous with the reaction bed. This series technique should reduce the particulate load on down-flow beds and may improve the overall efficiency.

After evaluation of the filter beds, studies will involve hydrochlorination followed directly by fluorination to ascertain the extent to which uranium can be recovered from the system. Conditions for fluorination, such as fluidizing gas velocity and bed temperatures, will be similar to those used during hydrochlorination. Since the material to be fluorinated (uranium and minor constituents of Zircaloy) comprises such a small amount of the total material in the system (being of the order of one percent), fluorine gas efficiencies may be low, but gas recycle can be used for economy. The heat load should be low and of little concern. It should be possible to use the same beds several times, thus minimizing handling of bulk materials. The uranium hexafluoride concentration in the off-gas will be relatively low and varying with time so that efficient cold trapping will be necessary. Satisfactory uranium material balances for consecutive hydrochlorination and fluorination steps will be necessary for proper process evaluation.

b. Corrosion of Metals in Zirconium Tetrachloride Vapor (J. J. Barghusen, D. Raue)

A series of corrosion tests has been made to evaluate possible materials of construction which would be exposed to zirconium tetrachloride vapor at approximately 375 C. Tests of 35- and 170-hr duration were performed in an atmosphere (2000 mm Hg pressure) of zirconium tetrachloride at 365 to 375 C with coupons of A-nickel, Monel, Inconel, 347-stainless steel, and sintered nickel metal. The coupons were suspended in a nickel bomb which was placed in a tube furnace.

Corrosion rates, expressed in mils/month, were calculated from the area and the observed weight loss of the specimens after the corrosion films were removed by light rubbing and by washing in warm water. Results (see Table 37) were similar for all four metals in that, after an initial period of relatively high corrosion, the corrosion rate levels off. Values of 0.2 mil/month or less were obtained for all cases for the 170-hr tests. The lower weight losses noted for stainless steel and Monel for the longer-term tests may be attributed to incomplete removal of the corrosion film.

Table 37

CORROSION TESTS IN ZIRCONIUM TETRACHLORIDE VAPOR

Equipment: 2-in.-diameter nickel bomb
Temperature: 365 to 375 C
$ZrCl_4$ Pressure: 2000 mm Hg absolute

Metal	Duration of Test (hr)	Surface Area (sq in.)	Weight Loss (mg/sq in.)	Corrosion Rate[a] (mils/mo)
A-nickel	35	2.22	1.8	0.3
A-nickel	170	2.18	2.2	0.1
Inconel	35	1.40	2.6	0.4
Inconel	170	1.40	3.4	0.1
Monel	35	2.22	9.7	2.0
Monel	170	2.20	6.8	0.2
347 stainless steel	35	2.24	6.3	1.0
347 stainless steel	170	2.24	5.0	0.2

[a] 30-day month.

C. Conversion of Uranium Hexafluoride to Uranium Dioxide
(I. Knudsen, H. Hootman,* N. Levitz, M. Jones, J. Kincinas)

A fluid-bed process for the preparation of ceramic-grade uranium dioxide from uranium hexafluoride is being studied for application to the production of nuclear fuel. Uranium hexafluoride is reacted with steam to form uranyl fluoride which is then reduced to uranium dioxide with mixtures of hydrogen and steam. The reactions have been carried out simultaneously in a single reactor and in separate steps. Uranium losses from the system have been consistently below 0.01 percent. High sintered densities (from 93 to 97 percent of theoretical: see ANL-6183, page 123, and ANL-6231, page 134) have been obtained in pellet-fabrication tests. The tests reported this quarter conclude the work on the two-step procedure. A topical report is in preparation.

1. Steam Hydrolysis of Uranium Hexafluoride

Final operability tests of the fluid-bed steam hydrolysis of uranium hexafluoride have been completed. Stable bed behavior was demonstrated within a range of operating conditions and for continuous

*Resident Student Associate from Michigan College of Mining and Technology.

periods up to 25 hr in duration. A total of 56 hr of running time was accumulated during this report period and 300 kg of uranyl fluoride were produced.

Improved operations were reported last quarter (see ANL-6379, page 182) as a result of modifications to the 3-in.-diameter Monel column which permit entrainment and separate collection of fines produced in the bed. The filter vessel, previously mounted integrally above the bed, was placed to the side and a 1-in. diagonal pipe from the reactor connects the two units. Fines discharged off the filters by blow-black, instead of returning to the bed, collect in the lower part of the vessel and are periodically withdrawn.

Experiments were made to determine the latitude of some of the variables one could use and still maintain operability of the unit. It was found that the unit had quite satisfactory stability and the following results were obtained. A small increase in average bed particle size was noted between Runs 62D and 62E (see Table 38) when steam superficial velocity was increased from 0.5 to 1.0 ft/sec. This was probably due to greater elutriation at higher velocities. A greater change in bed particle size was effected by increasing the recycle rate. In Run 62F, an increase in recycle rate of 70 percent caused an almost 25 percent reduction in average bed particle size over a 10-hr period. Lowering of the recycle rate to the normal value (nearly 14 percent by weight of the feed rate) during the last $1\frac{1}{2}$ hr resulted in rapid growth and the starting average bed particle size was again approached.

Table 38

CONDITIONS FOR STEAM HYDROLYSIS OF URANIUM HEXAFLUORIDE

Equipment	3-in.-diameter Monel reactor
Temperature	200 to 225 C
UF_6 Feed Rate	100 g/min
Bed Height (static)	18 in.

Run No.	Run Duration (hr)	Steam Superficial Velocity (ft/sec)	Steam Excess (%)	Recycle Rate (-60 +200 mesh) % of UF_6 Fed	Average Size of Hourly Samples (μ)	Size Range of Hourly Samples (μ)
62D	7.5	0.5	115	13.7	308	303-315
62E	12.0	1.0	330	13.7	327	314-346
62F	11.5	0.5	115	23.7	275	252-306
64A	25.0	0.8	245	15.6[a]	350	316-361

[a]Recycle rate higher due to coarser seed material.

The 25-hr continuous run (Run 64A) demonstrated satisfactory reliability. Conditions were held fixed near 230 C, 100 g/min uranium hexafluoride feed, and approximately 245 percent excess steam,

corresponding to a superficial fluidizing gas velocity of 0.8 ft/sec. The recycle rate was slightly higher, nearly 15.6 percent, because of the use of a coarser seed material. Product removal was from the bottom through the automatic (bed-level controlled) valve.

Several items of operational interest may be reviewed here:

a. The pipe size or section connecting the primary reactor with the filter chamber should be enlarged so as to preclude any plugging due to deposit of entrained material. The one-inch line used in this work required vibration and rapping to keep it open. Insertion of a smooth one-inch tube (the existing line contained several pipe joints) relieved the problem appreciably.

b. The sintered metal filters, three 9-in.-long bayonets (Micro-metallic Co., Grade G) for most of the work, were operated with an automatic venturi blowback system which delivered a reverse fractional second pulse of air on a one-minute cycle. Additional positive manual blowback was also provided. Filters were cleaned upon removal from the column by a reverse steam flow with the filter immersed in hot water. For the 25-hr run, three $9\frac{1}{2}$-in.-long cylindrical filters (Cuno Co.) were used and operated trouble-free.

c. The coating of uranyl fluoride found on the reactor walls would require removal, but only after extended periods of time. The action of the fluid bed apparently is not vigorous enough to maintain the walls free of this deposit. The overall amount of holdup can be determined by material balance.

In conclusion it can be emphasized that successful operation of a 3-in.-diameter fluid-bed reactor for the continuous steam hydrolysis of uranium hexafluoride has been achieved within the range of conditions discussed above. Problems associated with this unit, such as coating buildup, can be overcome by scheduling periodic clean-out of the reactor. Other problems, considered minor, can be circumvented by proper design.

2. Reduction of Uranyl Fluoride to Uranium Dioxide

The second step in the conversion of uranium hexafluoride to uranium dioxide by the two-step method involves the reduction of uranyl fluoride to uranium dioxide with hydrogen-steam mixtures. Previous work (see ANL-6379, page 185) showed the importance of gas composition and temperature, a 50-50 hydrogen-steam mixture appearing optimum along with high temperatures, near 650 C; material containing only 200 ppm residual fluoride was produced in 4-hr batch experiments.

The effects of gas velocity, bed depth, and feed particle size on the rate of fluoride removal (the criterion for degree of reduction) were studied in current batch fluidization experiments conducted in a 2-in. Monel reactor. All runs were conducted at 650 C with the optimized reactant gas mixture, 50 mole percent hydrogen-50 mole percent steam. Uranyl fluoride produced in the uranium hexafluoride-hydrolysis step was used as feed material.

Effect of Gas Velocity

The effect of gas velocity was studied in the range from 0.2 to 2.0 ft/sec with 3-kg beds of -40 +60 mesh size (minimum fluidizing velocity 0.25 ft/sec) uranyl fluoride at 650 C.

The conversion times of the beds were quite good within the fluidizing velocity range, 0.6 ft/sec or greater, requiring 4 hr or less to achieve fluoride specifications, <250 ppm residual fluoride (see Table 39). The run at subfluidizing velocity (0.2 ft/sec) resulted in 350 ppm residual fluoride in an equivalent period. High velocities, which introduced more reactants in a given period, resulted in higher rates of fluoride removal from the outset; for example, fluoride contents after one hour were near 0.2 percent for velocities near 2.0 ft/sec and over three percent for velocities below 1.0 ft/sec. Acceptable material was produced in less than 3 hr at the higher velocity, during which time nearly 15-fold excess hydrogen was used.

Table 39

THE EFFECT OF GAS VELOCITY ON THE CONVERSION OF URANYL FLUORIDE TO URANIUM DIOXIDE

Temperature: 650 C
Bed: 3 kg of uranyl fluoride (12.3 weight per cent fluoride)
Particle Size: -40 +60 mesh
Gas Composition: 50-50 hydrogen-steam by volume

Run No.	Superficial Velocity (ft/sec)	Weight Percent Fluoride in Sample Time (min)			
		60	120	180	240
28	0.2[a]	-	-	-	0.035
33	0.6	3.1	0.086	0.025	0.010
30	0 8	3.9	0.33	0.03	0.015
21	1.3	-	0.26	0.028	0.015
32	1.8	0.21	0.026	0 010	0.008
31	2.0	0.18	0.033	0.010	-

[a] Static-bed run; minimum fluidizing velocity 0.25 ft/sec.

Effect of Particle Size

Overall fluoride removal was found to improve with decreasing particle size. Several runs in which 3-kg beds of different average sized particles were used are compared in Table 40. The average particle diameter was calculated by the formula

$$D_{vs} = W/\sum (W_1/D_1) \quad ,$$

where W and W_1 are the weight of sample and sieve fraction, respectively, and D_1 is the mean diameter of the sieve fraction. After a 4-hr reaction time, results showed 200 and 80 ppm residual fluoride for the 630- and 335-μ beds, respectively.

Table 40

THE EFFECT OF FEED PARTICLE SIZE ON CONVERSION OF URANYL FLUORIDE TO URANIUM DIOXIDE

Temperature: 650 C
Bed: 3 kg of uranyl fluoride (12.3 weight percent fluoride)
Gas Composition: 50-50 hydrogen-steam by volume

Run No.	Superficial Velocity (ft/sec)	Average Particle Diameter[a] (μ)	Weight Percent Fluoride in Sample after Time (min)			
			60	120	180	240
15	2.0	630	0.50	0.06	-	0.02
39	1.5	380	0.48	-	-	0.01
32	1.8	335	0.21	0.03	0.01	0.008

[a] Average particle diameter expressed by the formula: $D_{vs} = W/\sum (W_1/D_1)$, where W and W_1 are the weight of sample and weight of sieve fraction, respectively, and D_1 is the average diameter of the sieve fraction.

Effect of Bed Depth

The conversion rate was found to change with bed depth expressed as the "length over diameter" (L/D) ratio.

Bed weights of 3, 6, 7.5, and 9 kg of uranyl fluoride gave static L/D ratios of approximately 3, 5, 6, and 7. All beds were reduced to less than specification grade (250 ppm) fluoride content within 4 hr. The results

are listed in Table 41. From these data it would appear that conversion is not hampered by increasing bed depth, at least not within the L/D range tested. Deeper beds were not tested because of the limited capacity of the reactor vessel.

Table 41

THE EFFECT OF BED DEPTH ON CONVERSION OF URANYL FLUORIDE TO URANIUM DIOXIDE AND ON PARTICLE BREAKUP

Temperature: 650 C
Bed Composition: ~50% -20 +40 screen fraction
~50% -40 +60 screen fraction
Superficial Velocity. 1.5 ft/sec

Run No.	Static Bed Depth (L/D)	Weight Percent Fluorine in Sample Time (min) 120	240	300	360	Breakup Index[a] (-60 basis)
34	7	0.10	0.018	0.008	0.007	0.55
37	6	0.10	0.022	0.016	0.014	0.56
38	5	0.05	0.019	0.010	0.014	0.56
39	3	0.48	-	-	0.010	0.65

[a]Breakup index = weight fraction of final bed below the minimum size in the starting bed.

Particle breakup when expressed in terms of "Breakup Index" (see Table 41) does not appear to vary appreciably with bed depth except in the most shallow bed. The increased breakup may be due to increased bed agitation in low "L/D" ratio beds. Typical starting and final bed particle size distribution follows:

Mesh Size	Fraction in indicated size range +20	+40	+60	+100	+200	+325	-325
Starting Bed	0.01	0.55	0.41	0.03	-	-	-
Final Bed	0.01	0.14	0.30	0.28	0.17	0.08	0.02

The tap bulk density of the dioxide product was found to vary from 4.2 to 4.8 g/ml. Individual particle densities have been determined as follows: 9.675 g/ml in xylene, 9.228 g/ml in water, and 6.22 g/ml in mercury, the last value giving an indication of overall internal voidage. Reactor corrosion resulted in 100 to 130 ppm nickel in the product beds.

D. Calcination Studies in Small-diameter Columns
(J. W. Loeding, J. Kincinas, E. Johanson*)

Work continued on establishing the feasibility of using small-diameter columns for continuous fluid-bed calcination operations. This application is intended primarily for these systems involving nuclear criticality, such as the processing of highly enriched uranium or plutonium solutions and those systems where a reduction in the total quantity of off-gas is desirable.

The technique used, positioning of the feed atomizing nozzle in the bottom of the calciner and directing it upwards, thus permitting the atomizing gas (together with gaseous decomposition products) to be used as the fluidizing medium, represents a major departure from the more usual process of spray-injecting the feed into the side of a fluid-bed reactor.[29]

Work thus far has utilized aluminum oxide granules as bed material, calcination temperatures of about 335 C, and 1 M aluminum nitrate solution as feed at rates from 8 to 16 ml/min. Following initial work in glass equipment, stainless steel equipment was employed as shown in Figure 35.

FIGURE 35
2 1/4-IN. DIAMETER EXPERIMENTAL STAINLESS STEEL CALCINER

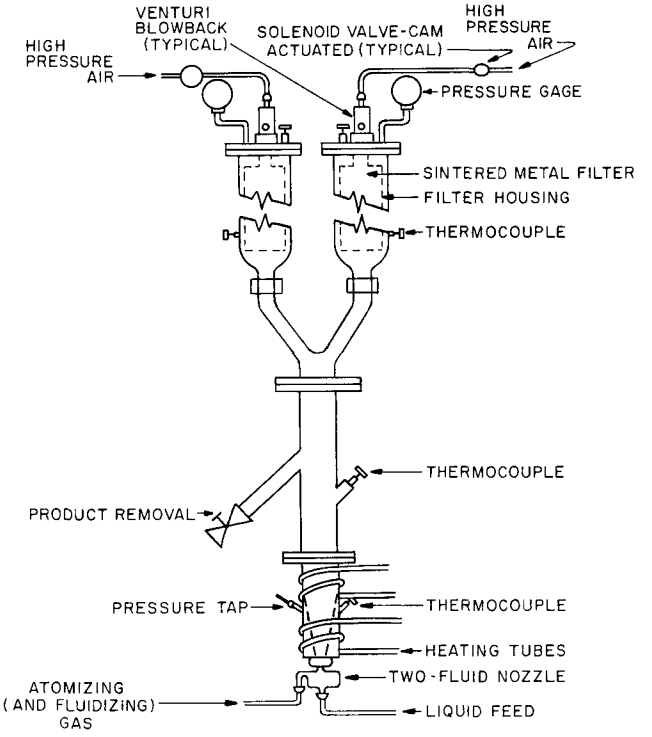

*Co-op student from Northwestern University.

[29] Jonke, A. A., et al., The Use of Fluidized Beds for the Continuous Drying and Calcination of Dissolved Nitrate Salts, Nuclear Science and Engineering 2, 303-319, (1957).

(The dual filters and blowback system are a recent equipment change and have not been used as yet.) The $2\frac{1}{4}$-in. column is tapered at the bottom to correspond to the angle of the feed spray. Results from several of the runs performed in this equipment are shown in Table 42.

Table 42

OPERATING CONDITIONS AND RESULTS OF CALCINATION RUNS

Equipment: 2 1/4-in.-diameter stainless steel calciner
Nozzle: Modified extended tip. Pressure type.
Bed Weight: 325 g
Bed Size: 100 percent -20 +80 mesh
Liquid Feed: 1 M $Al(NO_3)_3$

Run No.	Bed Temp (C)	Feed Rate (ml/min)	Atomizing Air Rate (scfm)	Air-to-liquid Rate Ratio (v/v)	Period of Operation (hr)	Comments
SD 18	325	9.9	0.72	2050/1	1.3	High air rate produced excessive fines (22% < 140 mesh)
SD 18A	325	10.3	0.60	1700/1	1.2	Slight fines production (2% < 140 mesh)
SD 20	335	8.9	0.60	1900/1	5.2	Moderate fines production (6% < 140 mesh)
SD 21	340	16.6	0.60	1020/1	1	Found small caking at nozzle (2% < 140 mesh)
SD 26	330	9.7	0.60	1740/1	4.3	Found small agglomerates on nozzle (~2% < 140 mesh)
SD 27	340	8.7	0.54	1740/1	6	Moderate fines production (5% < 140 mesh)
SD 28	330	14.0	0.54	1070/1	3	Negligible fines production (1% < 140 mesh)

Runs 18 and 18A were made to compare the effect of atomizing air rates on the product particle size. The higher rate of Run 18 resulted in the formation of excessive fines, over 22 percent less than 140 mesh in only 1.3 hr of operation. Run 18A, in an equivalent period at reduced air rates, resulted in only about two percent less than 140 mesh. The other runs reported were made to verify these results and to determine whether reduced air-to-liquid rate ratios (a measure of the degree of success obtained in reducing the off-gas volume) were practicable. This ratio can be reduced by either reducing the atomizing air rate or increasing the liquid feed rate or both. The longest of these runs (Run 27) utilized an air-to-liquid rate ratio of 1740, which is approximately equal to the ratio used in earlier work in a 6-in.-diameter calciner with horizontal spraying (ANL-6322). Run 28 represents the best results to date, a ratio of 1070 being achieved. Operations were smooth and the amount of less than 140 mesh particles produced was only 1.1 percent.

There has been virtually no evidence of particle growth in any of the runs, and fines production, at least in short runs, also seems to be no problem. Greatest concern at the present time is with operational reproducibility. Since several runs were interrupted shortly after the switchover from water (used during startup) to aluminum nitrate feed because of the formation of agglomerates in the bed, a review of the startup procedure will be made. Future work will also attempt to reduce further the air-to-liquid rate ratio.

III. REACTOR SAFETY

The oxidation, ignition, and combustion processes of uranium, zirconium, plutonium, and other metals and their compounds are being studied to provide information to aid in minimizing the hazards associated with handling these materials.

A program of theoretical studies has been initiated to relate quantitatively ignition results to isothermal oxidation data. Isothermal data from experiments with zirconium, covering the range from 400 to 900 C, was used to calculate theoretical temperature-time curves corresponding to shielded ignition tests. Calculations were made by a stepwise method using a simple heat transfer model. Theoretical ignition temperatures were obtained for single pieces of zirconium having specific areas of 5, 50, 500, and 5000 sq cm/g.

Previous experimental studies of zirconium by the shielded ignition method used flowing helium to shield the specimen while it was brought to temperature. Helium flow was then switched to oxygen and it was determined visually whether ignition occurred or not. It was not entirely clear how much preoxidation of the specimens occurred while the sample was heating. A brief experimental study was, therefore, made of zirconium ignition under conditions where no preoxidation could occur. Results indicated that preoxidation effects encountered in studies by the helium flow method were negligible except for the finest foils (highest specific area) studied. Further experimental studies were made by the helium flow method to test the effect of ends or edges exposed to oxygen. Edge effects were found to be significant for large wires (low specific area). Ignition was able to occur at lower temperature at exposed sharp edges.

Comparison of theoretical ignition temperatures with experimental values was then made after it was certain that preoxidation and edge effects were not complicating the experimental results. Ignition temperatures agreed within approximately 100 C.

Efforts to calculate burning curve ignition temperatures with uranium by similar methods failed. Failure was attributed to a lack of isothermal oxidation data above 300 C. Studies were, therefore, undertaken of the isothermal oxidation of uranium between 300 and 600 C. The studies were made in a metal "heat sink" reaction cell in which specimens were pressed against metal heat sinks by a spring. This was effective in preventing excessive self-heating. Preliminary data with Argonne base uranium, "β-quenched," showed that low-temperature rates could be extrapolated to 400 C. Reaction rates then decreased slightly between 400 and 500 C. Rates began to rise rapidly with temperature above 500 C.

Studies of burning propagation along uranium and zirconium foil strips are continuing. Simultaneous measurements of propagation rates and burning temperatures have been obtained by means of a photoelectric pyrometer. Studies were concentrated on the effects of additions of halogenated hydrocarbons to the air. Results were obtained for a number of halogenated hydrocarbons. The effectiveness of the compounds in reducing burning propagation rates and temperatures was believed due to their tendency to decompose thermally at or very near to the oxidizing metal surface. Fragments produced in the decomposition were able to react with oxygen in the gaseous diffusion zone near the metal. This oxygen was, therefore, lost to the metal and was responsible for decreased rates and temperatures. Carbon tetrafluoride (CF_4) was ineffective in decreasing rates and temperatures, presumably because of insufficient thermal decomposition. Methyl and ethyl iodides were also ineffective because thermal decomposition occurred at lower temperatures at the outer edge of the diffusion boundary layer. In general, those compounds having optimum chemical stability, such as trifluorobromomethane (CF_3Br), methyl chloride (CH_3Cl), and chloroform ($CHCl_3$), were most effective.

Studies were made of the effect of halogenated hydrocarbons on burning curve ignition temperatures of uranium. Ignition temperatures were unaffected by small additions to the air of compounds containing only carbon, hydrogen, and fluorine atoms. Compounds containing bromine or chlorine atoms lowered the ignition temperatures significantly. Results suggested that there is an exothermal reaction between chlorine or bromine compounds and uranium dioxide.

Installation of apparatus in new plutonium glovebox facilities is complete. Apparatus has been assembled to study (1) burning propagation, (2) ignition, and (3) controlled oxidation. Controlled oxidations are carried out in a recording thermobalance which has been equipped with a specimen thermocouple. A magnetic amplifier is used to provide a recorded output so that there is not interference with the balance operation.

The experimental program to determine rates of reaction of molten reactor fuel and cladding metals with water is continuing. One method involves the rapid melting and dispersion of metal wires in a water environment by a surge current from a bank of condensers. A series of runs with uranium in heated water was completed. Results showed that considerably more reaction occurred in heated water than in room-temperature water. The uranium results were, therefore, consistent with previous results with zirconium. The findings added supporting evidence to the theoretical account of the zirconium-water reaction, which has been presented in previous quarterlies.

Water temperature in the uranium runs ranged from 100 to 125 C (water vapor pressure, 15 to 33 psia). Attempts to study the reaction in water at 200 C failed because of very extensive corrosion of the specimens during the run preparation period.

Particle sizes of residue from uranium runs by the condenser-discharge method are reported. Transient pressure traces from uranium indicated that the progression of slow reaction rates to explosive rates occurred over the temperature range from 1600 to 2500 C. Results were consistent with the findings for zirconium that particles smaller than 1000μ in heated water and 500μ in room temperature water could undergo the explosive reaction. Analyses of the hydrogen retained by the residue from uranium runs indicated that, at most, a few percent of the hydrogen generated during a run is retained by the partly oxidized metal.

A second method of studying metal-water reactions involves the rapid contact of steam with heated metal. In this method, the metal receives a "pressure pulse" of water vapor. The apparatus is entirely enclosed in a box heated to 105 C. Runs with 500 mm of water vapor reacting with molten aluminum at 800, 1000, and 1200 C are reported. Rates followed the cubic rate law; an activation energy of 21,700 cal/mole described the effect of temperature. A series of runs with aluminum-5 percent uranium alloys at 1200 C gave slightly less reaction than that obtained with pure aluminum.

The experimental work on metal-water reactions during nuclear reactor excursions was continued. Four transients were completed in TREAT on fuel pins with a uranium dioxide core (20 percent enriched) clad in 18-mil-thick stainless steel-304. The data obtained from these meltdowns in 25 C water are as follows:

	CEN Transient Number			
	64	67	65	66
Megawatt-second burst:	140	185	190	230
Millisecond period:	115	290	50	97
UO_2 core density, % of theor	89 (water logged)	98	89	98
% SS-H_2O reaction:	0 8	0 3	5 2	9 0
Final appearance of fuel pin clad:	two small ruptures, darkened area	intact, darkened central area	fragmented, partly melted	fragmented, partly melted
core:	distorted, cracked	radial cracks	fragmented, fine particles	fragmented, coarse particles

Correlation of the data on the experiments with uranium dioxide core pins indicate a progressive increase in the amount of cladding (SS-304)-water reaction as the reactor burst becomes more energetic. For periods in the range 48 to 121 ms, the extent of metal-water reaction is 1.2, 6.0, and 16.0 percent stainless steel reacted for energies of 200, 300, and 400 cal/g uranium dioxide, respectively. For these uranium dioxide core fuel pins, the dividing point between destructive and nondestructive transients (on fast periods of 49 to 121 ms) is a burst of about 130 Mw-sec or 174 cal/g of core. This corresponds to a peak central core temperature of 2200 C for adiabatic heating of the uranium dioxide.

An evaluation was made of previous data obtained in TREAT on mixed oxide-core fuel pins; the results indicate a threshold temperature of 2300 C (for the central core) for incipient destruction of the fuel pin. Thus, both pure and mixed oxide-core fuel pins have similar behavior with regard to the maximum allowable temperatures in transients on fuel elements submerged in nonflowing, room-temperature water.

A. Metal Oxidation and Ignition Kinetics
(L. Baker)

1. Theory of Metal Ignition
(L. Baker, J. D. Bingle, R. Koonz*)

Extensive studies of the ignition behavior of zirconium and uranium have been reported in previous quarterlies. Isothermal oxidation rates of these metals have also been reported. It is the purpose of the present study to determine the quantitative relationship between these two kinds of data. Such a relationship should exist if metal ignitions are purely thermal ignitions. A thermal ignition is merely an accumulation of heat, in which the reacting system is generating more heat than can be dissipated by heat loss mechanisms, leading to a rapidly increasing temperature. Ignition behavior, therefore, should be precisely predictable from isothermal rate data if a sufficiently accurate heat transfer model can be established.

Two experimental procedures have been used to study ignition. One of these is called the burning curve method and the other the shielded ignition method. In the burning curve method, samples are heated at a uniform rate (usually 10 deg/min) in a flowing oxidizing atmosphere. As the rate of reaction increases, the sample self-heats and finally ignites. A graphical intersection method is used to determine ignition temperature. In the shielded ignition method, samples are brought to a precisely

---

*Summer employee from Wabash College.

controlled temperature either in vacuum or in inert atmosphere. The oxidizing gas is then suddenly admitted and it is determined visually whether ignition occurs or not. A series of runs is used to determine the ignition temperature.

Efforts are underway to formulate mathematical models to describe both types of ignition experiment. Preliminary attempts to compute burning curve ignition behavior of uranium led to the conclusion that the existing isothermal data for uranium did not extend into the temperature range of interest, 300 to 600 C, and that extrapolation of data from below 300 C was not satisfactory. For that reason, experimental studies in the high-temperature range were begun. These studies will be described in a later section. Isothermal data with zirconium[30] covered the range from 400 to 900 C and was believed to cover adequately the temperature range of interest in ignition. Mathematical description of shielded ignitions of zirconium was, therefore, undertaken.

a. Mathematical Description of Shielded Ignition of Zirconium

The following cubic rate law was found to apply to zirconium over the temperature range from 400 to 900 C:

$$w^3 = 5.94 \times 10^{16}\, t \exp\left(-\frac{42{,}700}{RT}\right) \quad , \tag{1}$$

where w is the oxygen uptake in μg/sq cm, R is the gas constant, 1.987 cal/(mole)(C), T is metal temperature, K, and t is time in min. It is more convenient to work in units of thickness of metal reacted:

$$w = 10^6\, M_{O_2}\, \rho X / M_{Zr} \quad , \tag{2}$$

where M_{O_2} is molecular weight of O_2 (32 g/mole), M_{Zr} is atomic weight of Zr (91.22 g/gram atom), ρ is metal density (6.5 g/cu cm), and X is thickness of metal reacted (cm). The rate law then becomes

$$X^3 = 0.00501\, t \exp\left(-\frac{42{,}700}{RT}\right) \quad , \tag{3}$$

and in differential form

$$\frac{dX}{dt} = \frac{0.00167}{X^2} \exp\left(-\frac{42{,}700}{RT}\right) \text{cm/min} \quad . \tag{4}$$

---

[30] Porte, H. A., et al., J. Electrochemical Soc. 107, 506 (1960).

The heat balance per g of metal can be expressed as follows:

$$C_p \frac{dT}{dt} = Q\rho S \frac{dX}{dt} - hS(T - T_a) - \sigma \epsilon S(T^4 - T_a^4) \qquad (5)$$

Self-heating | Convection Heat Loss | Radiation Heat Loss

where C_p is specific heat [0.0808 cal/(g)(K)], Q is heat of reaction (2866 cal/g), S is specific area (sq cm/g), h is heat transfer coefficient [0.0005 cal/(sq cm)(sec)(K)], ϵ is emissivity (0.75), σ is the Stefan-Boltzmann constant [1.36×10^{-12} cal/(sq cm)(sec)(K^4)], and T_a is ambient temperature (constant for shielded ignition). Reasonable values for the heat transfer coefficient h and the emissivity ϵ were chosen arbitrarily for the initial calculations. The value for h was checked by measuring the difference between furnace temperature and sample temperature for inert cubes in the burning curve apparatus at 200 C. The fact that heat transfer coefficients usually increase somewhat with temperature was ignored in the present study.

Simultaneous solution of Equations 4 and 5 would yield the temperature-time history of a zirconium sample of specific area S, located in a furnace at temperature T_a when suddenly exposed to oxygen. Hand calculations were made by choosing a small time interval, usually 10^{-6} min.

Equations 3, 4, and 5 were expressed in finite difference form:

$$(\Delta X)^3 = 0.00501\ \Delta t \exp\left(-\frac{42{,}700}{RT_a}\right) \qquad (3A)$$

(First Interval)

$$\Delta X = \frac{0.00167}{X^2}\ \Delta t \exp\left(-\frac{42{,}700}{RT}\right) \qquad (4A)$$

(Succeeding Intervals)

$$\Delta T = \frac{Q\rho S}{C_p}\Delta X - hS(T - T_a)\Delta t - \sigma \epsilon S(T^4 - T_a^4)\Delta t \quad . \qquad (5A)$$

Reaction occurring during the first interval was calculated from Equation 3A. The temperature ΔT occasioned by reaction ΔX was computed from Equation 5A. New values of reaction X and temperature T were then calculated. The process was then repeated with the alternate use of Equations 4A and 5A. Values of ΔX decreased rapidly with time so that larger

time intervals could be used in later stages of calculation. Time intervals were chosen so that no more than a 20-degree temperature rise occurred in any one interval. In this way, it was often possible to determine whether a theoretical ignition (temperature runaway) occurred or not in 10 time intervals.

Results of calculations for specific areas of 5, 50, 500, and 5000 are summarized in Table 43. Examples of the calculated temperature-time curves for specific areas of 5, 50, and 500 are plotted in Figure 36. Calculations for material of low specific area (S = 5) indicated very large temperature rises (up to 500 C) for nonignition runs near the ignition temperature. Theoretical results will be compared with experimental results in a later section.

Table 43

RESULTS OF THEORETICAL CALCULATIONS OF ZIRCONIUM IGNITION

Specific Area (sq cm/g)	Initial Temp (K)	Initial Temp (C)	Peak Temp Rise (C)	Time to Peak (sec)	Ignited
5000	550	277	26	0.009	no
5000	600	327	∞	-	yes
500	650	377	37	0.054	no
500	700	427	∞	-	yes
50	850	577	137	0.48	no
50	900	627	∞	-	yes
5	1100	827	96	1.20	no
5	1150	877	132	1.20	no
5	1200	927	187	1.20	no
5	1300	1027	343	1.20	no
5	1350	1077	502	1.20	no
5	1400	1127	∞	-	yes

b. Measurement of Shielded Ignition Temperature of Zirconium

Results of shielded ignition tests with zirconium foils, made in a quartz tube furnace, were given in previous reports (see ANL-5974, page 94, and ANL-6145, page 154).

FIGURE 36
RATE OF TEMPERATURE RISE OF OXIDIZING ZIRCONIUM SPECIMENS

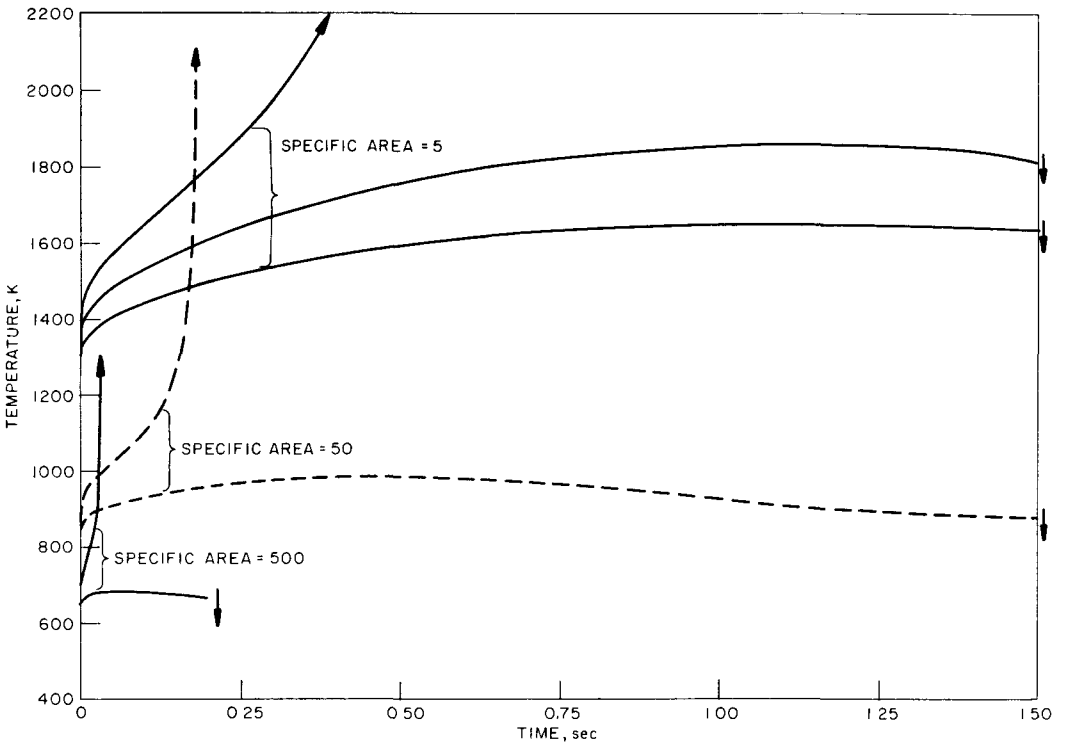

The furnace was brought to the test temperature with helium flowing from top to bottom through the tube. The zirconium sample, mounted on a thermocouple, was then suddenly inserted into the tube. After one to one and one-half minutes, the helium flow was switched to oxygen and it was determined whether ignition occurred or not.

It was decided to check these data for two reasons. It was not entirely clear how much pre-oxidation of the foil specimens occurred while it was reaching temperature equilibrium in flowing helium. The slightest contamination of the helium with oxygen or water vapor could conceivably produce an oxide film on the metal before the ignition test. It was also possible that the switch from the helium to oxygen was not sufficiently rapid. It was considered likely that pre-oxidation might have a marked effect on zirconium ignitions because of the highly protective nature of the films.

The other point in question concerned edge and end effects. The edge or the free end of a foil strip, considered separately from the bulk of the foil, has a greater effective specific area than the foil considered

as a whole. It was, therefore, of importance to determine whether edge effects gave rise to a lowered ignition temperature.

A brief study of zirconium ignition was, therefore, made under conditions where no pre-oxidation could occur. The zirconium foil specimens were spot-welded to large zirconium wires which, in turn, were welded to a platinum support structure. The entire assembly fit into 12-mm quartz tubing which was formed into vials. The vials were evacuated to 10^{-6} mm and sealed off while in vacuum. The zirconium wire sections and later the specimen foil were heated to ca. 1400 C for a few minutes by manipulating the vials in the field of a radiofrequency generator. This operation served to eliminate residual oxygen in the vial and caused the minute oxide film present at room temperature to diffuse into the metal. Foil surfaces had a bright luster following the induction heating. The entire vial was then heated to 1000 C in a furnace and it was determined that no decrease in the metallic luster occurred, the results suggesting that no significant oxide was formed from gas desorbed from the quartz surfaces.

Vials containing the bright zirconium foils were loaded into a reaction cell made of 2-in. stainless steel tubing, 10 in. long. Vials were clamped rigidly in place with asbestos-lined steel clamps. Provision was made for an externally operated screw to break the vials at one end located away from the specimen assembly. The reaction cell contained a large Pyrex window and fittings through which a flow of oxygen gas was passed. The entire reaction cell was heated to the test temperature during a run. The vial was then broken and it was determined visually whether ignition occurred or not.

Ignition temperatures obtained by the quartz vial method are compared in Table 44 with those obtained by the helium shielded method. Results showed that agreement between the two methods was excellent except for the foil of highest specific area (thinnest) tested. This foil, 0.007 mm thick, ignited nearly 100 degrees lower in the quartz vial apparatus. However, this 0.007-mm foil was so thin that it was impossible to polish (using 600 grit SiC paper) prior to the helium flow experiment as were the other foils. These experiments indicate that the helium flow method is satisfactory for all but the finest foils obtainable.

Studies to determine the magnitude of edge and end effects were made with zirconium wire specimens by the helium flow method. The use of wires of circular cross section eliminated the presence of an edge. Control runs were made with wires having a flat end exposed to the oxygen. These results are included in Table 44 and agree with foil data for specimens having the same specific area. Runs were also made with wires whose ends were shielded by rounding both ends of the wire and forcing them into holes drilled into $\frac{1}{4}$-in. lengths of $\frac{1}{4}$-in.-diameter stainless steel rods. The presence of the rods acted as heat sinks as well as shields to

prevent ignition at wire ends. Sufficient wire length (length/diameter greater than 30) assured that the wire midpoint was not affected by the presence of heat sinks at the wire ends. The results are given in the right-hand column of Table 44. Results with shielded and unshielded ends diverged for the two largest wires. Careful visual examination of ignition of the larger unshielded wires revealed that ignition began at one end and then propagated rapidly across the specimen. Wires with shielded ends appeared to ignite uniformly over the wire length.

Table 44

SHIELDED IGNITION TEMPERATURES OF ZIRCONIUM IN OXYGEN

Specimen Dimensions	Specific Area (sq cm/g)	Ignition Temp (C) by Method: Helium Flow Method, Ends Exposed	Quartz Vial Method, Ends Exposed	Helium Flow Method, Ends Shielded
Foils (2.5 mm wide x 22 mm long)				
0.94 mm thick	4.4	935	-	-
0.27 mm thick	12.9	833	795	-
0.13 mm thick	25.2	786	778[a]	-
0.02 mm thick	155	665	645	-
0.007 mm thick	441	600	508	-
Wires (30 mm long with ends exposed and 50 mm long with ends shielded)				
1.52-mm diameter	4.1	953	-	1036
0.76-mm diameter	8.1	896	-	932
0.38-mm diameter	16.2	847	-	833

[a]Underlined values are plotted in Figure 37.

c. Comparison of Theoretical and Experimental Ignition Temperatures

The experimental values of ignition temperature for zirconium foils and wires in oxygen are plotted in Figure 37. Results that were affected either by pre-oxidation effects (high specific area) or by end effects (low specific areas) were eliminated before plotting. The values used in the plot are underlined in Table 44. The theoretical results summarized in Table 43 are also plotted in Figure 37. It is apparent from the results that theoretical ignition temperatures are low at high specific areas and high at low specific areas although both curves have a somewhat similar shape. The upsweep of the theoretical curve in Figure 37 is due to the greatly increased radiation heat losses at high temperatures. The comparison of theoretical and experimental results

suggests that perhaps the emissivity value (0.75) used in the calculations was too high. The low, calculated temperature at high specific area indicates that perhaps the convection heat transfer coefficient [0.0005 cal/(sec)(sq cm)(K)] was too low, since heat losses at lower temperatures occur in large measure by convection. Future studies may include measurements of heat loss coefficients under conditions similar to those used in shielded ignition experiments.

FIGURE 37
SPECIFIC AREA DEPENDENCE OF ZIRCONIUM IGNITION

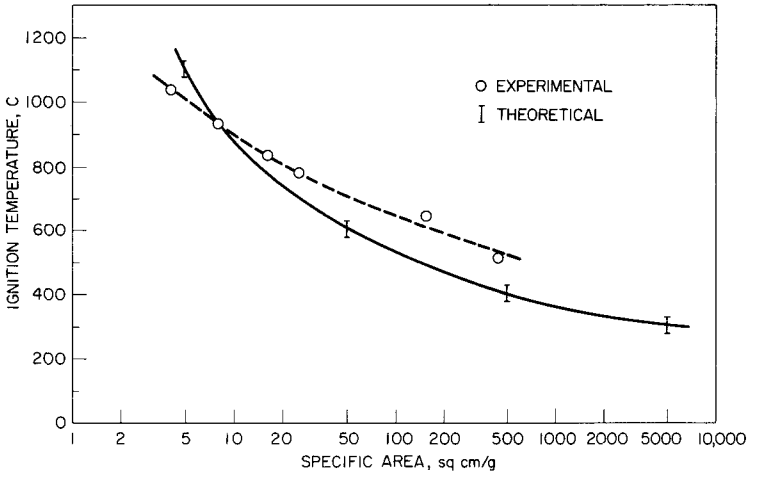

Theoretical temperature-time curves for specimens of low specific area, shown in Figure 36, indicated that it required over one second for the metal to reach a peak temperature before cooling occurred in nonigniting runs. Therefore, it appeared feasible to attach very fine thermocouples to the specimen wires and to obtain a direct comparison between calculated and measured rates of temperature rise for the large wires. Platinum, platinum-10% rhodium thermocouples (5-mil wires) were spot-welded to the center of 1.52-mm (60-mil) zirconium wire specimens. The ends of the specimen were shielded by stainless steel caps. The fine thermocouples were connected to a Visecorder high-speed oscillograph. The resulting temperature-time curves are compared with a theoretical curve for a sample of similar specific area in Figure 38. It is apparent that the experimental curves have the same general features as the theoretical curve. It is likely that much of the difference between experimental and theoretical curves are due to a lagging thermocouple response.

The combined theoretical and experimental studies of zirconium shielded ignition indicate that the course of ignition can be computed from isothermal rate data and a simple heat transfer model. This provides evidence that zirconium ignitions are thermal in character. An important point is that ignition behavior under conditions other than the shielded method may also be predicted from isothermal rate data if a heat transfer model can be found which adequately describes the environmental conditions.

FIGURE 38
COMPARISON OF THEORETICAL AND EXPERIMENTAL
TEMPERATURE CURVES FOR ZIRCONIUM IN OXYGEN

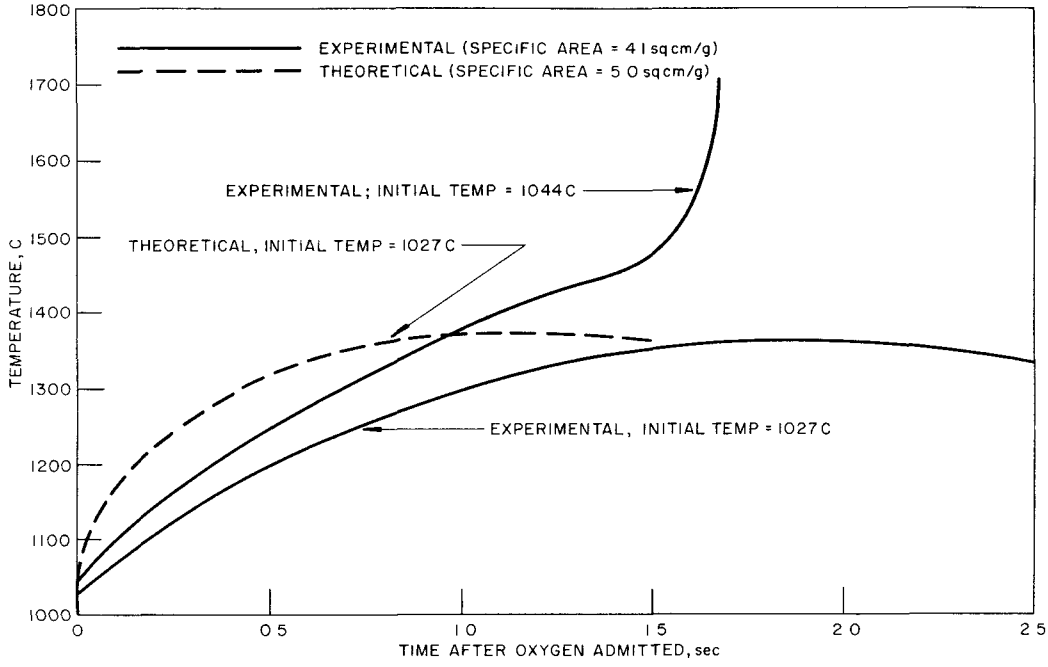

Conditions of the greatest practical importance involve aggregates of metal, not merely single pieces. Ignition temperatures of aggregates or powders are lower than those of single pieces of equal specific area because of the heat shielding effect of particles on each other. Future studies will be made of methods to introduce heat shielding effects into the heat transfer model.

2. Isothermal Oxidation of Uranium at High Temperature
(L. Baker, J. D. Bingle, G. Klepac,* R. Koonz**)

Efforts are underway to describe quantitatively temperature-time curves obtained experimentally with uranium by the burning curve method. This treatment should be similar to that reported for zirconium in the previous section. Isothermal rate data, covering the temperature range from 125 C to 300 C, for uranium were reported in ANL-5974, page 50. Ignition temperatures for single pieces, however, range from 325 to 600 C. Attempts to extrapolate the previous data were not satisfactory. It was therefore necessary to embark on a program of studies of the isothermal oxidation rates of uranium in the temperature range from 300 to 600 C.

---

*Summer employee from Carnegie Institute of Technology.

**Summer employee from Wabash College.

Previous studies up to 300 C were cut off because it was observed that the uranium cube specimens were self-heating as much as 25 C during a run at 325 C. It was, therefore, incorrect to assume that the controlled furnace temperature was also the metal temperature. The metal specimen was contained in a glass boat during these runs. Present studies were conducted with a massive metal "heat sink" reaction cell. Details of cell construction are shown in Figure 39. The uranium specimen, usually a one-cm cube, was compressed between two massive pieces of either aluminum or stainless steel by a stainless steel spring. The reaction cell was connected to the same apparatus used to measure volume additions to the system, while maintaining a constant pressure, that was used for the 125 to 300 C data. This apparatus is described in ANL-5974, page 41.

FIGURE 39
APPARATUS FOR ISOTHERMAL OXIDATION STUDIES AT HIGH TEMPERATURE

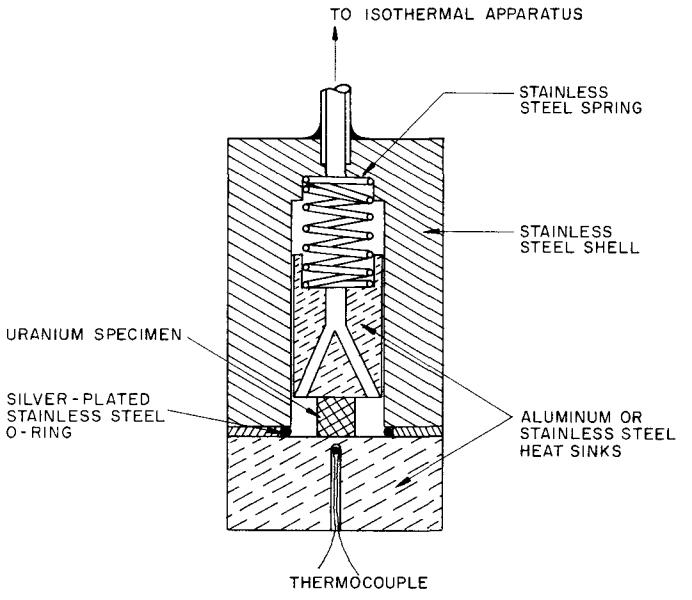

Preliminary studies over the temperature range from 300 to 600 C were made with Argonne-base (β-quenched) uranium. These runs were made with pure oxygen at 200 mm pressure. The nature of the oxidation curves is indicated in Figure 40. The curves correspond to the second-stage reaction reported previously. The slow, linear, first-stage reaction is barely perceptible in most of the high-temperature runs. Rates at 300 C decreased somewhat in later stages of the run. Rates accelerated somewhat as reaction progressed for runs in the range from 350 to 450 C. Rates again decreased with time for runs from 500 to 600 C. This behavior is apparent in Figure 40. Because of this, it was difficult to make precise comparisons between rates at differing temperatures. Data reported previously at temperatures below 300 C were the maximum

rates observed. Rates above 300 C were arbitrarily taken as the instantaneous rate occurring after 10,000-μg/sq cm oxidation. These rates are plotted as a function of reciprocal temperature in Figure 41.

FIGURE 40
OXIDATION OF URANIUM IN 200 mm OXYGEN AT VARIOUS TEMPERATURES

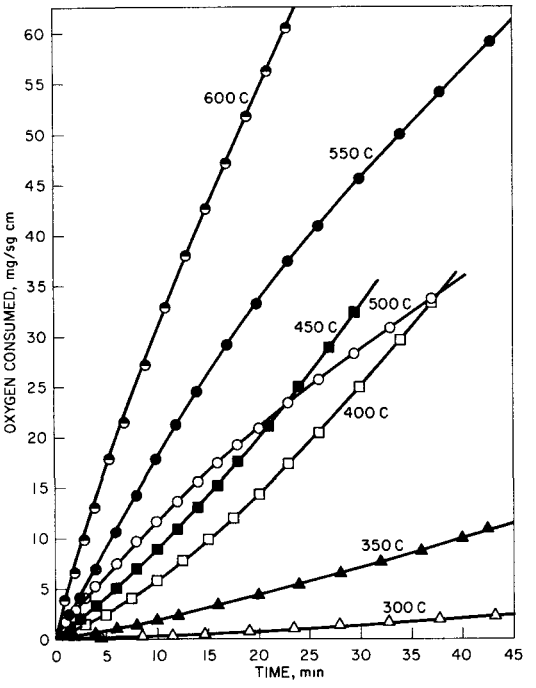

FIGURE 41
EFFECT OF TEMPERATURE ON OXIDATION RATE OF URANIUM IN 200 mm OXYGEN

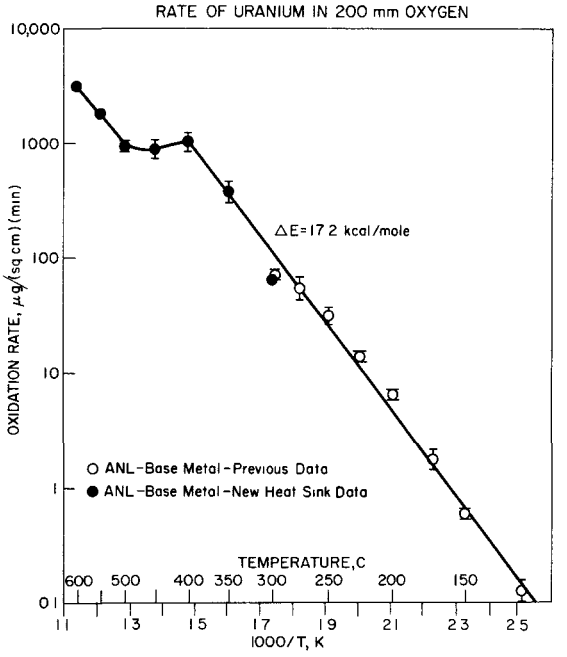

Figure 41 shows that the low-temperature rates cannot be extrapolated beyond 400 C. Rates between 400 and 500 C actually decrease with temperature. Rates above 500 C again increase rapidly with temperature. Further studies will be made with Battelle-base ("as cast") metal because of striking differences noted in the burning curve ignition behavior of the two metals. An effort to measure the metal temperature rise during runs in the "heat sink" apparatus is also under way. Data presented in Figures 40 and 41 must be considered tentative until additional runs can be completed, including measurements of self-heating under these conditions.

3. Burning Propagation and Ignition Studies - The Effect of Halogenated Hydrocarbons
(L. Leibowitz, L. W. Mishler)

The burning propagation rate, that is the rate of advance of a combustion zone along a wire or foil strip, has been used to compare the effects of various halogenated hydrocarbons on uranium and zirconium combustions in air. The dual pyrometer used in this work allows simultaneous measurements to be made of burning propagation rate and burning temperature (see ANL-6333, page 210).

It has been found that both the burning propagation velocity and the maximum burning temperature are lowered by the presence of a few percent in air of any one of a number of halogenated hydrocarbons (see ANL-6379, page 195). Some tests have recently been made with zirconium foil strips (0.02 x 3 mm) and additional work has been carried out with uranium (0.013 x 3 mm).

a. Burning Propagation Rates and Temperature

All of the data now available are listed in Table 45. Each value is an average of at least two runs, that is, two velocities and four temperatures. For convenience, the information is assembled so that comparisons can readily be made of the effect of variation in the constitution of the organic molecule. In group 1(a) are compared four molecules of the type CF_3-X. Clearly, CF_4 is nearly inert, producing only a small change in the burning propagation velocity. Note, however, that at the four percent level, an appreciable decrease in burning temperature is produced. Another significant point is that CHF_3 behaves much like the chlorine and bromine derivatives. The inhibiting effect is thus not caused only by halogen atoms.

Table 45

EFFECT OF VARIOUS CONTAMINANTS ON BURNING OF URANIUM AND ZIRCONIUM FOILS IN AIR

I. Uranium (foil 0.13 x 3.0 mm)

	Concentration (volume percent)			
	2		4	
Contaminant	v[a]	T[b]	v	T
None	0.52	1335	0.52	1335
	(a) CF_3-X			
CF_3-F	0.51	1220	0.49	1170
CF_3-H	0.43	1195	0.42	1165
CF_3-Cl	0.49	1180	0.41	1130
CF_3-Br	0.39	1170	0.38	1120
	(b) CH_3-X			
CH_3-Cl	0.41	1190	0.39	1165
CH_3-Br	0.42	1250	0.39	1175
CH_3-I	0.47	1275	0.49	1090[c]

Table 45 (Cont'd.)

I. Uranium (foil 0.13 x 3.0 mm) (Cont'd.)

Contaminant	Concentration (volume percent) 2 v[a]	2 T[b]	4 v	4 T
		(c) C_2H_5-X		
C_2H_5-Cl	0.40	1170	0.39	1070[c]
C_2H_5-Br	0.47	1220	0.35	1060[c]
C_2H_5-I	0.53	1210[c]	0.47	1100[c]
		(d) R-Cl		
CF_3-Cl	0.49	1180	0.41	1130
CH_3-Cl	0.41	1190	0.39	1165
C_2H_5-Cl	0.40	1170	0.39	1070[c]
		(e) R-Br		
CF_3-Br	0.39	1170	0.38	1120
CH_3-Br	0.42	1250	0.39	1175
C_2H_5-Br	0.47	1220	0.35	1060[c]
		(f) R-I		
CH_3-I	0.47	1275	0.49	1090[c]
C_2H_5-I	0.53	1210[c]	0.47	1100[c]
		(g) Increasing Chlorination		
CH_3Cl	0.41	1190	0.39	1165
CH_2Cl_2	0.36	1160	0.33	1130
$CHCl_3$	0.30	1120	0.32	1110
CCl_4	0.35	1110[c]	0.33	1025[c]
CHF_3	0.43	1195	0.42	1165
CHF_2Cl	0.40	1065	0.31	1020
$CHFCl_2$	0.38	1060	0.31	975
$CHCl_3$	0.30	1120	0.32	1110
CF_3Cl	0.49	1180	0.41	1130
CF_2Cl_2	0.37	1095	0.32	1040
		(h) Others		
He	0.48	1235	0.49	1260
Ar	0.47	1245	0.47	1275
N_2	0.51	1320	0.47	1290
CH_2BrCl	0.39	1175	0.31	1120
CH_3CHF_2	N. P.[d]		N. P.	

Table 45 (Cont'd.)

II. Zirconium (foil 0.02 x 3.0 mm)

Contaminant	Concentration (volume percent) 2 v	2 T	4 v	4 T
None	2.20	1540	2.20	1540
	(a) CF_3-X			
CF_3-F	1.59	1530	1.51	1535
CF_3-H	1.22	1380	1.17	1300
CF_3-Cl		N. P.		N. P.
CF_3-Br		N. P.		-
	(b) CH_3-X			
CH_3-Cl	2.15	1440	2.09	1350
CH_3-Br	1.93	1455	1.70	1330
	(c) R-Cl			
CF_3-Cl		N. P.		N. P.
CH_3-Cl	2.15	1440	2.09	1350
	(d) R-Br			
CF_3-Br		N. P.		-
CH_3-Br	1.93	1455	1.70	1330
	(e) Others			
He	2.39	1530	2.53	1525
Ar	2.53	1560	2.35	1560
CH_2BrCl	1.61	1380		N. P.
CH_3CHF_2	1.47	1295	1.40	1230

[a] v = Burning propagation velocity (cm/sec).

[b] T = Maximum burning temperature (C).

[c] Temperature uncertain due to excessive smoking.

[d] N. P. - Burning propagation would not occur.

Set I(b) clearly shows the relative ineffectiveness of the iodide CH_3I, whereas CH_3Cl and CH_3Br are quite similar to each other. This ineffectiveness of the iodide is shown also in I(c), where the ethyl halides are compared.

It is also possible to compare the effect of varying the radical R while maintaining the halogen atom X constant. In I(d) this is done for a set of chlorides. At the two percent level, CF_3Cl seems strangely ineffective, but there are no distinct differences between the CF_3, CH_3, and C_2H_5 chlorides. This is true also of the bromides and iodides, as is shown in I(e) and (f).

It seems clear from the comparisons shown in I(g) that increasing chlorination leads to increasing effectiveness of the molecule. Thus, in going from CHF_3 to $CHCl_3$, the burning propagation rate falls by about one-third.

Because of the effectiveness of CHF_3, it was decided to examine CH_3CHF_2, the only other readily available, suitable CHF compound. As shown in I(h), this compound completely inhibited burning propagation at the two percent level.

Burning of uranium in air is evidently controlled by the rate of diffusion of oxygen through a boundary layer of nitrogen around the combustion zone. In qualitative terms, the general inhibition observed here may be understood as a decomposition of the organic molecule in the boundary layer and reaction of the fragments with oxygen. The net effect is to lower the rate of diffusion of oxygen and, consequently, the rate of combustion. Some of the differences in effectiveness discussed above may be clarified if we consider some of the bond dissociation energies involved. Unfortunately, values are not available for all the compounds studied. Some pertinent values, however, are tabulated below.[31]

R-X Bond Dissociation Energies
(kcal/mole)

	X				
R	H	F	Cl	Br	I
CH_3	102	107	81	68	53
CF_3	103	121		65	
C_2H_5	96		83	65	51

Thus, the inertness of CF_4 may be attributed to the great stability of the C-F bond in that compound. Because of the weakness of the C-I bond, the iodides decompose readily outside the boundary layer and are effectively lost. Assuming a frequency factor of 10^{13} sec^{-1}, the first-order rate constants for decomposition of the methyl compounds of chlorine, bromine, and iodine, and for CF_3H are of the order of 10^1, 10^3, 10^5 and 10^{-2}, respectively, at 1500 K. For CF_4 the value is 10^{-5}. Evidently CF_4 is too stable to be effective while CH_3I is too unstable.

[31] Cottrell, T. C., The Strengths of Chemical Bonds, Butterworths Scientific Publications, London, (1958).

Some work was also done on zirconium combustion (see Table 45, Section II). The great effectiveness of CF_3Br and CF_3Cl is particularly striking. Burning propagation would not occur with these foils even at a concentration of two percent. The presence of a CF_3 group seems to be much more beneficial with zirconium than was the case with uranium. Some rough comparisons may be made by taking the ratio r of Zr:U of the fractional burning propagation rates for a given compound and concentration. Thus, for example, for CF_4 at 2 percent we find $r = (1.59/2.20)/(0.51/0.52) = 0.73$. Since $r<1$, CF_4 is relatively more effective with zirconium than with uranium. These values are almost identical for both 2 and 4 percent results and those that could be calculated are listed below:

Compound	r
CF_4	0.73
CHF_3	0.66
CH_3Cl	1.22
CH_3Br	1.02

The greater relative effectiveness of CF_3 derivatives in zirconium combustion may be due to the higher burning temperature. At 1750 K, again assuming a frequency factor of 10^{13} sec^{-1}, the first-order rate constant for dissociation of CF_4 is of the order 10^{-2}. A more extensive quantitative treatment of the burning propagation rate is being prepared and will be available shortly.

b. Ignition Temperature Studies

In considering possible applications of halogenated hydrocarbons to practical cases of metal fires (see above), it became important to explore the effects of these compounds on ignition temperature. The burning curve ignition temperature of 0.13-mm-thick uranium foil strips was measured in air containing small additions of various halogenated hydrocarbons. The results obtained are listed in Table 46. The important point to note is that CHF_3 and CH_3CHF_2 had very little effect on ignition temperature whereas all the chlorine- or bromine-containing compounds lowered the ignition temperature considerably. The two compounds mentioned were quite effective in lowering the burning propagation rate and burning temperature. However, the compound CH_3CHF_2 forms flammable mixtures with air. Suitable blending with other compounds might eliminate this hazard.

The ignition temperature results seem to indicate an exothermal reaction between the chlorine and bromine compounds and perhaps uranium dioxide, causing increased heat liberation and

lower ignition temperature. In any practical use of these agents as fire inhibitors a severe decrease in ignition temperature would not be desirable. Compounds containing only carbon, hydrogen, and fluorine seem attractive from this standpoint.

Table 46

BURNING CURVE IGNITION TEMPERATURES OF URANIUM FOILS IN AIR CONTAMINATED WITH CERTAIN HALOGENATED HYDROCARBONS

(Foil 0.13 x 3 mm)

Contaminant	Ignition Temperature (C) in Contaminant of Indicated Concentration (Volume Percent)	
	2	4
None	380	380
Argon	380	350
CHF_3	395	400
CH_3CHF_2	350	-
CH_3Br	340	300
CH_2BrCl	320	-
CF_3Cl	310	300
CH_3Cl	305	290
CF_3Br	285	270
$CHCl_3$	270	-

4. Plutonium-ignition Studies
(J. G. Schnizlein, D. F. Fischer)

Installations of equipment in the plutonium glovebox[32] facility are complete. Experiments have been resumed on ignition and burning of plutonium samples.

A view of the three module glovebox to be used for these studies is shown in Figure 42. Warning systems are provided for fire detection, air monitoring, radiation, ventilation, and criticality. Windows are $\frac{3}{8}$-in. laminated safety glass. A recirculating system provides dry air ($< 1\%$ relative humidity). Provision is made so that an inert atmosphere can be used on a once-through system.

---

[32]Malecha, R. F., et al., Low Cost Gloveboxes, presented at Eighth Hot Laboratory Conference in San Francisco, Calif., Dec. 13, 1960.

Figure 42

THREE-MODULE GLOVEBOX FOR PLUTONIUM IGNITION-OXIDATION STUDIES

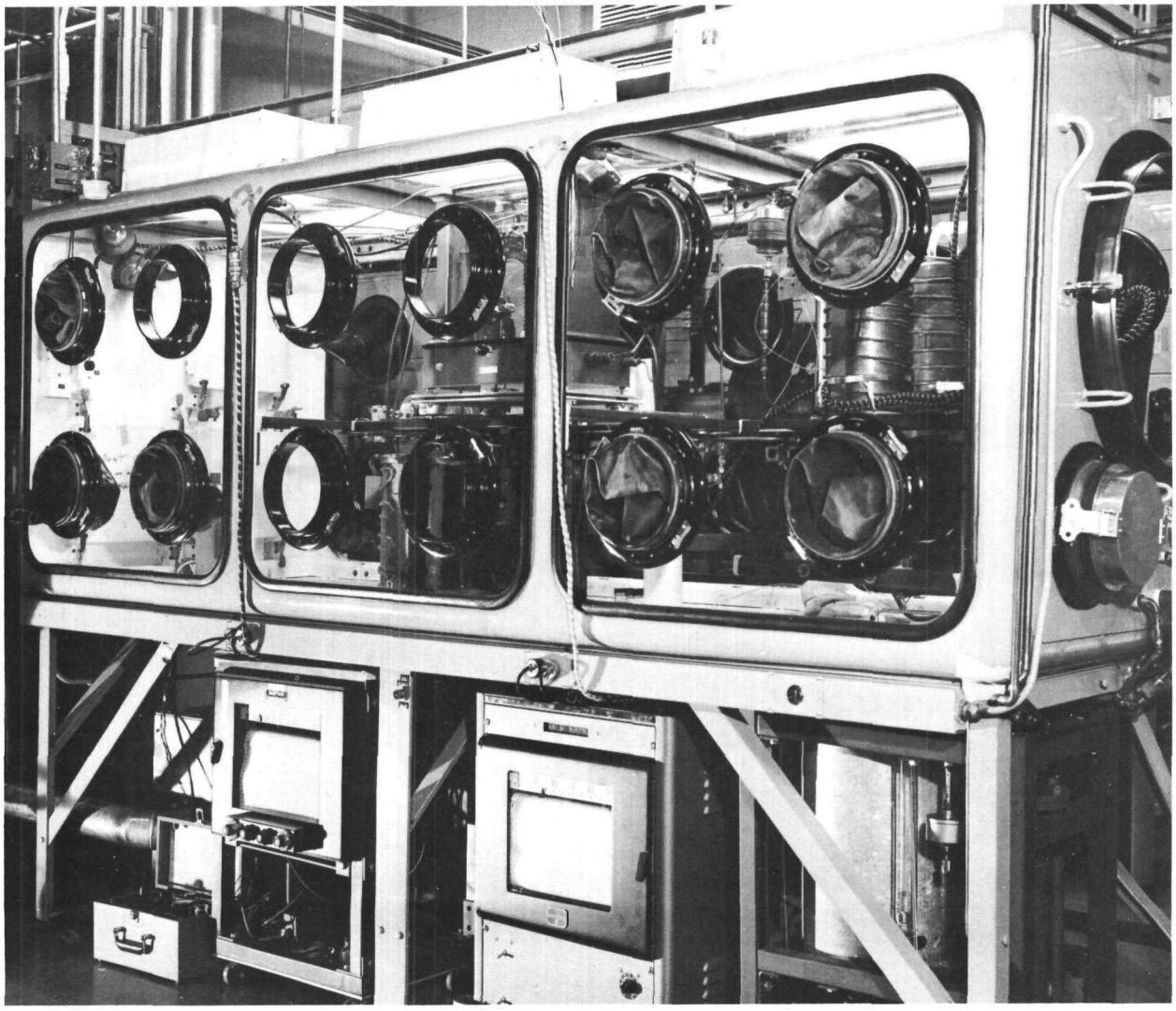

Apparatus has been assembled to do three types of experiments: (1) burning propagation, (2) ignition, and (3) controlled oxidation.

The propagation cell for enclosing the sample in a controlled atmosphere during propagation rate studies is illustrated in Figure 43. It consists of a 6-in. length of 4-in.-ID Pyrex pipe closed at one end by a circular window of $\frac{1}{4}$-in. plate glass and at the other by a metal plate fitted with supports for the sample, gas-inlet and outlet tubes, and insulated electrical leads. The apparatus is easily dismantled, and the sample supports and other parts are such that sample mounting and alignment can be accomplished readily.

Figure 43

BURNING PROPAGATION CELL
(Assembled)

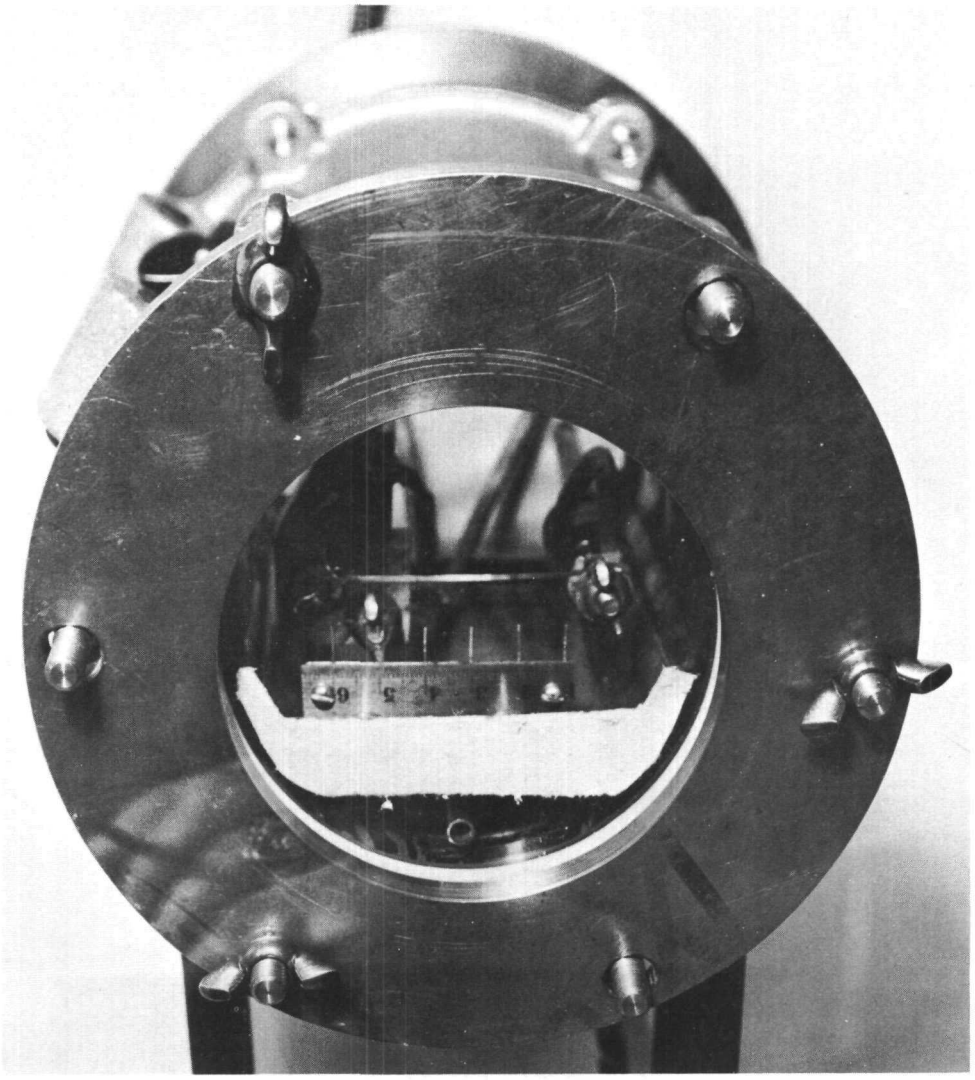

Photographic records of the burning propagation of the foil specimens will be made with a Fastax high-speed camera which offers speed ranges from 100 to 16,000 frames/second. The photo-beam lamps outside the module provide the necessary lighting. Precautions are taken to prevent glass breakage on the glovebox. The newly designed and developed two-color photoelectric pyrometer may also be used to record the burning propagation. This apparatus will simultaneously record the propagation rate and the burning temperature.

The samples for these experiments are obtained from foils. The foils are cut with a shear specially designed for this purpose. This same shear may be heated in case some foils are too brittle to cut at room

temperature. The strips are usually several centimeters long, 1 to 5 mm wide, and less than 1 mm thick. In the burning propagation apparatus, one end of a plutonium foil strip is attached to the nuts of the sample support. The other end of the specimen is touching a platinum ignition wire. This ignition wire is controlled by a switch and variac on the outside of the module. The cell is then assembled with gas-inlet and gas-exhaust lines in place. The controlled atmosphere (usually air or oxygen) gas line is turned on at the solenoid control panel underneath the module. The Fastax camera and beam lamps are mounted and positioned outside the module. After a time lapse of 10 min to flush the cell, the beam lamps are turned on, the ignition switch is triggered, and the camera is started as the sample ignites. After the sample ignites, the ignition switch is turned off. Upon completion of the run, the flowing controlled atmosphere is stopped and helium admitted if necessary.

Ignition experiments are conducted in 700-watt furnaces with water-cooled shells. A zirconia tube will be used as an inner protector liner for the reactor in both burning curve and shielded ignition experiments. The reactor is made of quartz and has a quartz optical flat window on top for observation purposes. The oxidizing gas will enter the bottom center, pass through the tube, past the sample, and out the top. The West programmer to be used for the programming of the burning curve experiments with plutonium and controlling furnace temperatures for shielded ignition studies presently has one programming cam to obtain the desired linear heating rates and controlled temperatures. From this one programming cam, linear heating rates from 1 deg/min to 15 deg/min (with seven intermediate rates) can be obtained by increasing or decreasing the gear ratio of the cam cycle. Presently the maximum programmed temperature and controlling temperature is 725 C.

In burning curve experiments the sample is heated in a controlled oxidizing atmosphere at a uniform rate of temperature increase. Thermocouples indicate the degree of self-heating of the sample over that of the surrounding gas stream. Ignition is observed visually and the ignition temperature is obtained graphically from the time-temperature trace.

In shielded ignitions the sample is inserted into a controlled temperature environment. Helium is used to protect the sample from oxidation when the thermocouple assembly is inserted into the hot reactor and until the sample equilibrium temperature is reached in approximately 7 to 10 min. At that time the helium is turned off and the oxidizing atmosphere is introduced. If the sample does not ignite after a minute or two, the oxidizing atmosphere is turned off and the helium readmitted. If the sample ignites, the helium is readmitted to quench the reaction. The thermocouple assembly is removed from the reactor and furnace and allowed to cool to room temperature before further dismantling. Procedures have been established so that is not necessary to have one's hands

in the boxes during the burning, ignition, or propagation experiment. Solenoid valves, controlled from outside the box, permit rapid switching from helium to air (or oxygen) and back to helium. This arrangement is essential for shielded ignitions and will be an added safety feature to permit quenching and extinguishing rapid reactions quickly in the apparatus. Also, the gases admitted to the glovebox pass through gas mask canister filters to prevent contamination of the lines outside the box.

Controlled oxidation behavior of plutonium and its alloys will be determined by gravimetric studies. Apparatus for these studies consists of an Ainsworth recording balance mounted over a water-jacketed, hinged, 1400-watt "heavy-duty" furnace (see Figure 44). The gases are controlled with the solenoid valves. Samples will be supported inside the furnace tube in a platinum basket hung from the balance pan. Helium or argon and an oxidizing gas will be available for the furnace tube apparatus.

Figure 44

PLUTONIUM THERMOGRAVIMETRIC APPARATUS

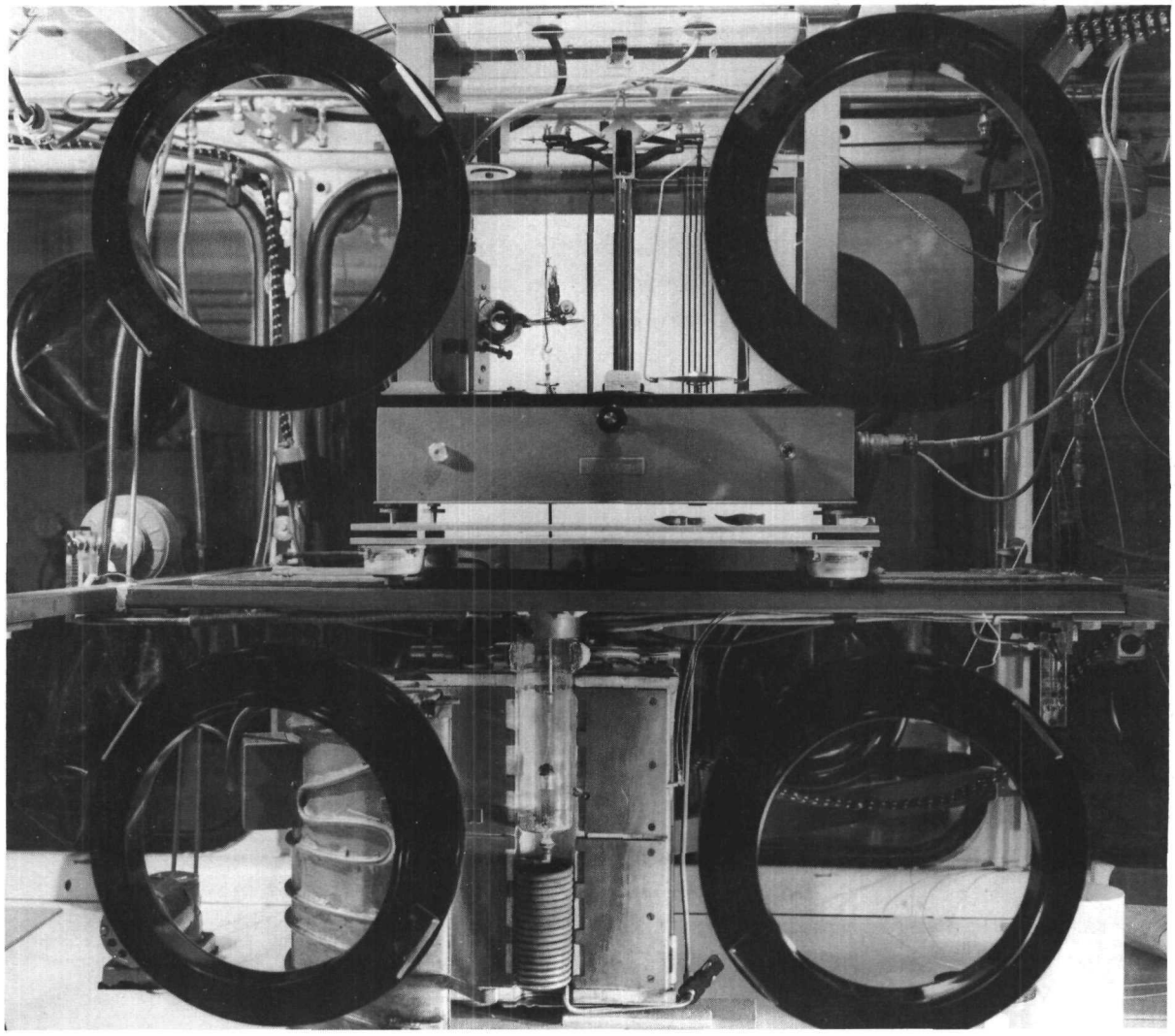

A baffle system minimizes the contamination of the glovebox atmosphere. Either burning curve experiments or isothermal oxidations can be performed, and weight gains measured.

This apparatus has been equipped with a Thermocouple transducer (visible in left side of balance case in Figure 44) which does not interfere with the balance operation. The temperature of the sample is converted to an electric signal which is recorded on a potentiometer recorder exterior to the glovebox. The movable portion consists of a thermocouple, a precision resistor, and a coil in series. The coil is interlocked with a toroidal magnetic amplifier. The thermoelectric output of the thermocouple causes current through the coil. The magnetic amplifier provides a potential proportional to the temperature. Calibration has demonstrated a precision of approximately 2 degrees.

With this added feature both temperature and weight of sample are continuously recorded. This will allow rapid appraisals of oxidation rates over a large range of temperatures.

B. Metal-Water Reactions
(L. Baker)

1. Condenser-discharge Method
(L. Baker, R. Warchal, R. Koonz*)

The condenser-discharge experiment is an attempt to obtain fundamental rate data under experimental conditions similar to those encountered during a serious accident in a nuclear reactor. Either a nuclear runaway or a sudden loss of coolant during operation of a water-cooled reactor could result in contact between very hot fuel and cladding metals with water or steam and might involve fine particles. The condenser-discharge experiment simulates the limiting case of a nuclear incident in that the heating time is very short and very fine metal particles are produced.

In the condenser-discharge experiment, metal wires are rapidly melted and dispersed in a water-filled cell by a surge current from a bank of condensers. The energy input to the wire is used to calculate the initial reaction temperature. The transient pressure measures reaction rate, the amount of hydrogen generated gives the extent of reaction, and the particle size of residue indicates the surface area exposed to reaction.

Analysis of results is based on one of the usual laws of metal oxidation (parabolic rate law) and on the laws of gaseous diffusion and heat transfer. In this way an attempt is made to interpret experimental work as it proceeds.

---

*Summer employee from Wabash College.

a. Uranium Runs in Heated Water

A series of runs with 30-mil uranium wires in the high-pressure reaction cell has been completed. The mean particle size of residue from the runs has also been determined. Water temperature ranged from 100 to 125 C (water vapor pressure 15 to 33 psia) in these runs. Results of the runs are given in Table 47. The new results in heated water are compared with previous results of runs in room temperature water in Figure 45. Runs in room-temperature water were reported in previous quarterly reports (see ANL-6145, page 161, and ANL-6183, page 141). The results show that considerably more reaction occurred in heated water than in room-temperature water. The uranium results are, therefore, consistent with previous results with zirconium.

Table 47

URANIUM-WATER REACTION DATA FROM HIGH-PRESSURE CONDENSER-DISCHARGE APPARATUS
(Uranium used: 30-mil wires)

Run	Calc Metal Temp (C) and Physical State	Ambient Water Temp (C)	Percent Reaction	Sauter Mean Particle Size (μ)	Appearance of Residue
244[a]	300, solid	119	1.9	2370[a,b]	Intact
247	1000, solid	113	2.5	1230[b]	Broken
246	1133, 75% liquid	116	6.7	1230[b]	Large pieces
253	1400, liquid	117	27.5	500	Particles
251	1600, liquid	106	32.4	370	Particles
245	1900, liquid	116	61.4	530	Particles
256	1900, liquid	124	51.8	420	Particles
252	2200, liquid	109	57.0	350	Particles
260	2300, liquid	104	71.9	480	Particles
257	2700, liquid	110	70.4	300	Particles
262	3000, liquid	104	103.7	140	Particles
258	3500, liquid	102	100.0	180	Particles
259	4100, liquid	104	94.7	200	Particles

[a]60-mil wire.

[b]Size of spheres that would have same surface to volume ratio as original wire.

FIGURE 45
RESULTS OF CONDENSER-DISCHARGE RUNS WITH URANIUM WIRES

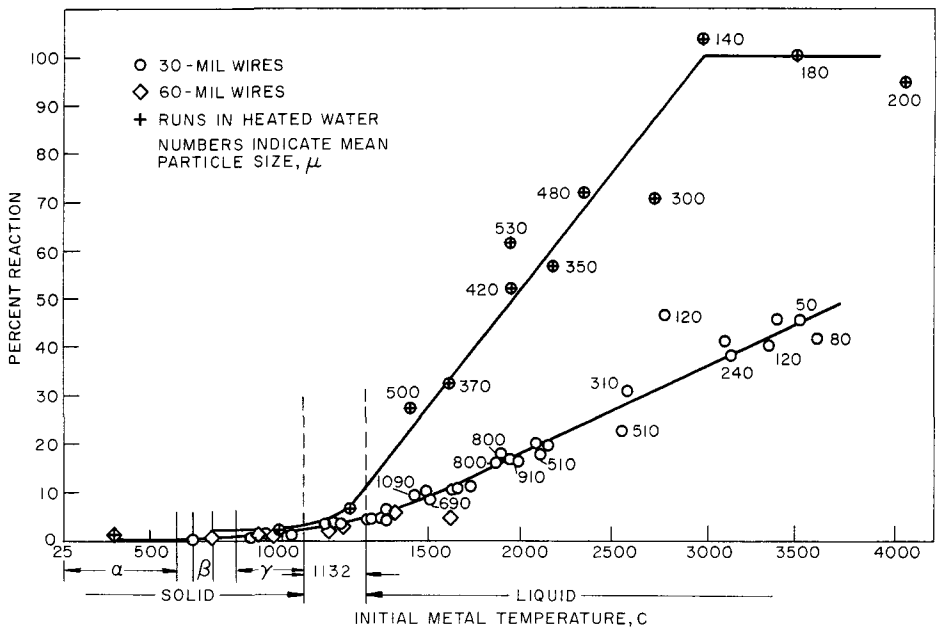

The more extensive reaction obtained in heated water was explained on the basis of a more rapid rate of gaseous diffusion of water vapor through the steam-hydrogen film in the case of zirconium. The same reasoning should apply to the uranium case. The fact that greater reaction in heated water also occurred with uranium further verifies the theoretical account of the zirconium-water reaction.

Attempts were made to study the uranium-water reaction in 200 C water. Specimen wires were approximately one-half corroded during the one-half to one-hour period in which the water in the reaction cell is heated and final run preparations are made. It was, therefore, not possible to conduct condenser-discharge runs in the usual way. The corrosion rates of bare uranium and the approximate time required to consume a specimen of 30-mil wire are shown in Table 48. Corrosion data in Table 48 show that only 2.6 hr are required to consume completely a specimen wire in water at 183 C. The corrosion data also indicate that less than one percent reaction occurred during the preparation period for runs in water at 100 C.

Larger particles formed in uranium runs were irregular in shape while the finer particles had a more nearly spherical shape. Measured particle sizes were averages of the longest and shortest dimensions of each particle counted. The average particle sizes reported in Table 47 and Figure 45 are therefore representative of the diameter of particles present while the metal was molten during the period of reaction, since presumably molten metal particles would have a nearly spherical shape. Measured average particle sizes are probably somewhat low for runs in which very extensive reaction occurred because of oxide flaking subsequent to reaction.

Table 48

RATES OF BARE URANIUM AQUEOUS CORROSION[a]

Temp (C)	Corrosion Rate[a] [mg/(sq cm)(hr)]	Time to Consume 30-mil Wire[b] (hr)
50	0.066	5400
100	2.7	130
183	139	2.6

[a]Reactor Handbook, 2nd Edition, Vol. 1, page 129.

[b]Approximate weight and surface area of 30-mil wire, one inch long = 250 mg and 0.7 sq cm.

Transient pressure traces were similar to those obtained with zirconium (see ANL-6333, page 214) in that they appeared to be composites of two reactions, one very fast and one much slower. This was interpreted to mean that some of the particles produced were capable of a very rapid reaction and some underwent only a slow reaction. A detectable fraction of the specimen underwent an explosive pressure rise when the initial metal temperature reached about 1600 C in either room-temperature or heated water. The entire samples showed the explosive pressure rises when initial temperatures reached about 2500 C. About one-half of the particles were capable of rapid reaction at initial metal temperatures of 1900 C. This behavior indicated that particle size and not metal temperature primarily determine the reaction rate. The results with uranium are consistent with the findings for zirconium that particles smaller than ca. 1000μ in heated water and 500μ in room-temperature water can undergo a very rapid reaction. The rapid reaction was postulated to occur by a hydrodynamic mechanism whereby the particles are driven through the water at high velocity by the evolving hydrogen. The high-speed motion causes an increase in the rate of gaseous diffusion of water vapor to the metal surface.

b. Studies of Residue from the Uranium-Water Reaction

Samples of residue from uranium runs were studied by X-ray diffraction* and metallographic techniques.** Analyses for retained hydrogen were performed by vacuum fusion analysis.† X-ray diffraction analyses of residue from six runs indicated the presence of only UO_2 and

*Performed by M. Homa and R. Schablaske.

**Performed by D. Anthes and M. Deerwester.

†Performed by Chemistry Division of ANL.

α-uranium. The residue included runs in heated water and room-temperature water, and covered the range of initial metal temperatures from 1400 to 4100 C. There was no evidence of higher oxides of uranium.

A photomicrograph of a uranium particle is shown in Figure 46. The central portion is uranium metal and the outer film is UO_2. The results of the determination of retained hydrogen are given in Table 49. The quantity of hydrogen that would be present if the sample retained all of the hydrogen generated by reaction is indicated in parenthesis in the table. The results indicate that only a few percent of the total hydrogen is retained by the residue. This finding justifies a previous conclusion that the procedure for collecting gaseous hydrogen can be used to determine the extent of metal reacted. The results indicate that some, but not all, of the equilibrium quantity of hydrogen is trapped in the metal during the rapid cooling process. The equilibrium solubility of hydrogen in uranium at one atmos goes from 17 to 28 ppm on melting at 1133 C.[33] The tendency of hydrogen to escape during cooling could explain the irregular shape of the larger particles generated during the reaction.

Figure 46

PHOTOMICROGRAPH OF OXIDIZED URANIUM PARTICLE FROM CONDENSER-DISCHARGE RUNS

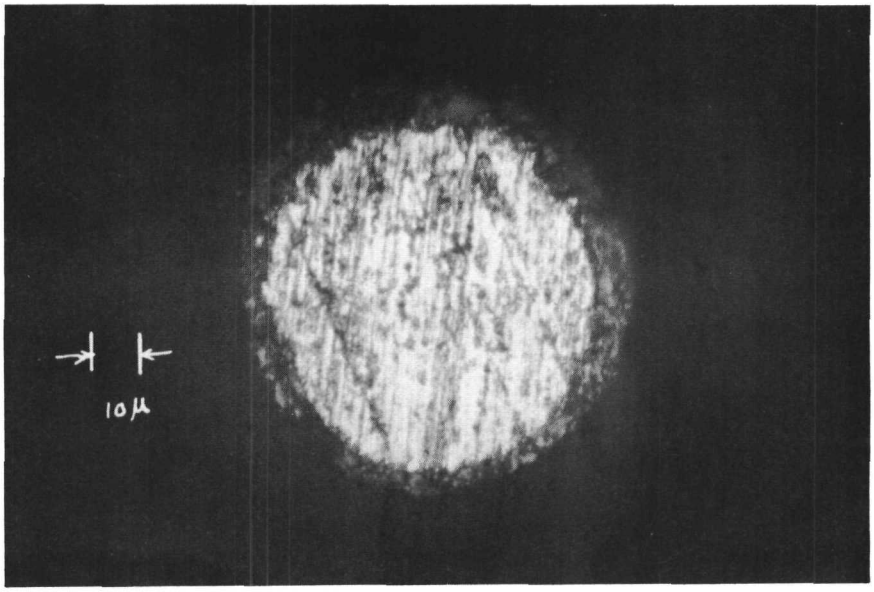

Initial metal temperature	1600 C
Extent of reaction by hydrogen analysis	10.7%

[33] Hansen, M., Constitution of Binary Alloys, McGraw-Hill Book Co., New York, (1958), page 803.

Table 49

RESULTS OF ANALYSIS FOR DISSOLVED HYDROGEN IN THE RESIDUE FROM URANIUM RUNS

Run	Calc Temp (C)	% Reaction (and total ppm)[a]	ppm Hydrogen (2 Det'n.)
165	1133, 40% Liquid	2.3 (390)	16-5
155	1650, Liquid	10.9 (1820)	19-12
153	1980, Liquid	16.8 (2780)	30-24
172	3220, Liquid	40.9 (6550)	98-61

[a]Total ppm is the parts per million of H that would be present if the solid residue (U + UO_2) retained the entire quantity of hydrogen generated.

2. Pressure-pulse Method
(D. Mason, P. Martin)

The pressure-pulse technique is a method of studying the kinetics of reaction of molten metals with water vapor under isothermal conditions. The results of this study should aid in the interpretation of data obtained from other metal-water studies, such as the condenser-discharge and TREAT experiments.

The metal is heated initially under high vacuum to outgas it. Depending on the temperature and the metal, argon may be introduced to a pressure between 3 and 16 mm to reduce vaporization of the sample. Heating is accomplished by an induction heater. When the sample is at the desired temperature, electronically controlled valves are operated in proper sequence to contact the molten metal with water vapor of known pressure for a specified period of time. A more complete description of the apparatus and operating procedure appears in a previous report (see ANL-6287, page 190).

a. Aluminum Runs

The results of the reaction of aluminum at 800, 1000, and 1200 C with water vapor (500 mm pressure) are shown in Table 50 and are plotted in Figure 47. It is apparent that the situation is quite different for aluminum than for the uranium and sodium results reported previously (see ANL-6379, pages 206 to 208). The reaction of steam with molten uranium and with molten sodium was controlled by diffusion and mixing processes within the reaction cell. It will be recalled that no temperature effects on the reaction rate were found (within experimental error). Since the rates were also much higher for sodium and uranium than those presently reported for aluminum, the aluminum rates cannot be controlled by the diffusion of water vapor to the surface.

Table 50

RESULTS OF THE REACTION OF ALUMINUM AT 800 TO 1200 C WITH STEAM AT 500 mm PRESSURE BY THE PRESSURE-PULSE METHOD

Reaction Time (sec)	Volume H_2 Evolved Per Unit Area (cc STP/sq cm)			Reaction Time (sec)	Volume H_2 Evolved Per Unit Area (cc STP/sq cm)		
	800 C	1000 C	1200 C		800 C	1000 C	1200 C
0.11	-	0.018	0.020	9.2	0.018	0.104	0.35
0.11	-	0.021	0.033	9.2	-	0.16	0.38
0.11	-	0.021	0.035	9.2	-	0.20	0.59
0.11	-	0.024	0.059	9.2	-	0.25	-
0.11	-	0.032	0.070	100	0.043	0.14	1.03
0.11	-	0.043	0.074	100	0.062	0.17	1.16
0.11	-	0.049	-	100	-	0.20	-
0.11	-	0.051	-	100	-	0.24	-
0.11	-	0.059	-	100	-	0.26	-
0.11	-	0.067	-	100	-	0.27	-
1.04	-	0.034	0.18	100	-	0.34	-
1.04	-	0.075	0.18	100	-	0.38	-
1.04	-	0.082	0.30	1000	0.091	0.71	1.82
1.04	-	0.102	0.36	1000	0.116	0.76	-
1.04	-	-	0.37	1000	-	0.91	-
1.04	-	-	0.45				

FIGURE 47
HYDROGEN EVOLUTION IN THE REACTION OF STEAM at 500 mm PRESSURE WITH ALUMINUM

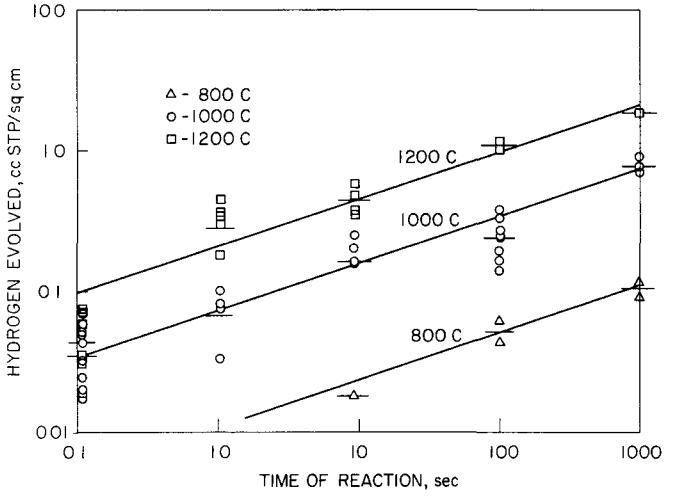

On Figure 47, the average values for each time and temperature are indicated by a horizontal line. The slopes of the straight lines which best fit the data were determined by least squares. The data for a contact time of 0.1 sec were somewhat scattered, so that these were not considered in the least-squares calculation. The least-squares slopes were 0.27 for 1200 C runs, 0.34 for 1000 C runs, and 0.36 for 800 C runs. These slopes correspond to n in the equation V (cc/sq cm) $\propto t^n$ (t in sec). The average of the n values is 0.32. A value of $n = \frac{1}{3}$ (cubic rate law) was, therefore, considered to represent the data adequately, and the lines on Figure 47 were drawn with a slope of $\frac{1}{3}$.

On Figure 48, the amount of hydrogen evolved is plotted vs. the cubic root of the time. The logarithms of the resulting slopes were plotted vs. 1/T in Figure 49. The slope of this plot corresponds to an activation energy of 21,700 cal/mole.

FIGURE 48
HYDROGEN EVOLVED vs (REACTION TIME)$^{1/3}$ FOR THE REACTION OF STEAM AT 500 mm PRESSURE WITH ALUMINUM

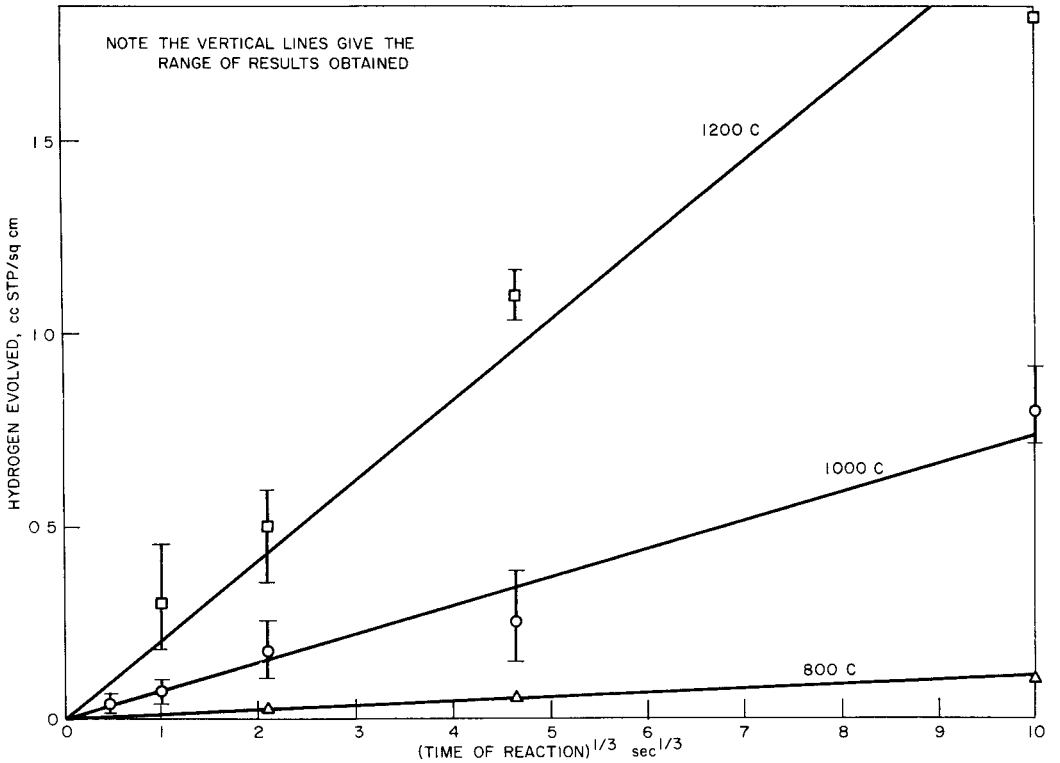

FIGURE 49
EFFECT OF TEMPERATURE ON THE RATE OF HYDROGEN EVOLUTION FOR THE REACTION OF STEAM AT 500 mm PRESSURE WITH ALUMINUM

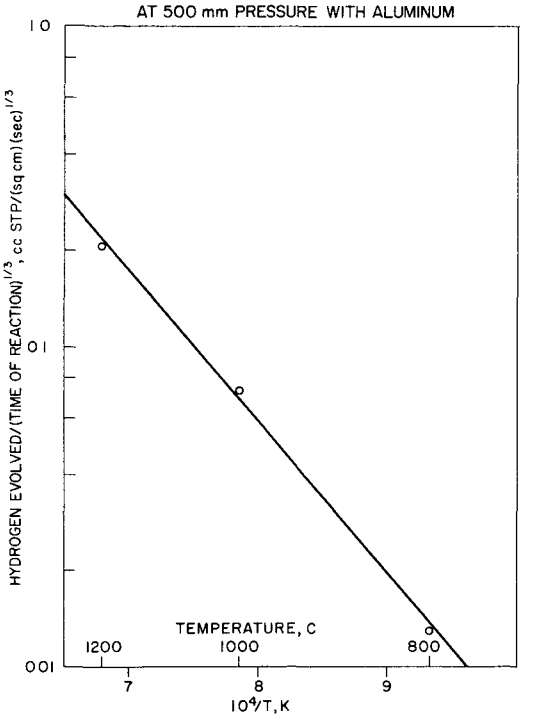

b. Aluminum-Uranium Alloy Runs

Shown in Table 51 are the results of the reaction of steam at 500 mm pressure with alloys of approximate composition 95 percent aluminum and 5 percent uranium. The data reported to date are at 1200 C. These results are also shown in Figure 50 (together with the average pure aluminum-steam data) and indicate that the small amount of uranium present has little effect on the reaction. The log-log plot for preliminary data with the alloy is best described by a curved line.

The alloys were prepared by melting weighed samples of aluminum and uranium just prior to each run.

Table 51

REACTION OF ALUMINUM-5 PERCENT URANIUM ALLOY AT 1200 C WITH STEAM AT 500 mm PRESSURE

Reaction Time (sec)	Vol H_2 Per Unit Area (cc STP/sq cm)	Reaction Time (sec)	Vol H_2 Per Unit Area (cc STP/sq cm)
1.04	0.26	100	0.42
1.04	0.25	100	0.50
9.2	0.28	1000	0.84
9.2	0.31	1000	1.14

FIGURE 50
HYDROGEN EVOLUTION IN THE REACTION OF STEAM AT 500 mm PRESSURE WITH ALUMINUM – 5% URANIUM ALLOYS AT 1200 C

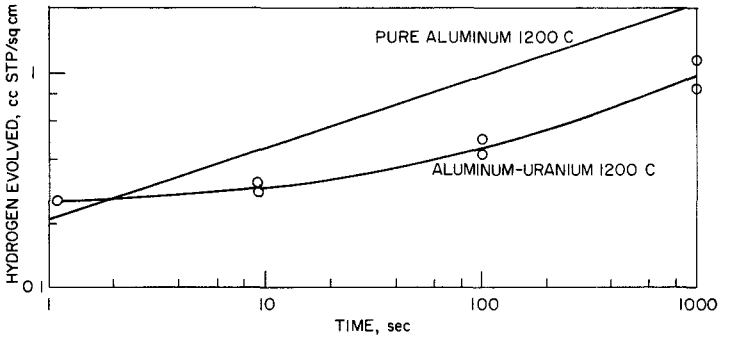

Three samples were later sectioned and the surfaces scanned by X-ray fluorescence spectrometry to determine the uniformity of the alloys produced. The greatest deviation of any part of any sample from the average value of all samples was 12.6 percent.

3. In-pile Testing in the TREAT Reactor*

(R. C. Liimatainen, R. O. Ivins, M. Deerwester, F. Testa)

The program of studying metal-water reactions initiated by a nuclear reactor burst is continuing. The technique consists of exposing fuel specimens immersed in water to a neutron pulse in the TREAT reactor. The purpose of this experimental work is threefold:

1. to determine the fraction of metal that reacts with water;

2. to determine the temperatures and pressures produced during the excursion; and

3. to determine the structural changes that take place in the fuel as a result of the rupture or meltdown; this includes metallographic and particle size evaluations.

a. Results of Recent Transients with Uranium Dioxide-core, Stainless Steel-304-clad Fuel Pins

During the present quarter, four transients were performed on uranium dioxide-core, stainless steel-304-clad fuel pins. Table 52 gives a summary of the experimental conditions, the characteristics of the reactor pulses, and the data obtained; the runs are arranged in increasing order of the energy of the reactor pulse. A photomicrograph of unirradiated uranium dioxide core material is given in Figure 51. Post-irradiation observations are presented in Figures 52 through 55 as macro and micro photographs. Particle size distribution for Runs CEN-65 and CEN-66 in which particles were formed are included in Figures 54 and 55. A typical oscillograph record of a run is included in Figure 55.

---

*The cooperation of the ANL Metallurgy Division (for furnishing the fuel pins) and of the ANL Idaho Division (for operation of TREAT) is gratefully acknowledged.

Table 52

SUMMARY OF IN-PILE DATA ON STAINLESS STEEL-WATER REACTIONS, URANIA-CORE FUEL PINS

Test conditions: Water initially at 25 C under 20 psia of helium pressure; fuel pins submerged in water
Composition of core: UO_2, 20% enriched
Core size: 0.33-in. diam x 0.50 in. long
Reaction: $Fe + H_2O \rightarrow FeO + H_2$
Cladding: 18-mil wall thickness of SS-304

	CEN Transient Experiment Number			
	64	67	65	66
Reactor Characteristics				
megawatt-second burst:	140	185	190	230
megawatt peak power:	147	83	1640	690
millisecond period:	115	290	50	97
Description of UO_2 Core				
% of theoretical density:	89 (water logged)	98	89	98
Thermal Neutron Dose				
nvt by gold foil activation:	1.2×10^{14}	2.6×10^{14}	1.6×10^{14}	1.8×10^{14}
Fission Energy Input to Pin				
cal/g core (Zr^{95}):	-	-	244	260
Peak Temp of Clad, C:	760	-	-	820
Peak Pressure Rise, psi:	-	-	-	60
Percent of Metal Reacted with Water:	0.8	0.3	5.2	9.0
Appearance of Fuel after Transient:				
clad:	Darkened zone in center, small ruptures in one end and in the center of jacket	Intact, darkened zone around central area of jacket	Fragmented, partially melted	Fragmented, partially melted
core:	Distorted, cracked, but UO_2 confined within jacket	Some radial cracking	Fragmented into fine particles	Fragmented into coarse particles

Figure 51

PHOTOMICROGRAPH OF UNIRRADIATED URANIUM DIOXIDE CORE

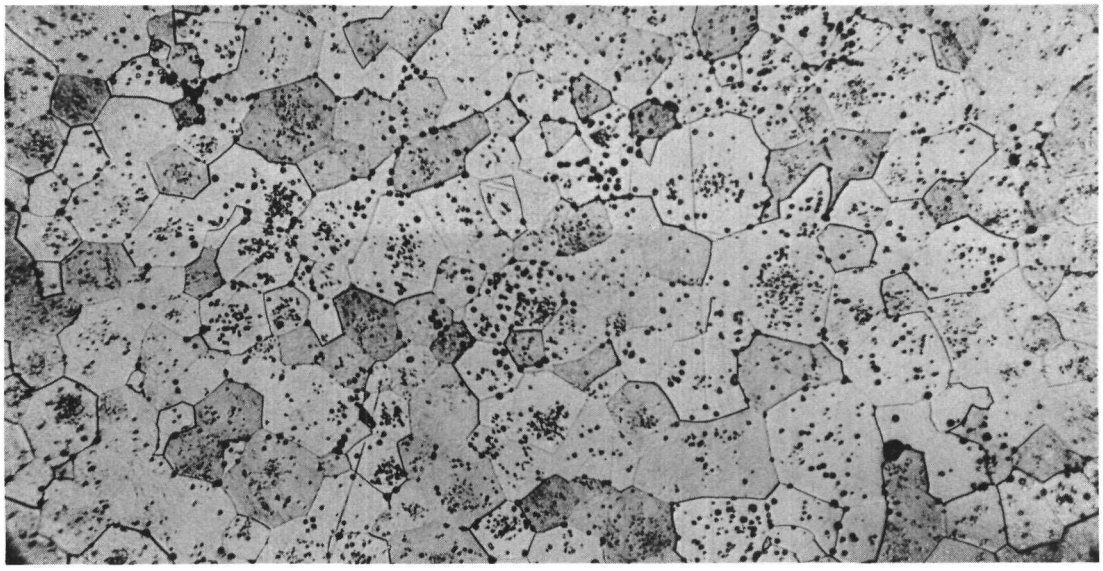

Scale
0.005
inch

etched with H_2O_2, H_2SO_4 10/1

Figure 52

TRANSIENT CEN-64: URANIA-CORE, STAINLESS STEEL-304-CLAD FUEL PIN
(Water Logged)

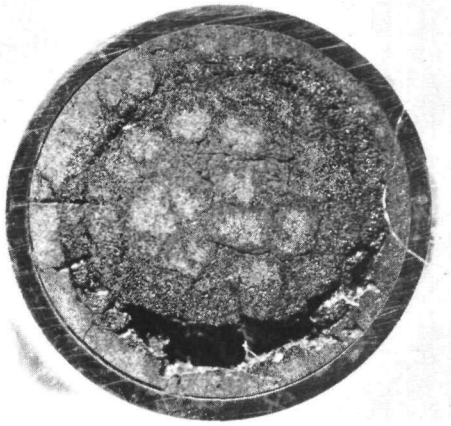

MACROGRAPH OF CROSS SECTION

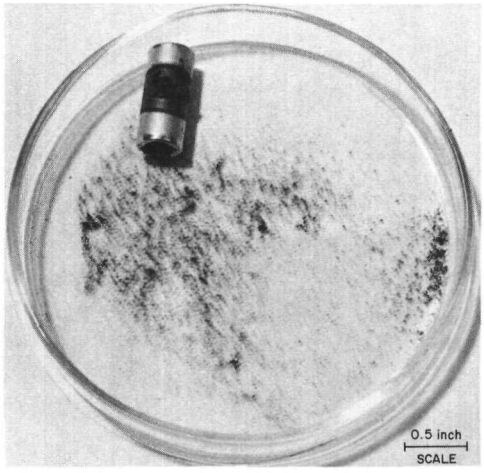

PHOTOGRAPH OF FUEL PIN

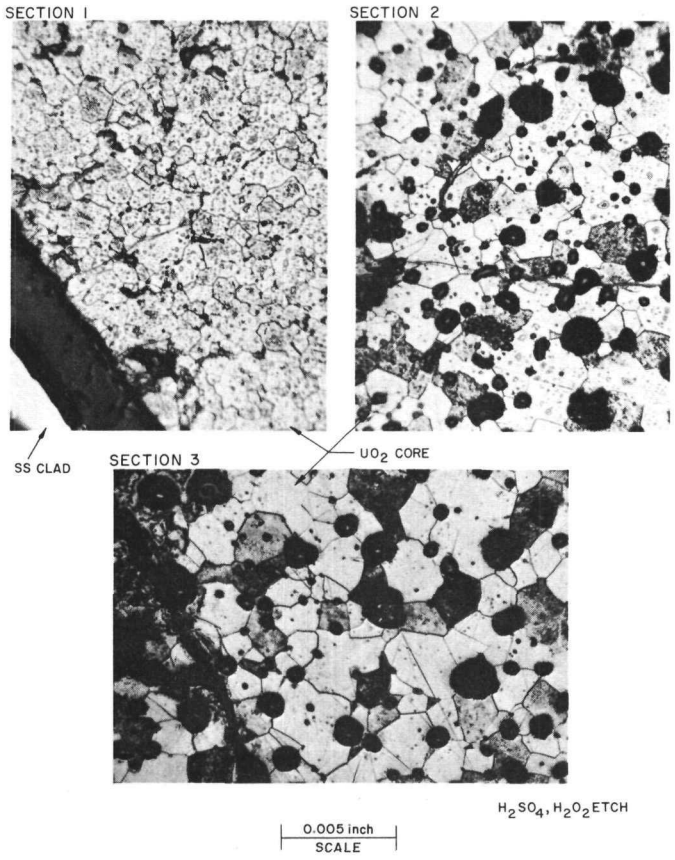

PHOTOMICROGRAPHS

140 mw-sec burst
147 mw peak power
115 ms period
0.8% SS-H_2O reaction

Figure 53

TRANSIENT CEN-67: URANIA-CORE, STAINLESS STEEL-304-CLAD FUEL PIN

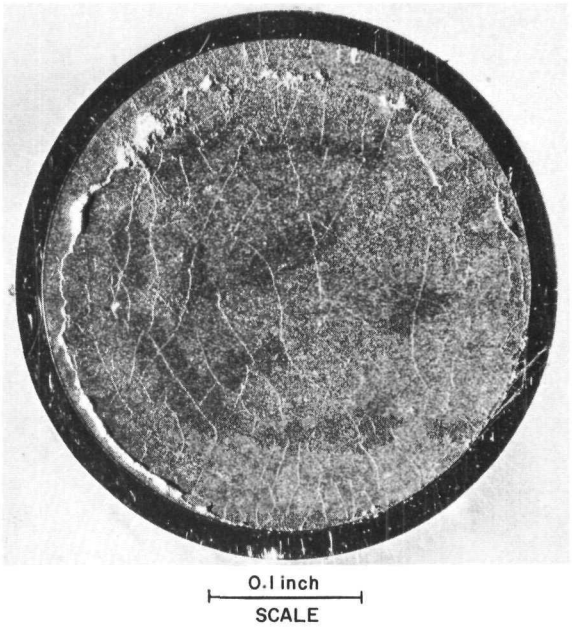

MACROGRAPH OF CROSS SECTION

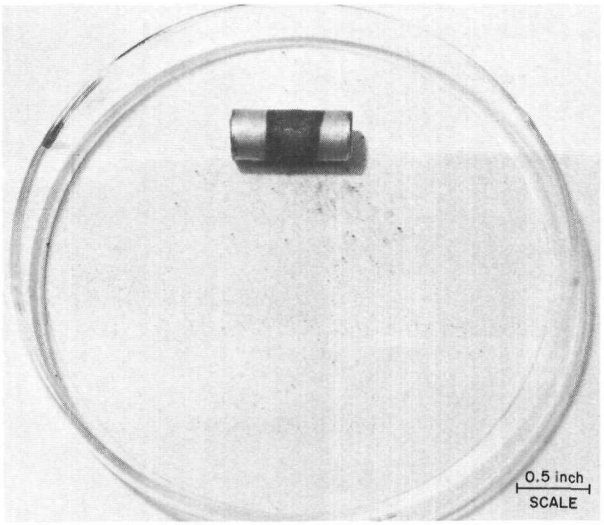

PHOTOGRAPH OF FUEL PIN

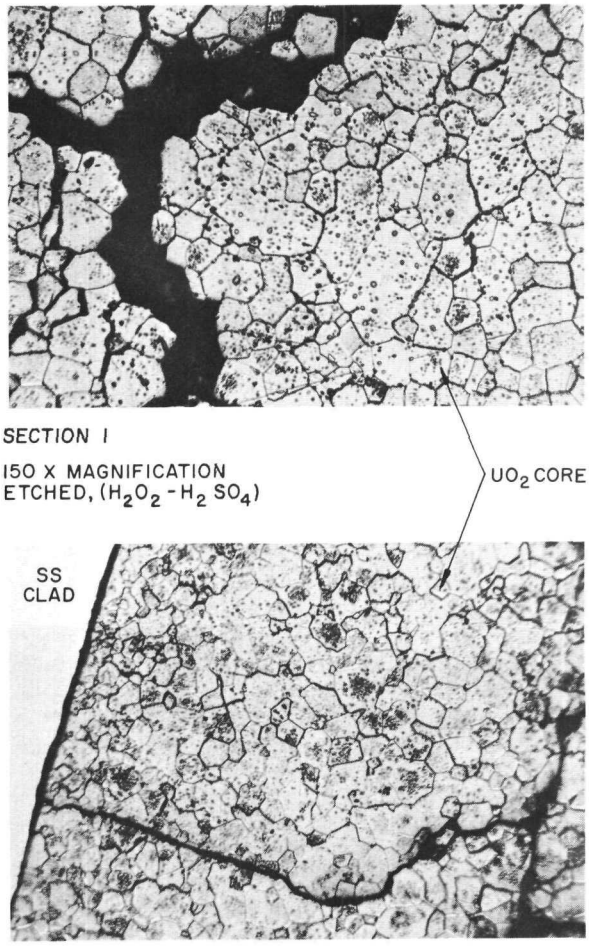

PHOTOMICROGRAPHS

185 mw-sec burst
83 mw peak power
290 ms period
0.3% SS-H_2O reaction

Figure 54

TRANSIENT-CEN 65: URANIA-CORE, STAINLESS STEEL-304-CLAD FUEL PIN

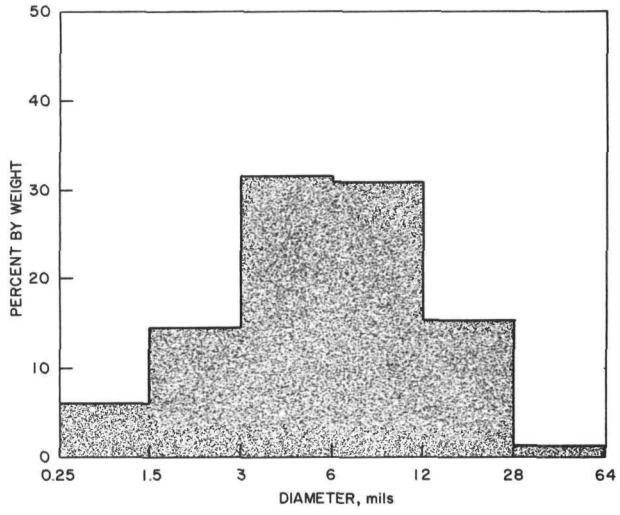

PARTICLE SIZE DISTRIBUTION
(Core and Cladding)
(Sieve Analysis)

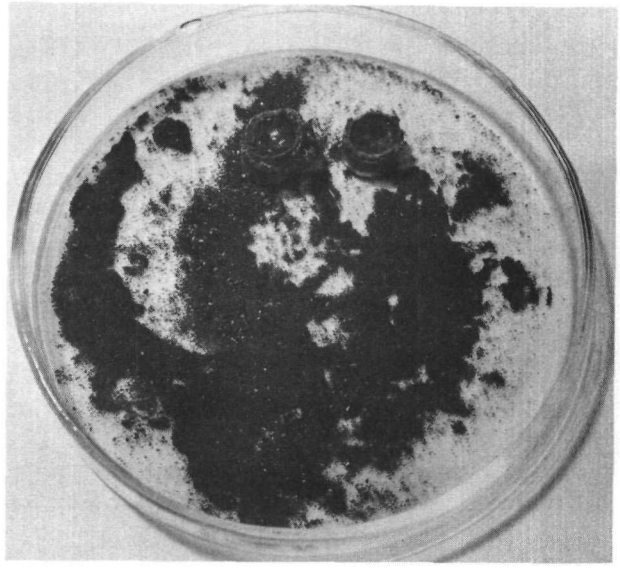

190 mw-sec BURST
1640 mw PEAK POWER
50 ms PERIOD
5.2% SS-H_2O REACTION

0.5 inch SCALE

PHOTOGRAPH OF FUEL PIN

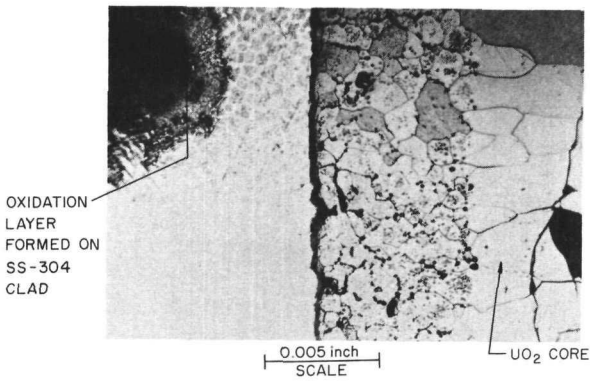

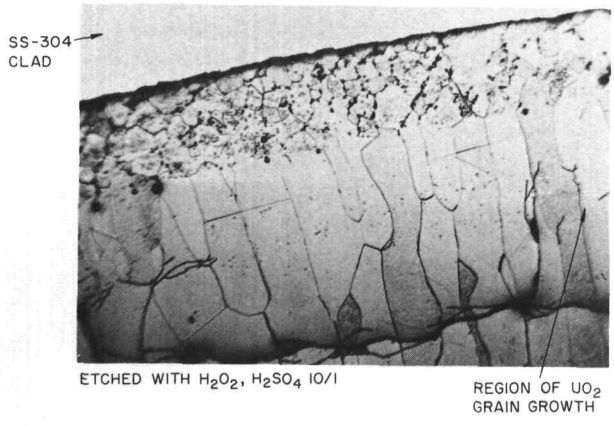

PHOTOMICROGRAPHS

Figure 55

TRANSIENT CEN-66: URANIA-CORE, STAINLESS STEEL-304-CLAD FUEL PIN

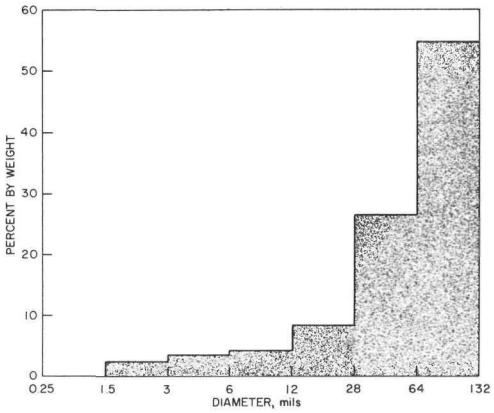

PARTICLE SIZE DISTRIBUTION
(Core and Cladding)
(Sieve Analysis)

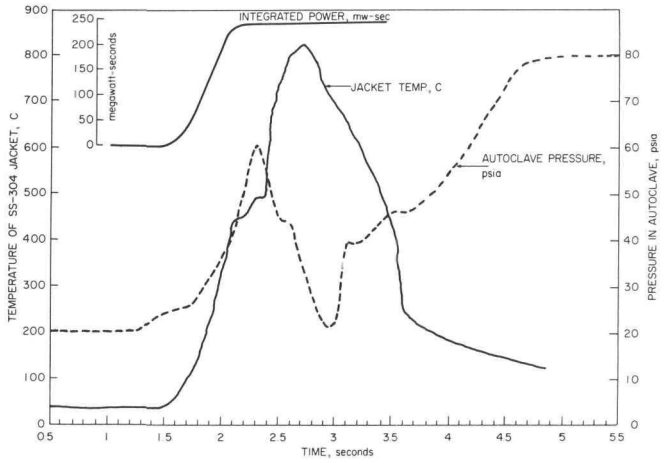

OSCILLOGRAPH RECORD OF RUN

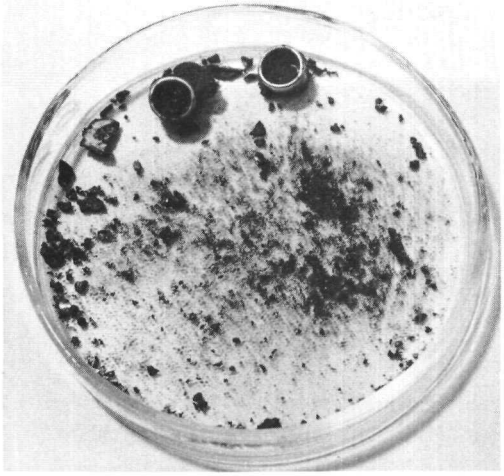

230 mw-sec BURST
690 mw PEAK POWER
97 ms PERIOD
9.0% SS-H_2O REACTION

0.5 inch SCALE

PHOTOGRAPH OF FUEL PIN

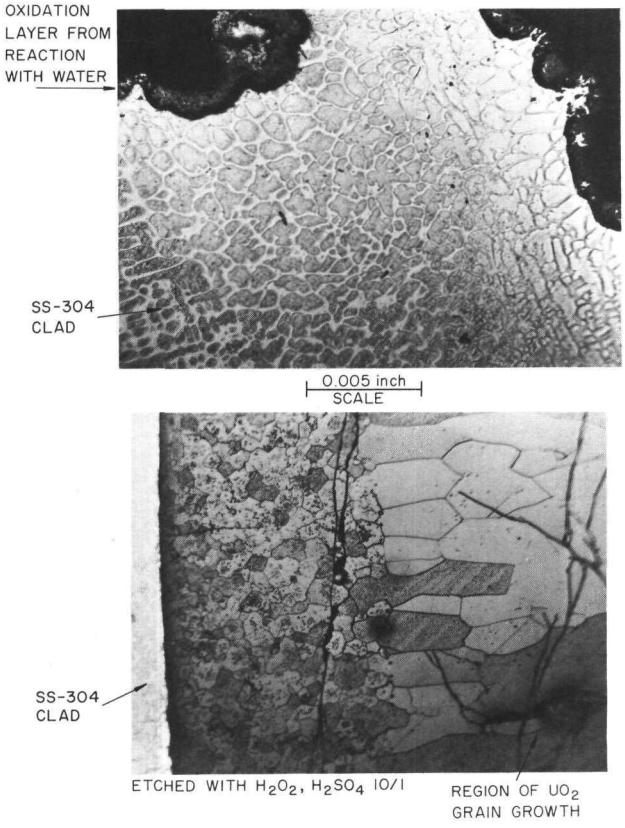

PHOTOMICROGRAPHS

Run CEN-64 was made with a water-logged core for comparison with a previous transient CEN-63. Run CEN-67 demonstrates the effect of a long (or "slow") period. Transients CEN-65 and 66 were made to obtain data on the meltdown behavior in water of uranium dioxide-core, stainless steel-304-clad fuel pins at energies intermediate to those obtained in the previous series.

An important phase of these in-pile studies is the determination of the particle size distribution which results when a fuel pin is fragmented and melted under water. Fragmentation occurred in Runs CEN-65 and CEN-66. In CEN-65 (see Figure 54), the 190 Mw-sec transient on a 50-ms period gave 5.2 percent stainless steel-water reaction with a peak in the distribution curve of from 3 to 28 mils. Run CEN-66 (see Figure 55), however, with 230 Mw-sec on a 97-ms period, gave a peak frequency (by weight) of from 64 to 132 mils. Thus, the shorter period appears to produce a larger fraction of fine particles. In CEN-65, 58.2 percent of the original weight of the fuel pin (core plus clad) was converted into particles. In CEN-66, 48.8 percent conversion into particles resulted. Before the transient, approximately 60 percent of the total weight of the fuel pin is the urania core.

By dissolving a sample of each size fraction (about one-half of the total was dissolved) and performing a uranium analysis the following results were obtained:

Particles Size Fraction, mils	UO_2 Concentration, Weight %	
	For CEN-65	For CEN-66
0.25-1.5	62	-
1.5 -3	55	88
3-6	81	78
6-12	81	80
12-28	85	74
28-64	72	69
64-132	-	76

From these results, it appears that the various fractions of particles contain a slightly higher ratio of urania to stainless steel than the original fuel pin. It also appears that there is no trend in the uranium dioxide concentration with particle size. Evidently, the shape of the particle size distribution curve for the total population of particles (core plus cladding) applies as well to either the oxide core or metal clad.

Various techniques are used to document the parameters of interest in this program. During the reactor burst itself, a record of the transient is obtained with an oscillograph. Figure 55 includes the oscillograph record from CEN-66; the integrated power curve shows that fission heating from the reactor pulse occurred within 0.6 sec. The peak jacket temperature measured by the thermocouple was 820 C; however, in view of the later visual observation of the extensive melting, the true metal temperature was more probably about 1450 C.

A comparison of the degree of destruction which resulted in CEN-65 and CEN-67 is of interest. Runs CEN-65 and 67 have very nearly the same energy input but periods of 50 and 290 ms, respectively. The 50-ms period gave rupture and partial melting of the clad with 5.2 percent stainless steel-water reaction, whereas with the 290-ms period the clad remained intact with only 0.3 percent metal-water reaction. This comparison shows the effect of a rather large change of reactor period.

Metallographic examination of the high-density urania core of the fuel pins (from Runs CEN-66 and 67) after transient irradiation showed radial and circumferential cracking. In Transients CEN-65 and 66 considerable grain growth in the central portion was apparent. A macrograph of the fuel pin after Transient Irradiation CEN-67 showed generalized cracking of the core. A comparison of Figure 51 with Figure 53 show the details of the cracking that occurred during a few seconds of heating and quenching in water.

If a ceramic core fuel element in a water-cooled reactor develops a defect, the pores and annular gaps can become partially filled with water. If such a fuel rod were then subjected to a power excursion, there could be an internal source of steam pressure which might promote dispersion of the core and cladding. To simulate such an event, two holes were drilled in the stainless steel-304 cladding (one on each end of the fuel pin) of the uranium dioxide-core fuel pin in Run CEN-64 (see Figure 52). The holes were each 0.035 in. in diameter. The pin was weighed, soaked overnight in water, and then weighed again. This water-logging treatment caused an increase in weight from 10.4066 to 10.4217 g. The fuel pin, with the punctured cladding, was then immersed in water inside the autoclave. A 140 Mw-sec reactor pulse on a 115-ms period caused a small rupture in the central part of the jacket; a small rupture also developed in one end of the fuel pin. There was no measurable increase in the diameter of the fuel pin (to within ±0.001 in.); however, there was a darkened central zone in the jacket indicating a high-temperature area which was oxidized by the water. From the measured amount of hydrogen produced, 0.8 percent of the stainless steel-304 cladding had reacted with the water. Observation of the core showed that cracking had occurred, as shown in the macrograph in Figure 52. A photomicrograph is also presented in Figure 52, which shows the grain structure of the oxide core at the edge of the pin.

The previously reported Transient CEN-63 with the same type of fuel pin, except that the core was not water logged, gave the following for a 120 Mw-sec transient on a 121-ms period:

(1) evidence for hot central zone (darkening);

(2) jacket remained intact, but showed a 7 percent increase in diameter;

(3) 0.3 percent metal-water reaction; and

(4) some cracking of core.

Thus, the results from CEN-63 and 64 are similar except for the behavior of the jacket. Evidently, when the jacket is completely sealed, swelling occurs from internal gas pressure; however, when the jacket is punctured, the holes permit the core to be vented and expansion of the jacket does not take place. It is possible that the rupture and slight increase in reaction for the case of the water-logged fuel could be caused by better heat transfer between the core and clad, which would create higher metal temperatures and, therefore, more reaction and a weakening of the metal. It is planned to conduct another similar experiment with a water-logged core, with the holes welded shut after the core has been saturated with water, and then subject the fuel pin to the reactor burst.

b. Summary of Results of Transients with Uranium Dioxide-core, Stainless Steel-304-clad Fuel Pins

Figure 56 summarizes the data that have been obtained to date on the in-pile studies of metal-water reactions for urania-core, stainless steel-304-clad fuel pins. From these results, the following tentative conclusions can be made.

1. There is a progressive increase in the amount of cladding-water reaction as the reactor burst becomes more energetic.

2. For reactor periods in the range from 48 to 121 ms, the period does not appear to be as important a parameter as the energy input in determining the amount of cladding-water reaction. However, with a very slow transient (such as a 290-ms period), there is less damage and less reaction relative to a faster transient.

3. For the 20 percent enriched urania-core fuel pins, clad in 18-mil-thick stainless steel-304, there is a threshold energy beyond which partial or total destruction of the fuel occurs depending on the energy input. For reactor periods from 48 to 121 ms, this dividing point is approximately 130 Mw-sec (or a specific energy input of 174 cal/g of core). This energy input corresponds to peak, adiabatic core temperature during the transient of 2200 C. This is to be compared with the melting point of uranium dioxide, which is 2730 C.

FIGURE 56
EXTENT OF STAINLESS STEEL-WATER REACTION
RESULTING FROM IN-PILE
MELTDOWNS OF URANIA CORE FUEL PINS

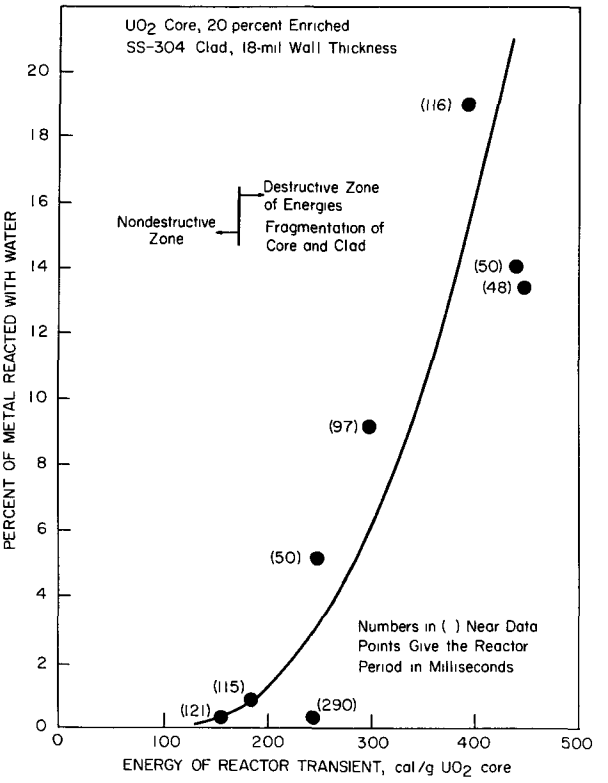

c. Evaluation of Structural Damage from Previous Experiments on Ceramic-core, Metal-clad Fuel Pins

Correlations have been presented in an earlier report (ANL-6333, page 236) on the chemical behavior of ceramic (mixed oxide)-core fuel pins in water. These data were given as the extent of metal-water reaction as a function of the energy input. Table 53 presents a summary which emphasizes the physical aspects of the results, which can be of use to reactor designers in making estimates of the allowable transients that a particular reactor can tolerate without destroying the integrity of the ceramic-core fuel. This summary brings out the interesting point that reactor transients which cause peak core temperatures greater than 2300 C give rise to rupture or melting of the core or clad (or both at very high energies). Less energetic transients (on periods from 60 to 105 ms) cause only cracking in the core, but no rupture of the cladding. Hence, for those transients which produce central core temperatures of from about 1000 to 2000 C, the core is still contained within the metal cladding even though structural changes have occurred in the core. Less energetic transients have not been investigated in this program since they are of no interest to the application of metal-water reactions to reactor safety; however, there is presumably some peak transient temperature less than 1000 C at which no changes (such as cracking) occur even in the core.

Table 53

SUMMARY OF SOME TREAT REACTOR TRANSIENTS PERTINENT TO THE BEHAVIOR OF CERAMIC-CORE[a] FUEL PINS IN WATER

	Characteristics of Neutron Pulse				Results		
Transient Number	Fission Energy Input, cal/g[b]	Reactor Period, ms	Rate of Energy Input at Peak of Reactor Burst, cal/(g)(sec)[c]	Cladding Metal Around Pellet	Appearance of Cladding after Transient	Calculated[d] Peak Core Pellet Temp (C) and Physical State	Observations on Ceramic Pellet after Transient
19	159	101	558	Al	no change	1050 Solid	Intact with a few fine cracks
56	254	105	592	Zr-2	no change	1650 Solid	Cracked
40	296	60	1753	SS-304	no change	1930 Solid	Extensive cracking
29	362	63	1504	Zr-2	hole in center	2360 Solid	Extensive cracking; some fragments
21	395	78	719	SS-304	no change	2550 Solid and Liquid	Central melting, radial and circumferential cracking
48	432	72	1321	SS-304	ruptured, partly melted	2550 Solid and Liquid	Fragmented into particles
23	474	60	1607	Al	ruptured, partly melted	2550 Liquid and Solid	Partially fused and fragmented into fine particles
30	517	62	1589	Zr-2	hole melted in center	~2750 Liquid	Melting, fine particles
49	609	50	2538	Zr-2	ruptured, melted	~3100 Liquid	Completely pulverized

[a] Composition of ceramic (mixed oxide) core: 81.5 w/o ZrO_2, 9.1 w/o CaO, 8.7 w/o U_3O_8, 0.7 w/o Al_2O_3, 93% enriched.
[b] Calculated from the correlation: (cal/g of oxide core) = (0.94)(Mw-sec).
[c] Calculated from the relationship cal/(g)(sec) = (Mw peak power) (cal/g)/(Mw-sec) .
[d] Adiabatic temp (no heat loss) from the equation: $Q\ (cal/g) = \int_{25}^{T_{max}} C_p dt$

Finally, it is appropriate to emphasize (to avoid confusion in interpreting or applying the results summarized in Table 53) that temperatures given are those calculated for the oxide core for adiabatic heating. During the actual transient experiments, the metal cladding temperatures have been measured (to date no thermocouples have been inserted into the oxide core) and these have commonly been about 1200 C. Thus if one asks, for example, would a fuel temperature of 1600 C during a fast transient in an oxide-core fuel pin in water result in a hazardous condition (assuming a stainless steel-304 clad), the answer would be 'no' if this temperature refers to that of the oxide core. If, however, the temperature in question refers to the cladding, then the stainless steel would have melted and partially reacted with the water.

It is also of interest to compare the mixed oxide-core fuel pins with the pure uranium dioxide-core fuel pins from the point of view of peak transient temperatures which begin to produce destruction of the fuel element. In the previous section on uranium dioxide-core fuel pins, it was noted that transients which caused the urania core to rise to 2200 C or less did not result in rupture or melting of the clad. The summary in Table 53 with mixed oxide-core fuel pins indicated that 2300 C was a peak threshold temperature for the central core. Thus, both the

pure and mixed oxide-core fuel pins appear to have substantially the same allowable temperature limit in a fast transient with the fuel pin initially at room temperature and submerged in water.

With regard to the application of these results, it is pertinent to note that the meltdown experiments were conducted in nonflowing water with a bulk temperature of ambient surroundings (~25 C). With other conditions (such as flow turbulence) it is possible that more heat could be dissipated and thus higher peak central temperatures tolerated without melting.

IV. REACTOR CHEMISTRY

The neutron capture cross sections of neptunium-237, erbium-170, gadolinium-158, lutetium-175, ytterbium-176, and molybdenum-98, are being determined in the fast neutron energy range. Preparations have begun for the determination of the yields of fission products in the region of mass 100 when the fissile isotopes uranium-233, uranium-235, and plutonium-239 are exposed to a fast neutron (fission spectrum) flux.

Operation of a regenerative lithium hydride fuel cell system for converting nuclear energy to electricity is being studied. The thermally regenerative emf cell system is one in which heat is used to disassociate lithium hydride, which is then re-formed in an electrochemical cell with the production of electric power.

The program of research in thermoelectricity methods for direct conversion of nuclear reactor heat energy into electrical power initiated last quarter (see ANL-6379, page 242) was continued. Measurements will be made in two limited areas, namely, liquid thermocouple systems and refractory solid thermal couple systems. Seebeck coefficients, electrical conductivities, thermal conductivities, and Hall coefficients of well-characterized materials may be determined. Current efforts are concerned with design, construction, and testing of equipment, and with some exploratory measurements.

The Reactor Decontamination Program is directed toward determination of the seriousness of fuel element ruptures in boiling water reactors and the determination of methods of decontamination of contaminated surfaces. Additional data have been obtained from a 16-day run made to determine whether zirconium-niobium content would reach an equilibrium value in a stainless steel loop which simulates the action of a boiling water reactor. The data indicated that the concentrations of all fission products, except ruthenium-103, reached a near equilibrium level after about 100 hr of loop operation. The concentration of ruthenium-103 continued to decrease to nondetectable levels. Current laboratory experiments on the decontamination of stainless steel 304 are being conducted using oxalic acid-base solutions containing hydrogen peroxide.

A. Determination of Nuclear Constants

(C. E. Crouthamel)

Fast neutron cross sections are being studied as a function of neutron energy for the nuclides erbium-170, gadolinium-158, lutetium-175, ytterbium-176, molybdenum-98, and neptunium-237. In the previous report, ANL-6379, the use and proposed uses of some of the rare earths as reactor control materials were discussed, and further details of the interest in all of the above nuclides are given there.

Preparations have been made for measurements of the fast fission neutron spectrum. The preliminary experimental work has been done in preparation for the determination of the yields of several fission products in the region of mass 100 for the fissile isotopes uranium-233, -235, and plutonium-239. Details of this work are given below.

1. Fast Capture Cross Sections
(D. C. Stupegia, E. H. Dewell, A. A. Madson)

Fast capture cross sections are being measured as a function of neutron energy by determining the absolute disintegration rate of the capture product when a target of known mass is irradiated in a known neutron flux. The neutron source is the reaction Li^7 (p,n) Be^7, from the bombardment of a lithium target with protons from the Van de Graaff accelerator. The available neutron energies range from about 0.3 to 2.2 Mev. The radioactivity of the activated samples is assayed with the multichannel scintillation spectrometer. Details of the experimental methods were given in the previous report (ANL-6379, pages 224 to 229).

Erbium-170

The neutron irradiation of this nuclide yields the 7.8-hr beta and gamma emitter, erbium-171. Twelve irradiations have been completed, covering the neutron energy range from 0.35 to 1.81 Mev. Gamma analyses of the targets have been taken and the decay curves followed.

Gadolinium-158

Two more irradiations of the oxide targets have brought the total to nine, covering the neutron energy range from 0.46 to 1.91 Mev. The activity measured is the 18-hr gadolinium-159, a beta and gamma emitter, and the gamma spectra have been recorded.

Ytterbium-176

Of the seven stable isotopes of ytterbium, three yield radioactive neutron capture products. The reactions are:

$$Yb^{174} \xrightarrow{n,\gamma} Yb^{175} \xrightarrow[101\ hr]{\beta,\gamma} Lu^{175}\ (stable)$$

$$Yb^{176} \xrightarrow{n,\gamma} Yb^{177} \xrightarrow[1.9\ hr]{\beta,\gamma} Lu^{177} \xrightarrow[6.8\,d]{\beta,\gamma} Hf^{177}\ (stable)$$

$$Yb^{168} \xrightarrow{n,\gamma} Yb^{169} \xrightarrow[32\,d]{K\ cap} Tm^{169}\ (stable)\ .$$

In the series of irradiations completed at this point, only the second reaction above was suitable for the measurement of the capture activity, since the half-lives of the other two capture products are too long. The present data, therefore, yield only the capture cross section of ytterbium-176.

Nine monoenergetic neutron irradiations have been carried out on ytterbium oxide targets in the energy range from 0.35 to 1.91 Mev, and the resulting gamma ray spectra have been analyzed.

Lutetium-175

When natural lutetium, containing 97.4 percent of lutetium-175 and 2.6 percent lutetium-176, is irradiated with neutrons, the following capture processes occur:

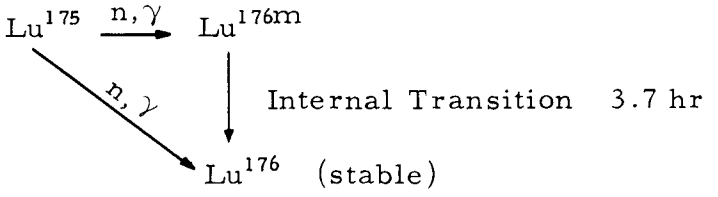

$$Lu^{176} \xrightarrow{n,\gamma} Lu^{177} \xrightarrow[6.8\,d]{\beta,\gamma} Hf^{177} \text{ (stable)}$$

Lutetium-175 yields two products; stable lutetium-176, and the 3.7-hr isomeric state of the latter. The activation of lutetium-176 yields the 6.8-day species, whose activity is too low to measure under the present conditions.

Eight irradiations of about 2 hr each have been carried out, covering the neutron energy range from 0.35 to 1.61 Mev, and the gamma ray spectra have been analyzed.

Molybdenum-98

Eight irradiations of about 4 hr each have been completed with metallic molybdenum targets using neutron energies between 0.46 and 2.12 Mev. Natural molybdenum contains 7 stable isotopes, of which three, molybdenum-92, -98, and -100, yield radioactive capture products, which are 6.9-hr Mo^{93m}, 67-hr Mo^{99}, and 15-min Mo^{101}. In the gamma-ray analyses following irradiations, the 67-hr and the 15-min activities were clearly apparent, but the 6.9-hr activity, arising from molybdenum-92, a species with an exceptionally low capture cross section, was apparently not found. Data are available, therefore, to measure the cross sections of molybdenum-98 and -100. The latter values are already available in the literature; therefore, these data will not be pursued, and attention will be given only to molybdenum-98.

Neptunium-237

Neutron activation of this nuclide gives the 2.1-day beta and gamma emitter, neptunium-238. Nine neutron irradiations have been completed, covering the neutron energy range between 0.46 and 1.30 Mev. Gamma analyses of the irradiated targets have been made and the data are being analyzed.

Absolute Beta Counting

In the determination of the capture cross section of each nuclide discussed above, it is necessary to know the absolute disintegration rate of the activation product. After irradiation, in each case, the irradiated target is analyzed for the gamma-ray spectrum of the activation product by means of the sodium iodide crystal and the 256-channel analyzer. The absolute disintegration rate corresponding to the observed gamma spectrum, or a convenient part of it, is determined by comparing this spectrum with that of a known activity of the same species counted in the same geometry. It is necessary, therefore, to determine the absolute disintegration rate of the species of interest. This has been done and will be done by one or both of two methods of 4π beta counting. The first and older method used here is the proportional counting technique, wherein a sample of the activity in solution is evaporated onto a thin mounting, and ideally 100 percent of the beta rays are counted. This apparatus has been used successfully for absolute beta counting in the present program. Another 4π beta-counting system has now been put into operation. This is a liquid scintillation system, in which a solution of the radioactive sample is introduced directly into a liquid scintillator solution, which is coupled with a photoelectric tube and an amplifying system. This method is faster, more convenient, and subject to fewer corrections than the proportional method. The liquid scintillation counter is now being used for absolute beta counting of activation products associated with the isotopes whose cross sections are being measured.

2. Neutron Total Cross Section of Uranium-233

(D. C. Stupegia)

A report of this work, detailed in the previous report (ANL-6379, pages 228 to 229), has been accepted for publication in the Journal of Nuclear Energy (Reactor Science).

3. Fast Fission Yields in the Region of Mass 100

(D. C. Stupegia, E. H. Dewell, A. A. Madson)

A common method of determining the degree to which a reactor fuel has undergone fission is to assay a fission product of well-known yield. For thermal fission of the major reactor fuels, the yields are well known as a function of fission fragment mass. With the increased attention being directed to studies of fast reactors, it has become necessary to know certain

fission yields in fast neutron spectra in the anticipation of their use in burn-up determination. These data, however, are not well known, and are not, in general, expected to be the same as the thermal values.

A fast reactor, such as EBR-I or EBR-II, has a neutron spectrum with a most probable neutron energy of about 0.3 Mev. If one wished to use fission-yield data as a burnup standard, one would want data for a spectrum closely approximating that of the reactor in question. However, it is not practical to determine fission yields in all possible fast spectra. A convenient fast neutron spectrum is the unmoderated fission spectrum, which has a most probable neutron energy of about 0.7 Mev. The fission yield of cesium-137 was determined[34] in a fission spectrum and the value was subsequently used to calculate, on the basis of cesium-137 analysis, the degree of burnup in fissile samples irradiated in EBR-I. In this fission-yield work on cesium-137, it was found that the yield in uranium-235 fission rises from 5.9 percent with thermal neutrons to 6.3 percent with fission neutrons (most probable energy, 0.7 Mev). Therefore, if one assumes that the rise from the thermal to the fast value is monotonic, one concludes that there is little difference between the yields in the fission neutron spectrum and the fast reactor spectrum (most probable energy 0.3 Mev).

Recent plans have been made to measure burnup by the assay of fission products other than cesium-137. In samples of high burnup, an attractive procedure is the colorimetric determination of technetium (Tc^{99}). For very short irradiations, a useful monitor is 67-hr molybdenum-99. In this mass region of the fission product distribution, it is expected that the fission yields will vary appreciably with neutron energy and with mass of the fissioning species, because of the presence of a fine structure peak in this part of the curve. In the present work it is planned to measure the fission yields of zirconium-95 and -97, niobium-97, technetium-99, and molybdenum-99.

The apparatus used is a neutron flux converter and associated fission chamber. The flux converter is a cup of enriched uranium which completely surrounds (1) the fissile sample being studied, (2) a thin fission monitoring sample of the same species, and (3) a fission chamber, which counts fissions in the thin sample. Since the enriched uranium cup is thick enough to be black to the reactor thermal neutrons, in which the apparatus is immersed, and the uranium itself a poor moderator, the samples inside the cup are exposed to an essentially unmoderated fission neutron spectrum. The numbers of fissions in the heavy and light samples are proportional to their respective masses. Then, having counted the number of fissions in the light sample, and having separated the given fission product from the heavy sample, and measured its disintegration rate, the yield of the fission product is thereby determined.

---

[34] Kafalas, P., and Crouthamel, C. E., J. Inor. and Nuclear Chem, 4, Nos. 5 and 6, 239 (1957).

Light and heavy samples of uranium-233 have been prepared for the first irradiations. The light samples contain about 4 μg plated on a circle of 1-cm diameter. The heavy samples consist of 1-cm-diameter discs of about 0.2 g uranium dioxide. Procedures for the separation of fission product molybdenum, niobium, and zirconium have been prepared, and will be used following the uranium-233 irradiations.

B. Thermally Regenerative Emf Cell
(C. E. Crouthamel, M. Foster, R. Heinrich, R. Eppley)

Studies are being directed toward the development of a regenerative cell to convert heat into electricity. This cycle requires regeneration of the cell product, that is, the physical separation and return of the anode and cathode reactants to complete the cycle. The product of the particular cell being investigated is lithium hydride, which is dissolved in molten lithium chloride-potassium chloride. Lithium ions are formed at a molten lithium metal anode floating on the surface of the molten salt electrolyte and contained in an Armco iron ring. Hydride ions are formed at the melt-Armco iron diaphragm interface in the base of the cell. Hydrogen enters the cell by diffusing through the solid Armco iron diaphragm.

The polarization of a cell with a lithium electrode, consisting of a pool of liquid lithium metal, and a hydrogen electrode, consisting of a 10-mil Armco iron diaphragm, has been investigated as a function of applied load by means of a small reference lithium electrode. The hydrogen pressure was maintained at 757 mm Hg; no stirring of the melt was done during these measurements. The data are shown in Figures 57 and 58 for both forward and reverse (discharge and charge) operation of the cell. It is clearly indicated that the majority of the voltage polarization is due to the hydrogen electrode. For example, at a current density of 2 amps/sq ft on the hydrogen electrode, a polarization of about 275 mv was measured during cell discharge, while at the same current density measured at the lithium electrode under the same conditions about 10 mv is measured.

The cell, when operated as a battery, can be considered as an ideal battery in series with a fixed resistance (due, e.g., to lead resistance) and a variable resistance (due to the passage of current). The latter resistance tends to zero as the rate of current flow tends to zero. The fixed resistance of the cell (lead resistance plus any fixed internal resistance) was estimated as 0.4 ohm. This value was used to estimate the efficiency of the cell operating as a battery and is given by

$$\text{efficiency} = (E/E^0)\,(R_{Total}/R_{Load})$$

where: E = voltage drop across external lead resistance R_{Load},
E^0 = open circuit voltage, and
R_{Total} = R_{Load} plus 0.4.

A graph of cell efficiency vs. R_{Total} is given in Figure 59.

FIGURE 57
POLARIZATION OF HYDROGEN ELECTRODE OF THE
THERMALLY REGENERATIVE LITHIUM HYDRIDE CELL

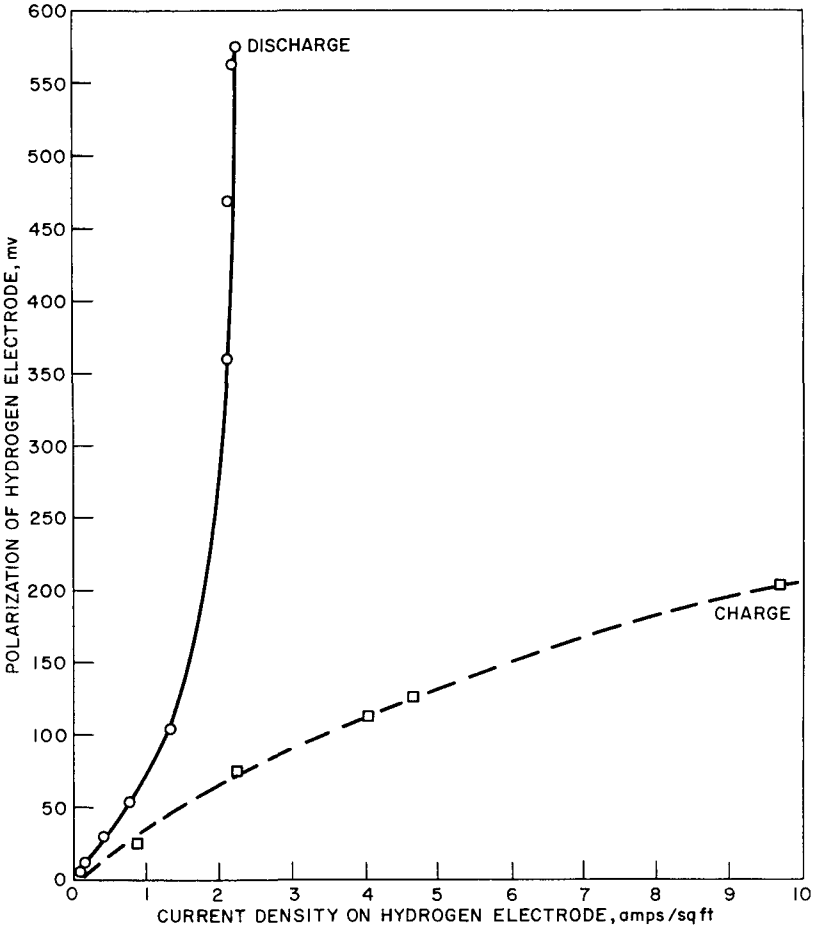

FIGURE 58
POLARIZATION OF LITHIUM ELECTRODE OF THE
THERMALLY REGENERATIVE LITHIUM HYDRIDE CELL

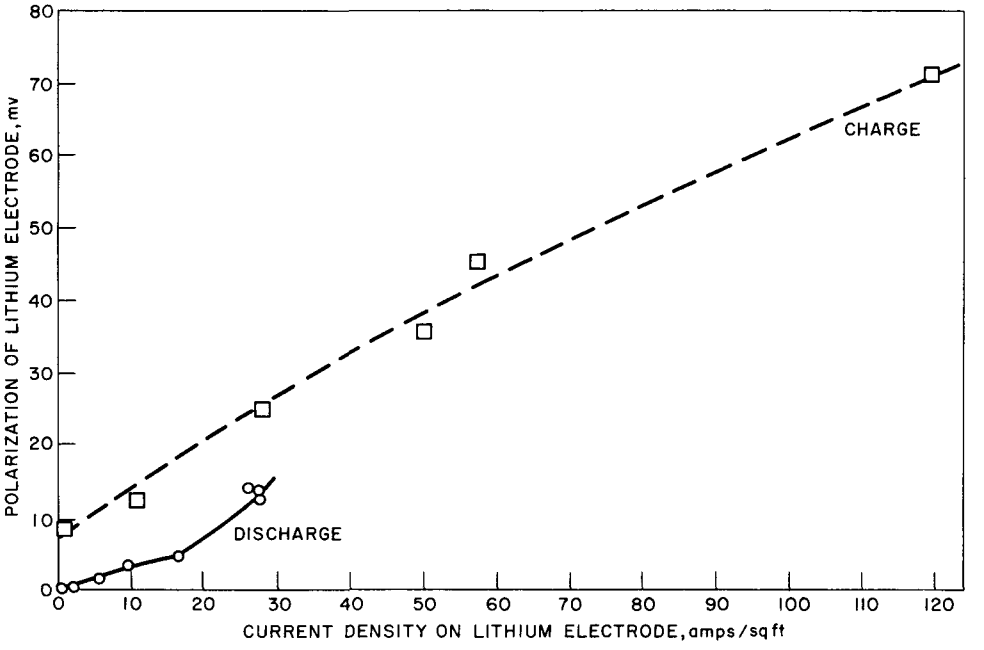

FIGURE 59
CELL EFFICIENCY AS A FUNCTION OF R_{TOTAL}

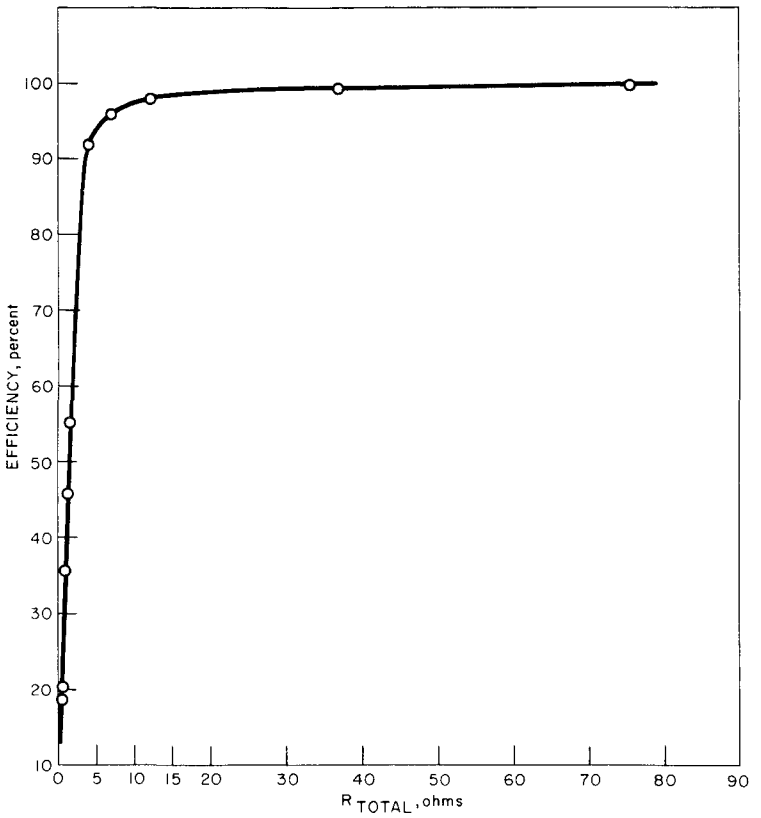

Polarization of the hydrogen gas electrode in the lithium hydride regenerative cell is substantial, and it has been shown that the degree of polarization is dependent upon the amount of hydrogen gas diffusing through the hydrogen diaphragm-electrode. Independent studies of hydrogen diffusion are now being conducted to provide a suitable metal diaphragm which will supply hydrogen to the cell at higher rates and which will also be compatible with the cell environment.

Since hydrogen diffusion rates of the order of 1 to 25 cu cm/(sec)(sq ft) of diaphragm area are desired, the rates of different materials compatible with the cell will be measured by means of a constant-pressure apparatus. This apparatus differs from that of earlier investigators in that the actual volume of hydrogen gas diffused through the diaphragm is observed at constant pressure. Previous investigators were concerned primarily with slower diffusion rates and observed small pressure changes at constant volume. The apparatus for this measurement is now complete and diffusion data will be reported in the next quarterly report.

C. Thermoelectricity Research
(R. K. Edwards)

A program of fundamental research in thermoelectricity has been initiated to contribute to the future technological development of direct conversion of nuclear reactor heat energy into electrical power by means

of the thermocouple effect. Two limited areas of research have been selected as of special interest. Liquid thermocouples are under investigation because of favorable experimental factors and because very little work has been and is being carried out with such materials. Refractory solid thermocouple systems form the other major area, since they are considered to be of particular interest to reactor energy conversion.

The experimental program consists of measurements of Seebeck coefficients, electrical conductivities, thermal conductivities, and Hall coefficients of well-characterized materials. These measurements are necessary for the elucidation of transport mechanisms for the charge carrier and for evaluation of material efficiencies. Current efforts are concerned with equipment design, construction, testing, and with some exploratory measurements.

1. Liquid Thermocouple Systems
(R. K. Edwards and P. Danielson)

Liquid systems containing elements in the area of the periodic system centering about the element tin will be investigated. The particular area chosen is that for which solid state investigations have shown many semiconducting compounds of promising thermoelectric efficiencies. An example is the compound indium antimonide, which has been extensively studied in the solid state and, to a limited extent, above its melting point. The solid state investigations were necessarily limited to the very narrow composition range of the compound. The present investigation will study the Seebeck coefficients throughout the complete composition range of the indium-antimony system in the liquid state. The equipment is assembled and ready for the initial measurements.

2. Refractory Solid Thermocouple Systems
(M. Tetenbaum)

For high-temperature use, a refractory, broad-band semiconductor is required if the thermoelectric properties are to be favorable over a large temperature interval. The lanthanide and actinide sulfide systems are highly refractory and have phases with electron concentrations in the semiconducting range. The uranium and thorium sulfide systems and their solid solutions have been selected for the initial studies.

Although a small amount of experimental work on refractory sulfides has been reported, it appears that measurements of thermoelectric parameters have been made on materials which were poorly defined as to stoichiometry. It was decided, therefore, that the present program would place strong emphasis on a preparation of sulfides of well-defined compositions.

a. Preparation of Uranium Monosulfide*

A small quantity of uranium monosulfide has been prepared with the equipment available in the Chemistry Division. The design of the equipment was essentially that of Eastman et al.[35] Uranium in the form or a small bar (initially cleaned in concentrated nitric acid and subsequently electropolished in a sulfuric acid-glycerine bath) was converted to the powdered hydride by reaction with purified hydrogen at approximately 200 to 250 C for several hours. The system was then evacuated and the hydride decomposed at a relatively low decomposition temperature (250 C) in order to avoid sintering of the finely divided product. The product was sulfided by reaction with hydrogen sulfide gas overnight at approximately 500 to 600 C. The crude sulfide was transferred (via a dry box) to a tungsten crucible and homogenization was effected by heating the charge slowly to 2100 C under high vacuum. X-ray analysis of the sintered product from the homogenization procedure showed uranium monosulfide (cubic structure, sodium chloride type) as the major phase and uranium oxysulfide (tetragonal) as the minor component.

An attempt was made to purify and, at the same time, to sinter this material into a usable shape for subsequent measurements of thermoelectric parameters. The product from the homogenization procedure was ground and cold pressed into a small pellet, inserted into a close-fitting tantalum crucible, and heated inductively in vacuum for several hours at approximately 2000 C. After cooling, it was found that the material in the crucible could not be conveniently removed in one piece, and it was necessary, therefore, to sacrifice the crucible in order to remove the material, which was then in the form of small, irregular pieces.

The material recovered from the tantalum crucible was reground, cold pressed into a pellet, placed in a tungsten crucible (large compared to the diameter of the pellet) and slowly heated under high vacuum to a temperature of approximately 2200 C. The crucible was held at this temperature for approximately $1\frac{1}{2}$ hr.

Chemical analysis of the sintered mass gave a sulfur content corresponding to $US_{1.03}$. Uranium oxysulfide (insoluble in 3.6 N sulfuric acid) was not detected. X-ray analyses and resistivity measurements are in progress.

---

* The assistance and guidance of Robert Walters of the Chemistry Division in the preparation of this material is gratefully acknowledged.

[35] Eastman, E. D., Brewer, L., Bromley, L. A., Gilles, P. W., and Lofgren, N. L., J. Am. Chem. Soc. 72, 4019 (1950).

D. Reactor Decontamination
(W. B. Seefeldt)

The Reactor Decontamination Program has two principal objectives: 1) to determine experimentally in pilot-plant equipment the degree of contamination to be expected in the steam phases of a boiling water reactor system in the event of fuel-cladding failure, and 2) to find suitable methods of removing deposited activity from internal surfaces, should it be necessary because of excessive radiation levels. The pilot-plant equipment used for the first objective consists of a stainless steel type 304 loop that simulates the action of a boiling water reactor. Fuel ruptures are simulated by inserting tracer activities of irradiated metallic uranium. In a parallel effort, studies are being made in the laboratory to find suitable means of removing deposited activities.

Additional data from a 16-day loop run show that the concentrations of all fission products, except ruthenium-103, reached a near equilibrium level after about 100 hr of loop operation. The concentration of ruthenium-103 continued to decrease to nondetectable levels. The specific depositions of fission products related to vapor (microcuries of fission product deposited per microcurie in vapor, $\mu c/sq\ cm \div \mu c/cu\ cm$) varied from 34 to 100 for cerium, zirconium-niobium, and ruthenium, and from 4 to 8 for iodine, cesium, and barium-lanthanum. Extrapolation of these results to a reactor system under specified conditions indicates that contamination of a 6-in. steam line would not result in sufficient deposition to jeopardize approach to the line for maintenance purposes.

The results of the decontamination of the liquid phase of the loop are presented. These include radiation measurements, material balances, and decontamination factors.

Current laboratory efforts are being directed at the modification of an oxalic acid-hydrogen peroxide reagent system developed by Oak Ridge National Laboratory; the modification is directed toward use in the vapor phases of boiling water reactor systems. Early data developed on laboratory contaminated stainless steel type 304 surfaces indicated that the decontaminations from zirconium-niobium-95 and cerium-141 were generally good (decontamination factors in excess of 100). Decontamination of ruthenium-103 was erratic. In recent experiments, the decontamination capability of this reagent on loop contaminated specimens was found to be considerably less (2.5 to 7), and efforts are being made to determine the cause of this reduction. Significant improvements were not obtained by varying the peroxide-oxalic acid ratios between 0.5 and 6.0.

Studies of the stability of oxalic acid-hydrogen peroxide mixtures were extended to include measurements at room temperature. Good stability was indicated in that the greatest pH change observed in one week was from 4.0 to 4.8.

1. Loop Studies
(D. Grosvenor, C. Bally)

A stainless steel type 304 loop which simulates the action of a boiling water reactor has been installed in a shielded cell in order to study the effects of simulated ruptures of fuel elements. It is of interest to know how much and what kind of fission products will distribute through the system in order to ascertain the degree to which maintenance might be impaired in a practical system should failure of fuel cladding occur. Fuel ruptures are simulated in the loop by introducing irradiated metallic uranium. Fission products are released as the uranium corrodes in the circulating water. Deposition of activity in the steam disengaging space is monitored by inserting a metallic sample strip. This is removed following a run, cut into convenient lengths, and counted in a 256-channel gamma scintillation spectrometer. This is correlated with similar information obtained from liquid and condensed steam samples.

In the preceding report period, partial results of a 16-day loop run (U4) were reported (see ANL-6379, page 245). The principal incentive for the run was to determine whether the fission product compositions of the circulating liquid reached what might be considered equilibrium levels. This is important since the objective of the loop experiments is to relate fission product deposition on metal samples in the vapor phase with the entrained fission product content of the steam, which, in turn, is a function of fission product content of loop water. The fission product patterns (as a function of time) obtained and presented in ANL-6379 suggested that for all fission products monitored, except ruthenium, correlatable deposition data could be obtained. This is possible if variations of concentration by a factor of five around some central value were acceptable and provided that the loop was operated for 100 hr prior to increasing the steam velocity of the desired value. The first 100 hr need to be excluded because most of the concentrations decreased by one to two orders of magnitude during that period. Good ruthenium data appear difficult to obtain, for its concentration continued to decrease through the entire run. The fission product concentration of the loop liquid are presented again in Figure 60. The curves presented in this report differ from those in the preceding report in that the new curves are the result of a statistical least-squares treatment. The curves were matched to polynominals of the fourth power and points deviating by more than three standard deviations were discarded.

Data presented below on fission product content of the steam, resulting disengaging factors, and fission product deposition on the metal sample strips are new information. During the last half of the run, after some reasonable sort of equilibrium of liquid content had been achieved, condensed steam samples were taken at regular intervals. These samples were similarly scanned on the 256-channel gamma scintillation spectrometer and the results processed through the IBM 650 computer. Plots of the fission product content of the vapor as a function of time (not included here) showed a reasonably consistent composition. Following the completion of

FIGURE 60
FISSION PRODUCT CONTENT OF LOOP LIQUID AS A FUNCTION OF TIME
(Curves are result of least squares to fourth power polynomial; points exceeding 3σ have been discarded (<10% of data))

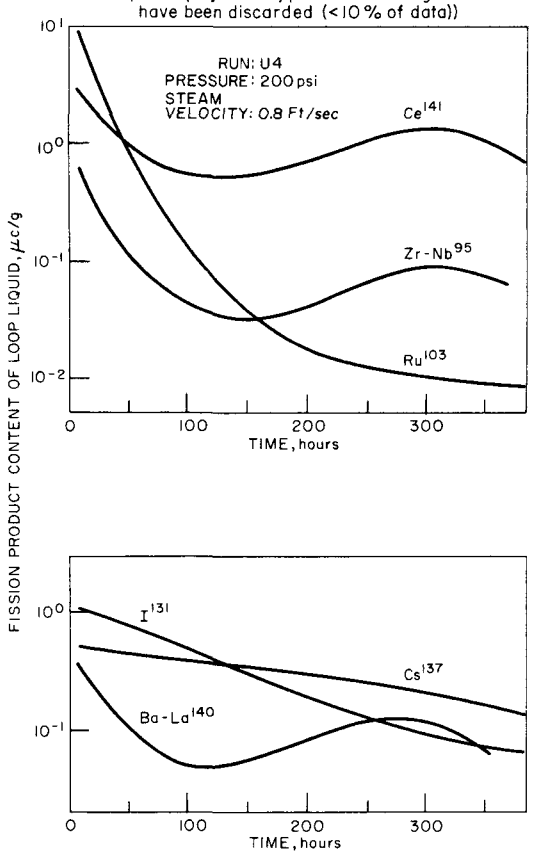

the run, the sample strip of stainless steel type 304 was removed, and several sections from the upper portions of the vapor phase were scanned. Table 54 and Figures 61 and 62 contain the results obtained from the analyses of liquid and condensed steam samples as well as of the metal sample strip. It is evident that cerium was the predominant activity contained in the liquid and steam. The disengaging factors for three of the fission products, iodine, cesium, and zirconium, ranged from 4 to 7 x 10^{-3}. The corresponding ruthenium factor was depressed while those of cerium and barium-lanthanum were high. The data thus suggest that some small enrichment of ruthenium occurred in the vapor while a depletion was observed for cerium and barium-lanthanum. Similar observations regarding cerium and ruthenium were made in Run U-3. The deposition data for fission products on stainless steel shown in Figure 62 indicate that the predominant activities deposited were those of cerium, ruthenium, and zirconium. To normalize the data, a ratio, termed specific deposition, was calculated. This was obtained by dividing the actual deposition, measured as μc/sq cm, by either the liquid or the vapor content, measured in μc/cu cm. The specific deposition related to vapor is the more significant insofar as it is the vapor content that determined deposition. However, the specific deposition for the liquid has been calculated for extrapolation to systems where the vapor content may be unknown. The much greater adsorption of cerium, ruthenium, and zirconium over that of iodine, cesium, and barium is immediately evident.

Specific deposition data such as have been calculated are useful, with limitations, for extrapolation to reactor systems. In a following section these data have been used to calculate radiation levels from a hypothetical 6-in. pipe line under specified reactor conditions.

In the preceding report period, the progress of the loop decontamination (liquid phase) as monitored by radiation measurements was given. It was shown that this series of solution treatments reduced the original radiation level of 5 to 30 r/hr to levels between 50 and 250 mr/hr.

Table 54

STEAM DISENGAGING FACTORS AND SPECIFIC DEPOSITION ON STAINLESS STEEL TYPE 304 FOR RUN U4

Conditions:

Steam Pressure: 200 psi
Steam Velocity: 0.8 ft/sec
Run Length: 16 days

Fission Product	Liquid Content (mc/cc)	Vapor Content (mc/cc)	Metal Deposition (mc/sq cm)	Steam Disengaging Factor[b]	Specific Depositions (cm)[a] Liquid Related x10³	Specific Depositions (cm)[a] Vapor Related
Ce	1.0	8.8×10^{-5}	3.0×10^{-3}	1.13×10^{4}	3.0	34
I	1.1×10^{-1}	2.5×10^{-5}	1.1×10^{-4}	4.4×10^{3}	1.0	4.4
Ru	1.0×10^{-2}[c]	2.0×10^{-5}	2.0×10^{-3}	0.5×10^{3}	80	100
Cs	1.75×10^{-1}	2.8×10^{-5}	1.5×10^{-4}	6.25×10^{3}	0.86	5.4
Zr	8.0×10^{-2}	1.1×10^{-5}	8.0×10^{-4}	7.3×10^{3}	10	73
Ba-La	8.6×10^{-2}	3.9×10^{-6}	3.0×10^{-5}	2.2×10^{4}	0.35	7.7

[a] Deposition (μc/sq cm) ÷ liquid or vapor fission product content (μc/cc).

[b] Disengaging factor is defined as the ratio of activity in the liquid phase to that in the steam phase.

[c] This value of the ruthenium content of the liquid is about the lowest good value obtained before data began to scatter because an insufficient quantity was present.

FIGURE 61
STEAM DISENGAGING FACTORS AND FISSION PRODUCT CONTENT OF LIQUID AND VAPOR FOR RUN U4

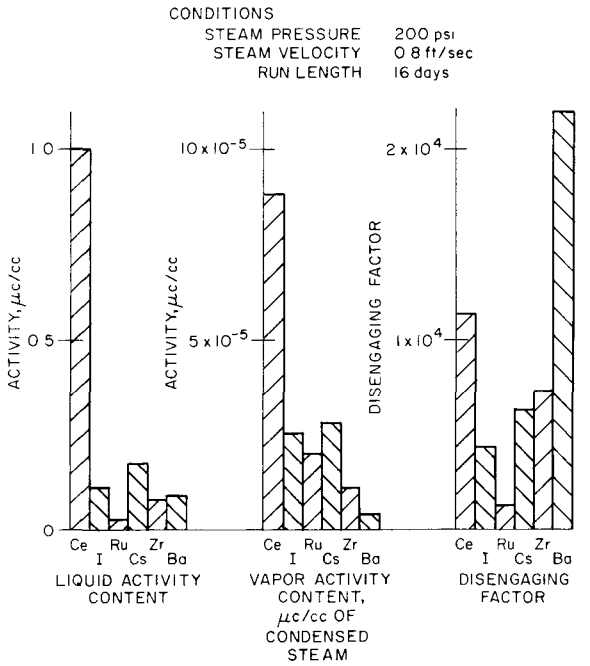

FIGURE 62
DEPOSITION OF VARIOUS FISSION PRODUCTS ON STAINLESS STEEL TYPE 304 IN RUN U4

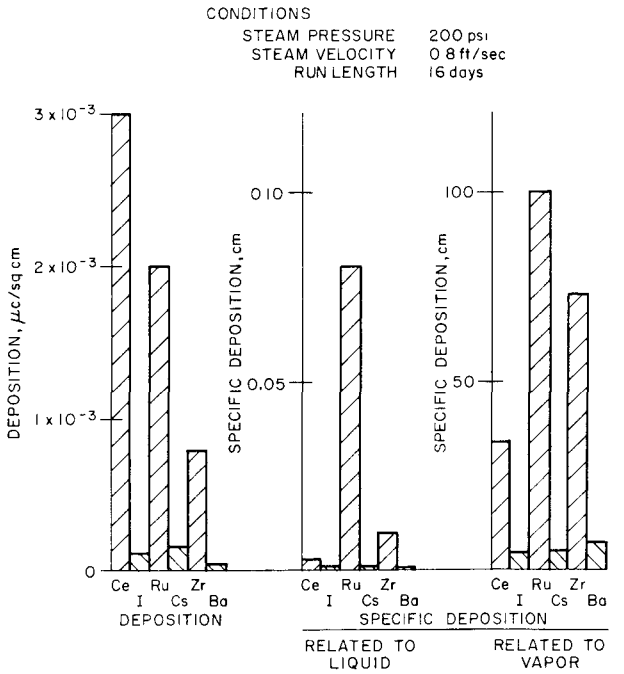

The lowest decontamination factors obtained were on the heated test section. In general, factors were low in the portions of the loop in which uranium was not likely to settle. Best results were obtained on the lower horizontal crossover. The bulk of the decontamination observed occurred with the first solution which removed approximately 54 percent of the contained uranium. Since the first solution was intended primarily as a uranium dissolvent, the possible conclusion that it is a good decontaminant is not warranted.

Additional data from the decontamination are now available and are reported below.

Following the run, the liquid portion of the loop was decontaminated by a series of four solution treatments. The first two consisted of carbonate-bicarbonate-peroxide solutions circulated for 7 hr and 5 hr, respectively, at 50 C. The purpose of circulating this solution was to dissolve the contained uranium. The third treatment was with an oxalate-peroxide solution which was circulated for 7 hr at room temperature. This solution was intended to remove deposited fission products from the metallic surfaces. The fourth treatment, 72 hr with 12 percent nitric acid, was used to dissolve uranium further and to decontaminate in the event that the first solutions were effective. The nitric acid, though not seriously considered for plant use, is considered effective for such purposes. The compositions of the solutions are listed at the top of Table 55. The fission product content and uranium content of each of the decontaminating solutions were obtained. From these data it was possible to calculate the amount of each isotope removed by each solution. These in turn were converted to percentages, which are shown in Table 55.

Table 55

ACTIVITY AND URANIUM RECOVERY DATA DURING DECONTAMINATION OF LOOP FOLLOWING RUN U4

Solution 1:	Solution 2:	Solution 3
0.25 M $NaHCO_3$ 0.25 M Na_2CO_3 0.5 M H_2O_2 3.4 g/l EDTA 1 g/l 8-hydroxyquinoline	0.5 $K_2C_2O_4$ 3 M H_2O_2 1 M Acetic Acid 0.18 M K Ac	12% Nitric Acid

Solution	Treatment Time (hr)	Percent of Total Activity or Uranium Recovered in Each Solution[a]						
		Ce^{141}	Ru^{103}	Nd^{147}	Cs^{137}	Zr^{95}	Ba^{140}	U
Loop Drainings, Acidified	0	1.0	1.3	1.6	0.9	0.4	3.4	0.5
Solution 1	7 (50 C)	39	56	30	54	50	26	54
Solution 1, Fresh Batch	5 (50 C)	27	14	36	23	25	28	26
Solution 2	7 (Room Temp)	21	6.5	29	12	14	30	3.5
Solution 3	72 (Room Temp)	12	22	3	9.9	9.8	11.8	15
Total Recovered		$5.6 \times 10^5 \mu c$	$4.45 \times 10^4 \mu c$	$2.66 \times 10^5 \mu c$	$5.49 \times 10^4 \mu c$	$4.12 \times 10^5 \mu c$	$3.41 \times 10^4 \mu c$	22 g
Percent of Amount Charged		76	25	-	49	72	56	65

[a] Quantities of iodine in solution were too low to be analyzed.

In addition, activity to uranium ratios were obtained for each solution to determine whether the decontamination observed was due solely to the dissolution of uranium or whether independent removal of activities had been achieved (see Table 56). Eighty percent of the uranium that was recovered was removed with the carbonate-peroxide dissolvent while somewhat less than four percent was removed by the oxalate-peroxide decontaminant. As expected, the percentage of fission products removed by the oxalate-peroxide decontaminant exceeded the percentage of uranium removed, but not by as large a factor as might be desired. Additional substantial uranium recovery was effected by the nitric acid. Material balances were in general poor, ranging from 49 to 76 percent for all fission products except ruthenium-103, for which it was 25 percent.

Table 56

ACTIVITY TO URANIUM RATIOS IN DECONTAMINATING SOLUTIONS FROM RUN U4

Identification	Fission Product Activity to Uranium Content, $\mu c/mg$[a]					
	Ce	Ru	Nd	Cs	Zr	Ba
Solution 1[b] (carbonate-peroxide)	18	2.1	6.7	2.5	17	0.75
Solution 1, fresh batch (carbonate-peroxide)	26	1.1	17	2.2	18	1.6
Average of Solution 1	22	1.6	12	2.3	17.5	1.2
Solution 2 (oxalate-peroxide)	130	3.3	90	7.5	69	12
Solution 3 (nitric acid)	22	3.1	2.6	1.8	13	1.4
Uranium charge to loop	42	9.0	-	3.3	23	9.0
Acidified loop drainings	50	5.5	38	4.6	16	11

[a] Insufficient iodine found in solutions to calculate meaningful ratios.

[b] See Table 55 for compositions.

To gain a better insight into the character of the several decontamination treatments, activity to uranium ratios ($\mu c/mg$) were calculated; these are presented in Table 56. The ratios for acidified loop drainings and and for the uranium charged to the loop are also included for general interest. If one assumes that the activity in the carbonate-peroxide dissolvent is solely from the dissolved uranium oxide and that the ratios shown are, as a

result, characteristic of this oxide, a basis exists for evaluating how much of the activity in the oxalate-peroxide decontaminant is from deposited activity and how much from uranium oxide. For example, the average activity/uranium ratio for zirconium is 17.5 in the carbonate-peroxide dissolvent. If the oxalate-peroxide decontaminant had dissolved only uranium, its ratio also would be expected to be 17.5. The difference between the 69 shown and 17.5 is then interpreted to represent activity removed from surfaces independently of uranium. When properly weighed for the amount of uranium actually contained in the decontaminant, the amount of zirconium removed independently of uranium is 77 percent. Similar analyses of cerium, ruthenium, neodymium, cesium, and barium result in the following percentages: 85, 56, 88, 72, and 91 percent. These results indicate that the oxalate-peroxide decontaminant is not as effective with ruthenium as compared with the other fission products. The ratios for nitric acid suggest that its ability to dissolve uranium is greater than its ability to decontaminate surfaces.

When the ratios given in Table 56 for the uranium charged and for the acidified loop drainings are compared with the ratios for the decontaminating solutions, it is evident that some preferential leaching of fission products occurred during the loop run. The evidence is quite marked for cerium and barium, less so for cesium and zirconium.

Extrapolation of Deposition Data to Radiation Level in Hypothetical 6-in. Vapor Space Pipe

The specific depositions related to liquid contents obtained above were used to determine radiation levels in a hypothetical situation by investigating the occurrences in a 6-in. steam line. (This line of necessity must be of stainless steel type 304 since it was on this kind of sample strip that the data were obtained.) The Dresden reactor was used as a reference for calculation of liquid-phase activities which might be associated with a fuel rupture. The assumptions used for the calculation are listed in Table 57. Time was not used as a parameter for the calculation for the variation of specific deposition has not been obtained in loop runs as a function of exposure time. The assumption which is most open to question is the 0.1 percent of the total reactor fission products in the reactor water. It should also be emphasized that the values of pressure and steam velocity are at variance with Dresden condition (1000 psi, 0.4 ft/sec vapor velocity in the steam drum). The results indicate that ruthenium and zirconium are the principal contributors to the radiation level. These two species are responsible for radiation levels of 8.5 and 11.6 mr/hr, respectively. The values are not high and would not jeopardize approach for maintenance purposes. It is perhaps significant that barium-140 with its high gamma energy of 1.6 Mev contributes only a small fraction to the total. Cerium, iodine, and cesium are likewise relatively insignificant.

Table 57

CALCULATED DEPOSITION IN HYPOTHETICAL VAPOR PHASE 6-IN. STEAM LINE BASED ON LOOP RUN U4

Conditions Assumed:	Dresden Reactor, equilibrium fission product content
Power Level:	626 Mw
Fissions/sec:	1.95×10^{19}
System Water Volume:	70,000 gal
Percentage Fission Products in reactor water:	0.1
Specific Fission Product Deposition:	as determined in loop run U4
Physical Geometry:	6-in. pipe (SS304)
Radiation:	Calculated for line source at distance of 1 ft
Steam Velocity:	0.8 ft/sec
Pressure:	200 psi

Fission Product	Fission Product Fission Yield (%)	Specific Deposition Related to Liquid (cm)	Gamma Energy Used (Mev)	Gamma Yield (%)	Radiation Level (mr/hr)
Ce^{141}	6.0	3×10^{-3}	0.145	70	0.14
I^{131}	3.1	1×10^{-3}	0.364	87.2	0.08
Ru^{103}	3.0	8×10^{-2}	0.50	90	8.5
Cs^{137}	6.15	8.6×10^{-4}	0.661	82	0.25
Zr^{95}	6.2	1×10^{-2}	0.75	200[a]	12
Ba^{140}	6.35	3.5×10^{-4}	1.6	100[b]	0.28

[a] 100 percent for Zr^{95} and 100 percent for Nb^{95} daughter.

[b] 100 percent for La^{140} daughter.

2. Laboratory Investigations (S. Vogler, H. Tyler)

The principal objective of the laboratory investigations is to study and evaluate decontamination or film-removal procedures by decontaminating reagents for reactor systems. In general, decontamination procedures developed at other sites are applicable to the primary circuits of pressurized water reactors. Investigations at this laboratory are directed toward the use of such reagents in the vapor space of boiling water reactors.

A current reagent under investigation is a solution of potassium oxalate and hydrogen peroxide at a pH of 4. This reagent was first suggested by the Oak Ridge National Laboratory for potential application in the Gas Cooled Reactor.

a. Decontamination of Stainless Steel with Oxalate-Peroxide Solution

In the past, decontamination experiments were usually performed with metal specimens which had been contaminated in laboratory equipment. The usual procedure consisted of heating a small piece (2 to 3 g) of irradiated natural uranium in deionized water in a stainless steel liner which was placed inside an autoclave. The water pressure was maintained at 600 psi for approximately one week. At this temperature the uranium reacted with the water to produce uranium dioxide and distributed the fission products into the water. The vaporizing water thus carried fission products up through the autoclave, in which deposition on the metal occurred. At the completion of an experiment, the contents of the liner were discarded and the liner rinsed clean. The liner was then cut into approximately one-in. squares. Squares obtained from the vapor space of the liner were then used as specimens for the decontamination experiments. Experiments with such samples had indicated good decontamination for cerium and zirconium (decontamination factors of approximately 200 and 1000) with poorer decontamination of about 5 to 10 for ruthenium (see ANL-6379, page 247).

Very few decontamination experiments had been done with loop-contaminated samples because only recently has the activity level been raised sufficiently high that vapor space samples of adequate contamination were obtained. The first experiments on loop-contaminated samples were on samples from Run U4. The decontamination factor obtained with these samples by means of the oxalate-peroxide reagent at 90 C was a rather poor 3 to 4, with little difference in this value from one fission product to another. The low decontamination obtained as compared with the higher results obtained on laboratory-contaminated samples was attributed at first to the low level of activity originally present on the loop samples, but is now believed to be a more complicated problem.

Currently, contaminated samples from Loop Run U5 have become available; these are the most active loop samples yet obtained. The first two experiments (see Table 58) were for the purpose of comparing the decontamination obtained with these more active samples with the results obtained with samples from Run U4 and with the results from autoclave-contaminated specimens.

Table 58

DECONTAMINATION OF STAINLESS STEEL WITH OXALATE-PEROXIDE SOLUTIONS

Samples: 304 SS Contaminated from Loop Run U5[a]

Activity: Ce ~3 x 10^3 cpm
Ru ~6 x 10^3 cpm
Zr ~6 x 10^3 cpm

Time: $\frac{1}{2}$ hr

Temp: 90 C

Exp No.	Reagent Concentrations[b] (mols/liter)		Decontamination Factor		
	$K_2C_2O_4$	H_2O_2	Ce	Ru	Zr
1	0.5	3.0	4.9	7.1	3.9
2	0.5	3.0	4.4	5.6	2.5
3	0.5	2.5	8.1	11.0	4.7
4	0.5	1.25	10	8.5	5.0
5	0.5	0.25	3.3	4.2	2.1

[a] Samples contaminated in the vapor phase of the loop while operating at 200 psi pressure and a steam velocity of 0.8 ft/sec.

[b] In all cases the reagent was originally at a pH of 4. In Experiment 1 this was achieved by the use of an acetate-acetic acid buffer. In the remaining experiments oxalic acid was used.

The decontamination results are in reasonable agreement with the results of the earlier loop run. In addition, decontamination experiments with the oxalate-peroxide reagent applied to loop-contaminated specimens from the liquid phase gave a decontamination factor of 4 to 5. From these data, it appears that an explanation for the poorer decontamination for loop samples should be sought in the difference in sample preparation and treatment during contamination of loop specimens and autoclave specimens.

These factors will be examined and correlated with the decontamination data in an effort to explain differences in the decontamination.*

It has been reported by Hickling and Rostron[36] that oxalic acid solutions containing hydrogen peroxide are excellent polishing agents for mild steel. In their work they show that the activity of the reagent is largely affected by the relative concentrations of the reagents. For example, with 0.1 to 0.3 molar oxalic acid in which the hydrogen peroxide is so low that the peroxide to oxalate ratio is less than 0.25, the metal appears to dissolve very slowly. When the hydrogen peroxide concentration is increased, so that the peroxide-to-oxalate ratio becomes greater than one, the rate of metal dissolution increases rapidly. Above a peroxide to oxalate ratio of 3.5, the metal appears passive.

It appeared interesting to examine whether such changes in the peroxide concentration would effect the reactions with stainless steel and hence the decontamination. Accordingly, Experiments 3 to 5 (results shown in Table 58) were performed. The results show essentially the same decontamination or at best a slight improvement over Experiments 1 and 2 in which the peroxide-to-oxalate ratios were six.

Qualitatively, the metal specimens at the completion of an experiment appeared to be little changed, and the brown oxide film was virtually unchanged.

The explanation of the differences in the ability to decontaminate loop specimens and laboratory-contaminated specimens may lie in the differences of pretreatment or of exposure conditions during contamination. The loop specimens are pre-filmed and contaminated in steam that is reasonably free of moisture; laboratory specimens probably "see" more liquid. A significant additional difference is the pressure (and hence also temperature during contamination). Loop specimens were contaminated at 200 psi, laboratory at 600 psi. This would suggest that activities deposited at high temperatures are more easily removed than those deposited at low temperatures. This is not consistent with experience at other sites with liquid systems. Additional experiments are required for clarification.

---

*The laboratory specimens were prepared by first carefully washing and degreasing the 304 stainless steel. The metal was placed in an autoclave containing water and maintained at a pressure of 600 psi for one week. This was termed preoxidation. The water in the autoclave was replaced and a small piece (~5 g) of irradiated natural uranium was added, and the autoclave was again heated to maintain a pressure of 600 psi for one week. Only the metal that was exclusively in the vapor space was used for decontamination experiments.

The loop specimens were degreased and preoxidized at 600 psi for 24 hr. Then, before the active run, the complete loop including the metal specimens was kept at 200 psi for 4 days with no vapor flow. Then, without interruption, the active run was begun and continued for 10 days at 200 psi and a vapor velocity of 0.8 ft/sec.

[36] Hickling, A., and Rostron, A. J., The Chemical Polishing of Mild Steel by Hydrogen Peroxide-Oxalic Acid Mixtures, Transactions Institute of Metal Finishing, 32, 229-261 (1955).

Stability of Oxalate-Peroxide Solutions

Previous experience with oxalate-peroxide solutions had indicated that at 90 C the stability of such solutions was approximately one hour. The deterioration of such a solution is marked by a rising pH due to the reaction of the oxalic acid with the peroxide. When the pH approached six, the hydrogen peroxide decomposed almost completely. When such a solution was buffered with acetic acid-acetate ion, the stability was increased.

The stability of such solutions at room temperature was also determined, and it was observed that standing for a period of over a week produced no significant changes in pH or hydrogen peroxide concentration (see Table 59).

Table 59

ROOM-TEMPERATURE STABILITY OF OXALATE-PEROXIDE SOLUTIONS

Solutions	
1	2
0.5 M $K_2C_2O_4$	0.5 M $K_2C_2O_4$
3.0 M H_2O_2	3.0 M H_2O_2
1.0 M $HC_2H_3O_2$	$H_2C_2O_4$ added to make pH = 4
0.175 M $NaC_2H_3O_2$	

Time (hr)	pH		H_2O_2 (M/L)	
	1	2	1	2
0	4.0	4.0	2.43	2.43
4	3.9	4.1	2.41	2.41
48	-	-	2.40	2.39
77	-	-	2.38	2.40
196	4.1	4.8	2.36	2.32

V. ROUTINE OPERATIONS
(H. G. Swope)

A. Waste Processing
(H. G. Swope, J. Harast, K. Bremer, G. Teats and R. Jarrett)

The total amount of liquid radioactive wastes processed during July, August, September, 1961 was 39,735 gal. The processing methods and quantity of wastes were as follows:

Process	Volume (gal)
Evaporation and Concentration	22,745
Filtration	11,160
Ion-Exchange (Cation, only)	2,750
Flocculation	2,490
Neutralization of HF Wastes	76
Absorption on Vermiculite	514
Total	39,735

B. High-level Gamma-irradiation Facility
(H. G. Swope, J. Harast, N. Ondracek, B. Kullen, R. Juvinall and V. Lemke)

A summary of irradiations performed in Racks M-1 and M-2 for July through September 1961 is given in Table 60.

Table 60

SUMMARY OF IRRADIATIONS PERFORMED IN RACKS M-1 AND M-2 DURING JULY THROUGH SEPTEMBER, 1961

	Rack M-1				Rack M-2			
Month	No of Samples[a]	No of Special Dosimetry Samples	Total Urn Units[b] Day	Total Urn Units[b] Night	No of Urns	No of Special Dosimetry Samples	Total Urn Units[c]	Dosimetry Units
July	413	122	790	1951	0	84	0	3
August	714	56	1556	2572	1	334	4	11
September	554	493	1755	2785	1	48	5	2
Totals	1681	671	4101	7308	2	466	9	16

[a] Equivalent to a No 2 sized can (3 7/16-in diam x 4 9/16 in high)
[b] 1 urn unit in Rack M-1 = 2×10^6 rad
[c] 1 urn unit in Rack M-2 = 200,000 rad